

University Of Alberta



0 0003 40431 41

PSR Report 1419-3

AIRBLAST FROM NUCLEAR BURSTS—ANALYTIC APPROXIMATIONS

Harold L. Brode

July 1987

Technical Report
CONTRACT No. DNA 001-85-C-0089

THIS WORK WAS SPONSORED BY THE DEFENSE NUCLEAR AGENCY
UNDER RDT&E RMSS CODE B 3460 85764XF 00003 25904D.

Prepared for
Director
DEFENSE NUCLEAR AGENCY
Washington, DC 20305-1000

QC
168.85
D46
B864
1987



PACIFIC-SIERRA RESEARCH CORPORATION
12340 Santa Monica Boulevard • Los Angeles, California 90025 • (213) 820-2200

SCI



EX LIBRIS
UNIVERSITATIS
ALBERTÆNSIS

REPORT DOCUMENTATION PAGE

| | | | |
|---|--|---|---|
| 1a. REPORT SECURITY CLASSIFICATION UNCLASSIFIED | | 1b. RESTRICTIVE MARKINGS | |
| 2a. SECURITY CLASSIFICATION AUTHORITY N/A since unclassified | | 3. DISTRIBUTION/AVAILABILITY OF REPORT | |
| 2b. DECLASSIFICATION/DOWNGRADING SCHEDULE N/A since unclassified | | | |
| 4. PERFORMING ORGANIZATION REPORT NUMBER(S) PSR Report 1419-3 | | 5. MONITORING ORGANIZATION REPORT NUMBER(S) | |
| 6a. NAME OF PERFORMING ORGANIZATION Pacific-Sierra Research Corporation | 6b. OFFICE SYMBOL (If applicable) | 7a. NAME OF MONITORING ORGANIZATION Director Defense Nuclear Agency | |
| 6c ADDRESS (City, State, and ZIP Code) 12340 Santa Monica Boulevard Los Angeles, California 90025-2587 | | 7b. ADDRESS (City, State, and ZIP Code) Washington, DC 20305-1000 | |
| 8a. NAME OF FUNDING/SPONSORING ORGANIZATION | 8b. OFFICE SYMBOL (If applicable) | 9. PROCUREMENT INSTRUMENT IDENTIFICATION NUMBER DNA 001-85-C-0089 | |
| 9c ADDRESS (City, State, and ZIP Code) | | 10. SOURCE OF FUNDING NUMBERS | |
| | | PROGRAM ELEMENT NO. | PROJECT NO. |
| | | TASK NO. | WORK UNIT ACCESSION NO. |
| 11. TITLE (Include Security Classification) AIRBLAST FROM NUCLEAR BURSTS--ANALYTIC APPROXIMATIONS | | | |
| 12. PERSONAL AUTHOR(S) Brode, Harold L. | | | |
| 13a. TYPE OF REPORT Technical Report | 13b. TIME COVERED FROM 841115 TO 871114 | 14. DATE OF REPORT (Year, Month, Day) 860930 | 15. PAGE COUNT |
| 16. SUPPLEMENTARY NOTATION This work was sponsored by the Defense Nuclear Agency under RDT&E RMSS Code B3460 85764 XF 00003 25904D. | | | |
| 17. COSATI CODES | | 18. SUBJECT TERMS (Continue on reverse if necessary and identify by block number) | |
| FIELD | GROUP | SUB-GROUP | Airblast Durations Fireballs |
| | | | Air Density Dynamic Pressure Free Air Burst |
| | | | Air Temperature Equation of State Height of Burst |
| 19. ABSTRACT (Continue on reverse if necessary and identify by block number) | | | |
| <p>Analytic approximations to nuclear blast and thermal radiation parameters are provided. Fits include overpressure, dynamic pressure, impulse, duration, shock velocity, density, temperature, particle velocity, shock reflections, and time of arrival. Height-of-burst effects are included for overpressure, dynamic pressure, and impulse. An approximation for the negative overpressure phase is included. Equations of state for air are provided in analytic form. The thermal radiation from the fireball from surface bursts, low air bursts, and high altitude bursts is characterized in simple forms.</p> | | | |
| 20. DISTRIBUTION/AVAILABILITY OF ABSTRACT <input type="checkbox"/> UNCLASSIFIED/UNLIMITED <input checked="" type="checkbox"/> SAME AS RPT. <input type="checkbox"/> DTIC USERS | | 21. ABSTRACT SECURITY CLASSIFICATION UNCLASSIFIED | |
| 22a. NAME OF RESPONSIBLE INDIVIDUAL Betty L. Fox | | 22b. TELEPHONE (Include Area Code) (202) 325-7042 | 22c. OFFICE SYMBOL DNA/STTI |

18. Subject Terms (Continued)

Impulse
Mach Reflection
Nuclear Bursts
Overpressure
Particle Velocity
Shock Reflection
Shock Velocity
Surface Burst
Time of Arrival
Yield Scaling
Negative Phase
Thermal Radiation

SUMMARY

Analytic approximations for many aspects of airblast from nuclear explosions are presented in this collection. Employing shock overpressure as an independent variable, shock front parameters are fit, including shock density, the specific heat ratio for shocks in sea-level air, shock velocity, peak particle velocity, peak dynamic pressure, shock temperature, and normal shock reflection factors in sea-level air.

Free-air (and surface) burst nuclear blast parameters are approximated, including such relations as peak overpressure versus range; shock radius versus peak overpressure; peak overpressure versus time of arrival; time of arrival versus peak overpressure; time of arrival versus shock radius; positive overpressure duration versus time of arrival; peak overpressure or range; overpressure impulse versus peak overpressure; overpressure and dynamic pressure versus time and range; overpressure impulse versus peak overpressure; overpressure and dynamic pressure versus time and range; overpressure impulse and dynamic pressure impulse versus overpressure or range; maximum (fireball) temperature versus peak overpressure; and negative underpressure versus peak overpressure and time.

Some blast parameters as a function of burst height are approximated, including overpressure and dynamic pressure versus burst height, ground range, and time. These fits are compared with results of detailed computer calculations.

The equations of state for air are fit, including both the thermal ($P = RT\rho$) and caloric [$E_\rho = P/(\gamma - 1)$] relations. Some of the fireball thermal radiation characteristics are given in further analytic approximations for surface bursts, air bursts, and high-altitude bursts.

PREFACE

This collection of airblast fits was prepared at the urging of Dr. George W. Ullrich (Defense Nuclear Agency/Shock Physics Aerospace Systems), and Mr. Clifton B. McFarland (Defense Nuclear Agency/Shock Physics Strategic Structures), who perceived a need for a single document summarizing the available analytical approximations.

In compiling these fits, the author relied upon many sources and individuals. In particular, the years of detailed curve fitting so diligently pursued by Stephen J. Speicher (a coauthor on numerous previous reports) are liberally represented in the approximations offered in this document, and in the reports noted in the reference section.

Special thanks are due Gilbert C. Binninger of Science Applications, Inc., La Jolla, California, and Fred Sauer of California Research & Technology, Inc., Pleasanton, California, for their thorough review and numerous suggestions.

CONVERSION TABLE

Conversion factors for U.S. customary to metric units of measurement.

| To Convert From | To | Multiply By |
|---|-----------------------------|-------------|
| Pounds per square inch (psi) | Kilopascals (kPa) | 6.8951 |
| Bars | Kilopascals (kPa) | 100.00 |
| Calories (cal) | Joules (J) | 4.183 |
| Feet (ft) | Meters (m) | 0.3048 |
| Inches (in.) | Meters (m) | 0.0254 |
| Kilotons (KT) | Terajoules (TJ) | 4.183 |
| Megatons (MT) | Terajoules (TJ) | 4183 |
| Kilofeet per second (kft/s) | Meters per second (m/s) | 304.8 |
| Kilofeet (kft) | Meters (m) | 304.8 |
| Kilofeet per cube-root kiloton (kft/KT ^{1/3}) | Meters per terajoule (m/TJ) | 189.2 |

TABLE OF CONTENTS

| Section | Page |
|--|--------|
| SUMMARY..... | iii |
| PREFACE..... | iv |
| CONVERSION TABLE..... | v |
| LIST OF ILLUSTRATIONS..... | viii |
| 1 INTRODUCTION..... | 1 |
| 2 SHOCK-FRONT VARIABLES..... | 4 |
| Conservation relations at shock front..... | 4 |
| Shock density..... | 6 |
| Specific heat ratio for shocks in sea-level air..... | 7 |
| Shock velocity..... | 11 |
| Peak particle velocity..... | 13 |
| Peak dynamic pressure..... | 13 |
| Shock temperature..... | 16 |
| Thermal equation of state for air..... | 18 |
| Normal reflection of shocks..... | 21 |
| Table of shock variables..... | 23 |
| 3 FREE-AIR AND SURFACE NUCLEAR BURSTS..... | 26 |
| Peak overpressure versus range (free-air burst)..... | 26 |
| Peak overpressure versus range (ideal-surface burst)..... | 29 |
| Test-surface peak overpressure versus range..... | 29 |
| Shock radius versus peak overpressure (free-air burst)..... | 29 |
| Peak overpressure versus time of arrival (free-air burst)..... | 30 |
| Peak overpressure versus time of arrival (surface burst)..... | 30 |
| Time of arrival versus peak overpressure..... | 31 |
| Time of arrival versus shock radius..... | 31 |
| Close-in time of arrival versus shock radius..... | 34 |
| Positive overpressure duration versus time of arrival (free-air burst)..... | 34 |
| Positive overpressure duration versus time of arrival (surface burst)..... | 36 |
| Positive overpressure duration versus peak overpressure (free-air burst)..... | 36 |
| Positive overpressure duration versus range..... | 38 |
| Overpressure impulse in positive phase versus peak overpressure (free-air and surface burst)..... | 38 |
| Overpressure versus time..... | 41 |
| Overpressure versus time (surface burst)..... | 41 |

TABLE OF CONTENTS (Concluded)

| Section | Page |
|---|---------|
| Duration of outward dynamic pressure versus peak overpressure..... | 43 |
| Dynamic impulse versus peak overpressure (free-air burst)..... | 45 |
| Dynamic impulse versus scaled range..... | 45 |
| Dynamic pressure versus time..... | 47 |
| Maximum temperature (fireball exposure) versus peak overpressure..... | 50 |
| Negative phase underpressure versus peak overpressure and time..... | 52 |
| Blast summary..... | 53 |
| 4 BLAST PARAMETERS AS FUNCTIONS OF BURST HEIGHT..... | 60 |
| Peak overpressure versus scaled burst height and scaled range..... | 60 |
| Overpressure versus time scaled range, and burst height..... | 71 |
| Peak dynamic pressure versus scaled burst height and scaled range..... | 120 |
| Scaled dynamic impulse versus scaled burst height and ground range..... | 133 |
| Dynamic pressure time versus scaled burst height and range..... | 136 |
| Height of target effect on maximum dynamic pressure contours..... | 144 |
| 5 EQUATION OF STATE FOR AIR..... | 146 |
| Caloric equation of state for air..... | 146 |
| Thermal equation of state for air..... | 147 |
| 6 THERMAL RADIATION..... | 151 |
| Airburst..... | 151 |
| Surface burst..... | 159 |
| Buried bursts..... | 160 |
| High-altitude bursts..... | 160 |
| 7 LIST OF REFERENCES..... | 172 |
| Appendices | |
| A OVERPRESSURE VALUES AS FUNCTION OF GROUND RANGE, BURST HEIGHT, AND TIME..... | 177 |
| B FORTRAN PROGRAM FOR OVERPRESSURE VERSUS TIME, BURST HEIGHT, AND GROUND RANGE..... | 179 |
| C LIST OF SYMBOLS..... | 183 |

LIST OF ILLUSTRATIONS

| Figure | | Page |
|--------|--|------|
| 1 | Shock-front parameters (in shock-front frame of reference)..... | 5 |
| 2 | Shock density versus shock overpressure in standard, sea-level air ($\rho_0 \approx 1.293 \text{ kg/m}^3$)..... | 8 |
| 3 | Specific heat ratio ($\gamma = C_p/C_v$) for shocks in standard, sea-level air versus shock pressure..... | 9 |
| 4 | Shock velocity versus shock overpressure in air at sea level..... | 12 |
| 5 | Peak particle velocity versus shock overpressure in air at sea level..... | 14 |
| 6 | Shock dynamic pressure relative to shock overpressure versus shock overpressure..... | 17 |
| 7 | Thermal equation of state for air versus temperature and density..... | 20 |
| 8 | Reflected shock conditions..... | 21 |
| 9 | Normal reflection factor versus shock overpressure for sea-level air..... | 24 |
| 10 | Peak overpressure versus shock radius for 1-KT free-air nuclear burst in standard, sea-level air..... | 27 |
| 11 | Scatter in percent of range to given peak overpressure for near-surface atmospheric nuclear tests.... | 28 |
| 12 | Time of arrival versus peak overpressure for 1-KT free-air burst at sea level..... | 32 |
| 13 | Product of time of arrival and peak overpressure ^{0.875} versus peak overpressure for 1 KT (T in milliseconds)..... | 33 |
| 14 | Time of arrival versus shock radius for 1-KT free-air burst..... | 35 |
| 15 | Fit compared to calculations: overpressure durations at 1 KT..... | 37 |

LIST OF ILLUSTRATIONS (Continued)

| Figure | | Page |
|--------|--|------|
| 16 | Fit compared to detailed calculation and 1-KT standard: overpressure impulse in positive phase (1-KT, free-air burst)..... | 39 |
| 17 | Fit compared to calculation: impulse in positive overpressure versus peak overpressure (1-KT, free-air burst)..... | 40 |
| 18 | Fit compared to calculation and 1-KT standard (scaled to 1-MT surface burst): dynamic pressure positive phase..... | 44 |
| 19 | Fit compared to calculation: dynamic impulse versus peak overpressure for 1-KT, free-air burst..... | 46 |
| 20 | Fit compared to calculation: scaled dynamic pressure impulse versus scaled range for 1-KT, free-air burst..... | 48 |
| 21 | Dynamic pressure versus peak overpressure and time (scaled for 1-MT surface burst)..... | 49 |
| 22 | Fit compared to calculation: maximum fireball temperature versus peak overpressure for 1-MT burst.... | 51 |
| 23 | Negative phase pressure versus time at scaled range of $0.1472 \text{ kft}/\text{KT}^{1/3}$ (570 psi)..... | 54 |
| 24 | Negative phase pressure versus time at scaled range of $0.2102 \text{ kft}/\text{KT}^{1/3}$ (213 psi)..... | 54 |
| 25 | Negative phase pressure versus time at scaled range of $0.3154 \text{ kft}/\text{KT}^{1/3}$ (74 psi)..... | 55 |
| 26 | Negative phase pressure versus time at scaled range of $0.4205 \text{ kft}/\text{KT}^{1/3}$ (37 psi)..... | 55 |
| 27 | Negative phase pressure versus time at scaled range of $0.5256 \text{ kft}/\text{KT}^{1/3}$ (23 psi)..... | 56 |
| 28 | Negative phase pressure versus time at scaled range of $0.6307 \text{ kft}/\text{KT}^{1/3}$ (15.5 psi)..... | 56 |

LIST OF ILLUSTRATIONS (Continued)

| Figure | | Page |
|--------|---|------|
| 29 | Negative phase pressure versus time at scaled range of $0.841 \text{ kft}/\text{KT}^{1/3}$ (9 psi)..... | 57 |
| 30 | Negative phase pressure versus time at scaled range of $0.9882 \text{ kft}/\text{KT}^{1/3}$ (6.7 psi)..... | 57 |
| 31 | Blast parameters for 1-MT surface burst..... | 59 |
| 32 | Ultra-high peak overpressure HOB versus ground range contours, scaled to 1 KT..... | 61 |
| 33 | Extremely high peak overpressure HOB versus ground range contours, scaled to 1 KT..... | 62 |
| 34 | Very high peak overpressure HOB versus ground range contours, scaled to 1 KT..... | 63 |
| 35 | High peak overpressure HOB versus ground range contours, scaled to 1 KT..... | 64 |
| 36 | Intermediate high peak overpressure burst height versus ground range contours, scaled to 1 KT..... | 65 |
| 37 | Intermediate peak overpressure burst height versus ground range contours, scaled to 1 KT..... | 66 |
| 38 | Intermediate low peak overpressure burst height versus ground range contours, scaled to 1 KT..... | 67 |
| 39 | Low peak overpressure burst height versus ground range contours, scaled to 1 KT..... | 68 |
| 40 | Very low peak overpressure burst height versus ground range contours, scaled to 1 KT..... | 69 |
| 41 | High peak overpressures versus scaled burst height and scaled ground range (ideal surface)..... | 72 |
| 42 | Fit compared to S-Cubed calculation (scaled): overpressure and scaled partial impulse versus scaled time to 0.07 ms, for $\Delta P_s = 548,300 \text{ psi}$, $y = 0$, $x = 18.896 \text{ ft}/\text{KT}^{1/3}$ | 79 |

LIST OF ILLUSTRATIONS (Continued)

| Figure | | Page |
|--------|---|------|
| 43 | Fit compared to S-Cubed calculation (scaled): overpressure and scaled partial impulse versus scaled time to 3.5 ms, for $\Delta P_s \approx 548,300$ psi, $y = 0$, $x = 18.896$ ft/KT $^{1/3}$ | 80 |
| 44 | Fit for overpressure and scaled partial impulse versus scaled time to 70 ms, for $\Delta P_s \approx 548,300$ psi, $y = 0$, $x = 18.896$ ft/KT $^{1/3}$ | 81 |
| 45 | Fit compared to S-Cubed calculation (scaled): overpressure and scaled impulse versus scaled time to 0.32 ms, for $\Delta P_s \approx 99,740$ psi, $y = 0$, $x = 33.068$ ft/KT $^{1/3}$ | 82 |
| 46 | Fit compared to S-Cubed calculation (scaled): overpressure and scaled impulse versus scaled time to 7 ms, for $\Delta P_s \approx 99,740$ psi, $y = 0$, $x = 33.068$ ft/KT $^{1/3}$ | 83 |
| 47 | Fit for overpressure and scaled impulse versus scaled time to 140 ms, for $\Delta P_s \approx 99,740$ psi, $y = 0$, $x = 33.068$ ft/KT $^{1/3}$ | 84 |
| 48 | Fit compared to S-Cubed calculation: overpressure and scaled impulse versus scaled time to 7 ms, for $\Delta P_s \approx 10,760$ psi, $y = 0$, $x = 69$ ft/KT $^{1/3}$ | 85 |
| 49 | Fit for overpressure and scaled impulse versus scaled time to 70 ms, for $\Delta P_s \approx 10,760$ psi, $y = 0$, $x = 69$ ft/KT $^{1/3}$ | 86 |
| 50 | Fit compared to DNA 1-KT standard (2W): overpressure and scaled impulse versus scaled time to 70 ms, for $\Delta P_s \approx 991.1$ psi, $y = 0$, $x = 154.6$ ft/KT $^{1/3}$ | 87 |
| 51 | Fit compared to DNA 1-KT standard (2W): overpressure versus scaled time to 100 ms, for $\Delta P_s \approx 98.59$ psi..... | 88 |
| 52 | Fit compared to DNA 1-KT standard (2W): scaled impulse versus scaled time to 100 ms, for $\Delta P_s \approx 98.59$ psi..... | 89 |
| 53 | Fit compared to DNA 1-KT standard (2W): overpressure versus scaled time to 250 ms, for $\Delta P_s \approx 10.01$ psi..... | 90 |

LIST OF ILLUSTRATIONS (Continued)

| Figure | | Page |
|--------|---|------|
| 54 | Fit compared to DNA 1-KT standard (2W): scaled impulse versus scaled time to 250 ms, for $\Delta P_s \approx 10.01$ psi..... | 91 |
| 55 | Fit compared to DNA 1-KT standard (2W): overpressure versus scaled time to 450 ms, for $\Delta P_s \approx 1.036$ psi..... | 92 |
| 56 | Fit compared to DNA 1-KT standard (2W): scaled impulse versus scaled time to 450 ms, for $\Delta P_s \approx 1.036$ psi..... | 93 |
| 57 | Fit compared to DNA 1-KT standard (2W): overpressure versus scaled time to 500 ms, for $\Delta P_s \approx 0.1086$ psi..... | 94 |
| 58 | Fit compared to DNA 1-KT standard (2W): scaled impulse versus scaled time to 500 ms, for $\Delta P_s \approx 0.1086$ psi..... | 95 |
| 59 | Fit compared to scaled SAI calculation: overpressure and scaled impulse versus scaled time to .13 ms, for 25 ft SHOB $\Delta P_s = 1,785,000$ psi..... | 96 |
| 60 | Fit compared to SAI calculation: overpressure and scaled impulse versus scaled time to .41 ms, for 25 ft SHOB, $\Delta P_s = 1,785,000$ psi..... | 97 |
| 61 | Fit compared to SAI calculation: overpressure and scaled impulse versus scaled time to .55 ms, for 25 ft SHOB, $\Delta P_s = 233,300$ psi..... | 98 |
| 62 | Fit compared to SAI calculation: overpressure and scaled impulse versus scaled time to 1.6 ms, for 25 ft SHOB, $\Delta P_s = 233,300$ psi..... | 99 |
| 63 | Fit compared to S-CUBED calculation: overpressure versus scaled time minus time-of-arrival to 7 ms, for 50 ft SHOB, $\Delta P_s \approx 9,000$ psi..... | 100 |
| 64 | Fit compared to S-Cubed calculation: scaled impulse versus scaled time minus time-of-arrival to 7 ms, for 50 ft SHOB, $\Delta P_s \approx 9,000$ psi..... | 101 |

LIST OF ILLUSTRATIONS (Continued)

| Figure | | Page |
|--------|---|------|
| 65 | Fit compared to S-CUBED calculation: scaled impulse versus scaled time minus time-of-arrival to 100 ms, for 50 ft SHOB, $\Delta P_s \approx 9,000$ psi..... | 102 |
| 66 | Fit compared to 8-lb charge data: overpressure versus scaled time to 10 ms, for 107-ft SHOB, $\Delta P_s \approx 1199$ psi..... | 103 |
| 67 | Fit compared to 8-lb charge data: scaled impulse versus scaled time to 10 ms, for 107-ft SHOB, $\Delta P_s \approx 1199$ psi..... | 104 |
| 68 | Fit compared to General Electric-TEMPO calculation: overpressure versus scaled time to 70 ms, for 60-m SHOB, $\Delta P_s \approx 110.5$ psi..... | 105 |
| 69 | Fit compared to General Electric-TEMPO calculation: scaled impulse versus scaled time to 70 ms, for 60-m SHOB, $\Delta P_s \approx 110.5$ psi..... | 106 |
| 70 | Fit compared to DIPOLE WEST data: overpressure versus scaled time to 220 ms, for 150-ft SHOB, $\Delta P_s \approx 10.15$ psi..... | 107 |
| 71 | Fit compared to DIPOLE WEST data: scaled impulse versus scaled time to 220 ms, for 150-ft SHOB, $\Delta P_s \approx 10.15$ psi..... | 108 |
| 72 | Fit compared to 200-ft SHOB Kaman AviDyne calculation: peak overpressure (from 1600 psi) versus scaled ground range (0 to 0.3 kft)..... | 109 |
| 73 | Fit compared to 200-ft SHOB Kaman AviDyne calculation: peak overpressure (100 to 15 psi) versus scaled ground range (0.3 to 0.9 kft)..... | 110 |
| 74 | Fit compared to 200-ft SHOB Kaman AviDyne calculation: peak overpressure (10 to 1.5 psi) versus scaled ground range (1 to 3.7 kft)..... | 111 |
| 75 | Fit compared to 200-ft SHOB Kaman AviDyne calculation: scaled overpressure impulse versus scaled ground range (to 1 kft)..... | 112 |

LIST OF ILLUSTRATIONS (Continued)

| Figure | | Page |
|--------|--|------|
| 76 | Fit compared to 200-ft SHOB Kaman AviDyne calculation: impulse versus scaled ground range (1 to 3.5 kft)..... | 113 |
| 77 | HOB isoimpulse curves: fit compared to 8-lb charge data, showing partial impulse contours for $0.5 \text{ ms}/\text{KT}^{1/3}$ | 114 |
| 78 | HOB isoimpulse curves: fit compared to 8-lb charge data, showing partial impulse contours for $2 \text{ ms}/\text{KT}^{1/3}$ | 115 |
| 79 | HOB isoimpulse curves: fit compared to 8-lb charge data, showing partial impulse contours for $10 \text{ ms}/\text{KT}^{1/3}$ | 116 |
| 80 | Partial impulse contours at very high overpressure for $0.5 \text{ ms}/\text{KT}^{1/3}$ | 117 |
| 81 | Partial impulse contours at very high overpressure for $2 \text{ ms}/\text{KT}^{1/3}$ | 118 |
| 82 | Partial impulse contours at very high overpressure for $10 \text{ ms}/\text{KT}^{1/3}$ | 119 |
| 83 | Peak dynamic pressure fit compared to Kaman AviDyne calculation, for surface burst, high-pressure region..... | 123 |
| 84 | Peak dynamic pressure fit compared to Kaman AviDyne calculation, for surface burst, intermediate region..... | 123 |
| 85 | Peak dynamic pressure fit compared to Kaman AviDyne calculation, for surface burst, low-pressure region..... | 124 |
| 86 | Peak dynamic pressure fit compared to Kaman AviDyne calculation, for scaled burst height of $200 \text{ ft}/\text{KT}^{1/3}$ | 124 |
| 87 | Peak dynamic pressure fit compared to Kaman AviDyne calculation, for scaled burst height of $250 \text{ ft}/\text{KT}^{1/3}$ | 125 |

LIST OF ILLUSTRATIONS (Continued)

| Figure | | Page |
|--------|---|------|
| 88 | Peak dynamic pressure fit compared to Kaman AviDyne calculation, for scaled burst height of 300 ft/ $KT^{1/3}$ | 125 |
| 89 | Peak dynamic pressure fit compared to Kaman AviDyne calculation, for scaled burst height of 400 ft/ $KT^{1/3}$ | 126 |
| 90 | Peak dynamic pressure fit compared to Kaman AviDyne calculation, for scaled burst height of 500 ft/ $KT^{1/3}$ | 126 |
| 91 | Peak dynamic pressure fit compared to Kaman AviDyne calculation, for scaled burst height of 600 ft/ $KT^{1/3}$ | 127 |
| 92 | Peak dynamic pressure fit compared to Kaman AviDyne calculation, for scaled burst height of 700 ft/ $KT^{1/3}$ | 127 |
| 93 | Peak dynamic pressure fit compared to Kaman AviDyne calculation, for scaled burst height of 750 ft/ $KT^{1/3}$ | 128 |
| 94 | Peak dynamic pressure fit compared to Kaman AviDyne calculation, for scaled burst height of 1000 ft/ $KT^{1/3}$ | 128 |
| 95 | Peak dynamic pressure fit compared to Kaman AviDyne calculation, for scaled burst height of 1250 ft/ $KT^{1/3}$ | 129 |
| 96 | HOB isopicnic contours from Kaman AviDyne calculations compared to fit for peak dynamic pressure (100 to 1000 psi)..... | 129 |
| 97 | HOB isopicnic contours from Kaman AviDyne calculations compared to fit for peak dynamic pressure (20 to 100 psi)..... | 130 |
| 98 | HOB isopicnic contours from Kaman AviDyne calculations compared to fit for peak dynamic pressure (8 to 20 psi)..... | 130 |

LIST OF ILLUSTRATIONS (Continued)

| Figure | | Page |
|--------|--|------|
| 99 | HOB isopicnic contours from Kaman AviDyne calculations compared to fit for peak dynamic pressure (3 to 8 psi)..... | 131 |
| 100 | HOB isopicnic contours from Kaman AviDyne calculations compared to fit for peak dynamic pressure (1 to 3 psi)..... | 131 |
| 101 | HOB isopicnic contours from Kaman AviDyne calculations compared to fit for peak dynamic pressure (0.4 to 1 psi)..... | 132 |
| 102 | HOB isopicnic contours from Kaman AviDyne calculations compared to fit for peak dynamic pressure (0.15 to 0.4 psi)..... | 134 |
| 103 | HOB isopicnic contours from Kaman AviDyne calculations compared to fit for peak dynamic pressure (0.08 to 0.15 psi)..... | 135 |
| 104 | HOB isopicnic contours from Kaman AviDyne calculations compared to fit for peak dynamic pressure (0.05 to 0.08 psi)..... | 135 |
| 105 | Scaled dynamic impulse fit versus scaled range and scaled burst height..... | 137 |
| 106 | Fit compared to Kaman AviDyne calculation: peak dynamic pressure for 200-ft SHOB versus scaled, close-in ground range..... | 139 |
| 107 | Fit compared to Kaman AviDyne calculation: peak dynamic pressure for 200-ft SHOB versus scaled, intermediate ground range..... | 140 |
| 108 | Fit compared to Kaman AviDyne calculation: peak dynamic impulse for 200-ft SHOB versus scaled, close-in ground range..... | 141 |
| 109 | Fit compared to Kaman AviDyne calculation: peak dynamic impulse for 200-ft SHOB versus scaled, intermediate ground range..... | 142 |

LIST OF ILLUSTRATIONS (Continued)

| Figure | Page |
|---|------|
| 110 Integration of Eq. (66) over positive phase compared to Kaman AviDyne calculations: dynamic impulse versus SHOB and scaled ground range..... | 143 |
| 111 Maximum dynamic pressure HOB/HOT contours for scaled target heights of scaled burst height and ground range where peak dynamic pressure is 90 percent of surface value..... | 145 |
| 112 Caloric equation of state for air--data..... | 149 |
| 113 Caloric equation of state for air--fit..... | 150 |
| 114 Fit compared to data average: normalized thermal radiation power pulse and thermal energy radiated versus normalized time..... | 153 |
| 115 Thermal fraction versus yield, near sea level airburst predictions..... | 156 |
| 116 Approximate transition from surface burst to airburst thermal radiation fraction versus burst height for yields from 1 KT to 10 MT [Eq. (97)]..... | 161 |
| 117 Thermal radiation fraction of total yield versus yield for burst altitudes up to 30 KM [Brode, 1968, Eq. (32)]..... | 164 |
| 118 Thermal radiation fraction of total yield versus yield for burst altitudes up to 30 KM [ENW, 1977]..... | 166 |
| 119 Thermal radiation fraction of total yield versus yield for burst altitudes up to 30 KM [EM-1, 1985]..... | 168 |
| 120 Comparison of thermal fractions as predicted by three formulae (Eqs. (101), (102), (103)) versus burst altitude for 1 KT..... | 169 |
| 121 Comparison of thermal fractions as predicted by three formulae (Eqs. (101), (102), (103)) versus burst altitude for 100 KT..... | 170 |
| 122 Comparison of thermal fractions as predicted by three formulae (Eqs. (101), (102), (103)) versus burst altitude for 10 MT..... | 171 |

SECTION 1

INTRODUCTION

Even before the first nuclear burst, the effect of height of burst (HOB) on the blast wave was considered important. The Hiroshima and Nagasaki bombs were detonated at considerable altitude in order to increase the range at which significant blast damage might occur.

Blast measurements were made on more than 90 atmospheric nuclear tests in the period 1951-1963.* A number of detailed hydrodynamic and radiation-hydrodynamic calculations have helped to explore the physical processes involved. Further measurements and understanding have come from simulated or analogous blasts created with chemical explosives. From each of those sources, we have gained information that has required further interpretation and simplification for application to targeting or to the design of survivable structures and military systems.

As a consequence, frequent efforts have been made to find useful analogs and algebraic formulae to represent the principal blast features. Some are derived from theoretical principles, some are the result of empirical fits to observations and test data. All attempt to simplify and quantify the complex physics of blast waves.

The analytic expressions for blast waves presented in this report are divided into three general classes. The first class (in Sec. 2) includes relations that can be expressed for shock-front variables, independent of yield and burst geometry. These Rankine-Hugoniot, or shock-front relations, become more complex for strong shocks in air, since the air molecules begin to disassociate and the air atoms begin to ionize as the strength of the shock grows and as the air temperature and pressure rise. Section 2 also includes the appropriate equation of state for air at the shock for both caloric and thermal

*A brief summary of atmospheric tests and a list of references are presented in Brode [1979]. An analysis of the resulting peak overpressure HOB data is provided in Brode [1981].

properties, i.e., for both internal energies and temperatures. Specifically, Sec. 2 deals with shock density, shock velocity, particle velocity at the shock (shock wind), peak dynamic pressure, shock temperature, and shock reflection factors. A tabular summary of those variables is included, along with peak overpressure, the ratio between pressure and energy density, i.e., the effective gamma-minus-one, and the gas "constant" for the thermal equation of state, i.e., the ratio of pressure to temperature times density.

The properties of a nuclear explosion in air, unaffected by any surface reflections (a "free-air" burst), have been described in detail by numerical radiation-hydrodynamic calculations, and have been used to describe surface bursts (assuming a surface burst is equivalent to a free-air burst of twice the yield). Some of those nuclear blast wave properties are described by simple algebraic fits in Sec. 3. The relations provided include peak overpressure versus shock radius; shock radius versus peak overpressure; peak overpressure versus time of arrival (TOA); TOA versus peak overpressure or shock radius; duration of positive overpressure versus TOA, peak overpressure, or shock radius; overpressure impulse (in the positive phase) versus peak overpressure; overpressure versus time; duration of positive dynamic pressure versus peak overpressure or shock radius; dynamic pressure versus time; maximum temperature versus peak overpressure; and time to maximum temperature versus peak overpressure.

Tabular listings are included here for peak overpressure, range, TOA, positive phase duration and impulse for overpressure, and dynamic pressure and maximum temperature in the shock or fireball (all for a 1-KT free-air burst).

Section 4 provides fits for peak overpressure versus burst height and ground range; overpressure versus time, burst height, and ground range; peak dynamic pressure and total positive dynamic impulse versus burst height and ground range; dynamic pressure versus time, burst height, and ground range; and some limits for dynamic pressure decreases (10 percent less than surface values) as functions of target height (in terms of ground range and burst height).

Section 5 provides a detailed fit to the caloric equation of state for air. The thermal equation of state for air is included in Sec. 2, Eq. (25).

The principal features of the thermal radiation from the fireball are given quantitative approximations in Sec. 6. That section includes times, peak power, energy radiated, and atmospheric transmission for both air and surface bursts.

Forty years of blast research have yielded an extensive data base, plus considerable confidence in many of the simplified analytic approximations presented here. However, airblast research in recent years has been proceeding at a rapid rate. Consequently, these fits for idealized conditions will need corrections, improvements, and additions within a few years. One of the areas being investigated most intensively is airblast over "nonideal" or "real" responding surfaces. There is already a need for simple representations of blast waves over such real surfaces for use in targeting and survivability analyses. The simplifications and analytic fits offered in this report may provide a logical point of departure for extensions into nonideal surface complexities and structure interaction models.

Appendix A provides overpressure values as a function of time, range, and burst height. These values are provided as test cases for those who have programmed the overpressure fit and wish to check for errors.

Appendix B is a Fortran listing of a program to calculate the overpressure as a function of time, burst height, and ground range.

While accuracy estimates are provided wherever possible, there is no adequate treatment of the variability and degree of unpredictability in airblast features. Measurements made during the atmospheric test program generally supported a variation exceeding plus or minus 20 percent on many blast features. A review of peak overpressure measurements by the author [Brode, 1981] emphasizes the data scatter and the lack of reproducibility in the nuclear blast over real surfaces. Clearly, the analytic expressions presented here cannot reflect such large uncertainties.

SECTION 2

SHOCK-FRONT VARIABLES

For shock waves in an ideal gas or fluid, all of the dynamic and thermodynamic variables at the shock front (density, particle velocity, shock velocity, dynamic pressure, temperature, etc.) can be expressed in terms of preshock conditions (ambient pressure P_0 , ambient air density ρ_0 , ambient air specific heat ratio γ_0 , ambient air temperature θ_0) and a single variable such as shock strength (e.g., peak overpressure). A number of such relations are derived in this section.

At high temperatures and pressures, air is not an ideal gas, which limits the utility of an ideal gas formulation for strong shocks in air. Since the effective specific heat ratio γ changes slowly with shock strength, analytical expressions for all of those parameters can be found which follow fairly simple forms; some are not unlike their ideal-gas counterparts. In addition, the influence of equation-of-state changes can be represented by a fit to γ at the shock condition in air.

Fits for peak dynamic pressure Q_s , shock velocity U_s , peak particle velocity u_s , peak density ρ_s , shock temperature θ_s , and normal reflection factor RF are offered as functions of the peak pressure P_s or peak overpressure ($\Delta P_s = P_s - P_0$), the preshock conditions (P_0 , ρ_0 , γ_0 , and ambient air sound speed C_0), and the shocked air specific heat ratio γ_s .

CONSERVATION RELATIONS AT SHOCK FRONT.

Conservation of mass, momentum, and specific internal energy across a shock front are represented in Fig. 1 and the following equations.

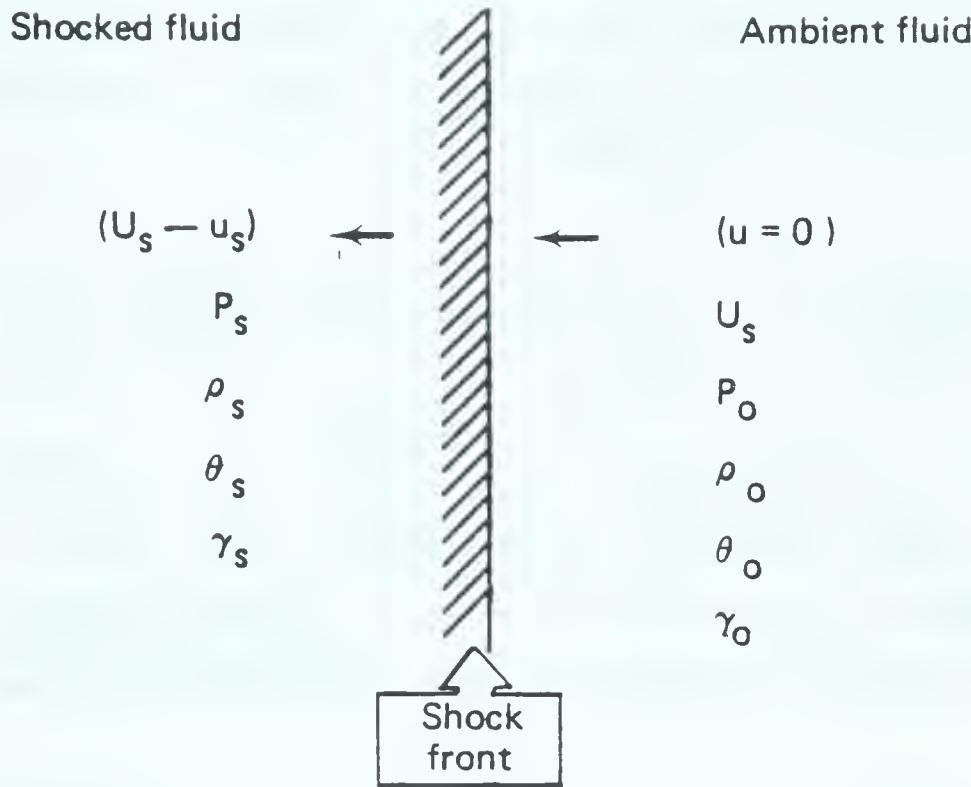


Figure 1. Shock-front parameters (in shock-front frame of reference).

$$\rho_o U_s = \rho_s (U_s - u_s) \quad (\text{mass}), \quad (1)$$

$$P_s - P_o = \rho_o u_s U_s \quad (\text{momentum}), \quad (2)$$

$$\frac{1}{2} U_s^2 + \frac{\gamma_o}{(\gamma_o - 1)} \frac{P_o}{\rho_o} = \frac{1}{2} (U_s - u_s)^2 + \frac{\gamma_s}{(\gamma_s - 1)} \frac{P_s}{\rho_s} \quad (\text{energy}). \quad (3)$$

Equation (3) may also be written as

$$E_s - E_o = \frac{P_s}{(\gamma_s - 1)\rho_s} - \frac{P_o}{(\gamma_o - 1)\rho_o} = \frac{(P_s + P_o)}{2} \left(\frac{1}{\rho_o} - \frac{1}{\rho_s} \right), \quad (4)$$

where E_s = shocked specific internal energy,

E_o = ambient specific internal energy.

Implicit in Eqs. (3) and (4) is the ideal gas relation for specific internal energy E :

$$E = P/[\rho(\gamma - 1)] ,$$

and (or)

$$P/\rho^\gamma = \text{constant} , \quad (5)$$

for adiabatic flows, in which γ is the specific heat ratio, $\gamma \equiv C_p/C_v$, where C_p is the specific heat at constant pressure, and C_v is the specific heat at constant volume, and where P = pressure and ρ = density.

SHOCK DENSITY.

Solving Eqs. (1), (2), and (3) for the shock density as a function of the peak pressure P_s leads to

$$\frac{\rho_s}{\rho_o} = \frac{\left(\frac{\gamma_s + 1}{\gamma_s - 1}\right)\left(\frac{P_s}{P_o}\right) + 1}{\left(\frac{\gamma_o + 1}{\gamma_o - 1}\right) + \frac{P_s}{P_o}} . \quad (6)$$

Expressed in terms of shock overpressure ($\Delta P_s \equiv P_s - P_o$), the relation becomes

$$\frac{\rho_s}{\rho_o} = \frac{\left(\frac{\gamma_s + 1}{\gamma_s - 1}\right) \frac{\Delta P_s}{P_o} + \frac{2\gamma_s}{\gamma_s - 1}}{\frac{2\gamma_o}{\gamma_o - 1} + \frac{\Delta P_s}{P_o}} . \quad (7)$$

This relation for sea-level air shocks is illustrated in Fig. 2. A fit to the shock density ratio ρ_s/ρ_0 for sea-level air shocks versus shock overpressure is also illustrated in Fig. 2. The fit is as follows:

$$\eta_s = \frac{\rho_s}{\rho_0} = \frac{86.06 + 5139\pi + 3480\pi^2}{86.06 + 926.3\pi + 243.8\pi^2 + 2.325\pi^3} + \frac{0.002985\pi^{2.473}}{1 + 3.57 \times 10^{-8}\pi^{6.221}}$$

$$+ \frac{374\zeta^2}{1 + 71.82\zeta^2} + \frac{3966\zeta^4}{1 + 1,136,830\zeta^8} + \frac{9.486\zeta^{2.567}}{1 + 5.911\zeta^{5.127}}$$

$$+ \frac{0.004599\zeta^{3.893}}{1 + 2.055 \times 10^{-5}\zeta^{6.139}}, \quad (8)$$

where $\pi \equiv \Delta P_s / 1000$,

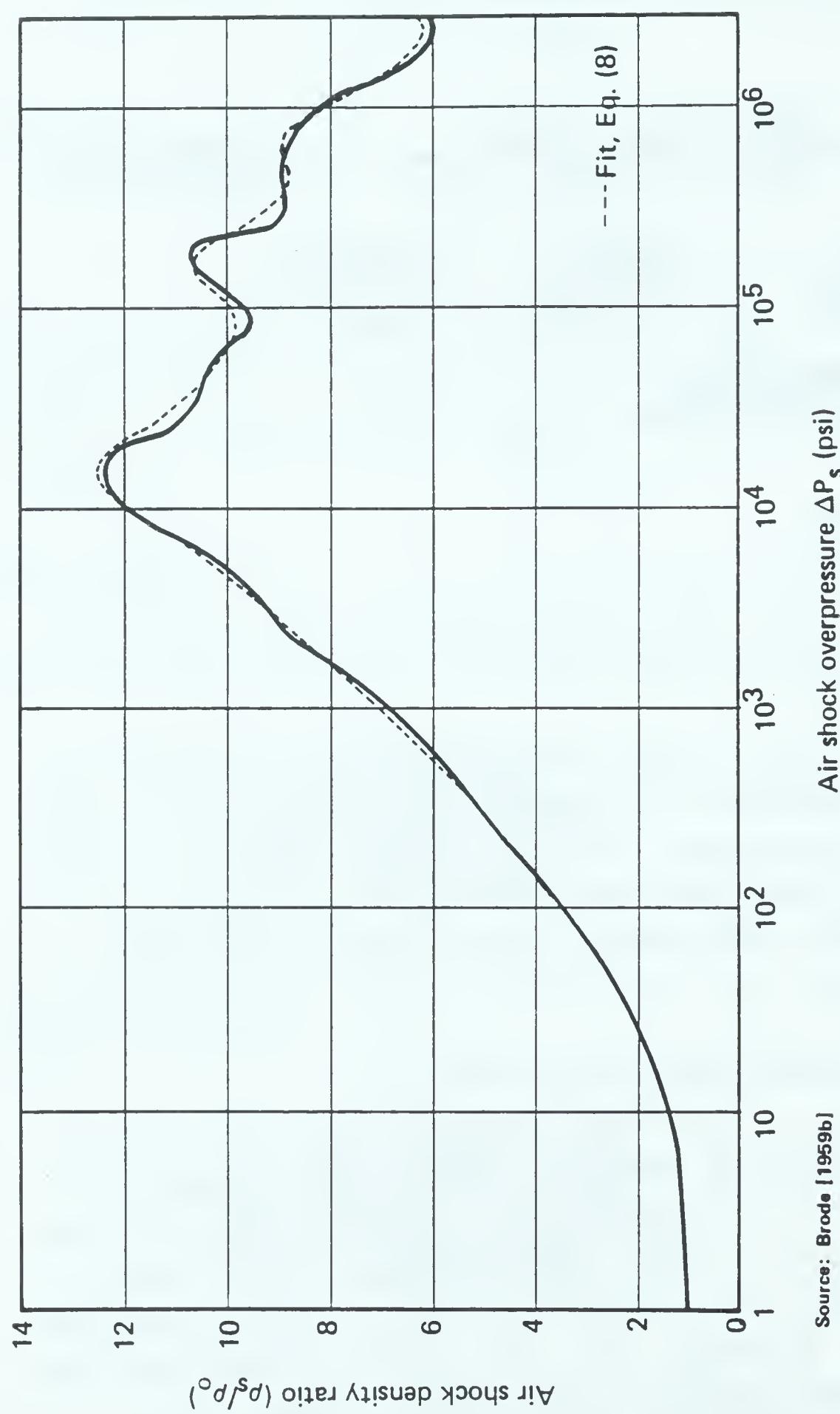
$\zeta \equiv \Delta P_s / 10^6$,

and ΔP_s is in pounds per square inch.

The fit is within 5 percent for all values of the overpressure. At very high overpressures ($>200,000$ psi) the adiabatic shock assumption is unlikely to be valid. For strong nuclear blast waves, radiative transport in the fireball can dissipate or redistribute shock energy and pressure, thus allowing further compression and higher densities.

SPECIFIC HEAT RATIO FOR SHOCKS IN SEA-LEVEL AIR.

The effective γ for air shocks (in standard sea-level air) is a slowly varying function of the shock strength. That dependence is illustrated in Fig. 3. For sea-level air, γ_s ranges between 1.17 and 1.67. It starts at $\gamma = 1.4$ for weak shocks, drops to 1.17 around 10,000 psi ($11,00^\circ\text{C}$), and eventually rises to 1.67 at very high pressures ($>10^7$ psi). According to Eqs. (6) and (7), this means that the shock density rises to nearly 13 times ambient at around 1 kb (15,000 psi), but is limited to only 4 times ambient at extremely high pressure ($>10^7$ psi).



Source: Brode [1959b]
Air shock overpressure ΔP_s (psi)

Figure 2. Shock density versus shock overpressure in standard, sea-level air ($\rho_0 \approx 1.293 \text{ kg/m}^3$).

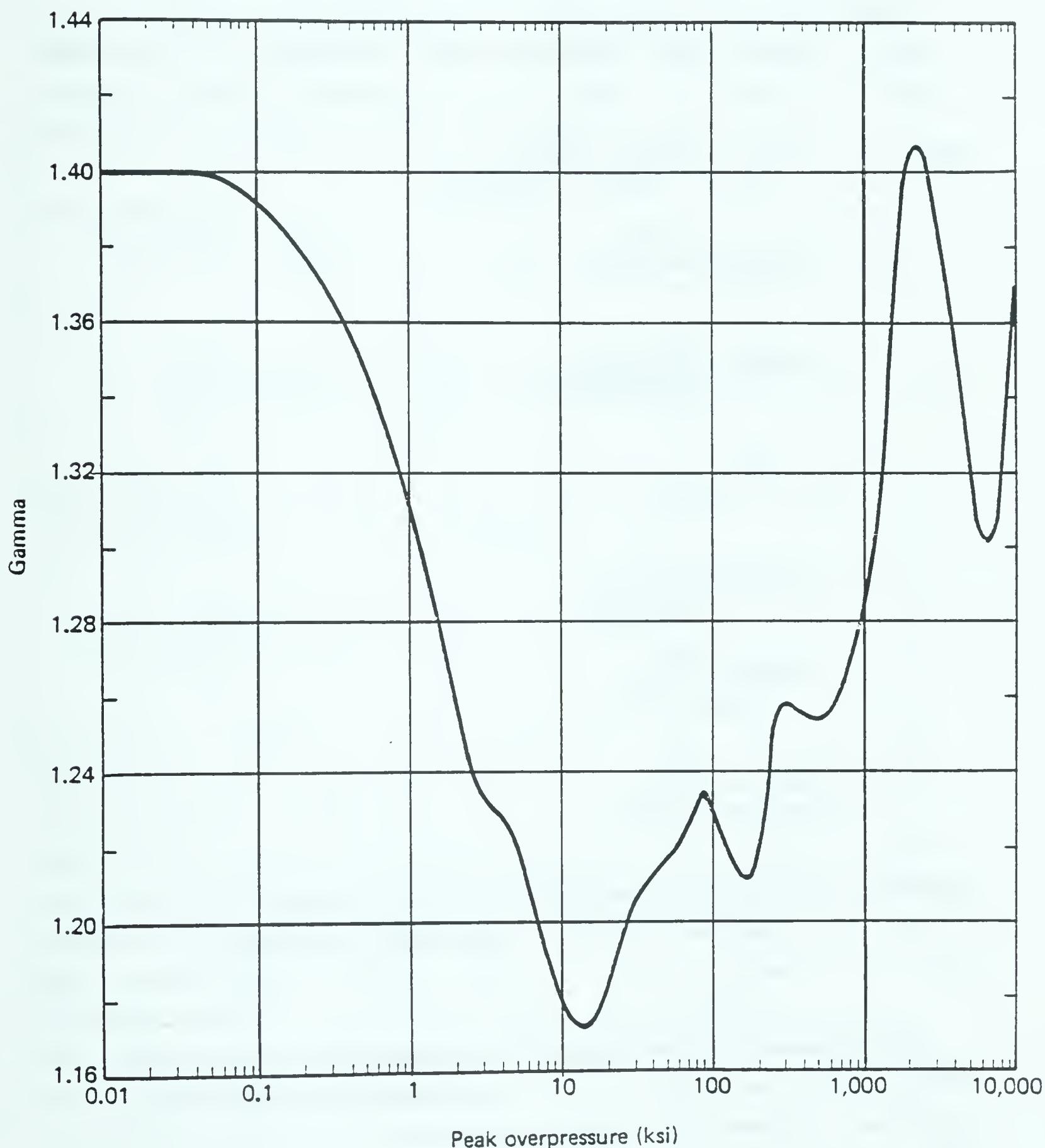


Figure 3. Specific heat ratio ($\gamma \equiv C_p/C_v$) for shocks in standard, sea-level air versus shock pressure.

An approximation to the specific heat ratio for shocks in sea-level air as a function of shock strength is as follows:

$$\gamma_s = 1 + A + B + C + D + E + F + G , \quad (9)$$

$$\text{where } A = \frac{0.4 + 2.399\pi + 116.4\pi^2}{1 + 5.812\pi + 293.2\pi^2 + 84.07\pi^3} ,$$

$$B = \frac{6.9 \times 10^{-5} \pi^{5.378}}{1 + 0.001089\pi^{5.378}} ,$$

$$C = \frac{9.565 \times 10^{-6} \pi^{3.122}}{1 + 7.288 \times 10^{-5} \pi^{3.122}} ,$$

$$D = \frac{762\zeta^4}{1 + 2.11 \times 10^8 \zeta^8} ,$$

$$E = \frac{70,246\zeta^{9.485}}{1 + 2.475 \times 10^6 \zeta^{10.09}} ,$$

$$F = \frac{0.06589\zeta^{2.536}}{1 + 0.08005\zeta^{3.742}} ,$$

$$G = \frac{3.931 \times 10^{-9} \zeta^8}{1 + 2.587 \times 10^{-8} \zeta^8} ,$$

and where $\pi \equiv \Delta P_s / 1000$, in kilopounds per square inch,

$\zeta \equiv \pi / 1000 = \Delta P_s \times 10^{-6}$, in megapounds per square inch.

This expression fits to within 3 percent of the curve in Fig. 3, which, in turn, is based on a fit to the equation of state for air--good almost everywhere to less than 5 percent error [Brode and Parkin, 1963]. (See also Sec. 5 of this report.)

As mentioned, however, at very high pressures, temperatures are also high, and radiative processes allow even higher shock

compressions. In a flow field dominated by radiation transport, shocks can reach much higher compressions because radiation can carry away the shock heating, thus lowering the shock pressure that would otherwise limit compression. For that reason, these adiabatic shock formulations may be inappropriate for nuclear blast waves much above 200,000 psi in sea-level air.

SHOCK VELOCITY.

Similarly, from Eqs. (1), (2), and (3),

$$U_s = C_o \left\{ \left[\frac{(\gamma_s + 1) \Delta P_s}{2 \gamma_o P_o} + 1 \right] \left/ \left[1 + \left(\frac{\gamma_o - \gamma_s}{\gamma_o - 1} \right) \frac{P_o}{\Delta P_s} \right] \right\}^{1/2} . \quad (10)$$

This expression is plotted in Fig. 4, using the γ_s of Eq. (9).

For an ideal gas of $\gamma = 1.4$, it reduces to

$$U_s = C_o \sqrt{\frac{\Delta P_s}{P_o}} \frac{(\gamma + 1)}{2\gamma} + 1 \approx 1.087 \sqrt{0.0583 \Delta P_s} + 1 \text{ kft/s} , \quad (11)$$

in which $C_o = \sqrt{\gamma P_o / \rho_o} \approx 1.087 \text{ kft/s}$ and P_o for sea level $\approx 14.7 \text{ psi}$. In air at sea level, this simple form [Eq. (11)] is within 5 percent correct for $\Delta P_s < 1,000,000 \text{ psi}$. As can be seen in the comparison plot of Fig. 4, the actual shock velocity is only slightly lower than the ideal gas simple form, and the dependence of shock velocity on the equation of state for air is minimal. For most purposes, this simple form is sufficiently accurate, since, in reality, the local variations in fireball growth far exceed 5 percent. Above $\approx 200,000 \text{ psi}$, the front velocity is increased by radiative effects, and, therefore, the Hugoniot expression is inadequate.

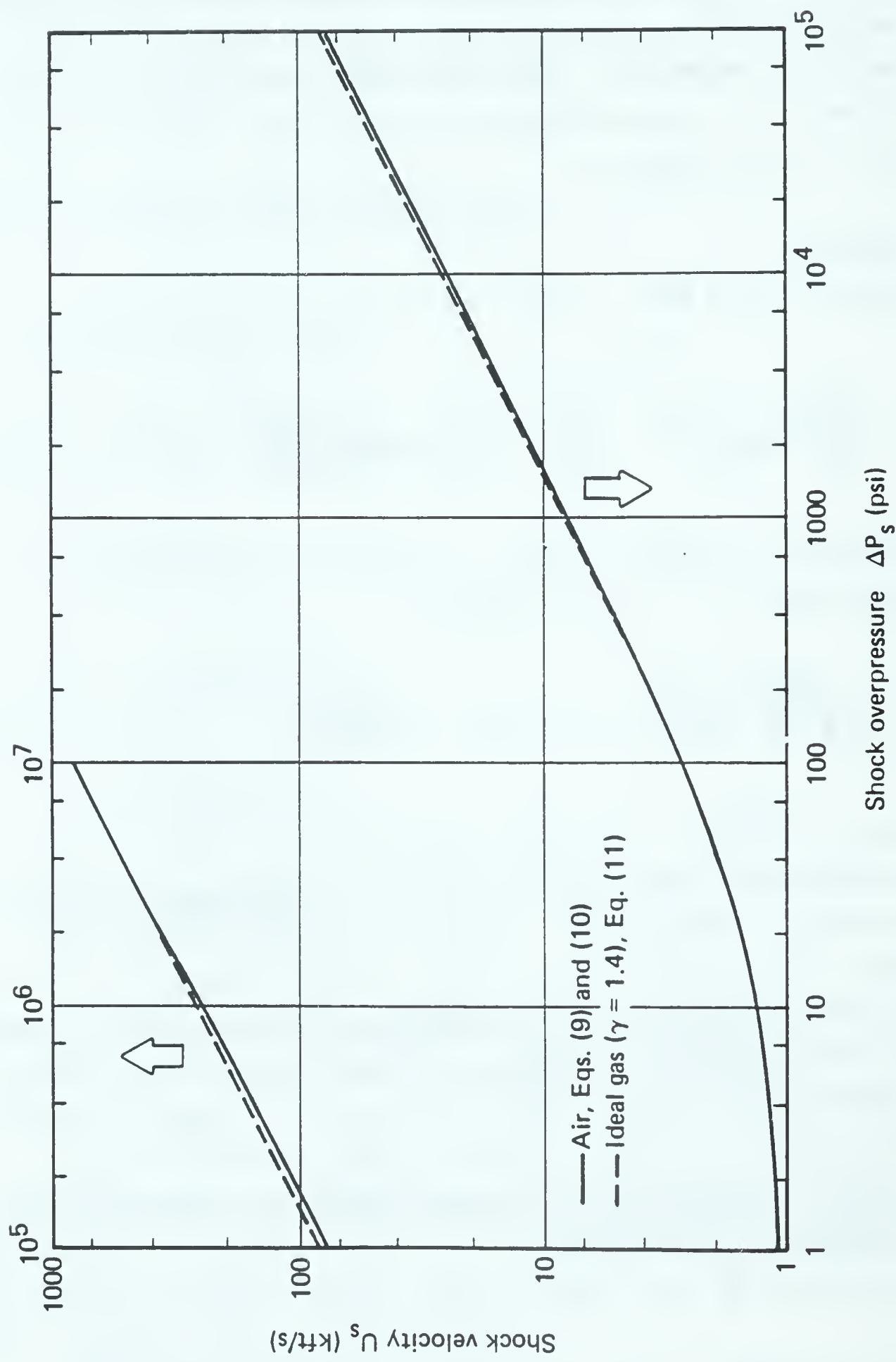


Figure 4. Shock velocity versus shock overpressure in air at sea level.

PEAK PARTICLE VELOCITY.

The air speed immediately behind an air shock can be written in terms of shock overpressure [from Eqs. (1), (2), and (3)] as

$$u_s = C_o \left\{ \frac{2\Delta P_s}{\gamma_o P_o} \frac{\left[\frac{\Delta P_s + P_o}{[(\gamma_s + 1)\Delta P_s + 2\gamma_s P_o]} \left(\frac{\gamma_o - \gamma_s}{\gamma_o - 1} \right) \right]}{[(\gamma_s + 1)\Delta P_s + 2\gamma_s P_o]} \right\}^{1/2} . \quad (12)$$

For an ideal gas of $\gamma_s = \gamma_o = 1.4$, this expression simplifies to

$$u_s = \frac{C_o \Delta P_s}{\sqrt{\gamma P_o [(\gamma + 1)\Delta P_s + 2\gamma P_o]/2}} \approx \frac{0.2188 \Delta P_s}{\sqrt{\Delta P_s + 17.15}} \text{ kft/s} . \quad (13)$$

This ideal gas form is valid for shocks in air to within 5 percent for $\Delta P_s < 1,000,000$ psi. The actual particle velocity is higher by about 4 to 5 percent between 10,000 and 50,000 psi, and by less than that elsewhere.

For strong shocks, i.e., for $\Delta P_s \gg P_o$,

$$u_s \approx C_o \sqrt{2\Delta P_s / [P_o \gamma_o (\gamma_s + 1)]} . \quad (14)$$

[Equation (9) can be used to find γ_s as a function of ΔP_s .]

The peak particle velocity as defined by Eqs. (12) and (9) is plotted in Fig. 5, and compared to the ideal gas form of Eq. (13).

PEAK DYNAMIC PRESSURE.

The blast wind pressure or dynamic pressure Q is defined as

$$Q \equiv \frac{1}{2} \rho u^2 . \quad (15)$$

At the shock front, using Eqs. (7) and (12), the peak dynamic pressure Q_s becomes

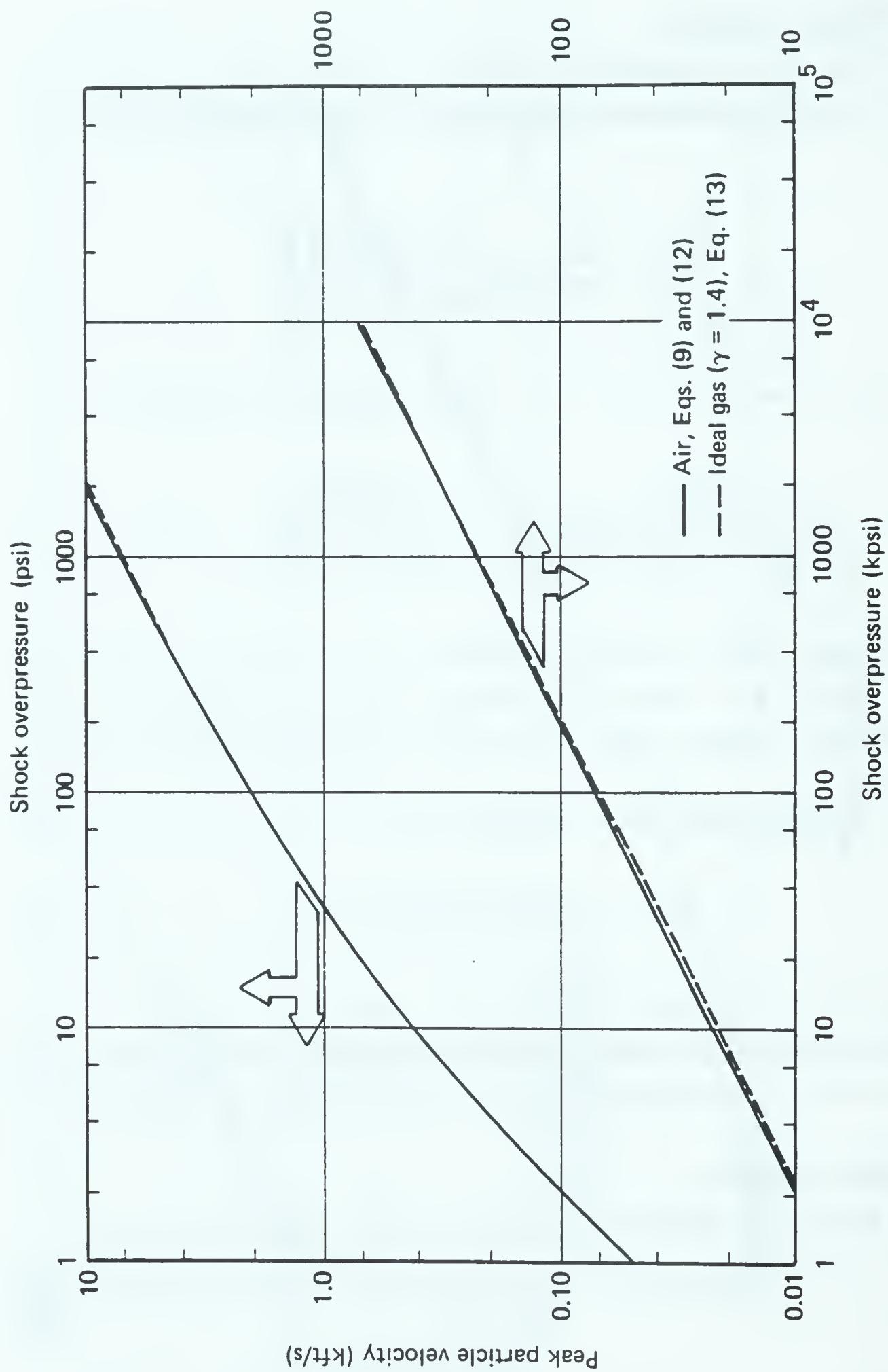


Figure 5. Peak particle velocity versus shock overpressure in air at sea level.

$$Q_s = \frac{\Delta P_s \left[\Delta P_s + P_o \left(\frac{\gamma_o - \gamma_s}{\gamma_o - 1} \right) \right] \left(\frac{\gamma_o - 1}{\gamma_s - 1} \right)}{2\gamma_o P_o + (\gamma_o - 1)\Delta P_s}. \quad (16)$$

For an ideal gas ($\gamma_s = \gamma_o = 1.4$) and standard conditions,

$$Q_s \approx \frac{\Delta P_s^2}{2\gamma P_o + (\gamma - 1)\Delta P_s} = \frac{\Delta P_s^2}{41.2 + 0.4\Delta P_s} \text{ psi.} \quad (17)$$

A better approximation for real air is

$$\begin{aligned} \frac{Q_s}{\Delta P_s} &= \frac{\pi(1 + 0.241\pi + 0.4376\pi^2)}{0.041 + 0.4\pi + 0.02891\pi^2 + 0.1015\pi^3} \\ &+ \frac{0.01251\pi^2}{1 + 9.649 \times 10^{-7}\pi^5} + \frac{7.29 \times 10^{-8}\pi^4}{1 + 2.61 \times 10^{-21}\pi^{12}} + \frac{9.763 \times 10^{-10}\pi^4}{1 + 6.957 \times 10^{-28}\pi^{12}} \\ &- \frac{5.052 \times 10^{-8}\pi^6}{1 + 1.368 \times 10^{-14}\pi^{12}} - \frac{6.021 \times 10^5\zeta^6}{1 + 3.541 \times 10^{12}\zeta^{12}} \\ &- \frac{2.17 \times 10^8\zeta^{14}}{1 + 1.62 \times 10^9\zeta^{15}} - \frac{0.7670\zeta^{2.839}}{1 + 0.1646\zeta^{3.678}}, \end{aligned} \quad (18)$$

where $\pi = \Delta P_s / 1000$ (ΔP_s in pounds per square inch),

$$\zeta = \pi / 1000.$$

The above expression is accurate to better than 3 percent for all overpressures less than 7,000,000 psi. If the last term is replaced by

$$- \frac{0.6805\zeta^3}{1 + 0.1230\zeta^4}, \quad (19)$$

the expression is accurate to better than 4 percent for overpressures less than 6,500,000 psi. The standard of comparison is Eq. (16) using Eq. (9) for γ_s . Again, above about 200,000 psi, for nuclear blast waves, the influences of radiation transport are likely to invalidate this adiabatic shock expression for peak dynamic pressure.

The ratio of peak dynamic pressure to peak overpressure is plotted in Fig. 6, and compared with the fit from Eq. (18). The figure shows that the quadratic dependence of dynamic pressure on overpressure at low overpressures gives way to something nearer linear dependence above 100 psi. Shock dynamic pressure is equal to shock overpressure at around 70 psi.

SHOCK TEMPERATURE.

The increased temperature in a shock front $\Delta\theta_s$ can be expressed, using the gas law relation $P = \rho R \theta$ and the Hugoniot equations [Eqs. (1), (2), and (3)] as:

$$\frac{\Delta\theta_s}{\theta_o} = \left(\frac{\Delta P_s}{P_o} + 1 \right) \left(\frac{R_o}{R_s} \right) \frac{\left(\frac{2\gamma_o}{\gamma_o - 1} + \frac{\Delta P_s}{P_o} \right)}{\left[\left(\frac{\gamma_s + 1}{\gamma_s - 1} \right) \frac{\Delta P_s}{P_o} + \frac{2\gamma_s}{\gamma_s - 1} \right]} - 1 , \quad (20)$$

in which R_o is the gas constant for air at standard conditions, R_s is the gas constant for shocked air, and θ_o is the ambient (preshock) temperature. For an ideal gas, $\gamma = \gamma_o = \gamma_s$, and $R_o = R_s$. The temperature ratio becomes:

$$\frac{\Delta\theta_s}{\theta_o} \approx \frac{(\gamma - 1)\Delta P_s}{\gamma P_o} \left(1 + \frac{\Delta P_s}{2P_o} \right) \left/ \left[1 + \left(\frac{\gamma + 1}{2\gamma} \right) \frac{\Delta P_s}{P_o} \right] \right. . \quad (21)$$

For standard conditions in air, $\gamma = 1.4$, $P_o = 14.7$ psi, $\theta_o \approx 273.2$ K, and

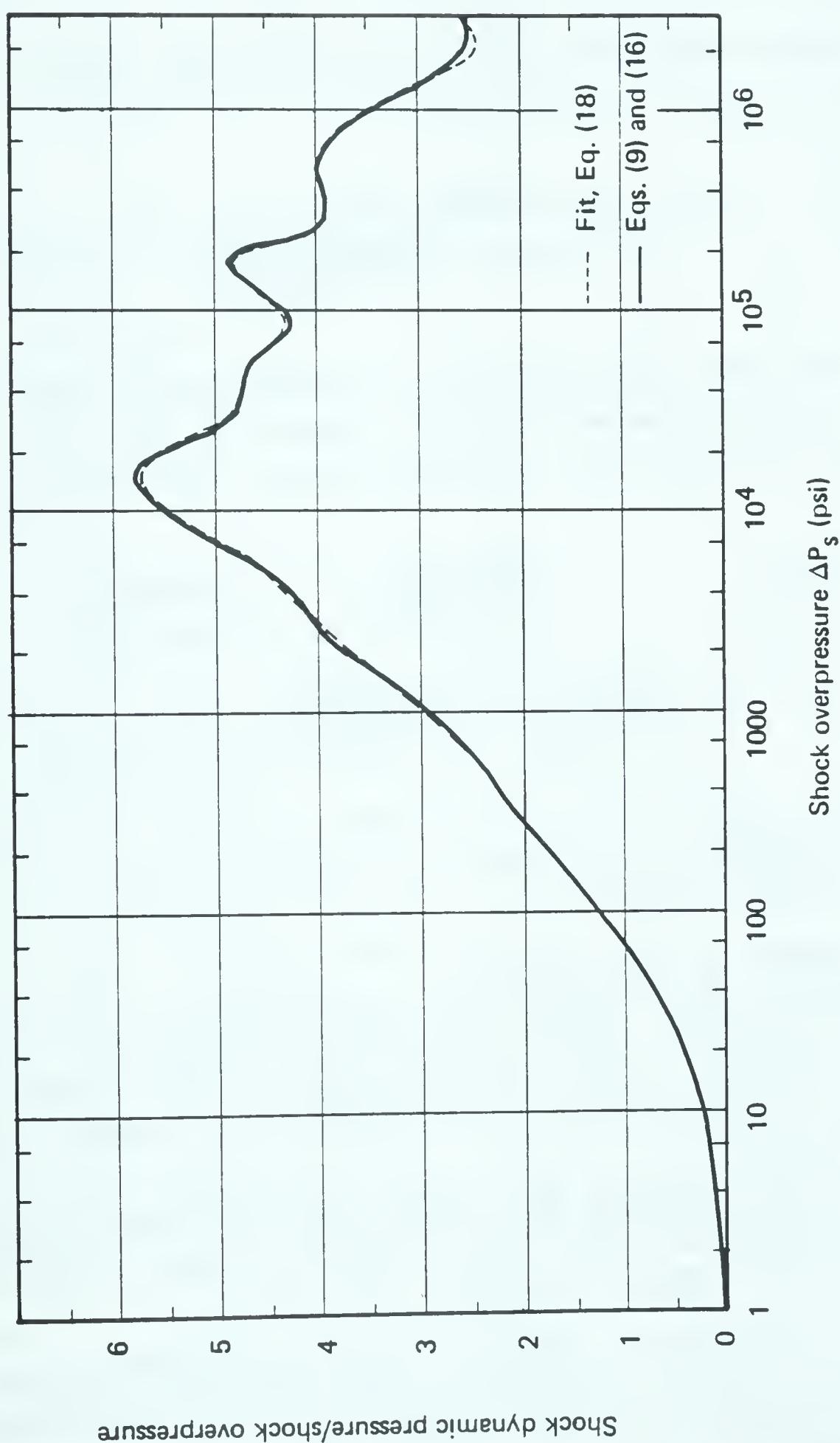


Figure 6. Shock dynamic pressure relative to shock overpressure versus shock overpressure.

$$\Delta\theta_s = \frac{5.31\Delta P_s(1 + 0.034\Delta P_s)}{(1 + 0.0583\Delta P_s)} {}^{\circ}\text{C} . \quad (22)$$

A better approximation to the shock temperature increase in air is given by:

$$\Delta\theta_s = \frac{5310\pi(1 + 34\pi)}{\left[1 + 58.3\pi + \frac{6.53\pi^{3.5}}{(1 + 0.2027\pi^2)}\right]} {}^{\circ}\text{C}. \quad (23)$$

A still better approximation to the temperature of a shock (in air at sea level, standard conditions) combines Eq. (20) with the following fit to the thermal equation of state on the Hugoniot:

$$\begin{aligned} \mathcal{R}_s/\mathcal{R}_o = v_s &= 1 + \frac{0.008168\pi^2}{(1 + 0.01807\pi^2)} + \frac{0.001924\pi^2}{(1 + 0.0005596\pi^2)} \\ &+ \frac{78.45\zeta^2}{1 + 10.12\zeta^2} + \frac{0.0009018\zeta^4}{1 + 0.0001484\zeta^4}, \end{aligned} \quad (24)$$

where $\pi \equiv \Delta P_s / 1000$,

$$\zeta \equiv \pi / 1000 = \Delta P_s \times 10^{-6}.$$

THERMAL EQUATION OF STATE FOR AIR.

Actually, the gas "constant" \mathcal{R}_s increases manyfold as the shock overpressure rises, so that at high pressures the real air shock temperature falls below the ideal gas temperature by factors ranging up to more than 16.

A relation between the gas constant \mathcal{R} and temperature and density allows the evaluation of Eq. (20) and the determination of the shock temperature as a function of the shock overpressure.

A fit to the thermal equation of state for air, based on properties of air derived by Gilmore [1955, 1959] and Hilsenrath, Green, and Beckett [1957] is as follows:

$$\frac{\mathcal{R}}{\mathcal{R}_O} = \frac{PV}{\mathcal{R}_O \theta} = v = 1 + \frac{4a\alpha^8}{1+a\alpha^8} + \frac{8.4b\alpha^3}{1+b\alpha^3} + \frac{2c\alpha^8}{1+c\alpha^8} + \frac{0.8d\beta}{1+d\beta} + \frac{0.2f\beta}{1+f\beta}, \quad (25)$$

where $\alpha = 10^{-4} \times \theta n^{-0.086}$ for θ in degrees kelvin, $n = \rho/\rho_0$,

$$\beta = \left(\frac{\alpha}{0.9746 + 0.0254n^{-0.21556}} \right)^{12},$$

$$a = 0.7778 \times 10^{-16},$$

$$b = 0.602 \times 10^{-3},$$

$$c = 0.5097 \times 10^{-3},$$

$$d = 2.20,$$

$$f = 0.971 \times 10^4,$$

with $\mathcal{R}_O = 0.04161$ for pressure in pounds per square inch, air temperature θ in degrees kelvin, density ρ in kilograms per cubic meter, and specific volume $V = 1/\rho$.

The thermal equation of state is illustrated in Fig. 7. The figure shows a plot of $PV/\mathcal{R}_O \theta$ versus temperature θ , which is the equivalent of the ratio of the gas constant to that for ambient sea-level air $\mathcal{R}/\mathcal{R}_O$. It is also a measure of the number of free particles per mole of air at a temperature θ and a density ratio n relative to the number in a mole of air at standard sea-level conditions. At a little less than 10,000 K, the oxygen and nitrogen molecules in air dissociate, and the relative number of particles rises by a factor of two. At extreme temperatures, like 1 million degrees, all the electrons are freed from the atoms, and the average number of particles (ions and electrons) rises to more than 16 per original air molecule.

Again, the changes in the gas constant ratio v are slow relative to density and pressure (or temperature) changes, so that simple iterative methods can be used to determine the proper thermodynamic state.

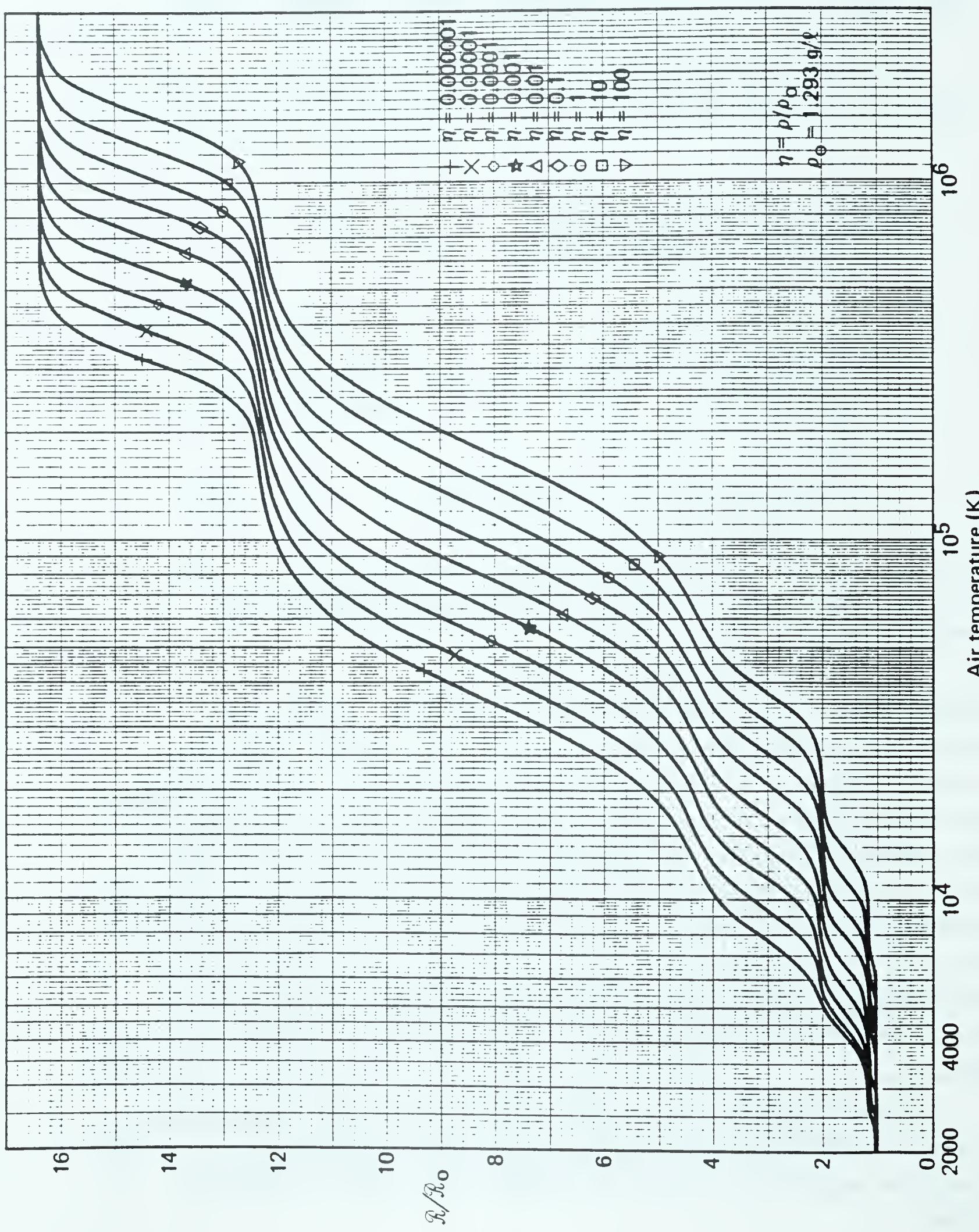


Figure 7. Thermal equation of state for air versus temperature and density.

NORMAL REFLECTION OF SHOCKS.

When a shock wave strikes a rigid plane head on (as illustrated in Fig. 8), the reflected shock conditions can be derived from conservation considerations similar to those expressed in Eqs. (1), (2), and (4), for mass, momentum, and energy across the reflected shock:

$$\rho_R U_R = (u_s + U_R) \rho_s \quad (\text{mass}), \quad (26)$$

$$P_R - P_s = (u_s + U_R)^2 \rho_s - U_R^2 \rho_R = u_s U_R \rho_R \quad (\text{momentum}), \quad (27)$$

$$\frac{P_R}{\rho_R (\gamma_R - 1)} - \frac{P_s}{\rho_s (\gamma_s - 1)} = \frac{P_R + P_s}{2} \left(\frac{1}{\rho_s} - \frac{1}{\rho_R} \right) \quad (\text{energy}), \quad (28)$$

in which subscripts R refer to conditions after reflection and subscripts s apply to shock values prior to reflection.

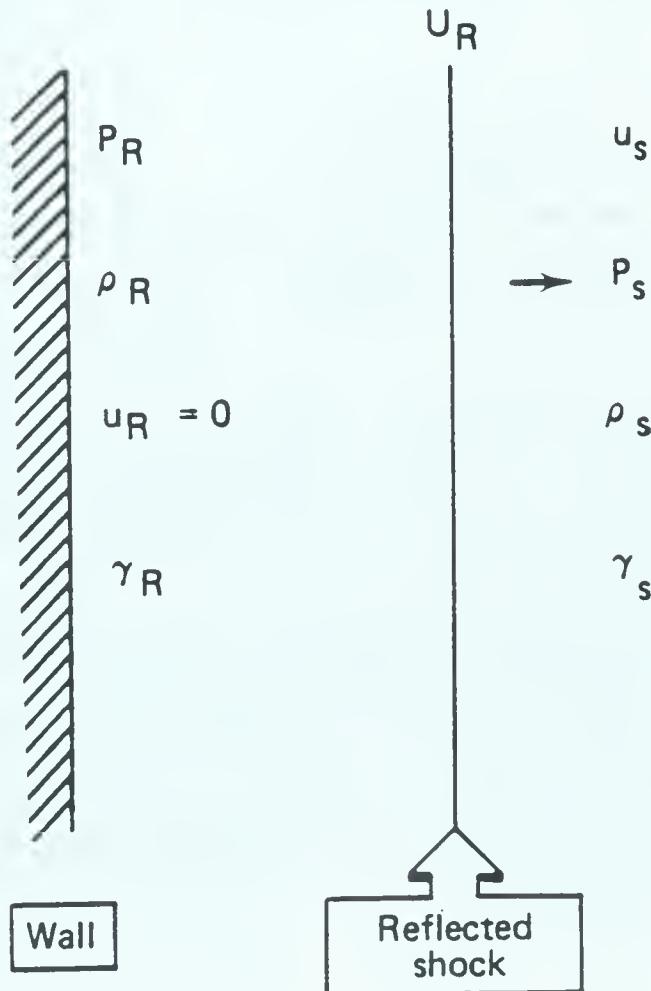


Figure 8. Reflected shock conditions.

Equations (26), (27), and (28) together with the usual Hugoniot relations [Eqs. (1), (2), and (4)], lead to a quadratic in the reflection factor $RF \equiv (\Delta P_R / \Delta P_S)$:

$$\left(\frac{\Delta P_R}{\Delta P_S} \right)^2 + \left(\frac{\Delta P_R}{\Delta P_S} \right) \left\{ \left(\frac{\gamma_s - \gamma_r}{\gamma_s - 1} \frac{P_o}{\Delta P_S} \right) - \left(\frac{\gamma_s + \gamma_r - 2}{\gamma_s - 1} \right) - (\gamma_r + 1) \times \frac{\left[\left(\frac{\gamma_o - 1}{\gamma_s - 1} \right) \Delta P_S - \left(\frac{\gamma_o - \gamma_s}{\gamma_s - 1} \right) P_o \right]}{[2\gamma_o P_o + (\gamma_o - 1)\Delta P_S]} \right\} - \left(\frac{\gamma_s - \gamma_r}{\gamma_s - 1} \right) \frac{P_o}{\Delta P_S} + \left(\frac{\gamma_r - 1}{\gamma_s - 1} \right) - \left[\left(\frac{\gamma_o - 1}{\gamma_s - 1} \right) - \frac{P_o}{\Delta P_S} \left(\frac{\gamma_o - \gamma_s}{\gamma_s - 1} \right) \right] \frac{[2\gamma_r P_o + (\gamma_r - 1)\Delta P_S]}{[2\gamma_o P_o + (\gamma_o - 1)\Delta P_S]} = 0 . \quad (29)$$

For an ideal gas (where $\gamma_r = \gamma_s = \gamma_o = \gamma$), that expression simplifies to:

$$RF \equiv \frac{\Delta P_R}{\Delta P_S} = \frac{2 + \left(\frac{3\gamma - 1}{2\gamma} \right) \left(\frac{\Delta P_S}{P_o} \right)}{1 + \left(\frac{\gamma - 1}{2\gamma} \right) \left(\frac{\Delta P_S}{P_o} \right)} = 2 + (\gamma + 1) \frac{Q_S}{\Delta P_S} , \quad (30)$$

in which ΔP_R is the reflected peak overpressure from a normally incident shock of peak overpressure ΔP_S in an ambient atmosphere of pressure P_o , and Q_S is given by Eqs. (16), (17), or (18). Equation (18), though, is an expression for $Q_S/\Delta P_S$ for a shock in real (sea-level) air, and is therefore inconsistent with the ideal gas assumption of Eq. (30).

For air at sea level, a better approximation to the reflection factor RF is given by the formula

$$RF \approx 2 + \frac{2.655\pi}{1 + 0.1728\pi + 0.001921\pi^2} + \frac{0.004218 + 48.34\pi + 6.856\pi^2}{1 + 7.997\pi + 3.844\pi^2}, \quad (31)$$

where $\pi = \Delta P_s / 1000$, (ΔP_s in pounds per square inch).

For a strong shock ($\Delta P_s \gg P_0$), the expression in Eq. (29) simplifies to

$$RF \approx 1 + \frac{2\gamma_R}{\gamma_s - 1}. \quad (32)$$

In Fig. 9, the reflection factor predicted by the approximation in Eq. (31) is compared with a more exact solution from Eq. (29) using the equation of state for air given in Sec. 5 [Eqs. (69) through (74)].

TABLE OF SHOCK VARIABLES.

The shock parameters treated in this section (and plotted in Figs. 2 through 7, and 9) are listed for a range of shock overpressures in Table 1, for standard, sea-level air. The specific heat ratio γ_s is from Eq. (9), the shock density ratio n_s from Eqs. (7) and (9), the shock velocity U_s from Eqs. (9) and (10), the peak particle velocity u_s from Eqs. (9) and (12), and the peak dynamic pressure Q_s from Eqs. (9) and (16). The ratio of the gas constants (thermal) v is given by Eq. (25); the shock temperature rise $\Delta\theta_s$ is provided by combining Eqs. (9), (20), and (25), and the normal reflection factor RF is arrived at from Eq. (29) and the equation-of-state for air, from Sec. 5, Eqs. (69) through (74).

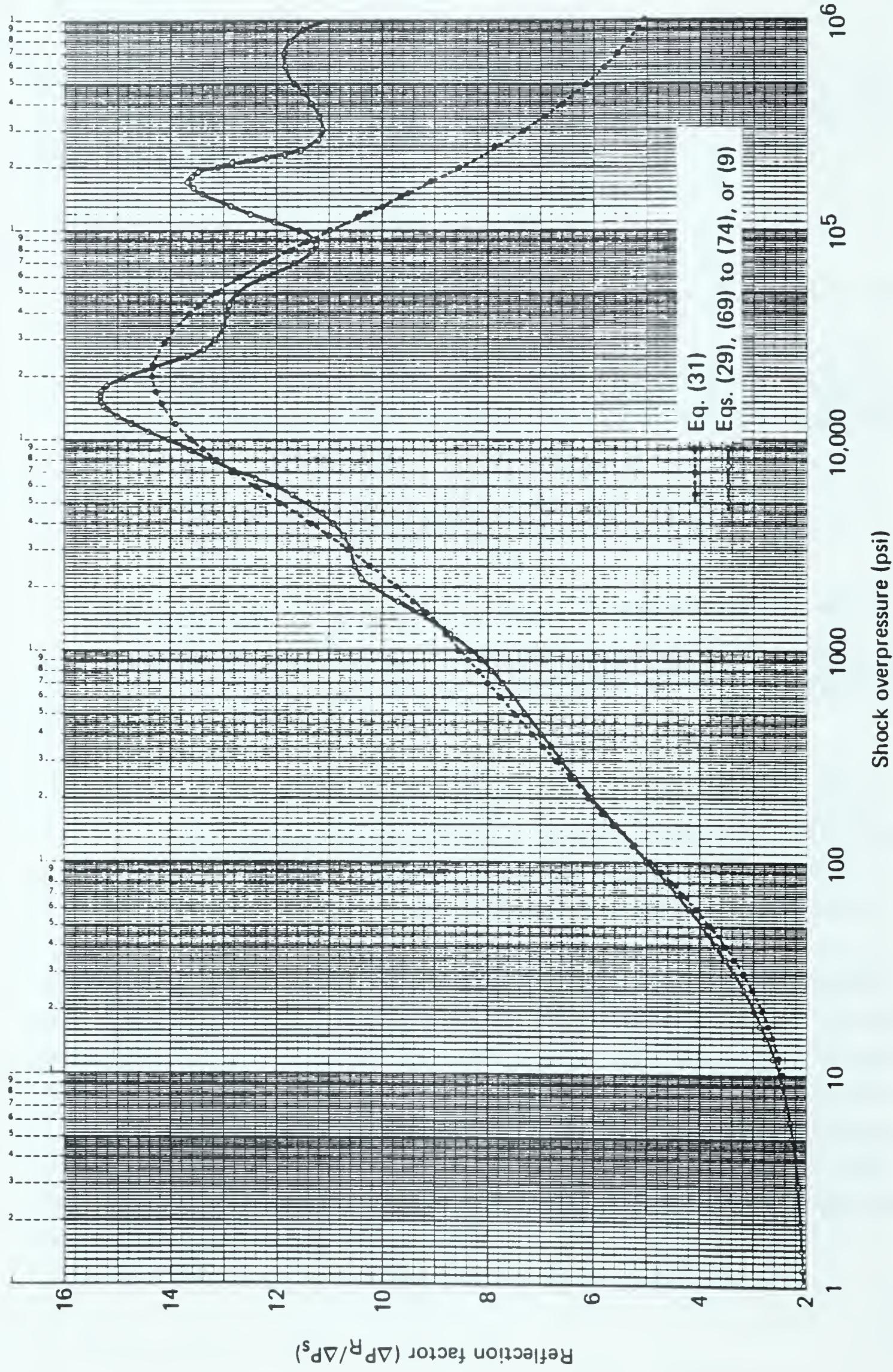


Figure 9. Normal reflection factor versus shock overpressure for sea-level air.

Table 1. Shock variables.

| ΔP_s (psi) | $\gamma_s - 1$ | η_s (ρ_s / ρ_o) | U_s (kft/s) | u_s (kft/s) | Q_s (psi) | v_s | $\Delta \theta_s$ (°C) | RF ($\Delta P_R / \Delta P_s$) |
|-----------------------|----------------|-----------------------------------|------------------|------------------|----------------|-------|---------------------------|-------------------------------------|
| .1 | .400 | 1.005 | 1.090 | .00527 | .000242 | 1.00 | 0.5 | 2.009 |
| .15 | .4 | 1.007 | 1.092 | .00789 | .000545 | 1.00 | 0.8 | 2.012 |
| .2 | .4 | 1.010 | 1.094 | .01051 | .00097 | 1.00 | 1.1 | 2.014 |
| .3 | .4 | 1.015 | 1.097 | .01571 | .00218 | 1.00 | 1.6 | 2.019 |
| .4 | .4 | 1.019 | 1.100 | .02089 | .00387 | 1.00 | 2 | 2.025 |
| .6 | .4 | 1.029 | 1.106 | .0312 | .00869 | 1.00 | 3 | 2.035 |
| .8 | .4 | 1.039 | 1.112 | .0413 | .01541 | 1.00 | 4 | 2.045 |
| 1 | .4 | 1.048 | 1.118 | .0514 | .0241 | 1.00 | 5 | 2.055 |
| 1.5 | .4 | 1.072 | 1.134 | .0760 | .0539 | 1.00 | 8 | 2.080 |
| 2 | .4 | 1.095 | 1.149 | .1000 | .0953 | 1.00 | 10 | 2.105 |
| 3 | .4 | 1.146 | 1.178 | .1462 | .2125 | 1.00 | 15 | 2.154 |
| 4 | .4 | 1.187 | 1.207 | .1903 | .3742 | 1.00 | 20 | 2.202 |
| 6 | .4 | 1.275 | 1.263 | .2728 | .8264 | 1.00 | 28 | 2.297 |
| 7 | .4 | 1.318 | 1.290 | .3116 | 1.1146 | 1.00 | 33 | 2.343 |
| 10 | .4 | 1.443 | 1.368 | .4200 | 2.214 | 1.00 | 45 | 2.478 |
| 15 | .4 | 1.636 | 1.489 | .5788 | 4.771 | 1.00 | 64 | 2.692 |
| 20 | .4 | 1.814 | 1.600 | .7179 | 8.137 | 1.00 | 82 | 2.891 |
| 30 | .4 | 2.129 | 1.803 | .9559 | 16.93 | 1.00 | 117 | 3.254 |
| 40 | .4 | 2.400 | 1.985 | 1.158 | 27.99 | 1.00 | 150 | 3.575 |
| 50 | .399 | 2.640 | 2.150 | 1.336 | 41.01 | 1.00 | 182 | 3.862 |
| 70 | .397 | 3.043 | 2.448 | 1.643 | 71.50 | 1.00 | 244 | 4.351 |
| 100 | .392 | 3.522 | 2.833 | 2.028 | 126.1 | 1.00 | 332 | 4.930 |
| 150 | .385 | 4.092 | 3.378 | 2.551 | 231.9 | 1.00 | 475 | 5.629 |
| 200 | .378 | 4.508 | 3.844 | 2.990 | 350.8 | 1.00 | 612 | 6.126 |
| 300 | .368 | 5.063 | 4.637 | 3.718 | 609.4 | 1.00 | 882 | 6.795 |
| 450 | .355 | 5.602 | 5.612 | 4.608 | 1035.5 | 1.00 | 1268 | 7.413 |
| 700 | .336 | 6.207 | 6.927 | 5.807 | 1822 | 1.00 | 1866 | 8.043 |
| 1000 | .312 | 6.831 | 8.207 | 7.002 | 2916 | 1.00 | 2486 | 8.559 |
| 1500 | .279 | 7.728 | 9.953 | 8.660 | 5046 | 1.00 | 3359 | 9.215 |
| 2000 | .252 | 8.569 | 11.409 | 10.074 | 7569 | 1.01 | 4045 | 9.758 |
| 3000 | .237 | 9.175 | 13.91 | 12.39 | 12263 | 1.10 | 5273 | 10.656 |
| 4000 | .228 | 9.565 | 16.02 | 14.34 | 17130 | 1.18 | 6313 | 11.375 |
| 6000 | .207 | 10.51 | 19.52 | 17.66 | 28530 | 1.24 | 8288 | 12.430 |
| 8000 | .191 | 11.35 | 22.45 | 20.47 | 41390 | 1.34 | 9530 | 13.132 |
| 10000 | .180 | 11.99 | 25.04 | 22.94 | 54940 | 1.46 | 10340 | 13.604 |
| 15000 | .172 | 12.56 | 30.60 | 28.16 | 86660 | 1.81 | 12030 | 14.20 |
| 20000 | .179 | 12.12 | 35.39 | 32.46 | 111200 | 2.08 | 14450 | 14.35 |
| 30000 | .207 | 10.65 | 43.61 | 39.51 | 144700 | 2.62 | 19750 | 14.13 |
| 40000 | .210 | 10.50 | 50.39 | 45.59 | 190000 | 3.12 | 22400 | 13.66 |
| 60000 | .218 | 10.16 | 61.83 | 55.74 | 274800 | 4.04 | 26900 | 12.64 |
| 80000 | .234 | 9.537 | 71.65 | 64.13 | 341500 | 4.76 | 32500 | 11.72 |
| 100,000 | .232 | 9.612 | 80.07 | 71.74 | 430600 | 5.19 | 37000 | 10.95 |
| 150,000 | .209 | 10.56 | 97.55 | 88.32 | 717200 | 5.90 | 44500 | 9.520 |
| 200,000 | .212 | 10.43 | 112.7 | 101.9 | 942900 | 6.74 | 52600 | 8.552 |
| 300,000 | .255 | 8.841 | 139.4 | 123.6 | 1176000 | 8.73 | 72000 | 7.341 |
| 400,000 | .2545 | 8.857 | 160.9 | 142.8 | 1571000 | 9.75 | 85800 | 6.619 |
| 600,000 | .254 | 8.873 | 197.1 | 174.9 | 2362000 | 11.0 | 113700 | 5.800 |
| 800,000 | .264 | 8.575 | 228.1 | 201.5 | 3030000 | 11.7 | 148000 | 5.346 |
| 1000,000 | .285 | 8.017 | 256.2 | 224.2 | 3508000 | 12.1 | 192000 | 5.060 |
| 1500,000 | .353 | 6.665 | 318.4 | 270.0 | 4249000 | 12.3 | 339000 | 4.659 |
| 2000,000 | .400 | 6.000 | 371.3 | 309.4 | 5000000 | 12.4 | 500000 | 4.449 |
| 3000,000 | .391 | 6.115 | 453.9 | 379.6 | 7672000 | 12.5 | 731000 | 4.234 |
| 4000,000 | .352 | 6.682 | 519.8 | 441.9 | 11363000 | 12.7 | 877000 | 4.124 |
| 6000,000 | .304 | 7.579 | 630.1 | 546.5 | 19740000 | 13.5 | 1089000 | 4.012 |
| 8000,000 | .316 | 7.329 | 729.4 | 629.9 | 25320000 | 15.1 | 1340000 | 3.956 |
| 10000,000 | .363 | 6.510 | 828.8 | 697.2 | 27550000 | 16.2 | 1760000 | 3.921 |

SECTION 3
FREE-AIR AND SURFACE NUCLEAR BURSTS

PEAK OVERPRESSURE VERSUS RANGE (FREE-AIR BURST).

An expression that is appropriate for overpressures in the range $0.07 < \Delta P_s < 400,000$ psi is

$$\Delta P_s \approx \frac{2}{r} + \frac{3}{r^{1.5}} + \frac{1.6}{r^3} \left[1 + \frac{105(10r)^4}{1 + 12,920(10r)^8} \right] \text{ psi,} \quad (33)$$

where r is scaled range in kilofeet per cube-root kiloton. In general, the agreement with a detailed one-dimensional calculation [Brode, 1959b] is within 5 percent. Extension to pressures below 2 psi is in agreement with the "Combined Airborne Polynomial" to within 5 percent, as well. The term in brackets is unnecessary for overpressures below 200 psi (viz., $r > 0.22 \text{ kft}/\text{KT}^{1/3}$). This fit is only 10 percent high at 600,000 psi. At the lower extreme, it is 20 percent high at 0.01 psi in comparison with the suggested curve, which is an extension of the Airborne curve and other (theoretical) extrapolations. The fit is in agreement with the 1-KT standard [Needham and Crepeau, 1981] to within 10 percent (beyond 20-m scaled range). The fit is plotted in Fig. 10.

The accuracy of the fit should not mislead the user into believing that such overpressures are repeatable or reproducible with comparable accuracy. A review of the original atmospheric nuclear test measurements suggests a much larger data scatter even for the controlled test-site conditions and surfaces. The scatter in test data far exceeds the few percent difference between "best-guess" curves and fits. Figure 11 is a graph of approximate data scatter, as derived from Brode [1981], plotted against peak overpressure. At the higher overpressure, the plot suggests a minimum uncertainty of 70 percent (from minimum to maximum datum), which translates into a pressure variation of a factor of 5. The uppermost curve in Fig. 11 roughly corresponds to a 2Σ limit; i.e., bounding about 95 percent of the

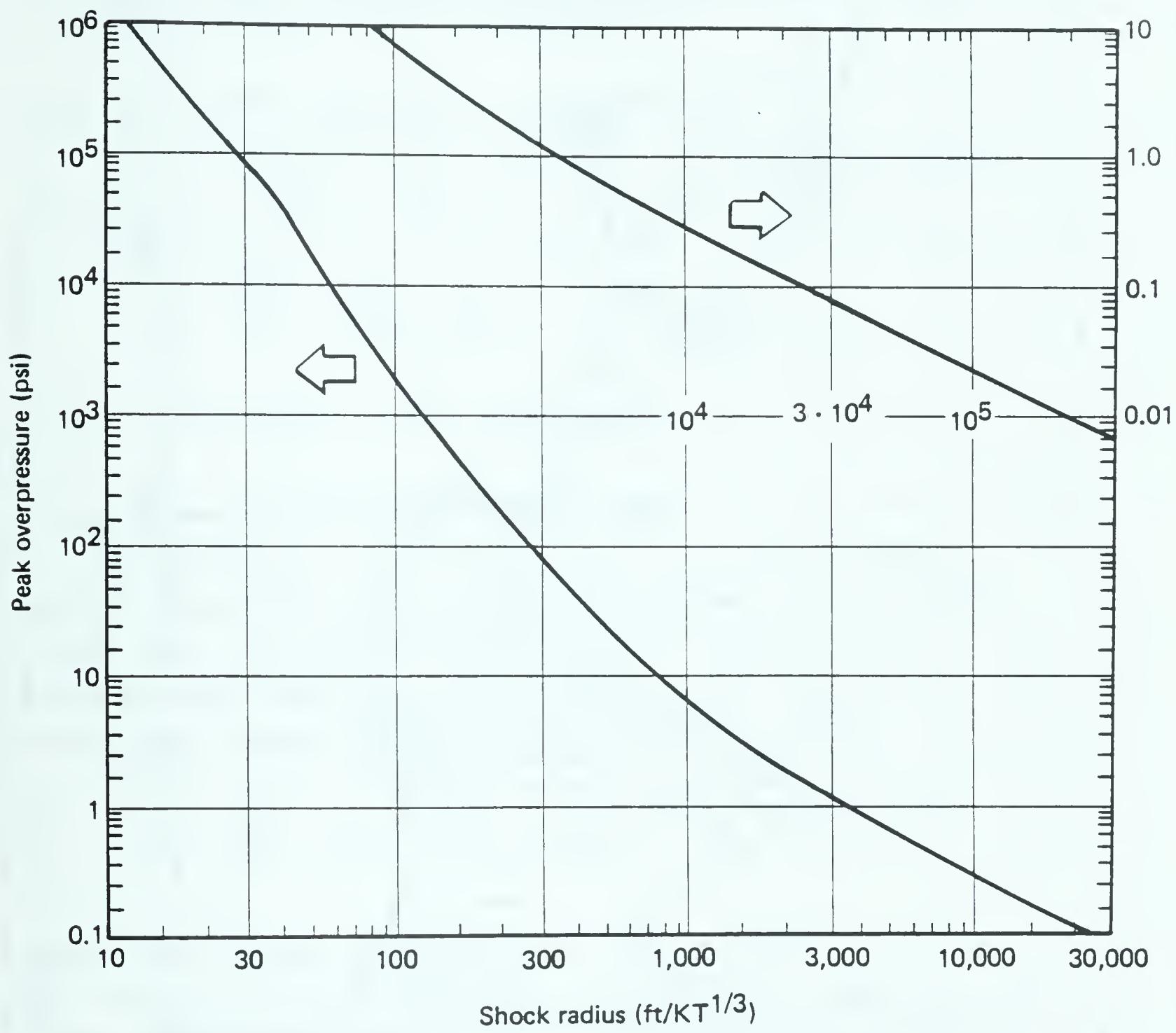


Figure 10. Peak overpressure versus shock radius for 1-KT free-air nuclear burst in standard, sea-level air.

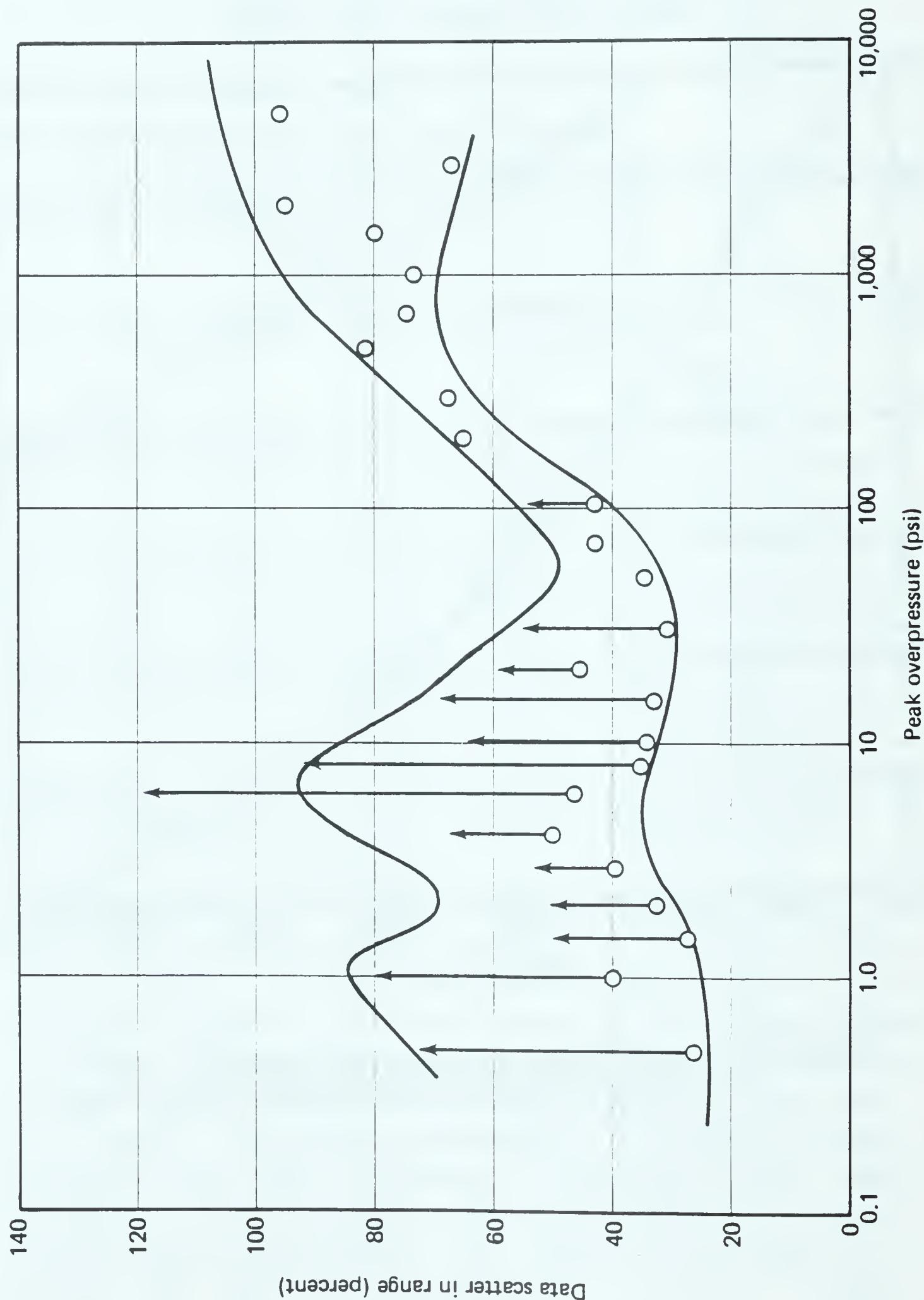


Figure 11. Scatter in percent of range to given peak overpressure for near-surface atmospheric nuclear tests.

data. The lower curve approximates a 1Σ value. The circles are estimates of the 1Σ value from the plots in Brode [1981], while the arrows represent a value of approximately 2Σ .

PEAK OVERPRESSURE VERSUS RANGE (IDEAL-SURFACE BURST).

The free-air curve can be recast for a rigid reflecting surface by using $2W$ in place of yield W in the scaled ground range x :

$$\Delta P_s = \frac{2.52}{x} + \frac{4.24}{x^{1.5}} + \frac{3.2}{x^3} \left[1 + \frac{41.7(10x)^4}{1 + 2035(10x)^8} \right] \text{ psi,} \quad (34)$$

where x is in kilofeet per cube-root kiloton.

TEST-SURFACE PEAK OVERPRESSURE VERSUS RANGE.

Overpressures from near-surface bursts in early atmospheric nuclear tests showed peaks generally below those of ideal surface bursts that can be approximated by scaling $1.8W$ rather than $2W$. The observed lower peaks were below 1000 psi and mostly above 8 psi. In that range, the approximation (using $1.8W$ scaling) becomes

$$\Delta P_s = \frac{2.4}{x} + \frac{4}{x^{1.5}} + \frac{2.9}{x^3} \text{ psi, for } 6 < \Delta P_s < 1000 \text{ psi.} \quad (35)$$

SHOCK RADIUS VERSUS PEAK OVERPRESSURE (FREE-AIR BURST).

The following fit can be used to search for the range to a given shock overpressure. Employing this fit saves one from the tedium of inverting the approximation of Eq. (33) for overpressure as a function of range. The fit is accurate to within 2 percent of Eq. (33):

$$sr = m \left[\frac{2.463}{\Delta P_s^{0.9846}} + \frac{1.176}{\Delta P_s^{1/3}} \left(1 + \frac{0.0004726\pi^{1.5}}{1 + 2.952 \times 10^{-6}\pi^3} \right) \right] \text{ kft.} \quad (36)$$

This approximation is for a free-air burst in which sr is the range in kilofeet; m , the scaling factor, is the cube-root yield in cube-root

kilotons; ΔP_s is in pounds per square inch; and $\pi = \Delta P_s / 1000$. (Note that sr is equal to $m \times r$.) The comparable range for an ideal-surface burst ($2W$) is $2^{1/3}$ (~1.26 times larger). For bursts over the (empirical) test-site surface ($1.8W$), the range is ~1.22 times larger than that for a free-air burst.

PEAK OVERPRESSURE VERSUS TIME OF ARRIVAL (FREE-AIR BURST).

The peak overpressure can also be expressed as a function of the scaled time of arrival:

$$\Delta P_s \simeq \frac{7000 + 5.18\tau^{0.75}}{0.007643 + \tau^{1.1334}} + \frac{7.11 \times 10^8 \tau^{2.973}}{1 + 430,800\tau^{4.656} + 3,052,000\tau^{6.535}} \text{ psi,} \quad (37)$$

where $\tau = T/m$,

$m = W^{1/3}$ (in cube-root kilotons),

$T = \text{time of arrival (in milliseconds)}$.

This fit to the time of arrival and peak overpressure is based on early detailed calculations [Brode, 1959b, 1966] scaled to 1 KT for pressures between $2 \leq \Delta P_s \leq 500,000$ psi. The fit is good to better than 4 percent below 50,000 psi, and to better than 3 percent below 10,000 psi.

PEAK OVERPRESSURE VERSUS TIME OF ARRIVAL (SURFACE BURST).

Using the $2W$ assumption for surface bursts, the fit from Eq. (37) becomes

$$\Delta P_s \simeq \frac{916,000 + 570\tau^{0.75}}{1 + 100.7\tau^{1.1334}} + \frac{3.58 \times 10^8 \tau^{2.973}}{1 + 146,900\tau^{4.656} + 674,300\tau^{6.535}} \text{ psi.} \quad (38)$$

TIME OF ARRIVAL VERSUS PEAK OVERPRESSURE.

Conversely, the time of arrival T can be expressed as a function of the peak overpressure (for a free-air burst) as:

$$T \simeq m \left(0.03394 + \frac{893}{\Delta P_s / 0.80424} + \frac{2015}{\Delta P_s} \right) \text{ ms}, \quad (39)$$

where $m \equiv W^{1/3}$ (in cube-root kilotons),

$W \equiv$ yield (in kilotons),

$\Delta P_s \equiv$ pounds per square inch.

For a surface burst, one uses $2W$. The above form is accurate to ± 2 percent for $2 \leq \Delta P_s \leq 100,000$ psi. This relation for a 1-KT, free-air burst is illustrated in Fig. 12.

As is evident in Fig. 12, the time of arrival is nearly inversely proportional to the overpressure. Actually, the product of time of arrival and peak overpressure to the fractional power 0.875 is a slowly varying function, and can generate a more readable curve. That relation is plotted in Fig. 13. The approximate proportionality means that the product of overpressure times arrival time to the 1.14 power is roughly constant ($\Delta P_s \times T^{1.14} \simeq \text{constant}$).

TIME OF ARRIVAL VERSUS SHOCK RADIUS.

The time of arrival T can also be represented in terms of the shock radius sr from a free-air burst [Brode, 1970].

$$T = \frac{0.54291m^3 - 21.185(sr)m^2 + 361.8(sr)^2m + 2383(sr)^3}{m^2 + 2.048(sr)m + 2.6872(sr)^2} \text{ ms}, \quad (40)$$

with sr in kilofeet, $m \equiv W^{1/3}$ (in cube-root kilotons), and $W \equiv$ yield (in kilotons).

This shock arrival-time form is limited to the range of the "Empirical 59" data [Moulton, 1960], namely, 620 μs to 26 s at 1 KT,

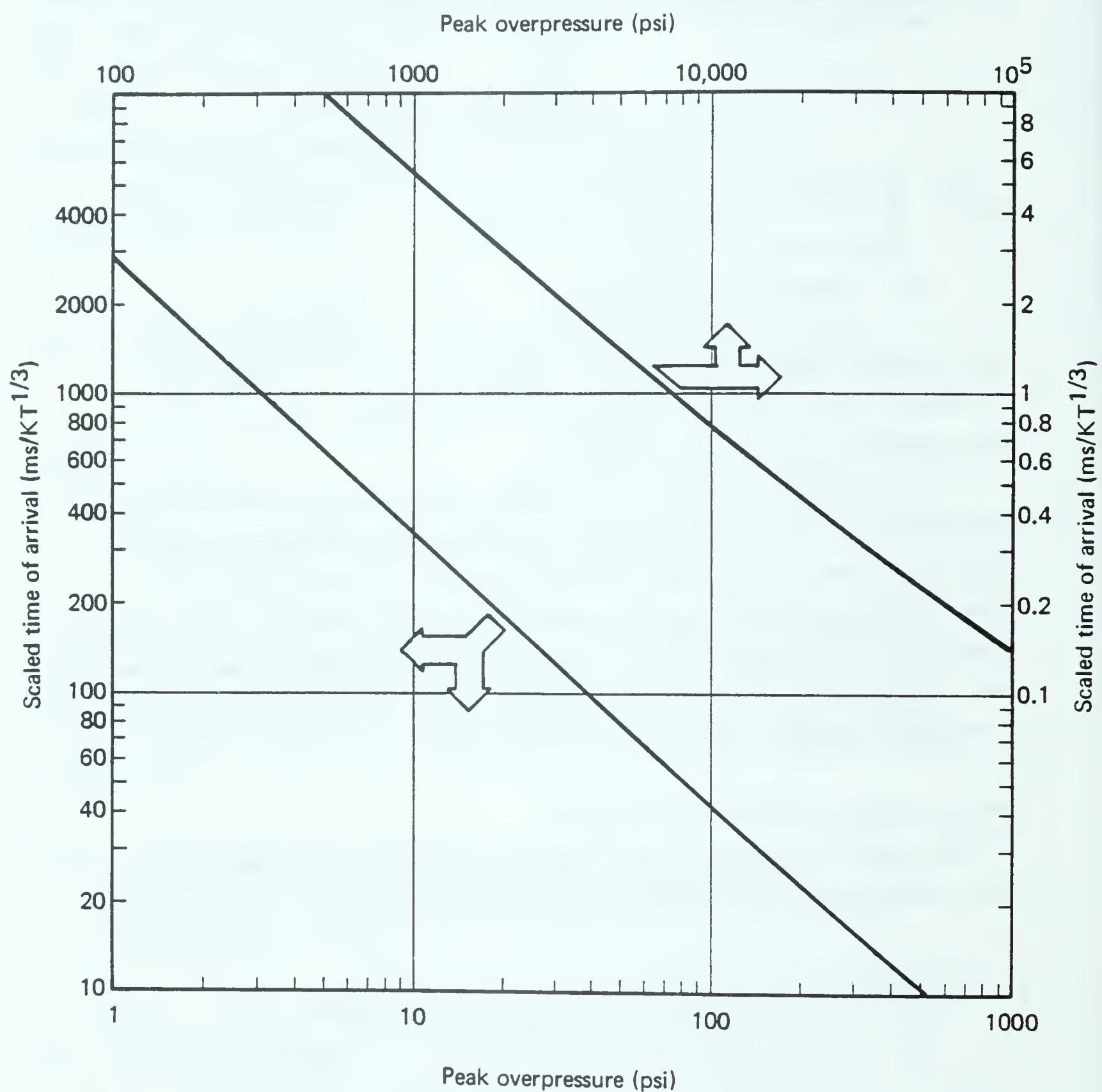


Figure 12. Time of arrival versus peak overpressure for 1-KT free-air burst at sea level.

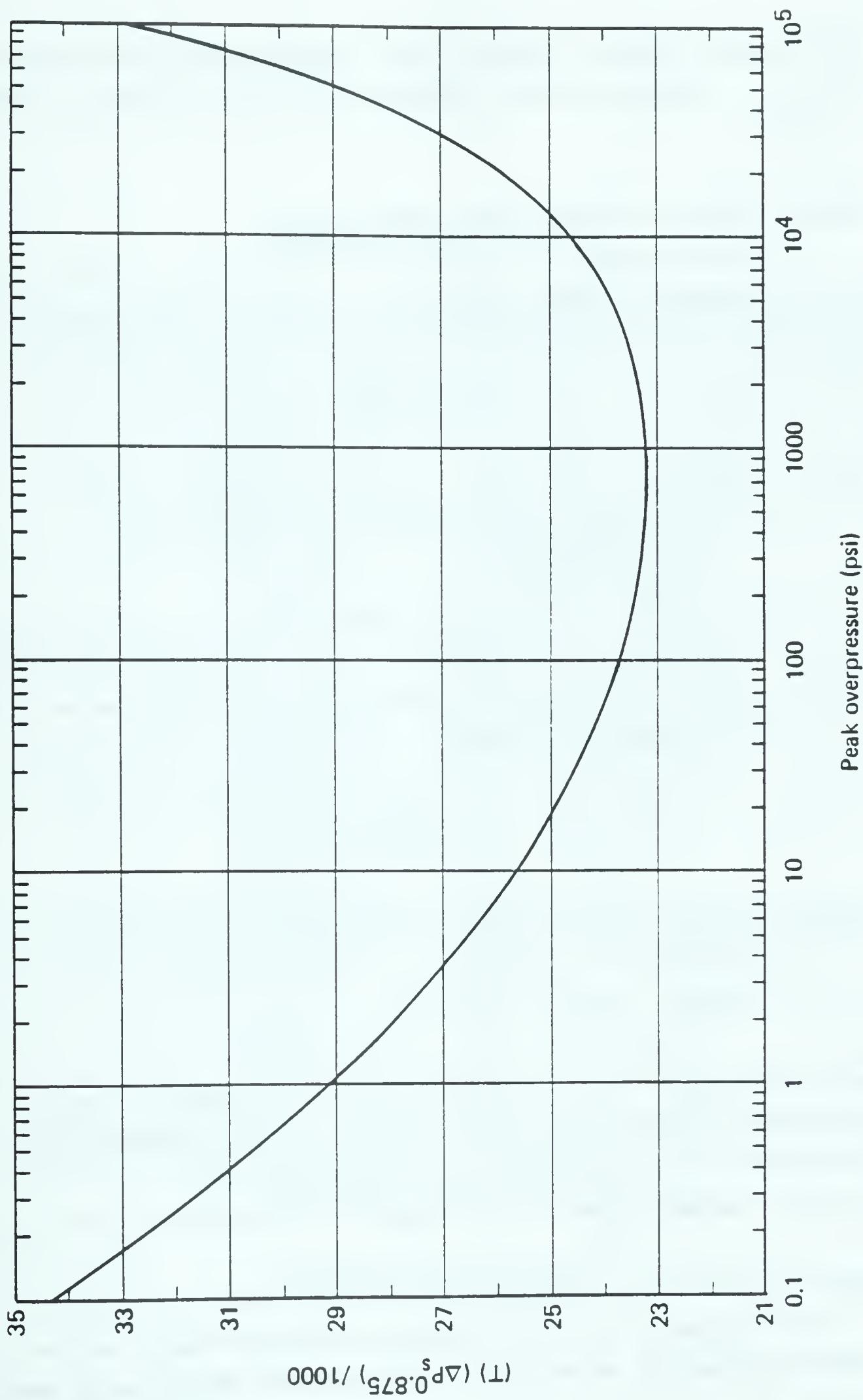


Figure 13. Product of time of arrival and peak overpressure^{0.875} versus peak overpressure for 1 KT (T in milliseconds).

which spans a range of free-air peak overpressures from 17,200 to 0.07 psi. (Use $2W$ in m for a surface burst; i.e., replace m with $m \times 2^{1/3}$.)

CLOSE-IN TIME OF ARRIVAL VERSUS SHOCK RADIUS.

For higher pressure (or earlier time of arrival T), the following fit is appropriate [Brode, 1970]:

$$T = \frac{a}{b + c} \quad \text{ms}, \quad (41)$$

$$\begin{aligned} \text{where } a &= [0.543m^3 - 21.8(sr)m^2 + 386(sr)^2m + 2383(sr)^3]sr^8, \\ b &= [2.99 \times 10^{-8}m^6 - 1.91 \times 10^{-4}(sr)^2m^4 + 1.032(sr)^4m^2 \\ &\quad - 4.43(sr)^6]m^410^{-6}, \\ c &= [1.028m^2 + 2.087(sr)m + 2.69(sr)^2]sr^8. \end{aligned}$$

Equation (41) is alternatively written in terms of the scaled range r in kilofeet per cube-root kiloton:

$$T = \frac{ma}{b + c}, \quad (42)$$

$$\begin{aligned} \text{where } a &= (0.543 - 21.8r + 386r^2 + 2383r^3)r^8, \\ b &= (2.99 \times 10^{-8} - 1.91 \times 10^{-4}r^2 + 1.032r^4 - 4.43r^6)10^{-6}, \\ c &= (1.028 + 2.087r + 2.69r^2)r^8, \end{aligned}$$

and is valid for $10^{-3} < T < 26,000$ ms at 1 KT. This more complex fit is advisable for pressures above 10,000 psi, or scaled times less than 0.6 ms/KT^{1/3}. This relation is plotted in Fig. 14.

For a surface burst, use $m = (2W)^{1/3}$.

POSITIVE OVERPRESSURE DURATION VERSUS TIME OF ARRIVAL (FREE-AIR BURST).

The duration of the positive phase for overpressure can be expressed variously as a function of overpressure, shock range, or time of arrival in a fit to detailed one-dimensional blast calculations [Brode, 1959b]:

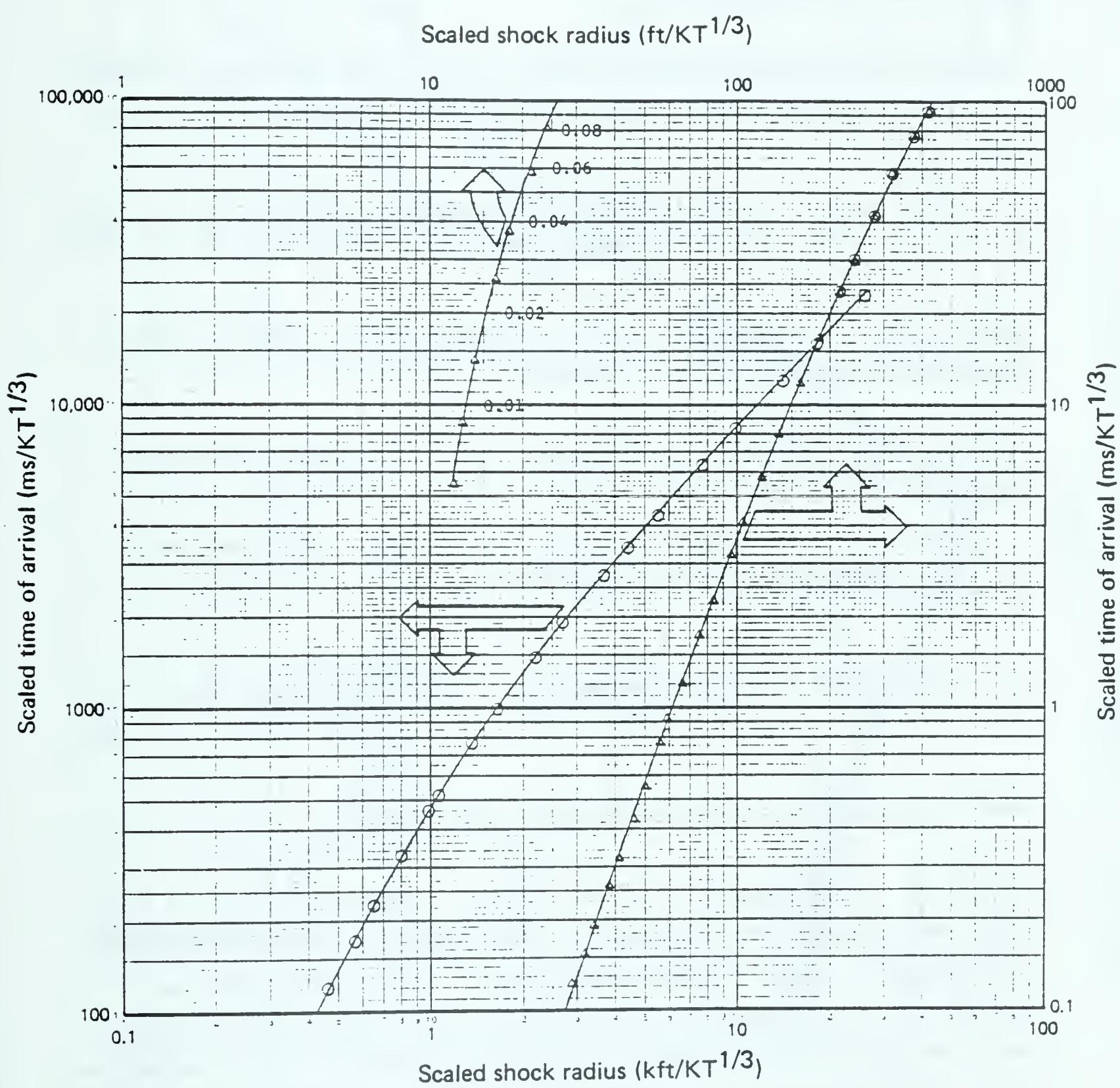


Figure 14. Time of arrival versus shock radius for 1-KT free-air burst.

$$D_p^+ \approx (m) \frac{(813,140m^2 + 11,412mT + 313T^2)}{(6,780m^2 + 444.7mT + T^2)} \text{ ms,} \quad (43)$$

where T is in milliseconds.

POSITIVE OVERPRESSURE DURATION VERSUS TIME OF ARRIVAL (SURFACE BURST).

For a surface burst, the form in Eq. (43) becomes

$$D_p^+ \approx (m) \frac{(1,626,300m^2 + 18,115mT^2 + 394T^2)}{(10,790m^2 + 560.3mT + T^2)} \text{ ms,} \quad (44)$$

where T is in milliseconds. It is assumed that the effect of the surface is to double the blast yield.

POSITIVE OVERPRESSURE DURATION VERSUS PEAK OVERPRESSURE (FREE-AIR BURST).

Expressed as a function of peak overpressure, the duration of positive overpressure can be approximated by

$$D_p^+ \approx (m) \left[-148.6 + \frac{497.3}{(1 + 18.68\pi^{0.6783})} + \frac{1629\pi^{0.8711}}{(1 + 6.477\pi^{0.8555})} \right] \text{ ms,} \quad (45)$$

where $\pi = \Delta P_s / 1000$, in kilopounds per square inch.

This form, in combination with Eq. (33), is compared in Fig. 15 with both the calculation to which it is a fit [Brode, 1959b] and the DNA 1-KT standard values [Needham and Crepeau, 1981]. The difference between those two predictions is typical of the uncertainty and expected variation (particularly at large distances) in blast parameters such as positive phase durations. For a surface burst, this form should be multiplied by $2^{1/3} \approx 1.26$ (i.e., use $2W$ in m).

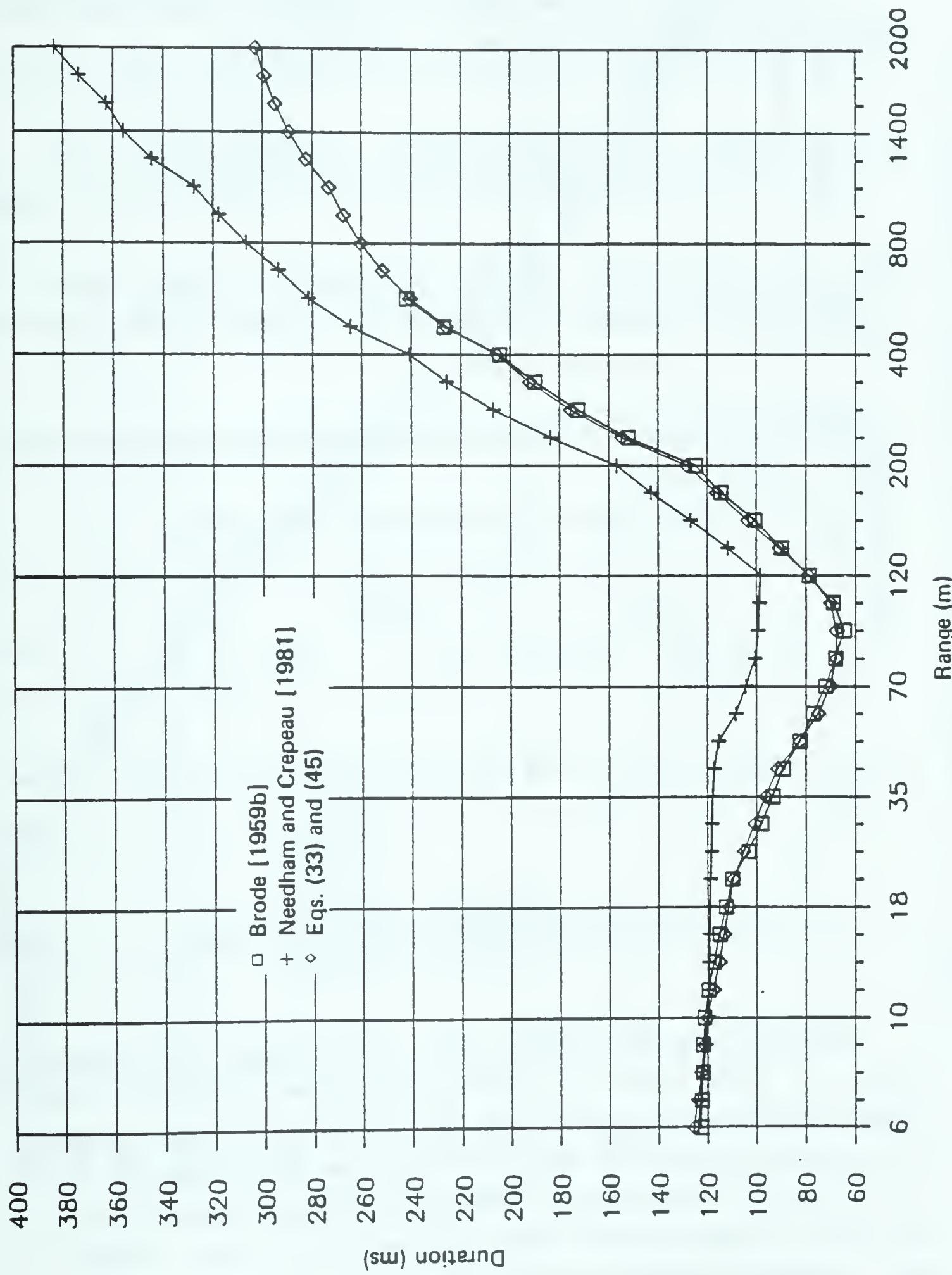


Figure 15. Fit compared to calculations: overpressure durations at 1 kT.

POSITIVE OVERPRESSURE DURATION VERSUS RANGE.

As a function of scaled range (1 KT, free-air burst), the duration of positive overpressure can be approximated by

$$D_p^+ = (m) \left[69.12 + \frac{46.19}{(1 + 3,000,000r^{7.217})} + \frac{4043r^{6.329}}{(1 + 37.16r^{5.621})} \right] \text{ ms}, \quad (46)$$

where r is scaled range in kilofeet per cube-root kiloton. Again, for a surface burst, D_p^+ should be increased by a factor of $2^{1/3}$, i.e., the free-air form for twice the yield.

OVERPRESSURE IMPULSE IN POSITIVE PHASE VERSUS PEAK OVERPRESSURE (FREE-AIR AND SURFACE BURST).

Positive phase impulse I_p^+ is defined by the integral

$$I_p^+ \equiv \int_T^{T+D_p^+} \Delta P(t) dt = m \int_{\tau}^{\tau+D_p^+/m} \Delta P(\sigma) d\sigma. \quad (47)$$

A simple approximation to this impulse as a function of peak overpressure is

$$I_p^+ = \frac{145 \Delta P_s^{1/2}}{(1 + 0.00385 \Delta P_s^{1/2})} \text{ m psi-ms.} \quad (48)$$

This fit, when used with Eq. (33), leads to the values compared in Fig. 16 versus radius. The impulse approaches a constant at small ranges and decays approximately as the inverse of the range elsewhere. For a surface burst, that expression should be multiplied by 1.26 (i.e., by $2^{1/3}$), which leads to replacing the coefficient 145 by 183. This form is good to better than 10 percent for $2 < \Delta P_s < 100,000$ psi. Comparison between the approximation as a function of peak overpressure and the detailed numerical results [Brode, 1964] is made in Fig. 17. In that plot, it is evident that impulse increases

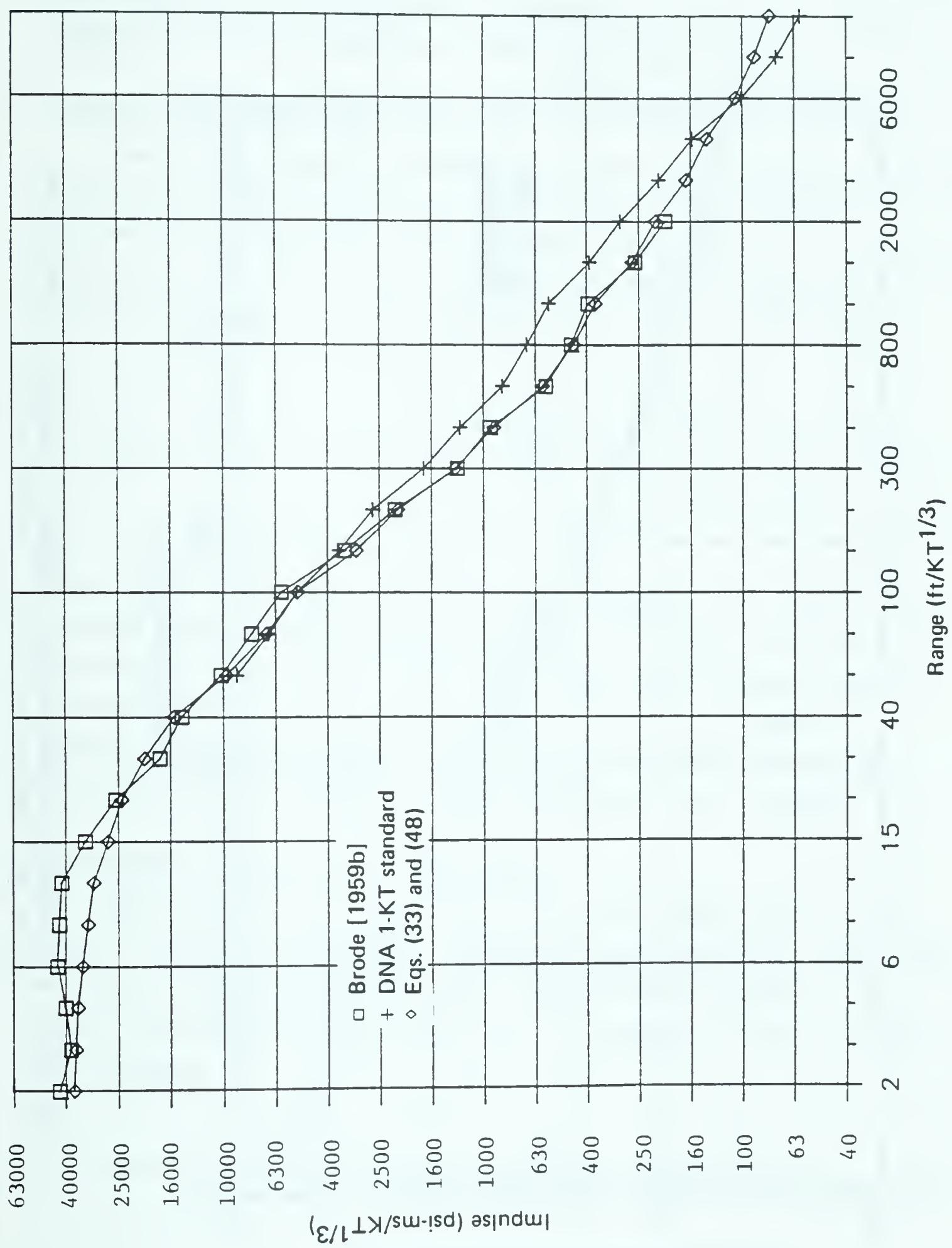


Figure 16. Fit compared to detailed calculation and 1-KT standard: over-pressure impulse in positive phase (1-KT, free-air burst).

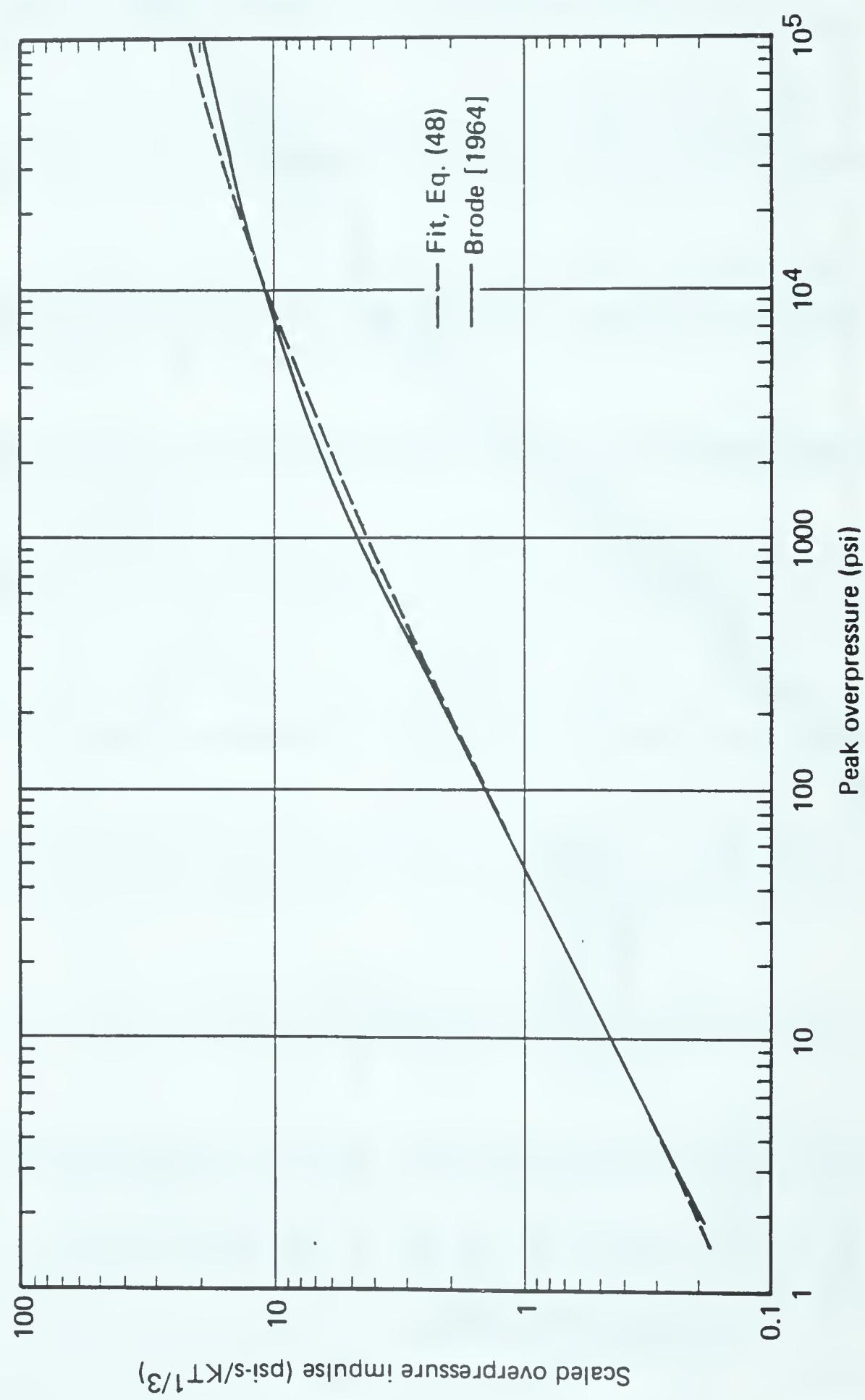


Figure 17. Fit compared to calculation: impulse in positive overpressure versus peak overpressure (1-KT, free-air burst).

approximately as the cube root of overpressure, but tends toward a constant at about a few thousand pounds per square inch.

OVERPRESSURE VERSUS TIME.

The following analytic expression is valid for overpressures less than about 15,000 psi. It is an approximate form, modified from earlier fits [Brode, 1970, 1978] for the overpressure in the positive phase as a function of time. In these fits, time is zero at the instant of burst:

$$\Delta P \approx \Delta P_s(\sigma) \left\{ 0.417 + 0.583 \left(\frac{\tau}{\sigma} \right)^6 \left[\frac{40 \left(\frac{\tau}{\sigma} \right)^6 + \tau^2}{40 + \tau^2} \right] \right\} \left(1 - \frac{\sigma - \tau}{D_p^+ / m} \right) \text{ psi,} \quad (49)$$

where $\Delta P_s(\sigma)$ is found in Eq. (37) and σ replaces τ , $\tau = T/m$, $\sigma = t/m$, T is the time of arrival (in milliseconds), t is the time after time of arrival ($t \geq T$, i.e., $\sigma \geq \tau$). Both T and t are measured from the instant of detonation. The scale factor $m = W^{1/3}$ (in cube-root kilotons) and D_p^+ is the duration of the positive phase [Eqs. (43) through (46)]. As before, for a surface burst, use $m = (2W)^{1/3}$.

OVERPRESSURE VERSUS TIME (SURFACE BURST).

Alternatively, one can use the zero burst height from the more complex equations for height of burst and range [Eq. (63) and Speicher and Brode, 1980a,b, 1981, 1984a,b]. When zero burst height is inserted and expressions are simplified, the calculation for a surface burst becomes

$$\Delta P \approx \Delta P_s(\tau) \left[f \left(\frac{\tau}{\sigma} \right)^g + (1 - f) \left(\frac{\tau}{\sigma} \right)^h \right] \left(1 - \frac{\sigma - \tau}{D} \right) \text{ psi,} \quad (50)$$

where

$$D = \left(\frac{1,641,000 + 24,630\tau + 416.2\tau^2}{10,880 + 619.8\tau + \tau^2} \right)$$

$$\times \left(\frac{0.001204\tau^{1.5}}{1 + 0.001559\tau^{1.5}} + \frac{0.5486\tau^{0.25}}{1 + 0.00357\tau^{1.5}} + \frac{-3.47\tau^{0.637}}{1 + 5.696\tau^{0.645}} + 1.0126 \right),$$

$$f = \frac{0.01477\tau^{0.75}}{1 + 0.005836\tau} + \frac{7.402 \times 10^{-5}\tau^{2.5}}{1 + 1.429 \times 10^{-8}\tau^{4.75}} + 0.4916$$

$$- \frac{3.077 \times 10^{-5}\tau^3}{1 + 4.367 \times 10^{-5}\tau^3} + \frac{9.94 \times 10^{-7}X^{4.13}}{1 + 2.1868 \times 10^{-6}X^{4.13}},$$

$$g = 87.58 - \frac{64.99\tau^{0.125}}{1 + 0.04348\tau^{0.5}},$$

$$h = 1.403 + \frac{0.05601\tau}{1 + 1.473 \times 10^{-9}\tau^{5}} + \frac{0.01769\tau}{1 + 3.207 \times 10^{-10}\tau^{4.25}}$$

$$- \frac{0.03209\tau^{1.25}}{1 + 9.914 \times 10^{-8}\tau^{4}} - \frac{0.1966\tau^{1.22}}{1 + 0.767\tau^{1.22}}.$$

and X is the scaled ground range in feet per cube-root kiloton.

Note that in this form, unlike Eq. (49), the peak overpressure is the peak at the time of shock arrival. The peak overpressure (ΔP_s) for this surface burst form can be approximated in various ways. Using Eq. (38), which is Eq. (37) with $2W$, leads to a convenient form in terms of arrival time.

Using $y = 0$ in the height of burst form from Speicher and Brode [1980b, as revised in 1981 and further revised in 1984a] (i.e., for a surface burst) leads to a function of scaled ground range somewhat different than the form of Eq. (34), namely:

$$\Delta P_s = \frac{10.47}{x^{1.22}} + \frac{2.9902}{x^{3.053}} - \frac{4.166}{1 + 0.6096x^{1.83}} - 0.2905 + \frac{0.0014x^2}{1 - 0.158x + 0.0486x^{1.5} + 0.00128x^2} \text{ psi,} \quad (51)$$

where x is scaled ground range in kilofeet per cube-root kiloton.

Equation (34) is preferred over Eq. (51). Eq. (34) is a bit simpler algebraically and is also a closer fit to the detailed one-dimensional calculation [Brode, 1959b]. Equation (51) is within 7 percent of Eq. (34) between 10,000 psi and 0.03 psi. The largest deviation occurs near 150,000 psi, a point in the detailed calculation just after the air shock has fully formed and the debris shock has overtaken it [at that point, Eq. (51) is low by -23 percent]. At closer ranges and higher pressures, details of the nuclear weapon become increasingly important, so that no general curve fit will be wholly correct. In addition, radiation transport plays an increasingly important role, making normal shock physics less applicable.

DURATION OF OUTWARD DYNAMIC PRESSURE VERSUS PEAK OVERPRESSURE.

The duration of the outward flow in the blast wave D_u^+ can be related to the peak overpressure (for a free-air burst) as

$$D_u^+ \approx m \left(\frac{317}{1 + 85\pi + 7500\pi^2} + \frac{6110\pi}{1 + 420\pi^2} + \frac{2113\pi}{1 + 11\pi} \right) \text{ ms,} \quad (52)$$

where $\pi = \Delta P_s / 1000$ (in kilopounds per square inch),

$m = W^{1/3}$ (in cube-root kilotons).

For a surface burst, substitute $2W$ for W , i.e., $m \approx 1.26m$. The fit is in good agreement with earlier calculations [Brode, 1959b, 1966], but it differs significantly from the 1-KT standard [Needham and Crepeau, 1981]. The difference is illustrated in Fig. 18 (scaled to 1-MT surface burst). Such a disparity between results of detailed

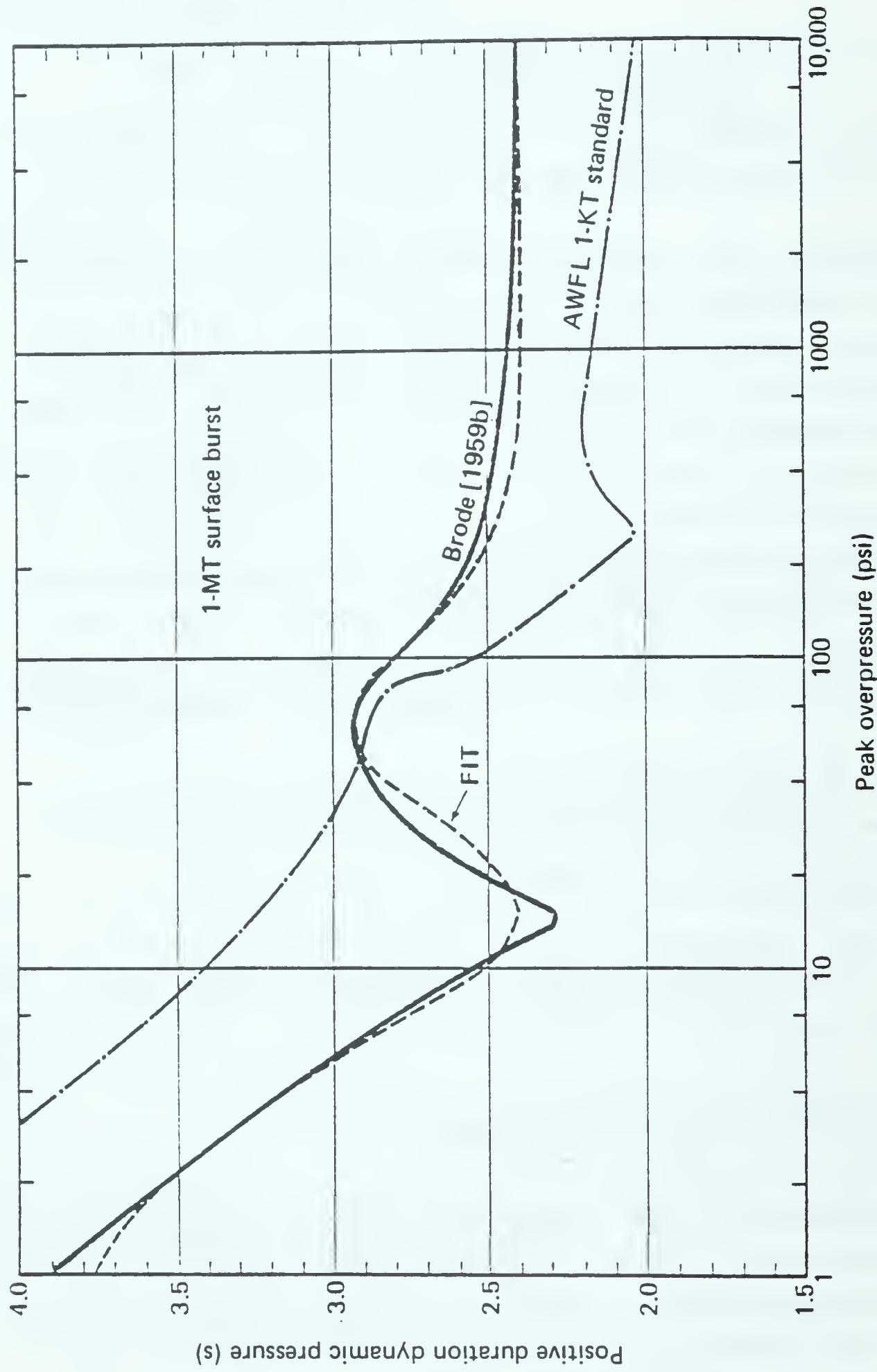


Figure 18. Fit compared to calculation and 1-KT standard (scaled to 1-MT surface burst): dynamic pressure positive phase.

numerical (one-dimensional) calculations is a measure of the differences introduced by dissimilarities in boundary and initial conditions, equations of state and opacities, and by various treatments of radiation transport, thermal radiation losses, and accumulated numerical errors in detailed computer calculations.

DYNAMIC IMPULSE VERSUS PEAK OVERPRESSURE (FREE-AIR BURST).

The dynamic impulse in the positive phase, defined as

$$I_u^+ = (1/2) \int_T^{T+D_u^+} \rho u^2 dt , \quad (53)$$

can be approximated as

$$I_u^+ \approx \frac{2.14 \Delta P_s^{1.637} (m)}{(1 + 0.00434 \Delta P_s^{1.431})} \quad \text{psi-ms.} \quad (54)$$

That form is within 10 percent of the scaled values from the detailed calculations [Brode, 1959b, 1966] for $3 < \Delta P_s < 10,000$ psi. It is high by nearly 20 percent at $\Delta P_s \approx 100,000$ psi. Figure 19 compares the dynamic impulse from the detailed calculations with that from this fit (Eq. 54).

DYNAMIC IMPULSE VERSUS SCALED RANGE.

A fit to the dynamic impulse versus range for the early calculations [Brode, 1959b] agrees to better than 10 percent for $0.0025 \leq r \leq 2 \text{ kft}/\text{KT}^{1/3}$. The relation, when scaled to a 1-KT free-air burst, is

$$I_u^+ = \left[\frac{18.8r^2}{10^{-6} + 0.06896r^3 + 0.5963r^{5.652}} + \frac{92.64}{(100r)^5} \right. \\ \left. + \frac{2935(r - 0.00597)(0.01 - r)(0.0003552 - r^4)}{10^{-10} + 0.003377r^{2.5} + 155.8r^8} \right] m \quad \text{psi-ms,} \quad (55)$$

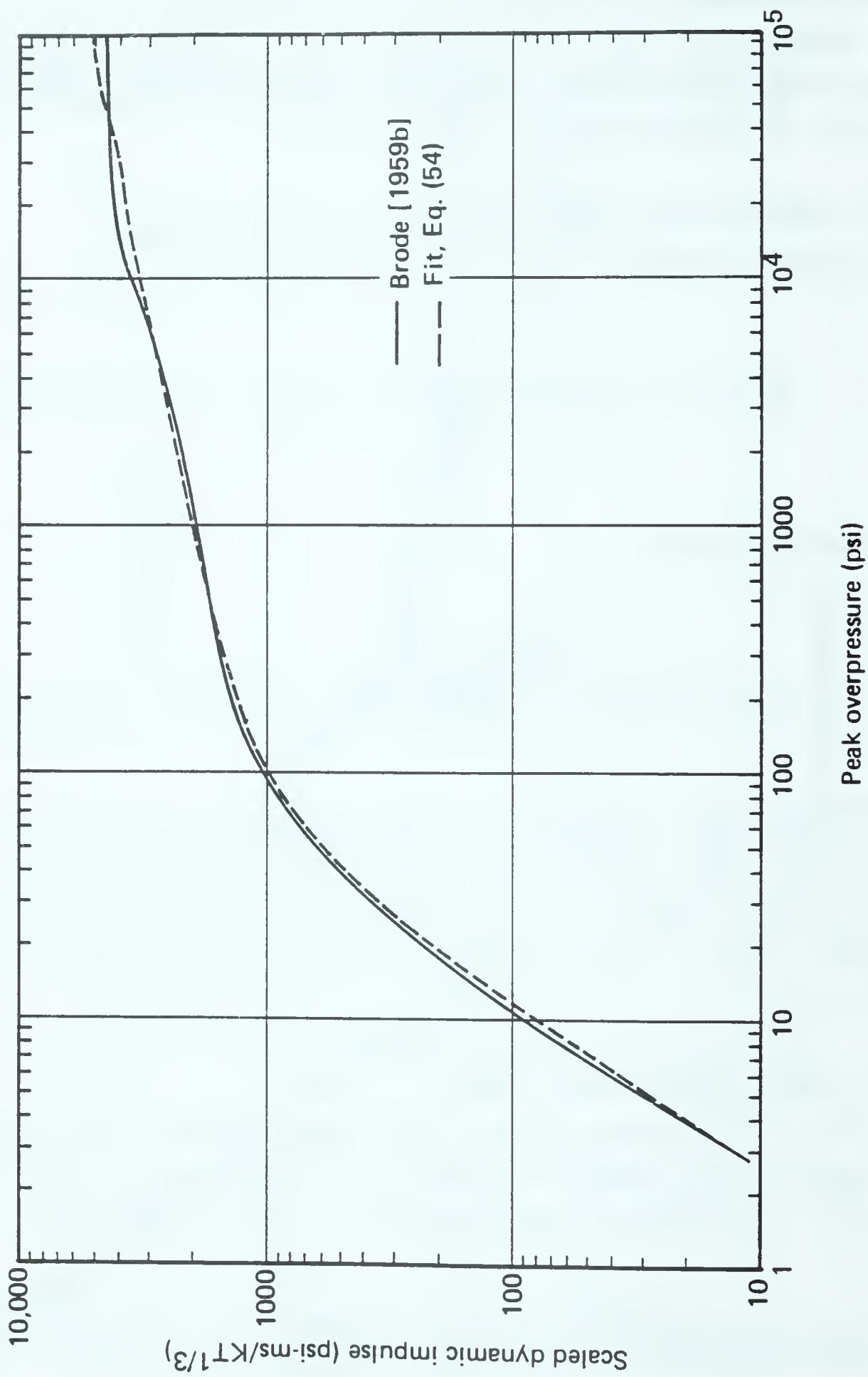


Figure 19. Fit compared to calculation: dynamic impulse versus peak overpressure for 1-kT free-air burst.

with $r = sr/m$, sr in kilofeet, $m = W^{1/3}$, and W in kilotons. This expression is illustrated in Fig. 20 and compared with the detailed calculation results to which it was fit. The fit is good to a few percent over the entire range. For a surface burst, $m = (2W)^{1/3}$.

DYNAMIC PRESSURE VERSUS TIME.

An older approximate analytic expression for dynamic pressure versus time covers the range $2 \leq \Delta P_x \leq 1000$ psi ($0.1 \leq Q_s \leq 3000$ psi) [Brode, 1964]:

$$Q(t) = Q_s (1 - \omega)^2 [d \exp(-aw) + (1 - d) \exp(-bw)] \text{ psi}, \quad (56)$$

in which $\omega = (t - T)/D_u^+$,

T = time of arrival [see Eqs. (39) through (41)],

t = time,

D_u^+ = duration of outward blast wind [see Eq. (52)],

Q_s = peak dynamic pressure in pounds per square inch [see Eqs. (16) through (18)],

$$d \approx \frac{1.06\pi^{0.035}}{1 + 147\pi^3} + \frac{2.13\pi^3}{1 + 67.9\pi^{3.5}},$$

$$a \approx 0.38\Delta P_s^{0.8605} \approx 145\pi^{0.8605},$$

$$b \approx 5.4\Delta P_s^{0.604} \approx 350\pi^{0.604}.$$

Equation (56) is valid for $1 \geq \pi \geq 0.002$ ksi ($1000 \geq \Delta P_x \geq 2$ psi).

These parameters are illustrated in Fig. 21 (scaled to 1-MT surface burst).

A relatively simple alternative surface burst formula for dynamic pressure versus time can be derived from the more complex fits to dynamic and overpressure versus HOB, ground range, and time [Speicher, 1983; Speicher and Brode, 1981; Brode, 1983]. That fit, when simplified for zero HOB, becomes essentially that of the shock or

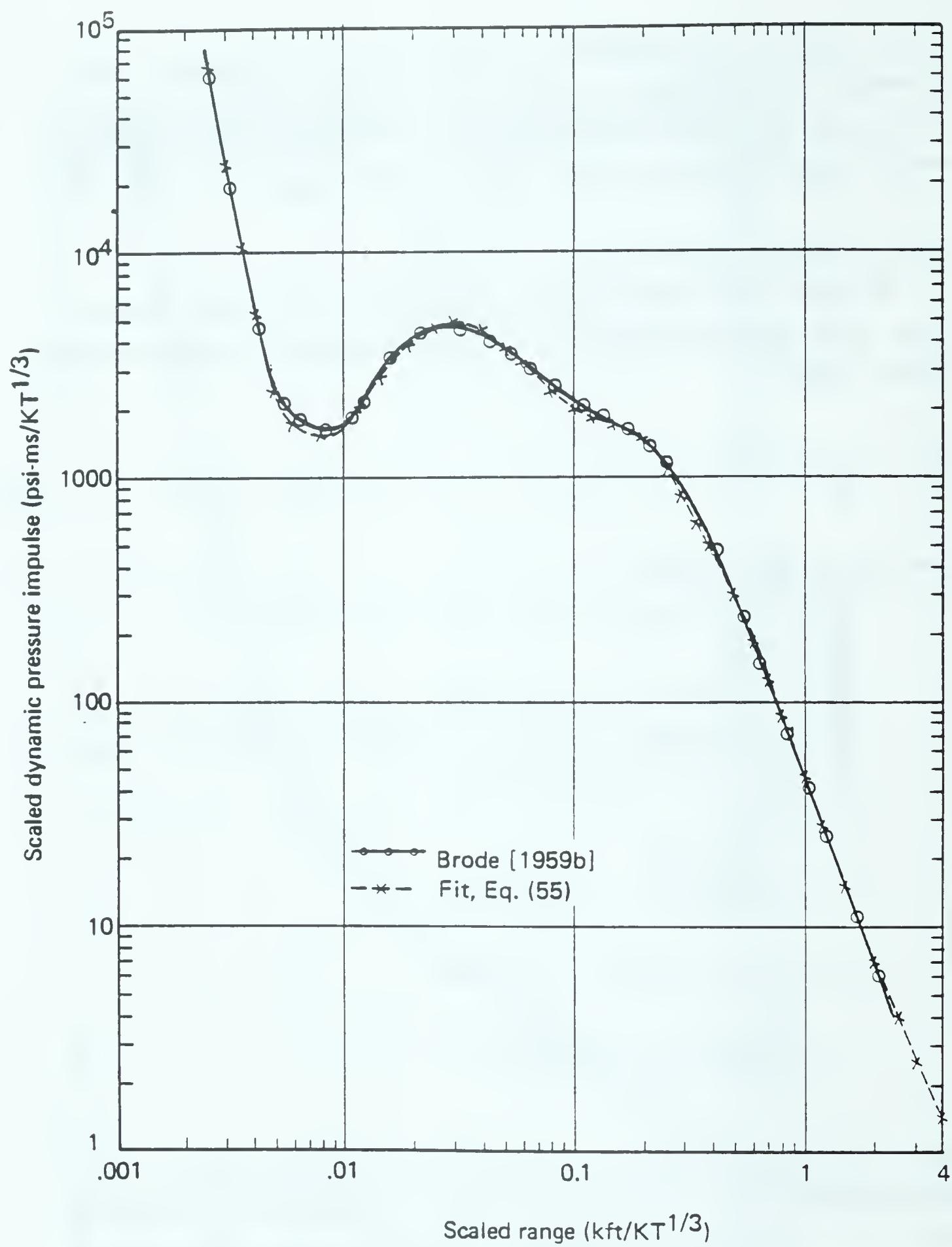
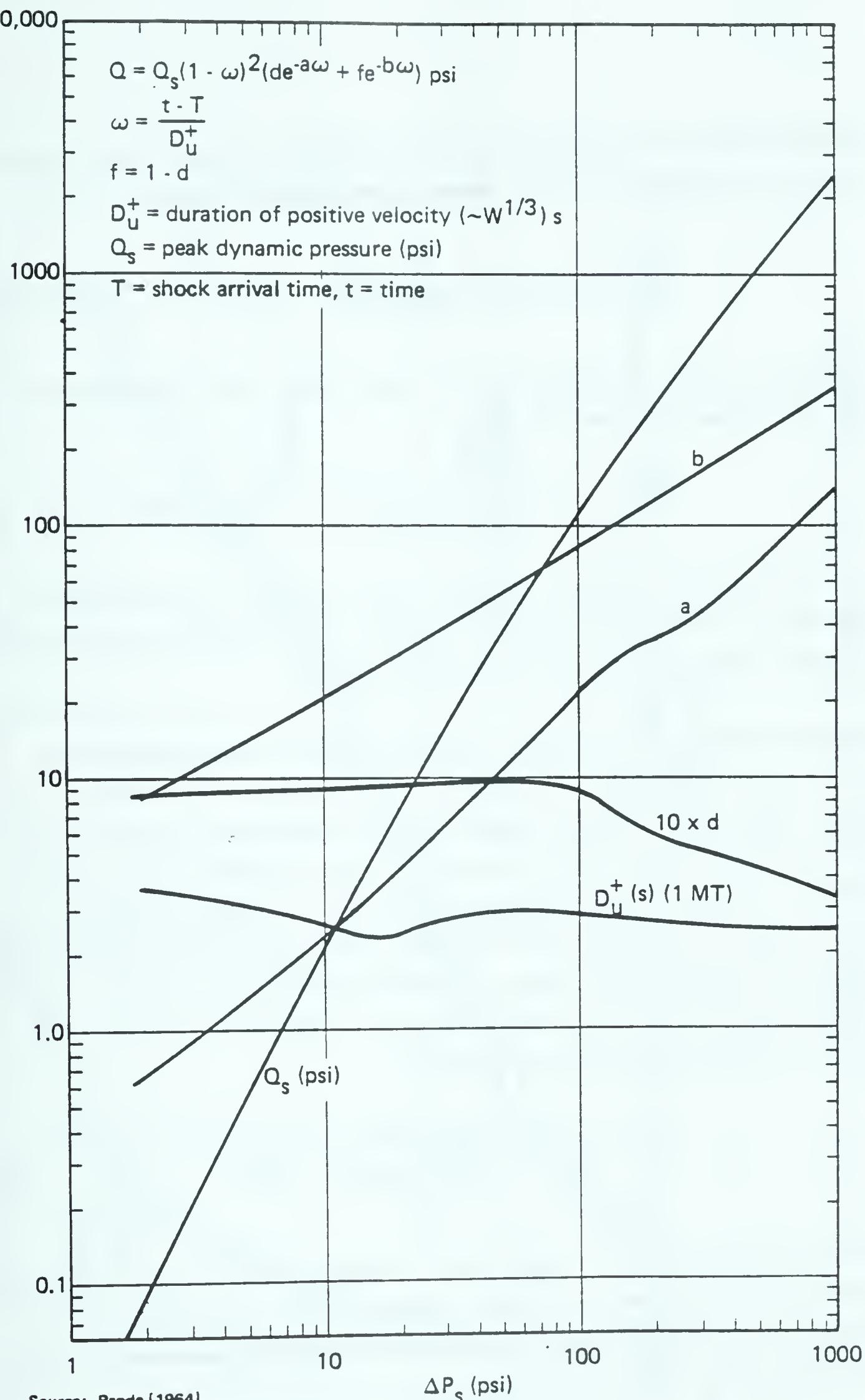


Figure 20. Fit compared to calculation: scaled dynamic pressure impulse versus scaled range for 1-KT free-air burst.



Source: Brode (1964)

Figure 21. Dynamic pressure versus peak overpressure and time (scaled for 1-MT surface burst).

Hugoniot form of the relation between dynamic pressure and overpressure, but extended to times after shock arrival [e.g., Eq. (17)]:

$$Q(x, \sigma) \approx \frac{2.5\Delta P^2}{102.9 + \Delta P} \quad \text{psi}, \quad (57)$$

In this fit, ΔP is defined by Eq. (50), except that the quantity D in Eq. (50) should be replaced by

$$D' = D[4.51 - 12.8x^{2.5}/(1 + 3.63x^{2.5})]. \quad (58)$$

This is not a wholly accurate form, since it is the result of a "quick fix" HOB fit for dynamic pressure time-histories, and has not yet been replaced by a more exact expression.

MAXIMUM TEMPERATURE (FIREBALL EXPOSURE) VERSUS PEAK OVERPRESSURE.

Another parameter of interest is the maximum temperature at a given range. The maximum temperature at overpressure levels above 100 psi occurs after shock arrival, as hotter fireball air expands past that point. That maximum temperature is somewhat dependent on yield, since the fireball of a megaton burst cools more slowly than that of a kiloton burst (even if cube-root scaling is applied). The rough fit of Eq. (59) is appropriate for a megaton and is based on earlier calculations by Brode [1959b]:

$$\theta_m \approx \frac{1090\pi^{3.26}}{1 + 35.6\pi^{2.75}} \quad 10^3 \text{°C}, \quad (59)$$

with π in kilopounds per square inch. More recently, improved opacities for air have led to slightly higher fireball temperatures at corresponding times, so that temperatures somewhat above those predicted by Eq. (59) are likely.

In Fig. 22, the fit is compared with the values from the radiation-hydrodynamic calculation [Brode, 1959b].

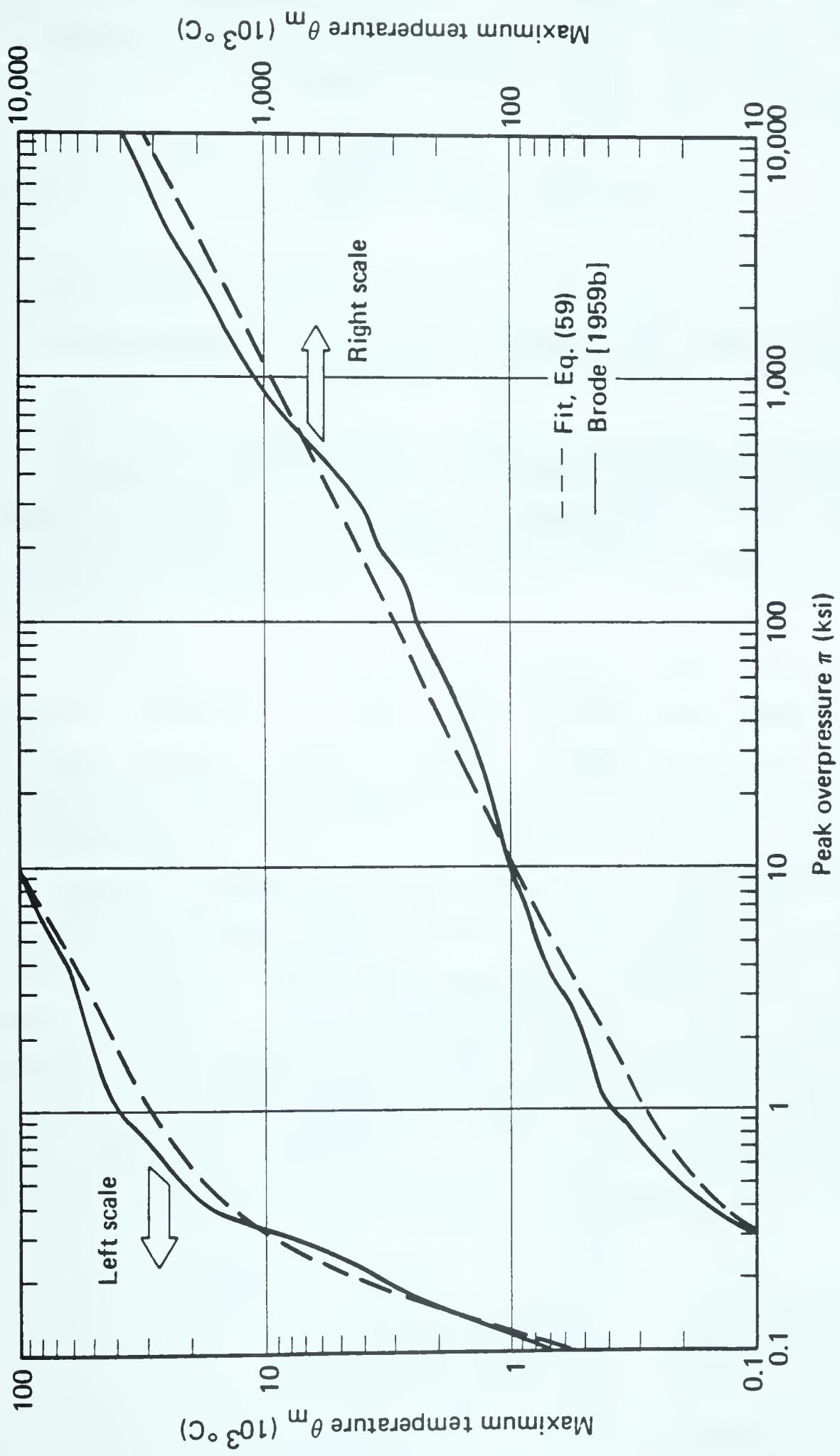


Figure 22. Fit compared to calculation: maximum fireball temperature versus peak overpressure for 1-MT burst.

The time to maximum temperature cannot be rigorously scaled; but assuming cube-root scaling, that time is roughly inversely proportional to the peak overpressure (free-air burst):

$$t_m \approx 19W^{1/3}/\pi = 19 m/\pi \text{ ms}, \quad (60)$$

where $\pi = \Delta P_s / 1000$ (in kilopounds per square inch) and W is yield in kilotons. This approximation, which is based on a calculation for a few megatons, is less reliable as the yield deviates from that.

NEGATIVE PHASE UNDERPRESSURE VERSUS PEAK OVERPRESSURE AND TIME.

The time-history of the negative overpressure ΔP_- , or underpressure, can be approximated for a free-air (or surface) burst by the algorithm

$$\Delta P_- = - \frac{P_0 A_n \tau (1 - \tau)}{1 + B_n \tau^2 + C_n \tau^3} \text{ psi}, \quad (61)$$

where P_0 = ambient pressure (14.7 psi),

$\tau = (t - t_n)/D_p^-$,

t = time after detonation,

t_n = time of beginning of negative phase,

= time to end of positive phase,

= time of arrival + duration of positive phase = $T + D_p^+$,

D_p^- = duration of negative phase = 1051 m (in milliseconds),

$m = W^{1/3}$ (in cube-root kilotons),

$$A_n = \frac{0.2532\Delta P_s}{(1 + 0.1262\Delta P_s)} + \frac{413.2(\Delta P_s/100)^4}{[1 + 668.1(\Delta P_s/100)^5]},$$

$$B_n = \frac{2.481\Delta P_s}{(1 + 0.004272\Delta P_s^{1.7})},$$

$$C_n = \frac{18.55(\Delta P_s / 100)^8}{[1 + 2.75(\Delta P_s / 100)^{7.335}]} ,$$

$$t_n = m \left(151.3 + \frac{2844}{\Delta P_s / 0.9638} \right)$$

$$= T + D_p^+ ,$$

[i.e., Eqs. (39) through (41), plus Eqs. (43) through (45)].

This fit is compared with an early detailed one-dimensional free-air calculation [Brode, 1959b] at overpressure ranges from 300 psi down to less than 5 psi in Figs. 23 through 30.

BLAST SUMMARY.

A number of free-air blast parameters (shock radius, time of arrival, overpressure positive phase, overpressure impulse, dynamic pressure duration, dynamic impulse, and maximum fireball temperature) are listed in Table 2 for shock overpressures ranging from 0.1 to 10,000,000 psi.

Figure 31 summarizes some of the shock parameters for a 1-MT surface burst versus peak overpressure. Several of the variables listed in Tables 1 and 2 are illustrated in that figure. They are time of arrival T , in milliseconds; shock radius GR , in feet; shock velocity U_s , in kilofeet per second; peak particle velocity u_s , in feet per second; peak dynamic pressure Q_s , in pounds per square inch; shock temperature increase $\Delta\theta_s$, in degrees centigrade; and maximum fireball temperature θ_m , in degrees centigrade.

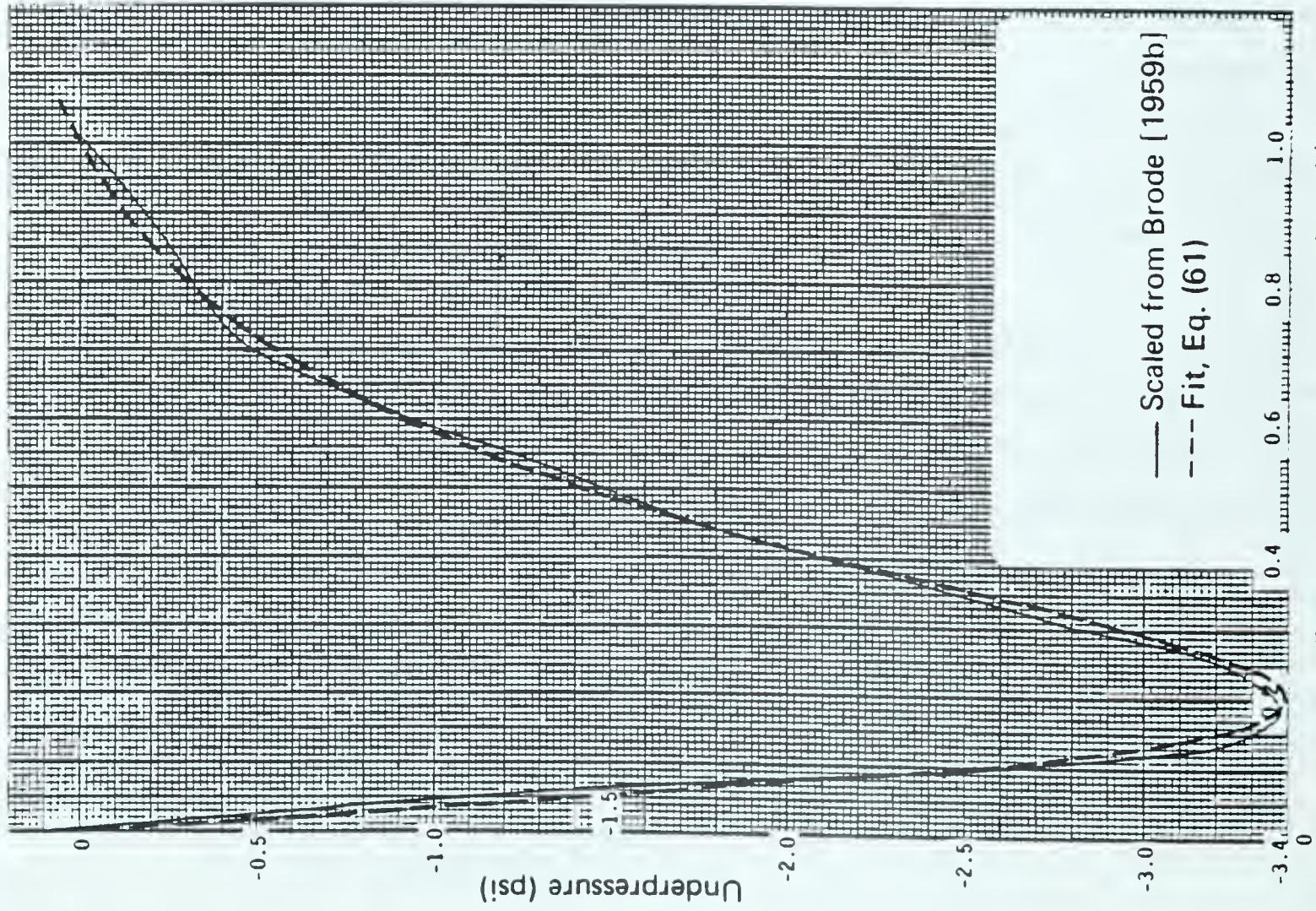


Figure 23. Negative phase pressure versus time at scaled range of 0.1472 kft/KT₁ (570 psia)

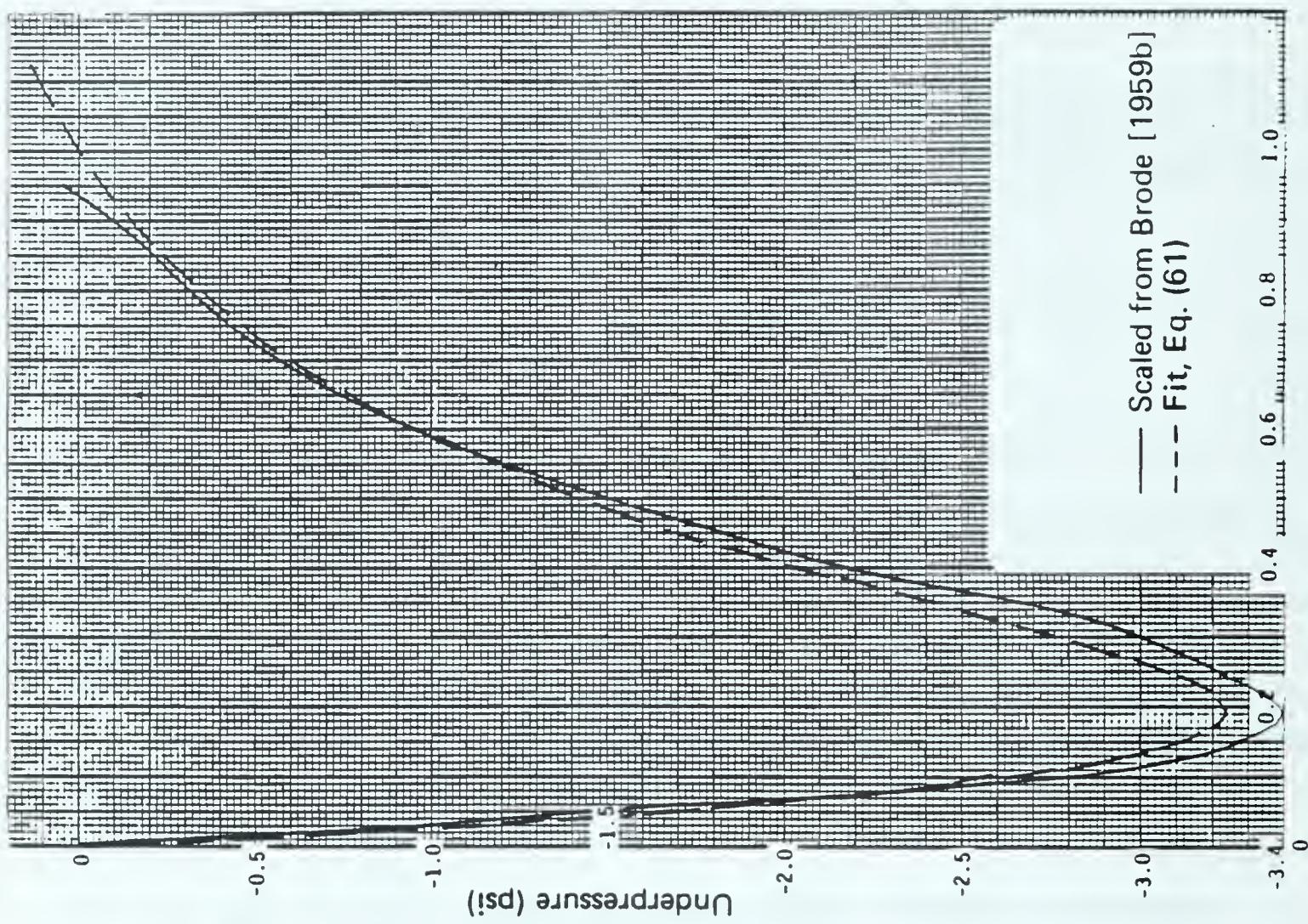


Figure 24. Negative phase pressure versus time at scaled range of 0.2102 kft/KT₁ (213 psia)

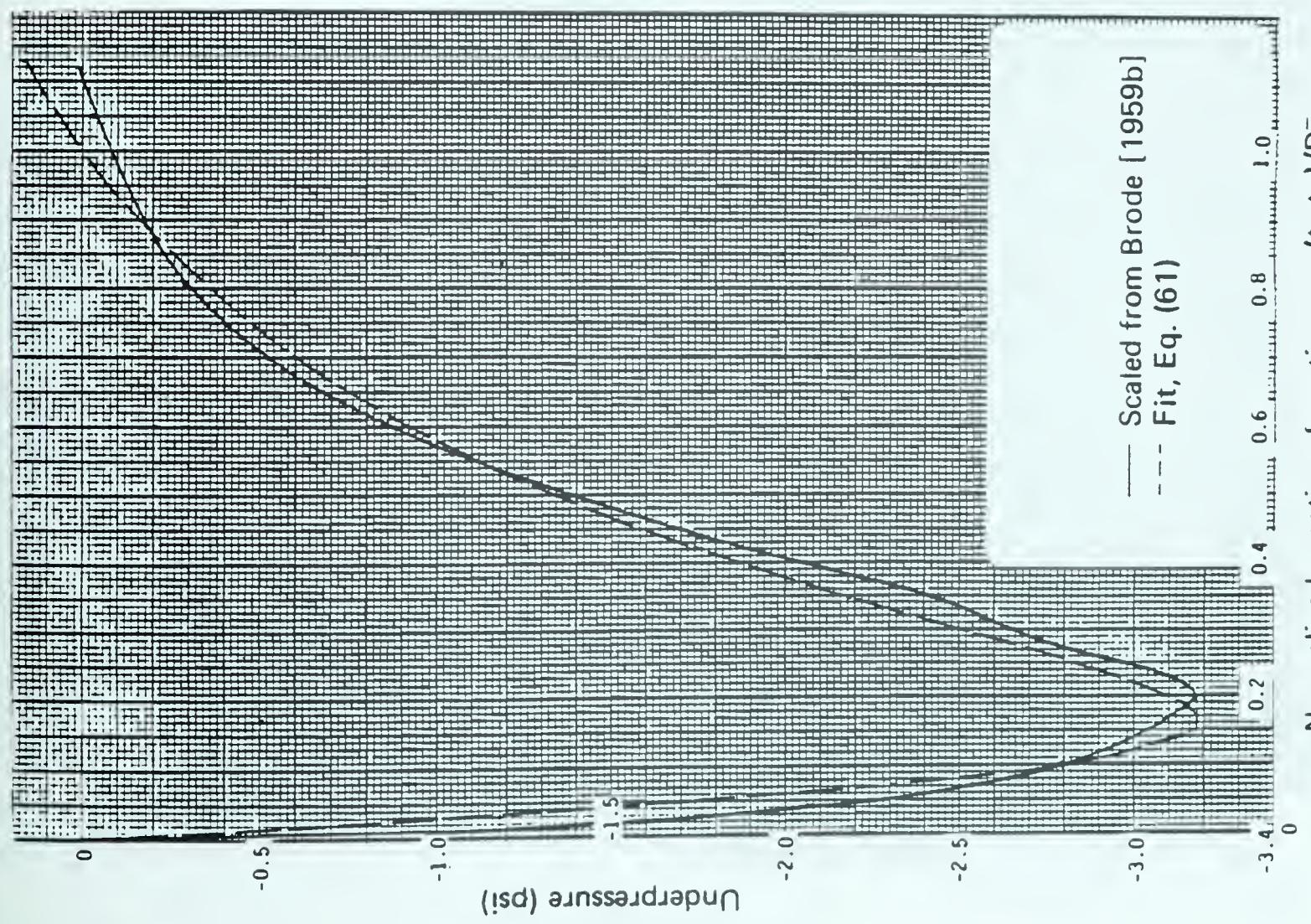


Figure 25. Negative phase pressure versus time at scaled range of 0.3154 kft/KT $\frac{1}{3}$ (74 psi).

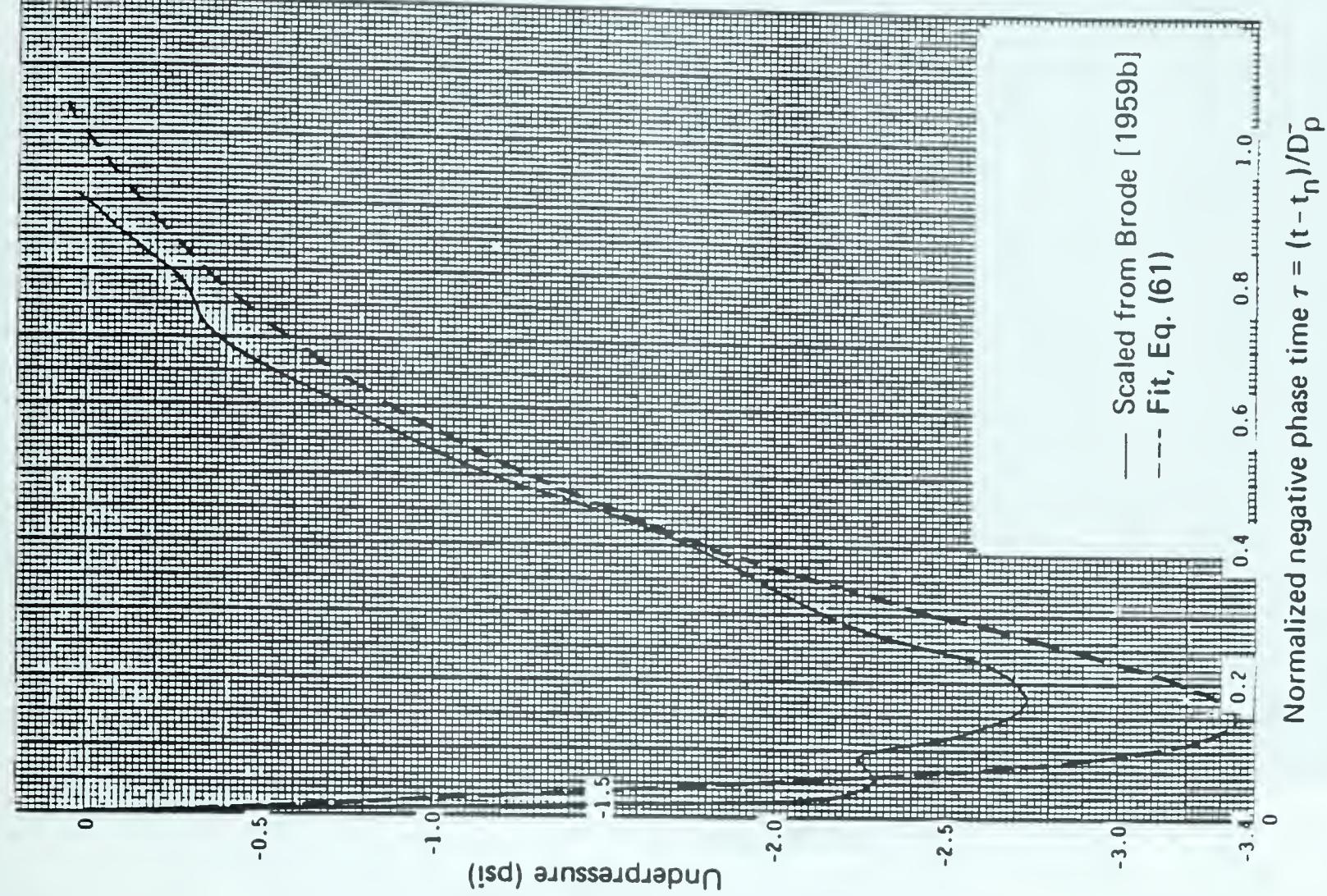
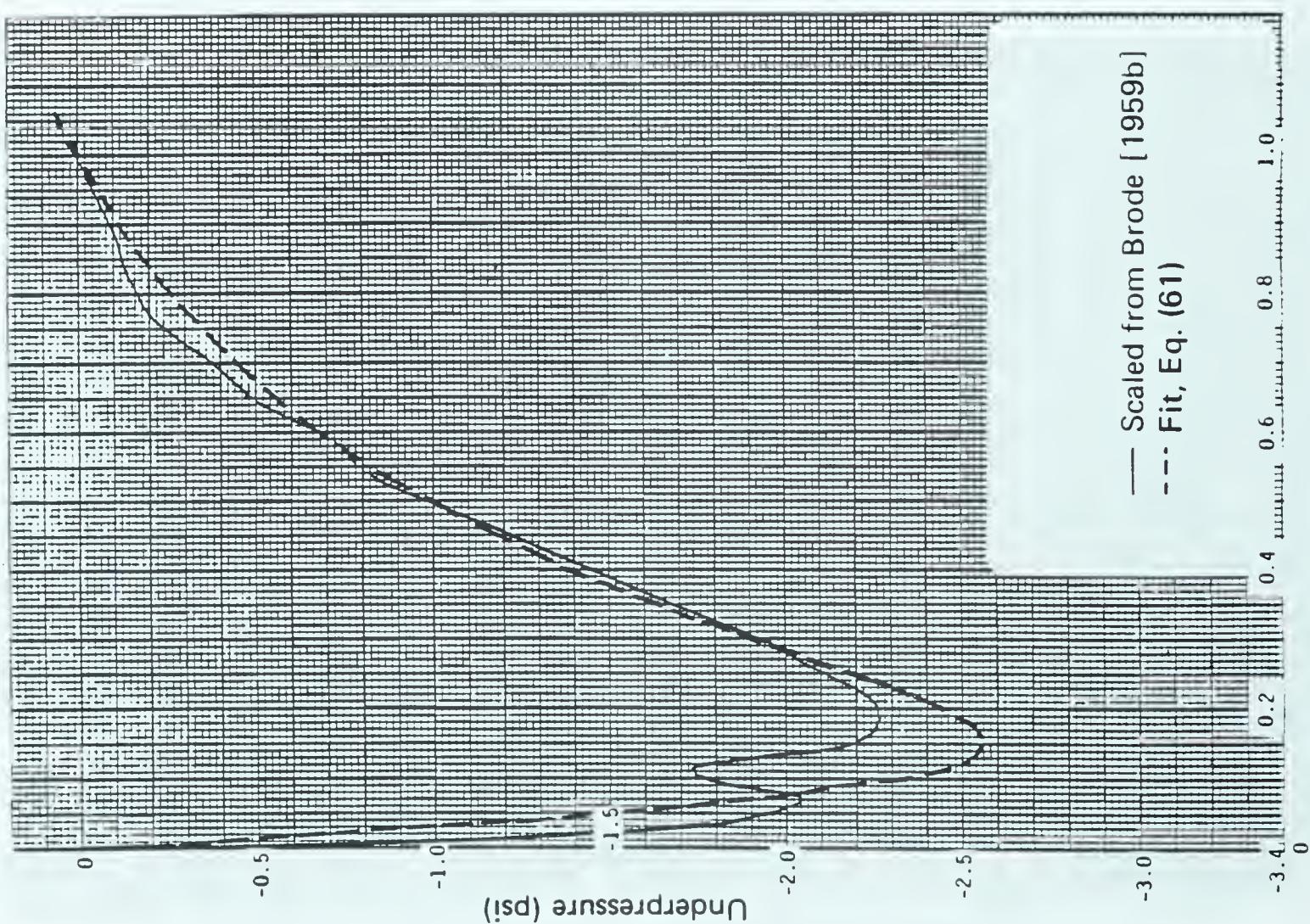
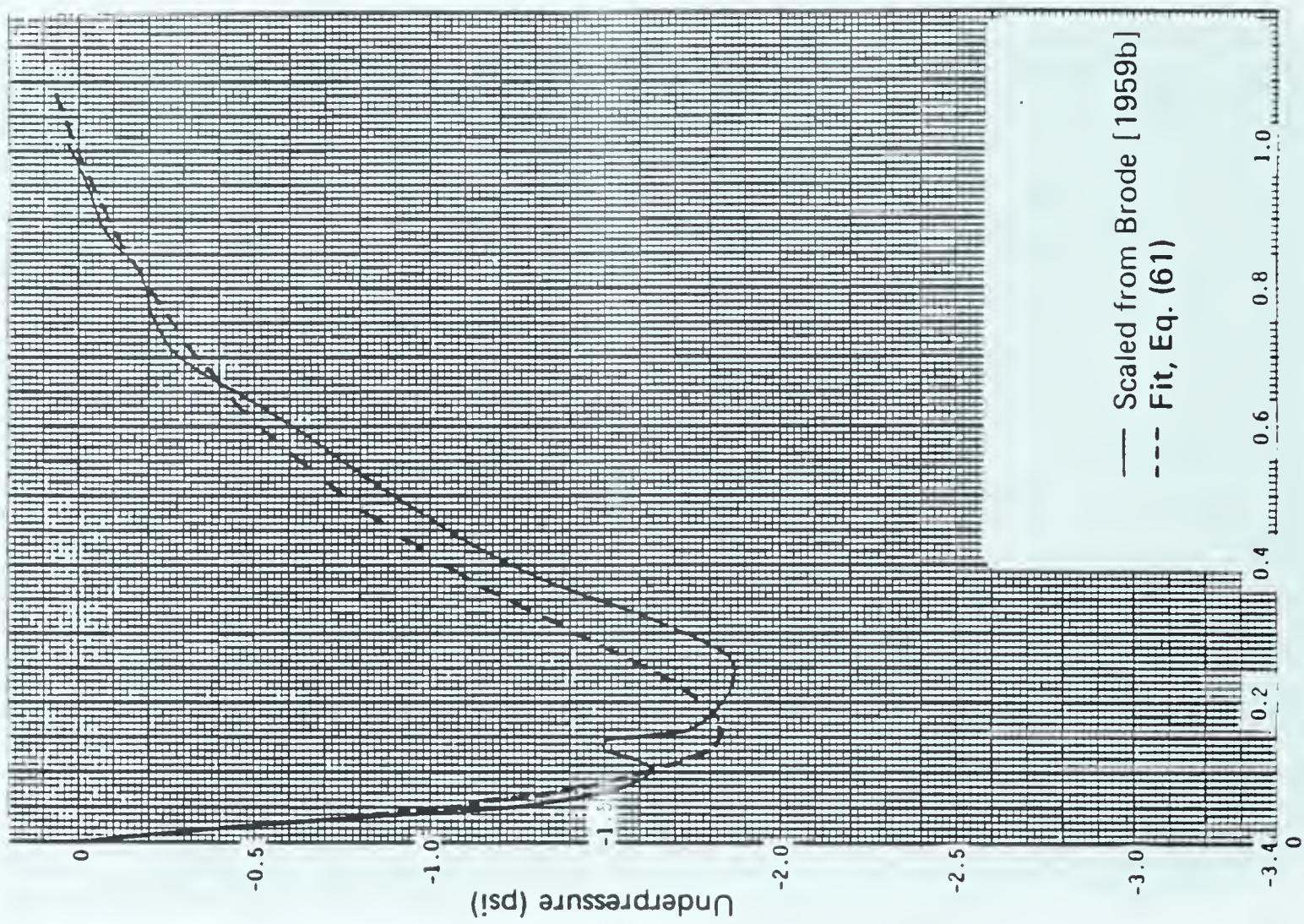


Figure 26. Negative phase pressure versus time at scaled range of 0.4205 kft/KT $\frac{1}{3}$ (37 psi).



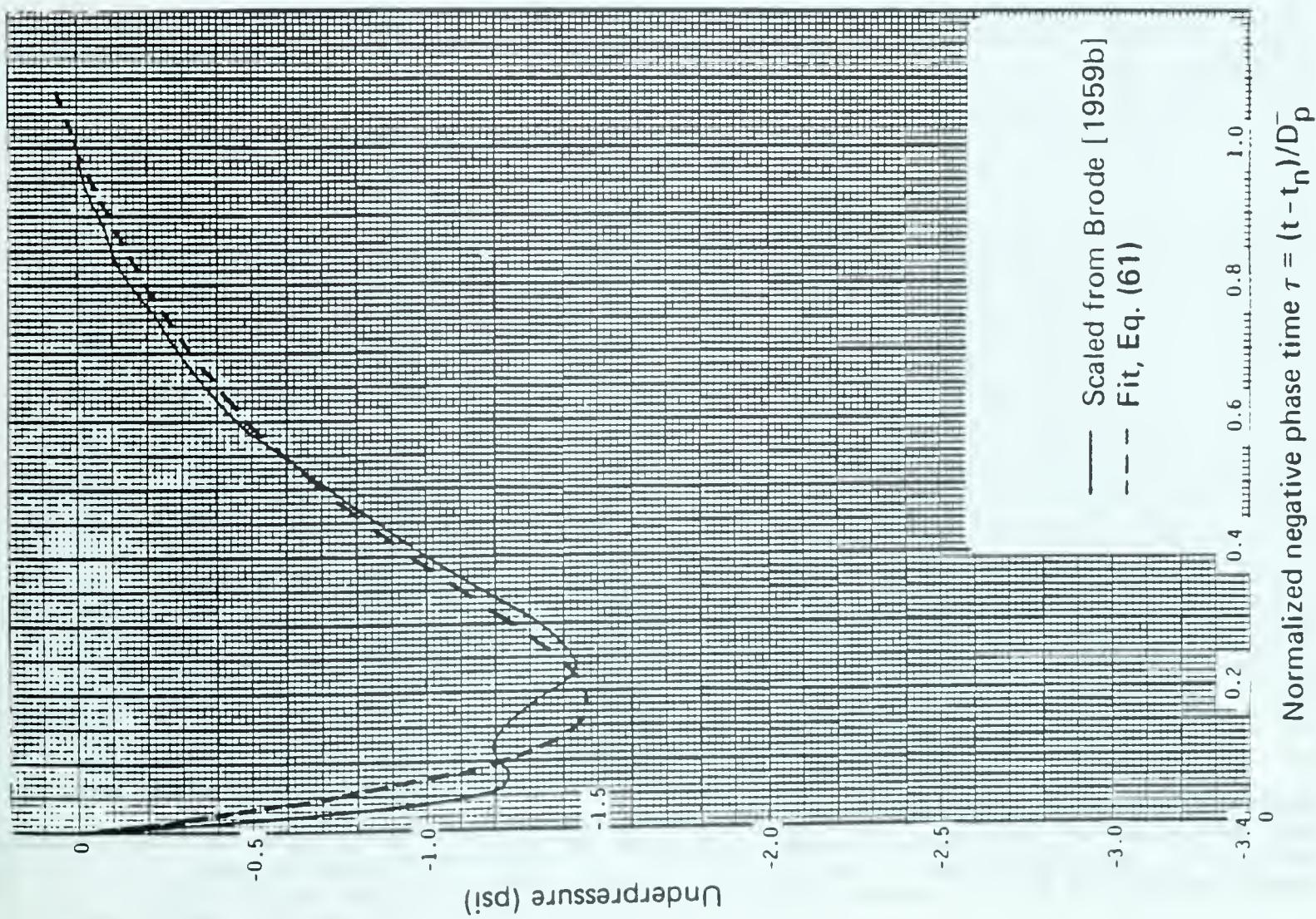


Figure 29. Negative phase pressure versus time at scaled range of 0.841 kft/KT₃ (9 psi).

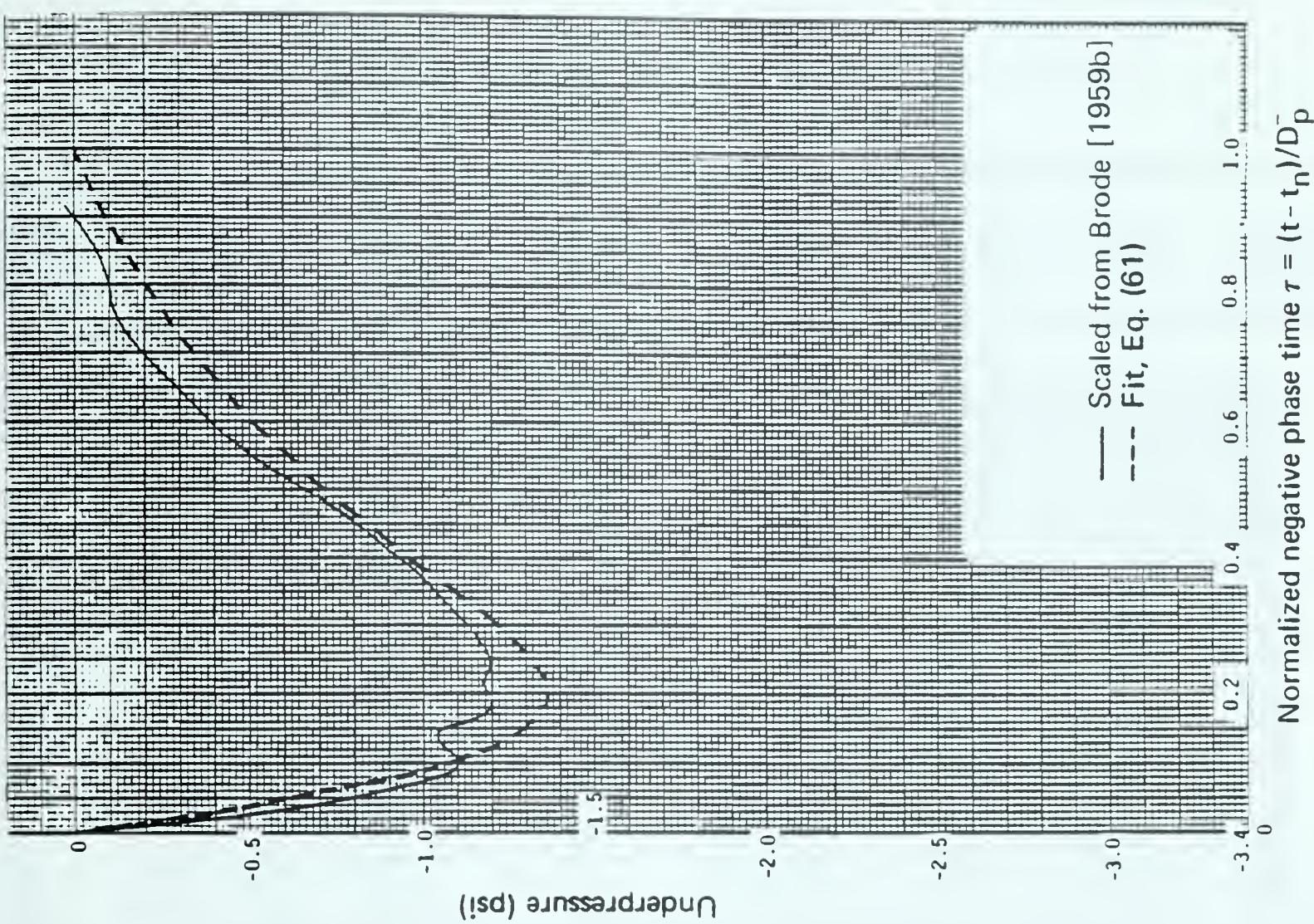


Figure 30. Negative phase pressure versus time at scaled range of 0.9882 kft/KT₁ (6.7 psi).

Table 2. Quantities for 1-KT free-air blast wave.

| Peak Overpressure ΔP_s (psi) | Shock Radius r_s (ft) | Time of Arrival T (ms/ $KT^{1/3}$) | Overpressure Positive Phase D_p^+ (ms/ $KT^{1/3}$) | Overpressure Impulse I_p^+ (psi-ms $KT^{1/3}$) | Dynamic Pressure Duration D_u^+ (ms/ $KT^{1/3}$) | Dynamic Impulse I_p^+ (psi-ms/ $KT^{1/3}$) | Maximum Fireball Temperature Θ_m (10^3 °C) |
|--------------------------------------|-------------------------|---------------------------------------|---|---|---|---|--|
| .1 | 26310 | 22760 | 332 | 45.8 | 315 | 0.0274 | 0.0005 |
| .15 | 18160 | 15550 | 327 | 56.1 | 314 | 0.0579 | 0.0008 |
| .2 | 14020 | 11890 | 322 | 64.7 | 313 | 0.0977 | 0.0011 |
| .3 | 9816 | 8161 | 315 | 79.2 | 311 | 0.203 | 0.0016 |
| .4 | 7667 | 6261 | 308 | 91.5 | 310 | 0.338 | 0.002 |
| .6 | 5467 | 4317 | 297 | 112 | 306 | 0.692 | 0.003 |
| .8 | 4335 | 3320 | 288 | 129 | 302 | 1.15 | 0.004 |
| 1.0 | 3639 | 2709 | 279 | 144 | 298 | 1.70 | 0.005 |
| 1.5 | 2680 | 1872 | 262 | 177 | 289 | 3.46 | 0.007 |
| 2 | 2178 | 1440 | 248 | 204 | 280 | 5.75 | 0.010 |
| 3 | 1650 | 994.0 | 226 | 249 | 264 | 11.8 | 0.015 |
| 4 | 1370 | 763.4 | 209 | 288 | 249 | 19.4 | 0.019 |
| 6 | 1069 | 525.9 | 183 | 352 | 226 | 38.8 | 0.028 |
| 7 | 977.3 | 456.3 | 173 | 380 | 217 | 49.9 | 0.032 |
| 10 | 801.0 | 328.9 | 151 | 453 | 200 | 87.4 | 0.045 |
| 15 | 648.0 | 227.1 | 126 | 553 | 191 | 156 | 0.064 |
| 20 | 562.2 | 174.9 | 110 | 637 | 195 | 226 | 0.082 |
| 30 | 465.0 | 121.5 | 91.5 | 778 | 211 | 358 | 0.117 |
| 40 | 409.0 | 94.05 | 81.4 | 895 | 224 | 475 | 0.15 |
| 50 | 371.5 | 77.22 | 75.5 | 998 | 230 | 579 | 0.18 |
| 70 | 322.9 | 57.50 | 69.8 | 1175 | 231 | 754 | 0.24 |
| 100 | 279.8 | 42.17 | 67.7 | 1396 | 222 | 961 | 0.56 |
| 150 | 239.1 | 29.72 | 69.1 | 1700 | 209 | 1210 | 1.88 |
| 200 | 214.5 | 23.21 | 72.0 | 1940 | 202 | 1390 | 4.02 |
| 300 | 184.6 | 16.39 | 77.4 | 2350 | 195 | 1630 | 9.36 |
| 450 | 159.5 | 11.57 | 83.5 | 2840 | 192 | 1790 | 16.3 |
| 700 | 136.4 | 7.903 | 89.9 | 3480 | 191 | 1890 | 23.7 |
| 1000 | 120.4 | 5.798 | 94.5 | 4090 | 191 | 1950 | 29.8 |
| 1500 | 104.7 | 4.064 | 99.0 | 4890 | 191 | 2060 | 37.3 |
| 2000 | 94.85 | 3.152 | 102 | 5530 | 191 | 2200 | 43.4 |
| 3000 | 83.67 | 2.106 | 105 | 6560 | 191 | 2460 | 53.5 |
| 4000 | 75.06 | 1.696 | 107 | 7370 | 191 | 2690 | 62.0 |
| 6000 | 65.64 | 1.177 | 110 | 8650 | 192 | 3060 | 76.3 |
| 8000 | 59.78 | 0.9091 | 111 | 9650 | 192 | 3350 | 88.4 |
| 10,000 | 55.68 | 0.7460 | 112 | 10500 | 192 | 3570 | 99.1 |
| 15,000 | 49.17 | 0.5270 | 114 | 12100 | 192 | 3970 | 121 |
| 20,000 | 45.26 | 0.4180 | 115 | 13300 | 192 | 4230 | 141 |
| 30,000 | 40.67 | 0.3100 | 117 | 15100 | 192 | 4530 | 174 |
| 40,000 | 37.92 | 0.2570 | 118 | 16400 | 192 | 4700 | 201 |
| 60,000 | 34.12 | 0.1936 | 120 | 18300 | 192 | 4880 | 247 |
| 80,000 | 31.00 | 0.1510 | 121 | 19600 | 192 | 4960 | 286 |
| 100,000 | 28.40 | 0.1206 | 122 | 20700 | 192 | 4940 | 321 |
| 150,000 | 23.91 | 0.07897 | 124 | 22500 | 192 | 4660 | 394 |
| 200,000 | 21.22 | 0.05719 | 125 | 23800 | 192 | 4300 | 456 |
| 300,000 | 18.11 | 0.03659 | 127 | 25500 | 192 | 3690 | 561 |
| 400,000 | 16.29 | 0.02583 | 128 | 26700 | 192 | 3260 | 650 |
| 600,000 | 14.10 | 0.01438 | 129 | 28200 | 192 | 2710 | 799 |
| 800,000 | 12.76 | 0.008623 | 131 | 29200 | 192 | 2390 | 926 |
| 1000,000 | 11.82 | 0.005415 | 132 | 29900 | 192 | 2180 | 1037 |
| 1500,000 | 10.30 | 0.002133 | 133 | 31100 | 192 | 1900 | 1275 |
| 2000,000 | 9.352 | 0.001029 | 135 | 31800 | 192 | 1760 | 1477 |
| 3000,000 | 8.163 | 0.0003522 | 136 | 32750 | 192 | 1670 | 1816 |
| 4000,000 | 7.414 | 0.0001623 | 138 | 33300 | 192 | 1660 | 2103 |
| 6000,000 | 6.475 | 0.0000514 | 140 | 34100 | 192 | 1750 | 2587 |
| 8000,000 | 5.882 | 0.00002485 | 141 | 34500 | 192 | 1920 | 2996 |
| 10,000,000 | 5.460 | 0.00001360 | 142 | 34800 | 192 | 2140 | 3357 |

Note: Shock radius, see Eq. (36); time of arrival, see Eq. (41); overpressure positive phase, see Eq. (43); overpressure impulse, see Eq. (48); dynamic pressure duration, see Eq. (52); dynamic impulse, see Eq. (55); maximum fireball temperature, see Eqs. (20) and (24), or Eq. (59).

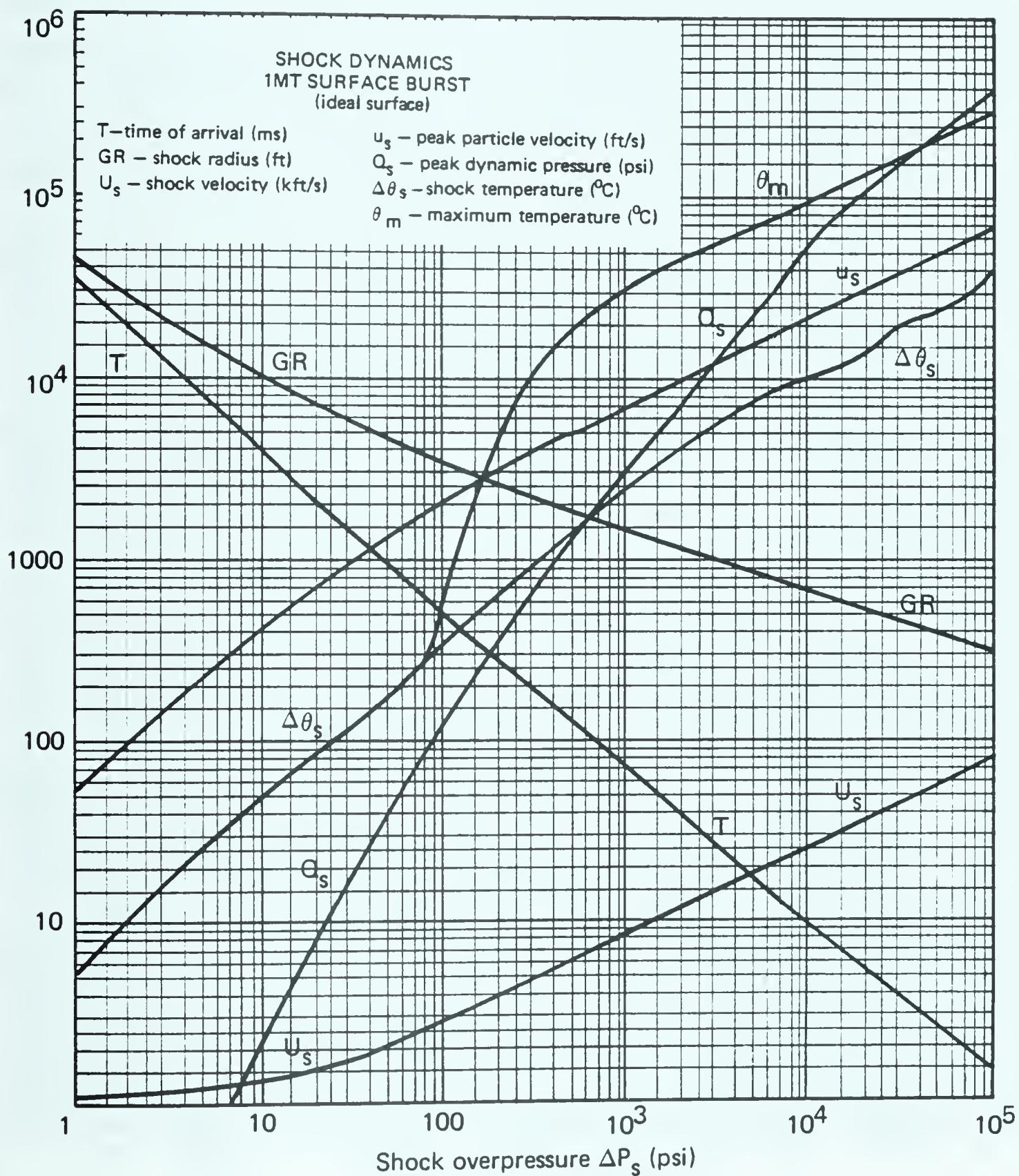


Figure 31. Blast parameters for 1-MT surface burst.

SECTION 4
BLAST PARAMETERS AS FUNCTIONS OF BURST HEIGHT

PEAK OVERPRESSURE VERSUS SCALED BURST HEIGHT AND SCALED RANGE.

An earlier fit to the peak overpressure HOB contours was valid up to pressures of 10,000 psi [Speicher and Brode, 1980b]. It was subsequently extended to much higher pressures [Speicher and Brode, 1984a]. The latter fit was illustrated to 3,000,000 psi, but the basis for that fit was restricted, at the time, to the old data (valid to 10,000 psi), to a calculation near zero burst height, which is called BM-3 [Pyatt, 1983], and to some low-altitude HULL calculations at 25 and 50 ft scaled height of burst (SHOB) [Pyatt and Wilkins, 1983]. Interpolation for bursts between zero and 200-ft SHOB was modestly successful, as borne out by comparison with results of subsequent calculations [Fry, Kamath, and Book 1985; Fry, 1986]. Those results, however, were not in as good agreement with some later HULL calculations at the low-burst altitudes [Pyatt, 1985]. Figures 32 through 40 span the range of the current fit, showing contours of constant peak overpressure plotted against scaled burst height and scaled ground range. Comparisons with calculation results from the Naval Research Laboratory (NRL), Washington, D.C., and S-Cubed, La Jolla, California, are plotted in Figs. 32 through 36. In those figures, the lines that indicate the onset of Mach reflection (X_m) and the locus of points where the second peak equals the first peak (X_e) are sometimes shown. Those curves are approximated analytically (along with the time dependence of pressure) in Eq. (63). For NRL calculations, agreement, in most cases, is within 20 percent on peak overpressure.

The fit for peak overpressure takes the form:

$$\Delta P_s = \frac{10.47}{r^{a(z)}} + \frac{b(z)}{r^{c(z)}} + \frac{d(z) \times e(z)}{1 + f(z) \times r^{g(z)}} + h(z, r, y) + \frac{j(y)}{r^{k(y)}} \quad \text{psi}, \quad (62)$$

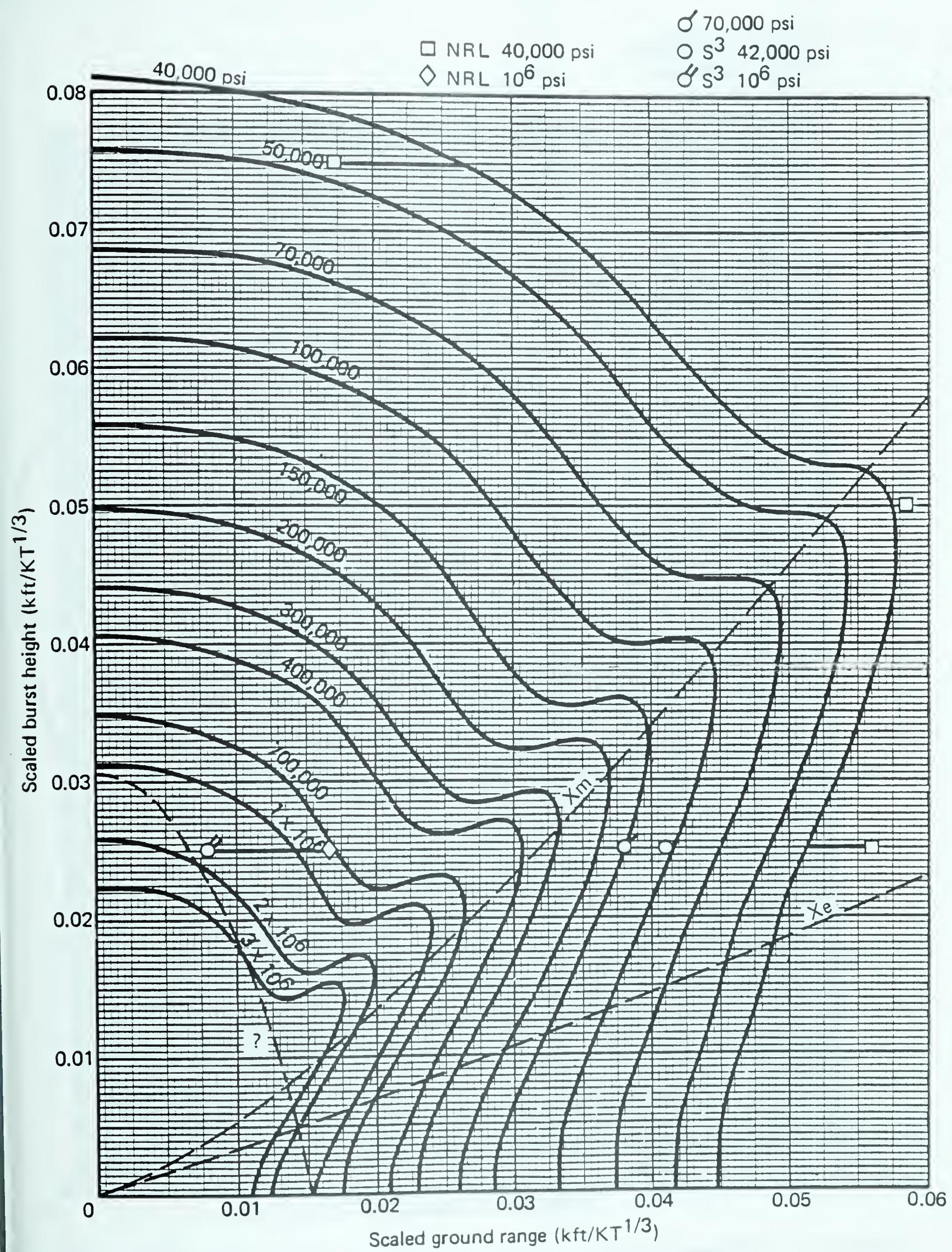


Figure 32. Ultra-high peak overpressure HOB versus ground range contours, scaled to 1 KT.

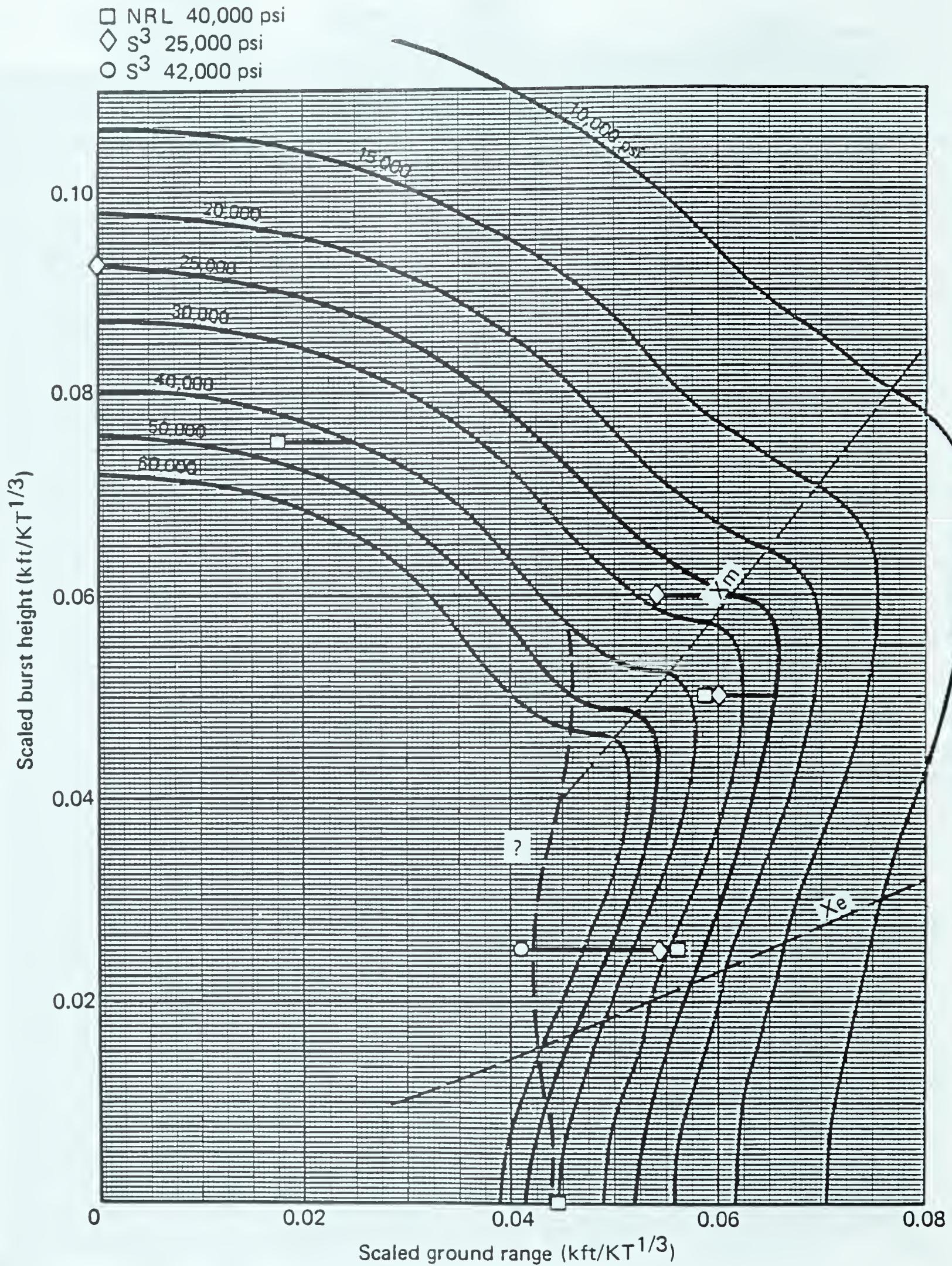


Figure 33. Extremely high peak overpressure HOB versus ground range contours scaled to 1 KT.

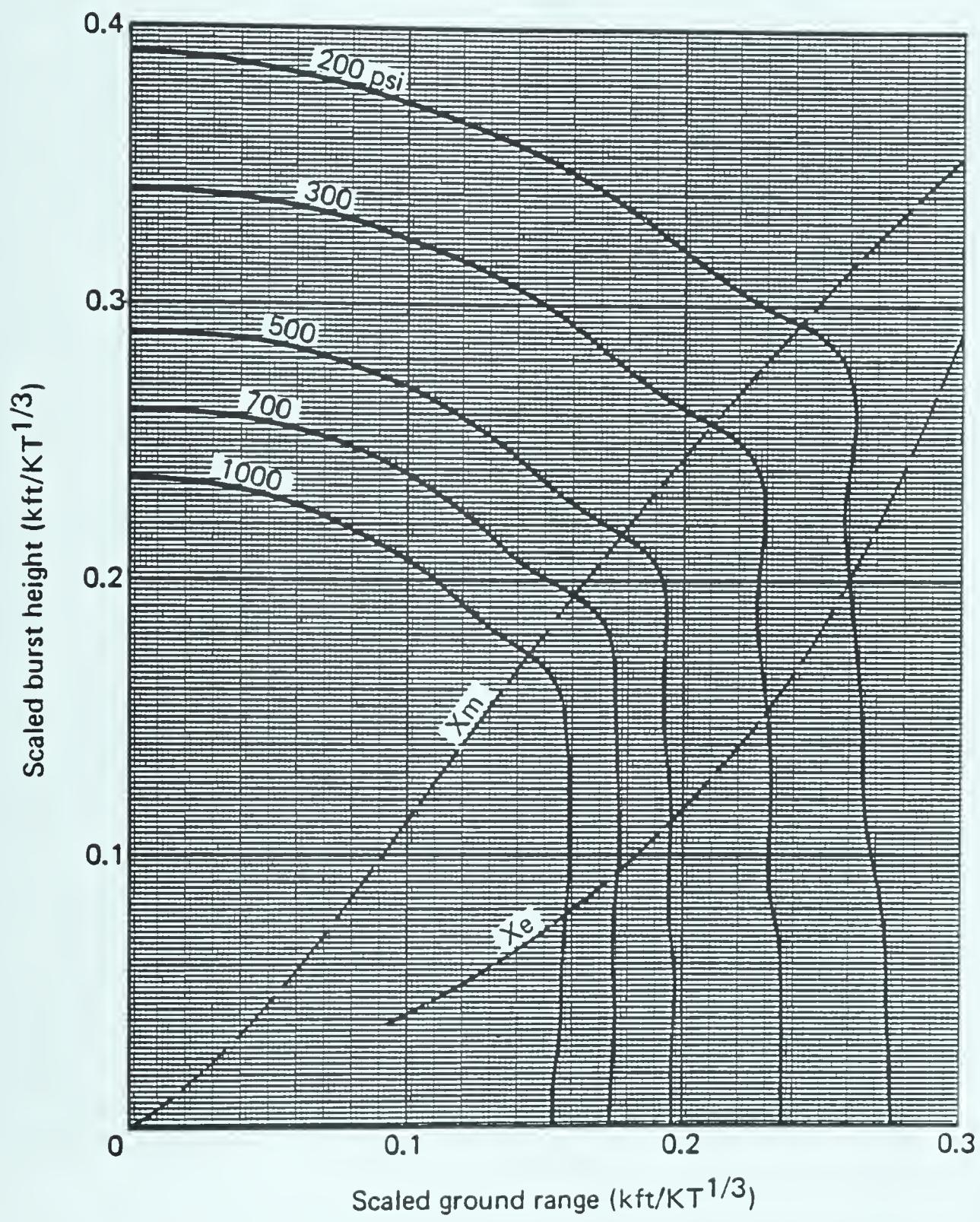


Figure 36. Intermediate high peak overpressure burst height versus ground range contours, scaled to 1 KT.

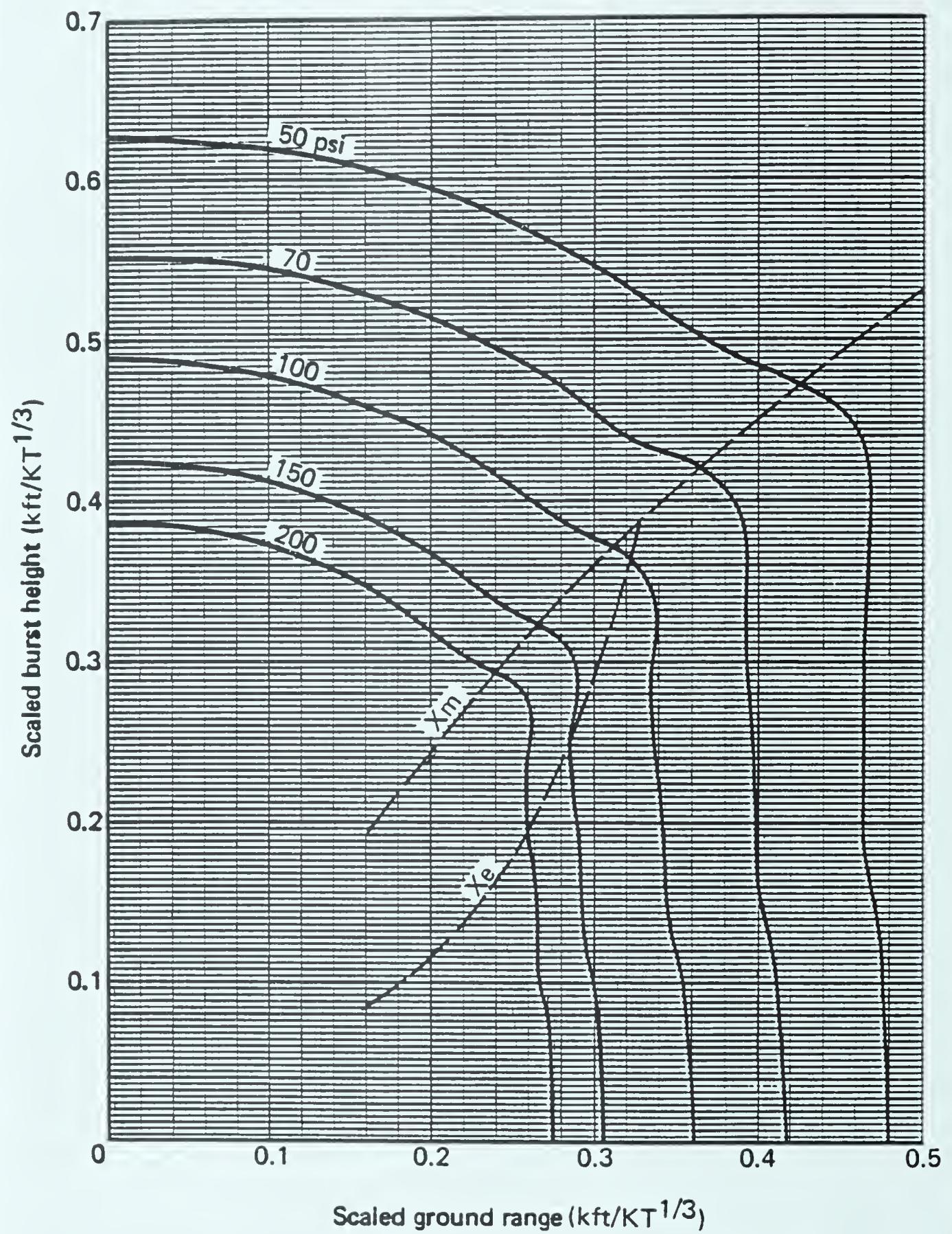


Figure 37. Intermediate peak overpressure burst height versus ground range contours, scaled to 1 KT.

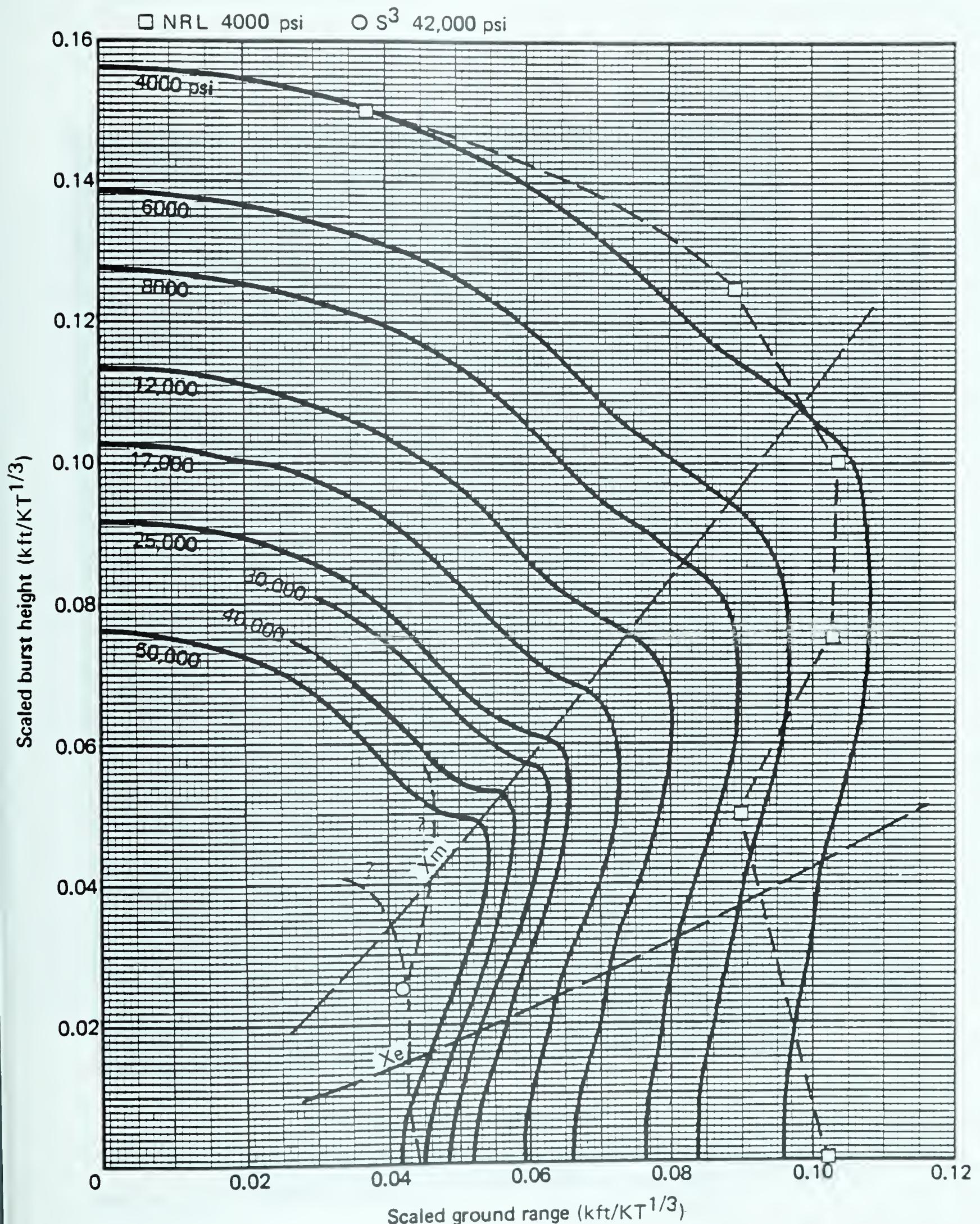


Figure 34. Very high peak overpressure HOB versus ground range contours, scaled to 1 KT.

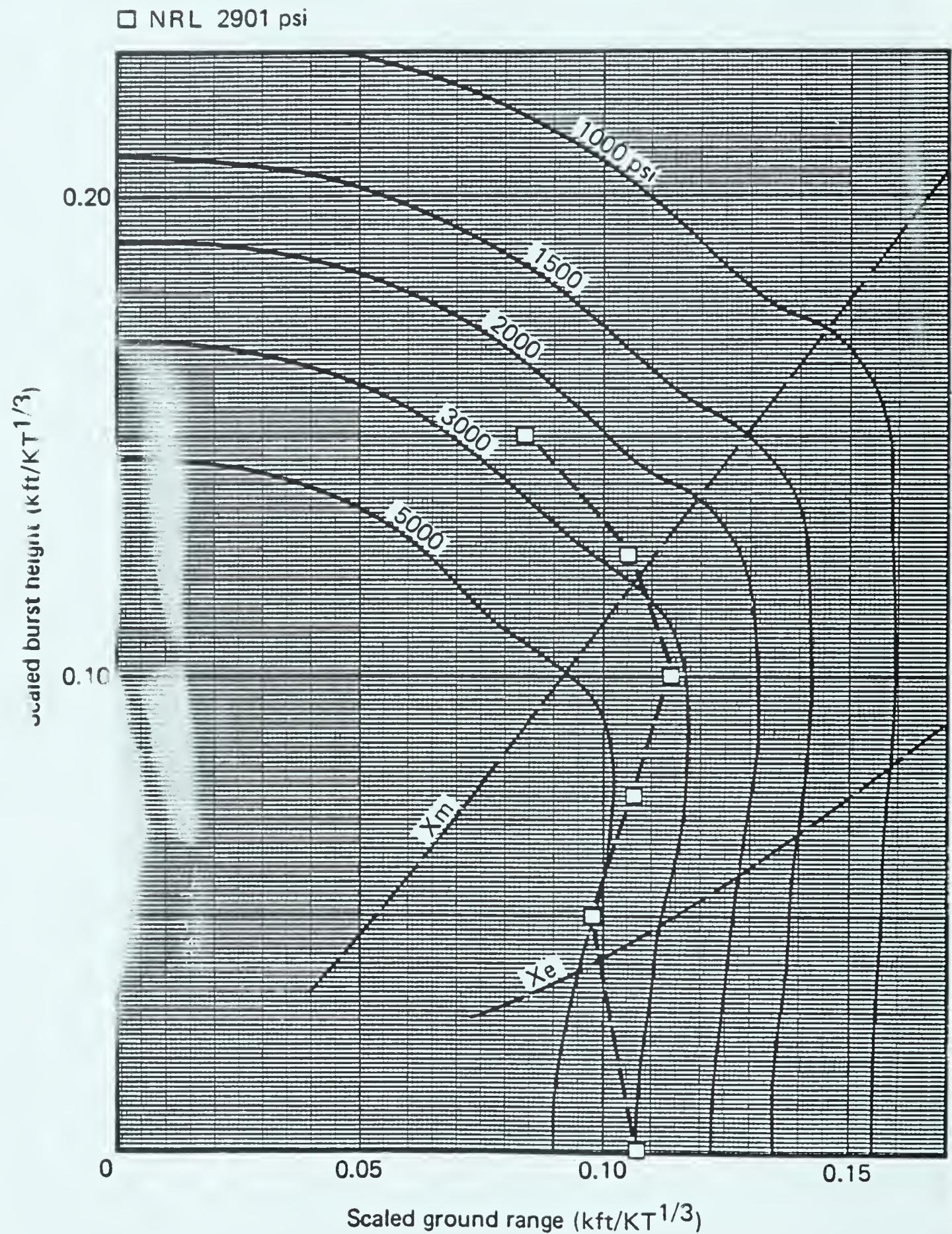


Figure 35. High peak overpressure HOB versus ground range contours, scaled to 1 KT.

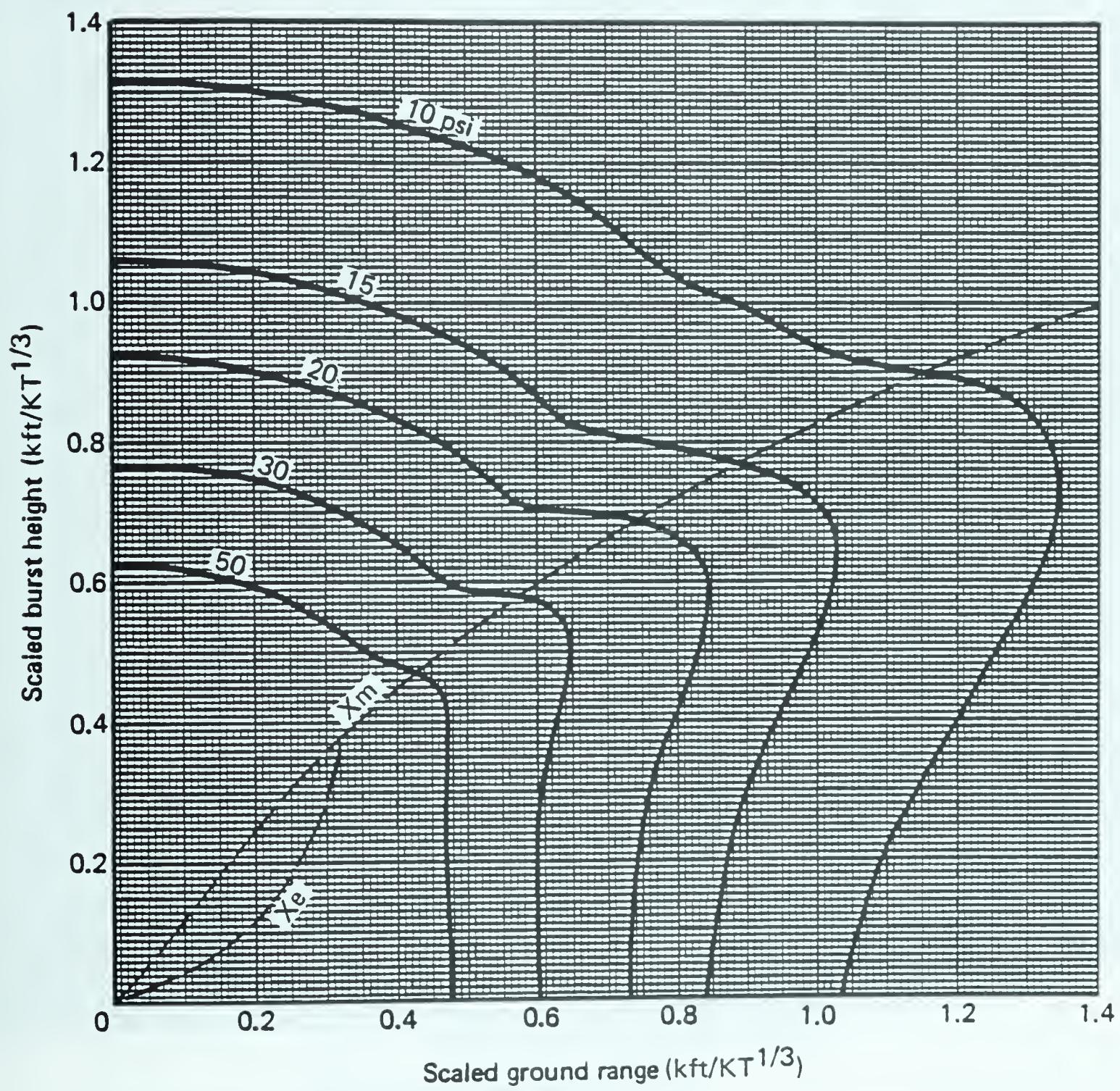


Figure 38. Intermediate low peak overpressure burst height versus ground range contours, scaled to 1 KT.

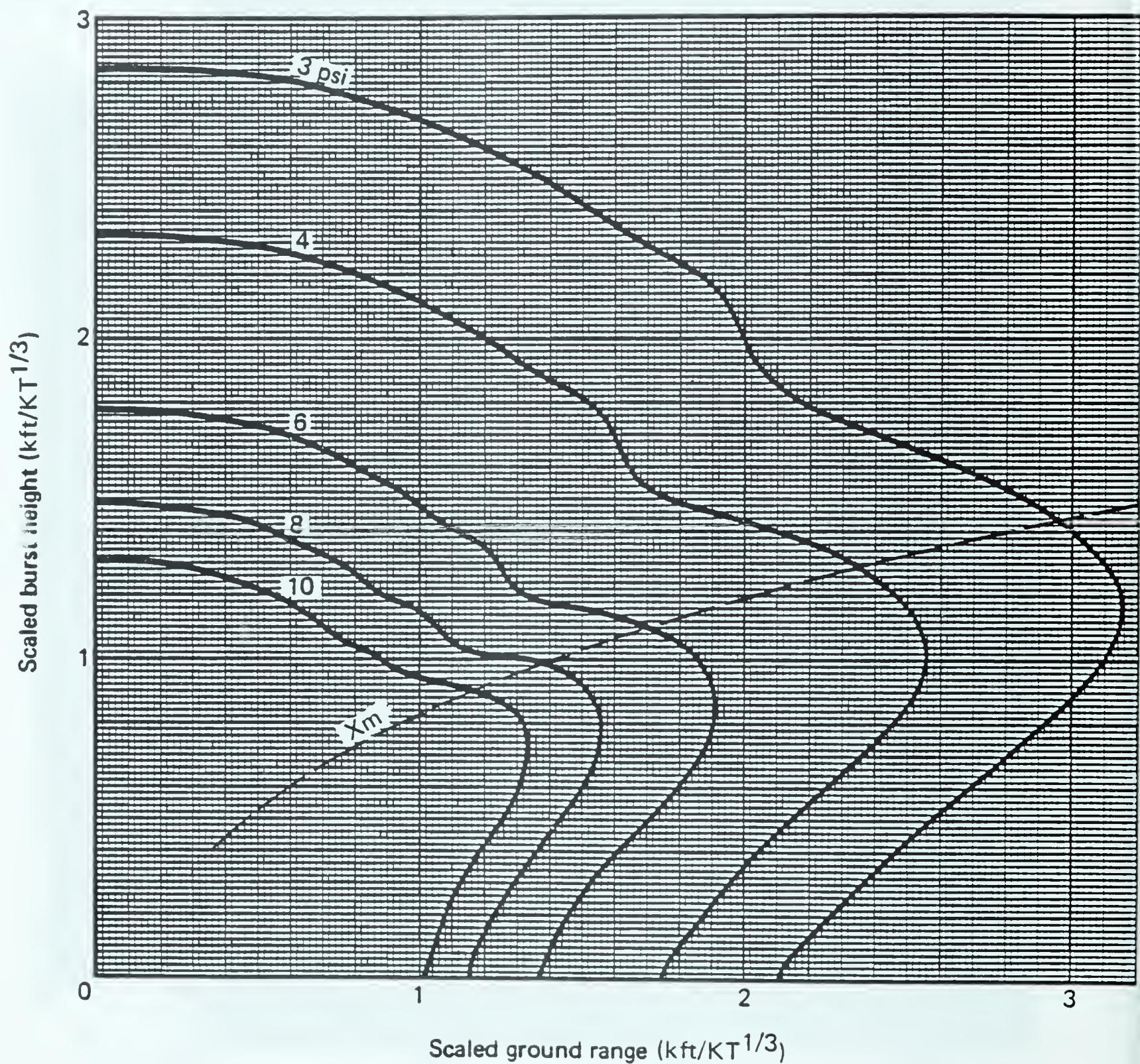


Figure 39. Low peak overpressure burst height versus ground range contours, scaled to 1 KT.

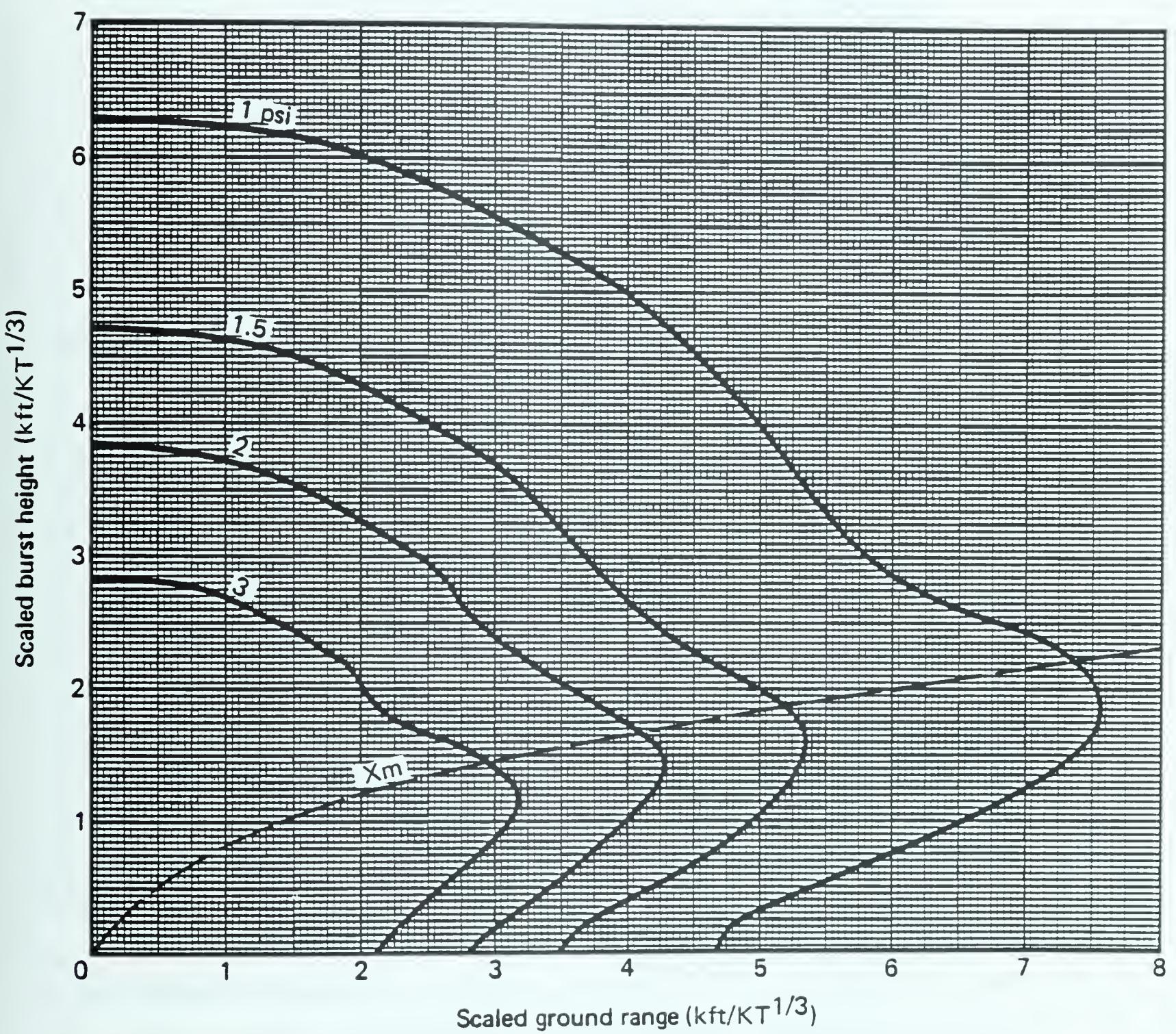


Figure 40. Very low peak overpressure burst height versus ground range contours, scaled to 1 KT.

where $r \equiv$ scaled slant range in kilofeet per cube-root kiloton
 $= \sqrt{x^2 + y^2}$,
 $x \equiv$ scaled ground range in kilofeet per cube-root kiloton, or
 $GR/m/1000$,
 $y \equiv$ scaled burst height in kilofeet per cube-root kiloton, or
 $H/m/1000$,
 $m \equiv W^{1/3}$ in cube-root kilotons (the scale factor),
 $W \equiv$ yield in kilotons,
 $GR \equiv$ ground range in feet,
 $H \equiv$ burst height in feet,
 $z \equiv H/GR = y/x$,

and where

$$a(z) = 1.22 - \frac{3.908z^2}{1 + 810.2z^5},$$

$$b(z) = 2.321 + \frac{6.195z^{18}}{1 + 1.113z^{18}} - \frac{0.03831z^{17}}{1 + 0.02415z^{17}} + \frac{0.6692}{1 + 4164z^8},$$

$$c(z) = 4.153 - \frac{1.149z^{18}}{1 + 1.641z^{18}} - \frac{1.1}{1 + 2.771z^{2.5}},$$

$$d(z) = -4.166 + \frac{25.76z^{1.75}}{1 + 1.382z^{18}} + \frac{8.257z}{1 + 3.219z},$$

$$e(z) = 1 - \frac{0.004642z^{18}}{1 + 0.003886z^{18}},$$

$$f(z) = 0.6096 + \frac{2.879z^{9.25}}{1 + 2.359z^{14.5}} - \frac{17.15z^2}{1 + 71.66z^3},$$

$$g(z) = 1.83 + \frac{5.361z^2}{1 + 0.3139z^6},$$

$$h(z, r, y) = \frac{8.808z^{1.5}}{1 + 154.5z^{3.5}} - \frac{0.2905 + 64.67z^5}{1 + 441.5z^5} - \frac{1.389z}{1 + 49.03z^5}$$

$$+ \frac{1.094r^2}{(781.2 - 123.4r + 37.98r^{1.5} + r^2)(1 + 2y)},$$

$$j(y) = \frac{0.000629y^4}{3.493 \times 10^{-9} + y^4} - \frac{2.67y^2}{1 + 10^7 y^{4.3}},$$

$$k(y) = 5.18 + \frac{0.2803y^{3.5}}{3.788 \times 10^{-6} + y^4}.$$

OVERPRESSURE VERSUS TIME, SCALED RANGE, AND BURST HEIGHT.

An earlier time-history fit, published by Speicher and Brode [1981], included the double peaks in the high overpressure reflection region of the HOB-range map (Fig. 41),* but was limited to peak overpressures less than 10,000 psi and more than 1 psi (or to 0.1 psi for a surface burst). Four sources formed the basis of that fit: (1) results of a calculation at 200 ft SHOB [McNamara, Jordano, and Lewis, 1977], (2) a composite free-air blast, 1-KT "standard" [Needham, Havens, and Knauth, 1975], (3) the results of a large-charge, high-explosive (HE) test series called DIPOLE WEST [Reisler, 1980], and (4) tests with 8-lb spheres of PBX-9404 (plastic bonded explosive) conducted and analyzed by Carpenter [1976], which concentrated on the higher overpressure regions of the early Mach reflections (100 to 2500 psi).

The fit reported here includes a recent extension to much higher overpressures [Speicher and Brode, 1984b]. It is unlikely that the fit will be useful at overpressures higher than 200,000 psi, because radiation transport is a dominant factor that near the burst. In a 1-MT surface burst, radiation dominates the fireball expansion out to a radius of about 250 ft (until the pressure drops to approximately 200,000 psi). The shock wave is not fully developed prior to that.

*In Fig. 41, the line depicting the locus of points where the second peak is just equal to the first peak (X_e) was first drawn by Carpenter [1976].

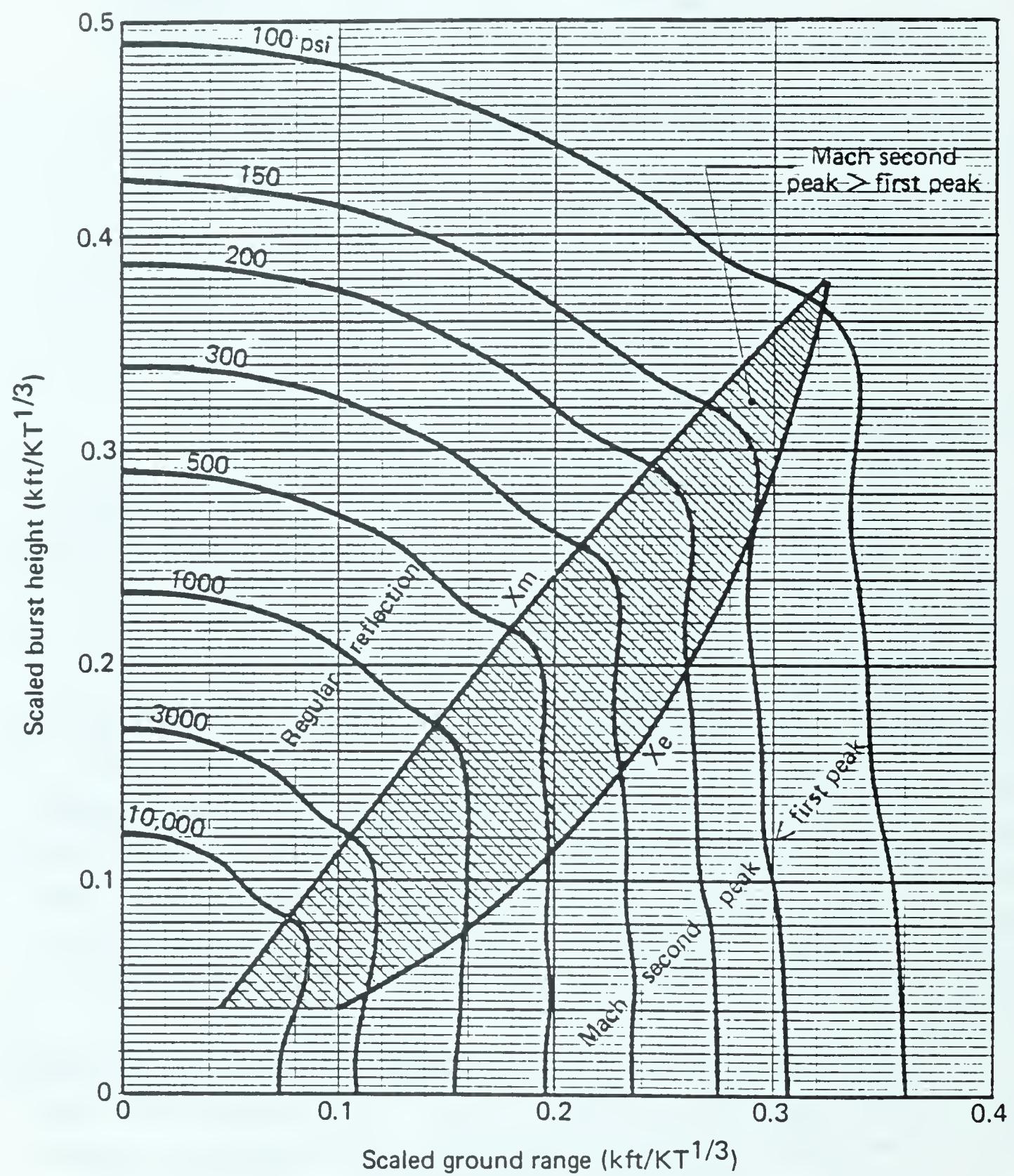


Figure 41. High peak overpressures versus scaled burst height and scaled ground range (ideal surface).

Although reflected pressures can rise above the incident shock pressure, much of the energy of an incident shock of 200,000 psi, on reflection, radiates away, allowing the density to rise without significantly altering reflected overpressure.

The changes to the fit given here were modeled after the close-in results of the surface burst BM-3 calculation [Pyatt, 1983] and HULL calculations at 25 and 50 ft SHOB [Pyatt and Wilkins, 1983]. However, the fit does not correspond well with calculations of the early Mach reflection; it predicts too great an impulse around the second peak. At an SHOB of 25 ft and scaled ground ranges of 30 to 100 ft, the partial impulse to 2 ms at 1 KT is high by as much as a factor of 2. That partial impulse correlates closely with blast damage to hardened surface-flush structures such as missile silos, so the error can have serious consequences. This section of the fit is being modified, and copies of the improved form will be distributed later. Elsewhere (at the surface or at SHOBs above 100 ft and scaled ground ranges beyond 100 ft), the fit is still quite good.

The time-history of overpressure at various ranges (X) and burst heights (Y) can be expressed as

$$\begin{aligned}\Delta P(X, Y, t) &= \Delta P_s (1 + a)(bv + c) \quad \text{for } X \geq X_m \text{ and } Y \leq 380 \text{ ft/KT}^{1/3}, \\ &= \Delta P_s \times b \quad \text{for } X < X_m \text{ or } Y > 380 \text{ ft/KT}^{1/3}.\end{aligned}\tag{63}$$

where ΔP ≡ overpressure in pounds per square inch,
 X ≡ scaled ground range in feet per cube-root kiloton,
or GR/m,
GR ≡ ground range in feet,
m ≡ $W^{1/3}$ in cube-root kilotons,
W ≡ yield in kilotons,

Y = scaled burst height in feet per cube-root kiloton, or
 H/m ,

H = height of burst in feet,

t = time after detonation in milliseconds,

ΔP_s = peak overpressure in pounds per square inch
[see Eq. (62)],

$$a = (d - 1) \left(1 - \frac{K^{20}}{1 + K^{20}} \right),$$

$$d = 0.23 + \frac{0.583Y^2}{26,667 + Y^2} + 0.27K + \left(0.5 - \frac{0.583Y^2}{26,667 + Y^2} \right) (K)^{d_2},$$

$$d_2 = 2.99 + \frac{31,240(Y/100)^{9.86}}{1 + 15,530(Y/100)^{9.87}},$$

$$K = \left| \frac{X_e - X_m}{X_e - X_m} \right|, \quad ,$$

X_m = onset of Mach reflection locus, scaled, in feet per cube-root kiloton,

$$= \frac{170Y}{1 + 60Y^{0.25}} + 2.89(Y/100)^{2.5},$$

X_e = locus of points where second peak equals first peak,
scaled, in feet per cube-root kiloton,

$$= \frac{3.039Y}{1 + 0.0067Y},$$

$$b = \left[f \left(\frac{\tau}{\sigma} \right)^g + (1 - f) \left(\frac{\tau}{\sigma} \right)^h \right] \left[1 - \frac{(\sigma - \tau)}{D} \right],$$

τ = scaled time of arrival in milliseconds per cube-root kiloton, based on Eq. (41),

$$= u(r) \quad \text{for } X \leq X_m,$$

$$= u(r_m) + w(r) - w(r_m) \quad \text{for } X > X_m,$$

$$u(r) = \frac{(0.543 - 21.8r + 386r^2 + 2383r^3)r^8}{- 2.99 \times 10^{-14} - 1.91 \times 10^{-10}r^2 + 1.032 \times 10^{-6}r^4 - 4.43 \times 10^{-6}r^6 + (1.028 + 2.087r + 2.69r^2)r^8},$$

r = scaled range in kilofeet per cube-root kiloton
 $= (X^2 + Y^2)^{1/2}/1000$

$$w(r_0) = \frac{(1.086 - 34.605r + 486.3r^2 + 2383r^3)r^8}{3.0137 \times 10^{-13} - 1.2128 \times 10^{-9}r^2 + 4.128 \times 10^{-6}r^4 - 1.116 \times 10^{-5}r^6 + (1.632 + 2.629r + 2.69r^2)r^8},$$

D = duration of positive phase in milliseconds,

$$= \left(\frac{1,640,700 + 24,629\tau + 416.15\tau^2}{10,880 + 619.76\tau + \tau^2} \right) \left[0.4 + \frac{0.001204\tau^{1.5}}{1 + 0.001559\tau^{1.5}} \right. \\ \left. + \left(0.6126 + \frac{0.5486\tau^{0.25}}{1 + 0.00357\tau^{1.5}} - \frac{3.47\tau^{0.637}}{1 + 5.696\tau^{0.645}} \right) s_2 \right],$$

$$s_2 = 1 - \frac{15.18(Y/100)^{3.5}}{1 + 15.18(Y/100)^{3.5}} - \left[\frac{0.02441(Y/10^6)^2}{1 + 9000(Y/100)^7} \right] \\ \times \left[\frac{10^{10}}{0.441 + (X/100)^{10}} \right],$$

$$f = \left(\frac{0.01477\tau^{0.75}}{1 + 0.005836\tau} + \frac{7.402 \times 10^{-5}\tau^{2.5}}{1 + 1.429 \times 10^{-8}\tau^{4.75}} - 0.216 \right) \times (s) + 0.7076$$

$$- \frac{3.077 \times 10^{-5}\tau^3}{1 + 4.367 \times 10^{-5}\tau^3} + f_2 - \left(0.452 - \frac{9.94 \times 10^{-7}X^{4.13}}{1 + 2.1868 \times 10^{-6}X^{4.13}} \right)$$

$$\times \left(1 - \frac{0.00015397Y^{4.3}}{1 + 0.00015397Y^{4.3}} \right),$$

$$s = 1 - \frac{1100(Y/100)^7}{1 + 1100(Y/100)^7} - \left[\frac{2.441 \times 10^{-14}Y^2}{1 + 9000(Y/100)^7} \right]$$

$$\times \left[\frac{10^{10}}{0.441 + (X/100)^{10}} \right],$$

$$f_2 = \left[0.445 - \frac{5.44r^{1.02}}{(1 + 100,000r^{5.84})} + \frac{7.571z^{7.15}}{(1 + 5.135z^{12.9})} \right.$$

$$\left. - \frac{8.07z^{7.31}}{(1 + 5.583z^{12.23})} \right] \left[\frac{0.4530(Y/10)^{1.26}}{1 + 0.03096(Y/10)^{3.12}} \right]$$

$$\times \left[1 - \frac{0.000019\tau^8}{1 + 0.000019\tau^8} \right],$$

g = early-time decay power,

$$= 10 + \left(77.58 - \frac{64.99\tau^{0.125}}{1 + 0.04348\tau^{0.5}} \right) \times (s),$$

$$h = 3.003 + \frac{0.05601\tau}{1 + 1.473 \times 10^{-9} \tau^5}$$

$$+ \left(\frac{0.01769\tau}{1 + 3.207 \times 10^{-10} \tau^{4.25}} - \frac{0.03209\tau^{1.25}}{1 + 9.914 \times 10^{-8} \tau^4} - 1.6 \right)$$

$$\times (s) - \frac{0.1966\tau^{1.22}}{1 + 0.767\tau^{1.22}},$$

$$v = 1 + \left[\frac{0.003744(Y/10)^{5.185}}{1 + 0.004684(Y/10)^{4.189}} + \frac{0.004755(Y/10)^{8.049}}{1 + 0.003444(Y/10)^{7.497}} \right.$$

$$\left. - \frac{0.04852(Y/10)^{3.423}}{1 + 0.03038(Y/10)^{2.538}} \right] \left(\frac{j^3}{6.13 + j^3} \right) \left(\frac{1}{1 + 9.23 \times K^2} \right),$$

$$c = \left\{ \frac{\left[1.04 - \frac{0.02409(X/100)^4}{1 + 0.02317(X/100)^4} \right] \times j^7}{(1 + a)(1 + 0.923j^{8.5})} \right\} [c_2 + (1 - c_2) \times \left(1 - \frac{0.09K^{2.5}}{1 + 0.09K^{2.5}} \right)] \times (c_3) \times \left\{ 1 - \left[\frac{(\sigma - \tau)}{D} \right]^8 \right\},$$

$$c_2 = \frac{23,000(Y/100)^9}{1 + 23,000(Y/100)^9},$$

$$c_3 = 1 + \left\{ \left(\frac{1.094K^{0.738}}{1 + 3.687K^{2.63}} \right) \left[1 - \frac{83.01(Y/100)^{6.5}}{1 + 172.3(Y/100)^{6.04}} \right] - 0.15 \right\}$$

$$\times \left(\frac{1}{1 + 0.5089K^{13}} \right),$$

j = ratio of time after TOA to time to second peak after TOA,

$$= \frac{11,860(\sigma - \tau)}{Y(X - X_m)^{1.25}}, \text{ or } 200 \text{ (whichever is less).}$$

In the above definitions for Eq. (63), the expression for free-air time of arrival u is the same as Eq. (42), and the scaling factor for it is $m = 1$; the expression w is also the same as Eq. (42), but with $m = 2^{1/3}$.

Examples showing how successful the fit is for Eqs. (62) and (63) are provided in Figs. 42 through 87. In those figures, the fit is compared with six sources of "data": the S-Cubed [Pyatt, 1983] surface-burst calculation (BM-3) scaled to 1 KT (Figs. 42 through 49); the DNA 1-KT standard [Needham and Crepeau, 1981] (Figs. 50 through 58); the 25 and 50 ft SHOB S-Cubed [Pyatt, 1983] calculations (Figs. 59 through 70); the tests of PBX-9404 8-1b HE spheres [Carpenter, 1976] (Figs. 71 and 72); the HULL calculation for 60-m SHOB [McNamara, Jordano, and Lewis, 1977] (Figs. 73 and 74); and the DIPOLE WEST data [Reisler, 1980] (Figs. 75 and 76).

The plots display overpressure versus time and impulse versus time. The diversity of data sources and the extensive range of the fit mitigate against its being everywhere close. However, the inherent uncertainty and expected variation in actual pressure histories and impulses are far larger than the 10 to 20 percent disparities between this analytic fit and the calculation results shown in these comparison plots. (Average discrepancies between fit and calculated pressures are of the order of only 4 percent).

The simple fit for positive phase overpressure impulse in a surface burst [Eq. (48)] predicts somewhat higher values than those for the integral of the time-history fit for zero burst height [time integral of Eqs. (62) and (63)]. The latter, while much more complex, was fit to the BM-3 cratering calculation impulses [Pyatt, 1983] in the close-in range (scaled ground range between 25 and 100 ft, or peak pressure between 1500 and 150,000 psi). The lower peak overpressure in the detailed calculations may not be correct, although further calculations are being made to verify that region of the BM-3 calculation. It has been suggested that the lower impulses may be due to the quenching effect of cratered material ejected into the fireball.

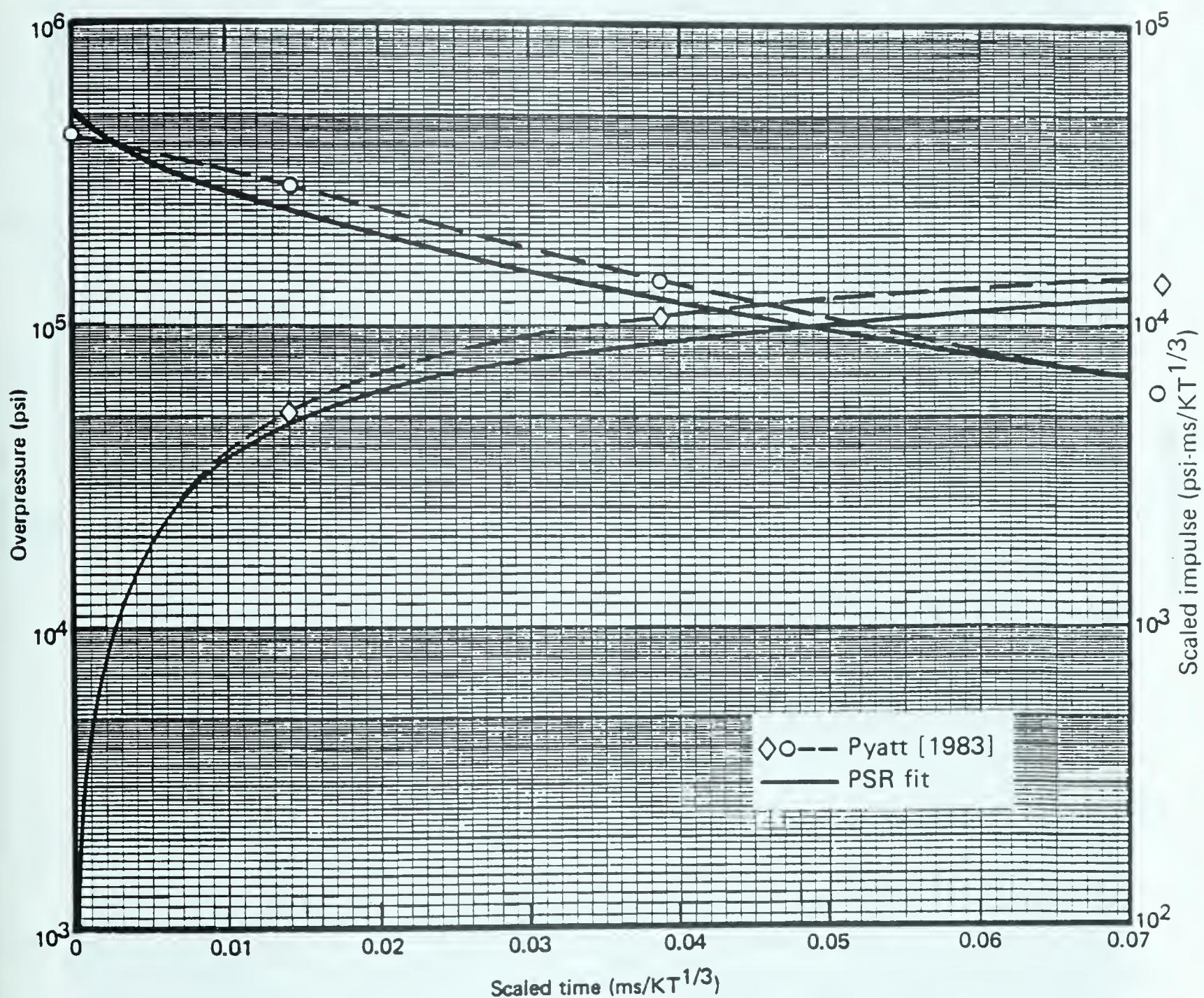


Figure 42. Fit compared to S-Cubed calculation (scaled): overpressure and scaled partial impulse versus scaled time to 0.07 ms, for $\Delta P_s \approx 548,300$ psi, $y = 0$, $x = 18.896$ ft/ $KT^{1/3}$.

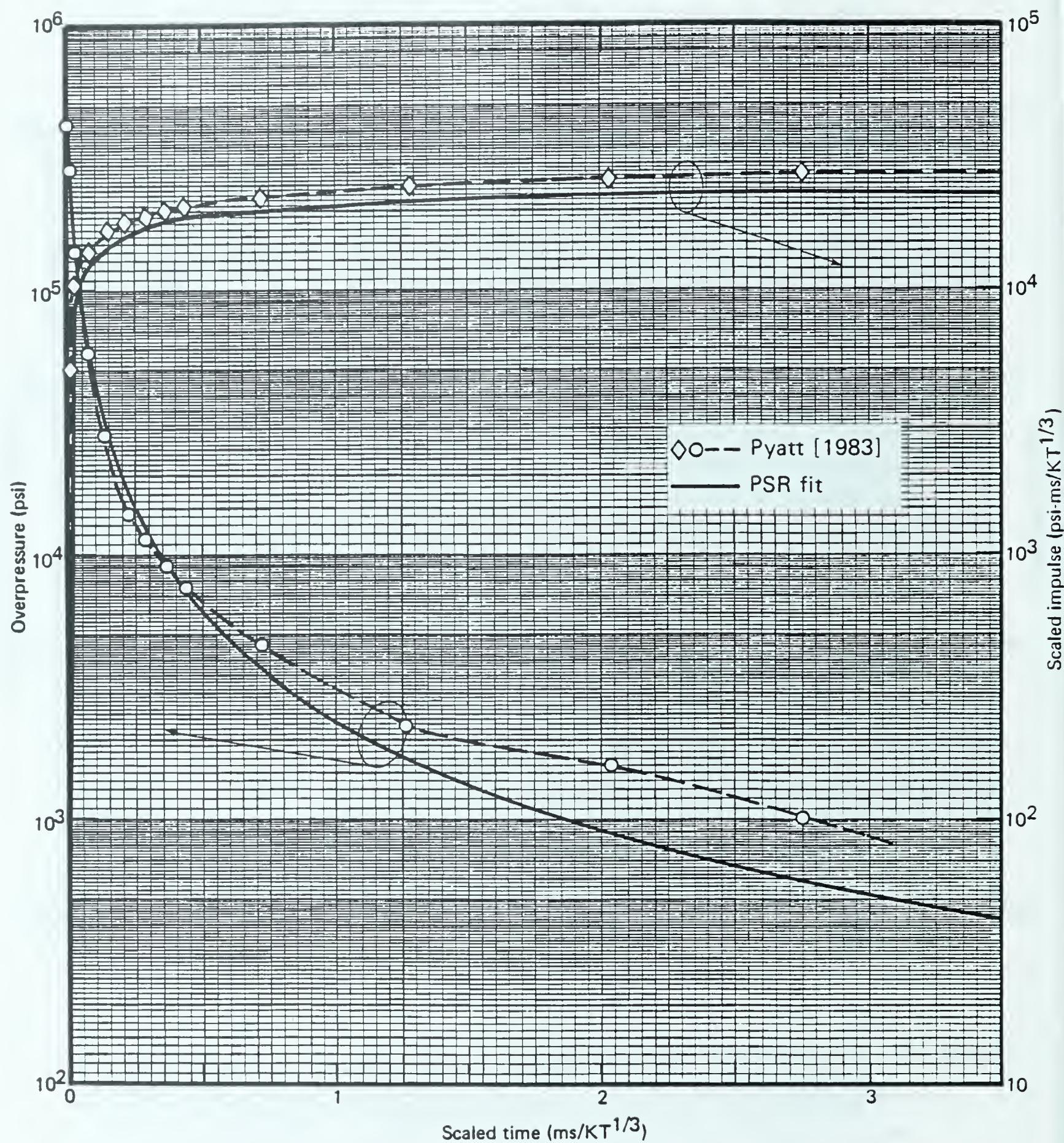


Figure 43. Fit compared to S-Cubed calculation (scaled): overpressure and scaled partial impulse versus scaled time to 3.5 ms, for $\Delta P_S \approx 548,300$ psi, $y = 0$, $x = 18.896$ ft/ $KT^{1/3}$.

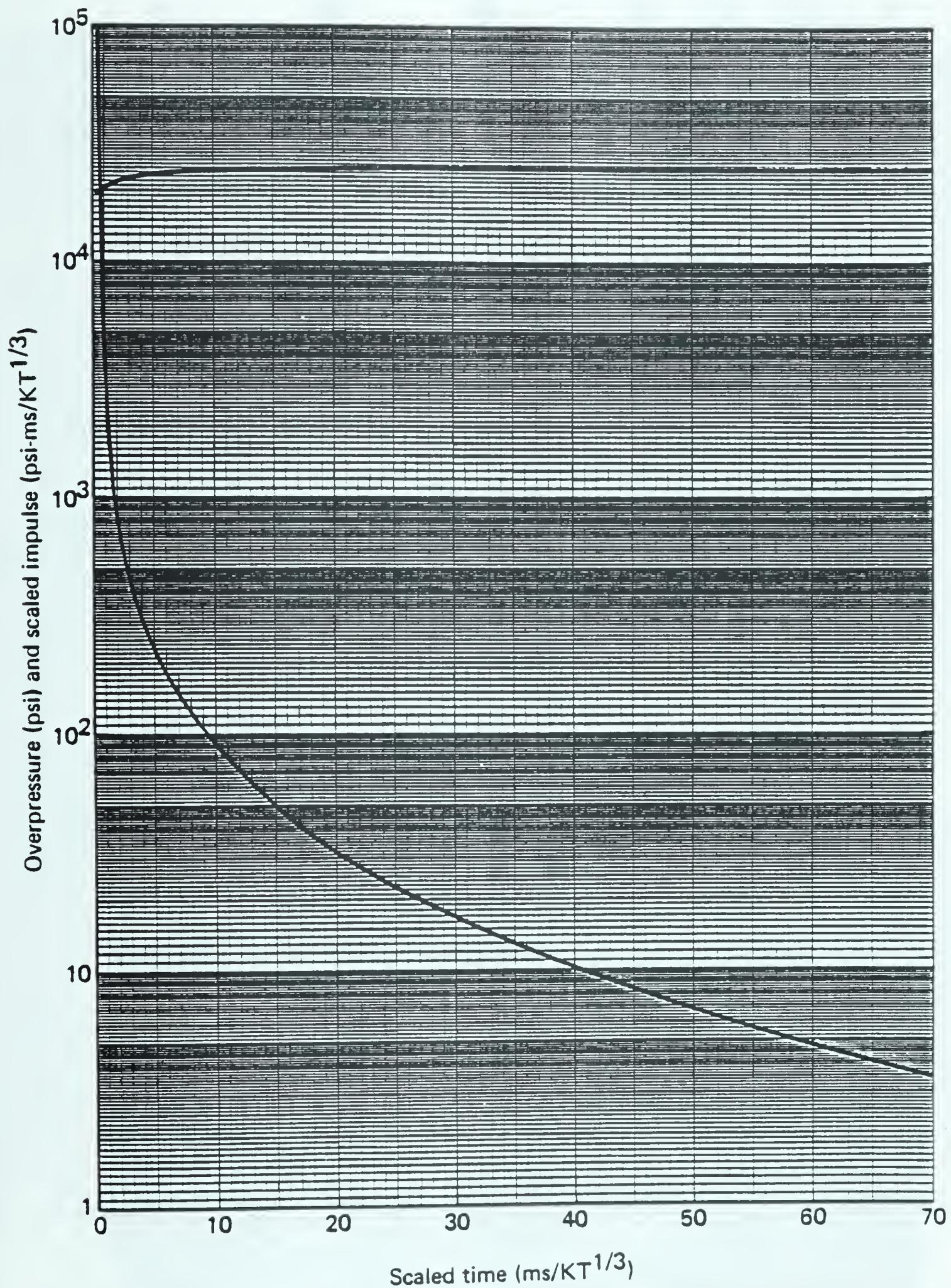


Figure 44. Fit for overpressure and scaled partial impulse versus scaled time to 70 ms, for $\Delta P_s \approx 548,300$ psi, $y = 0$, $x = 18.896$ ft/ $KT^{1/3}$.

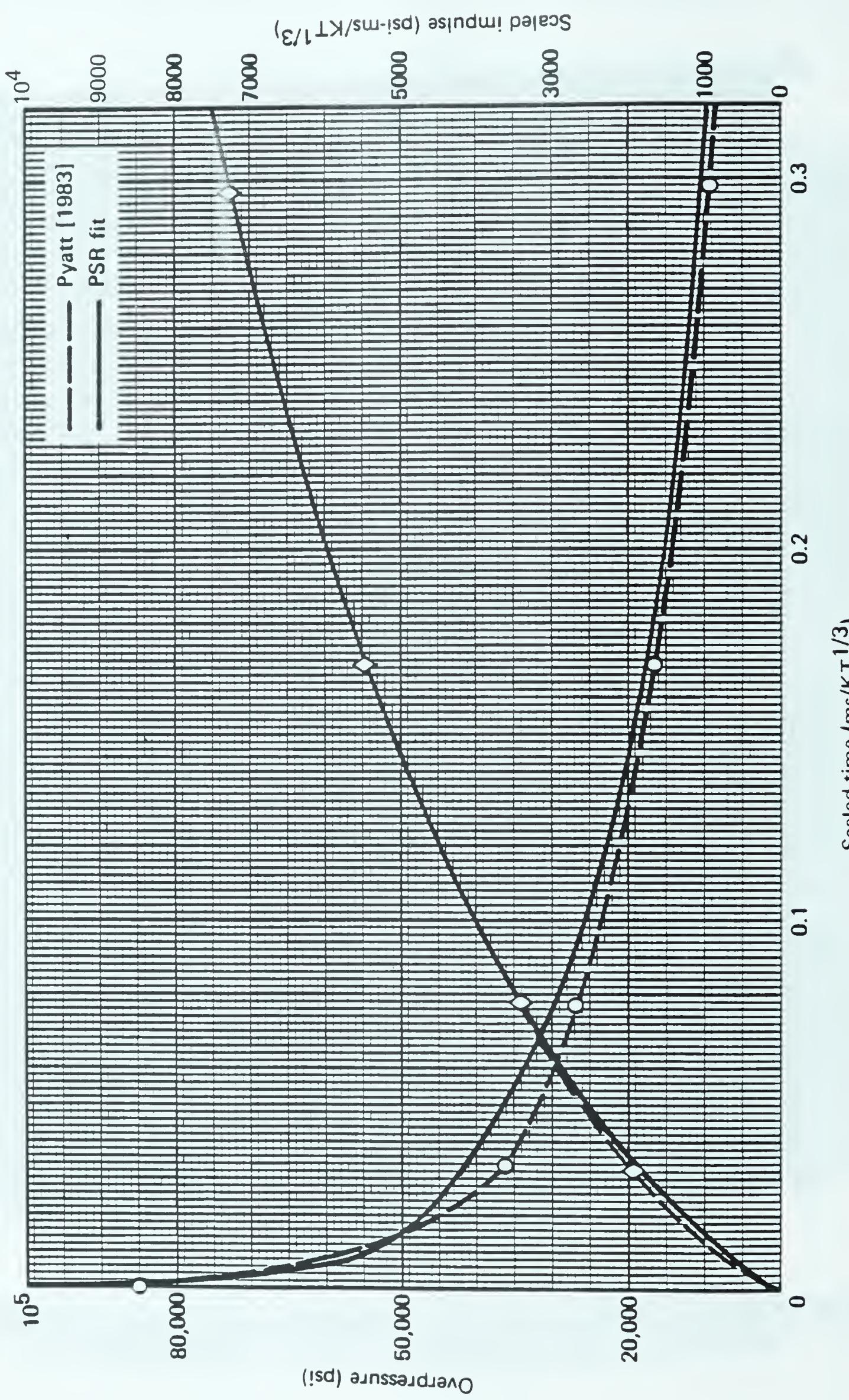


Figure 45. Fit compared to S-Cubed calculation (scaled): overpressure and scaled impulse versus scaled time to 0.32 ms, for $\Delta P_s \approx 99,740$ psi, $y = 0$, $x = 33.068$ ft/KT^{1/3}.

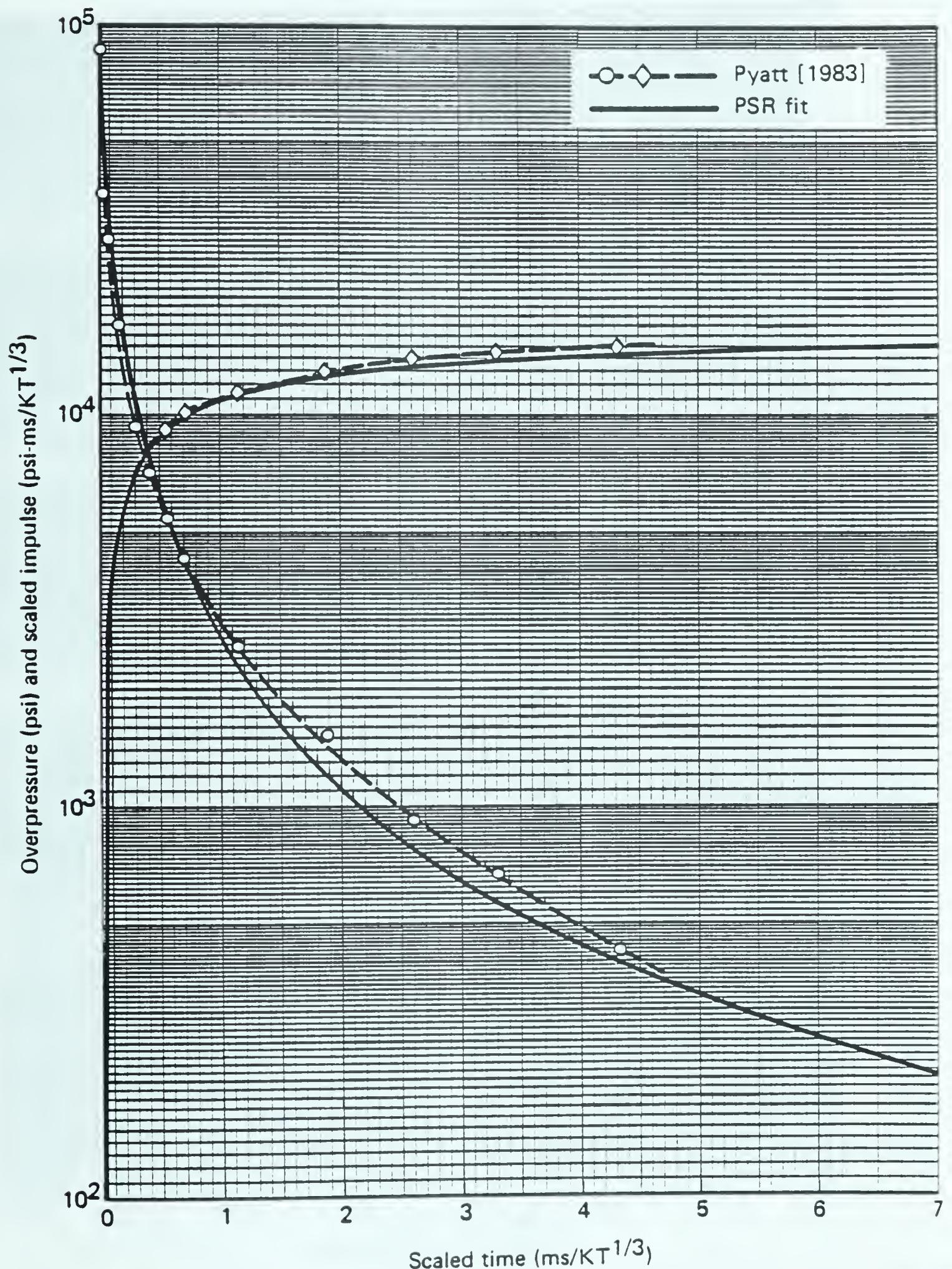


Figure 46. Fit compared to S-Cubed calculation (scaled): overpressure and scaled impulse versus scaled time to 7 ms, for $\Delta P_s \approx 99,740$ psi, $y = 0$, $x = 33.068$ ft/ $KT^{1/3}$.

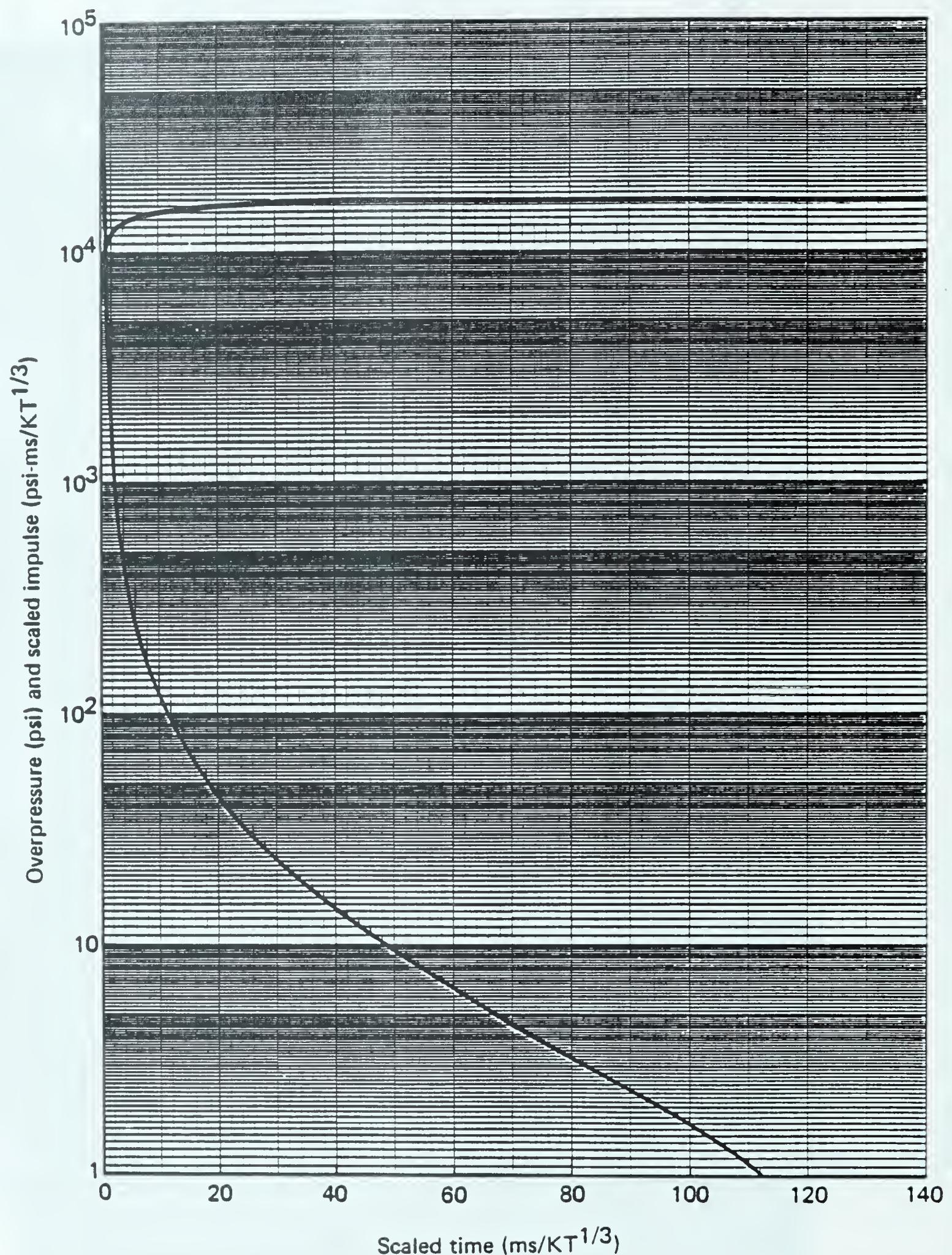


Figure 47. Fit for overpressure and scaled impulse versus scaled time to 140 ms, for $\Delta P_s \approx 99,740$ psi, $y = 0$, $x = 33.068$ ft/KT^{1/3}.

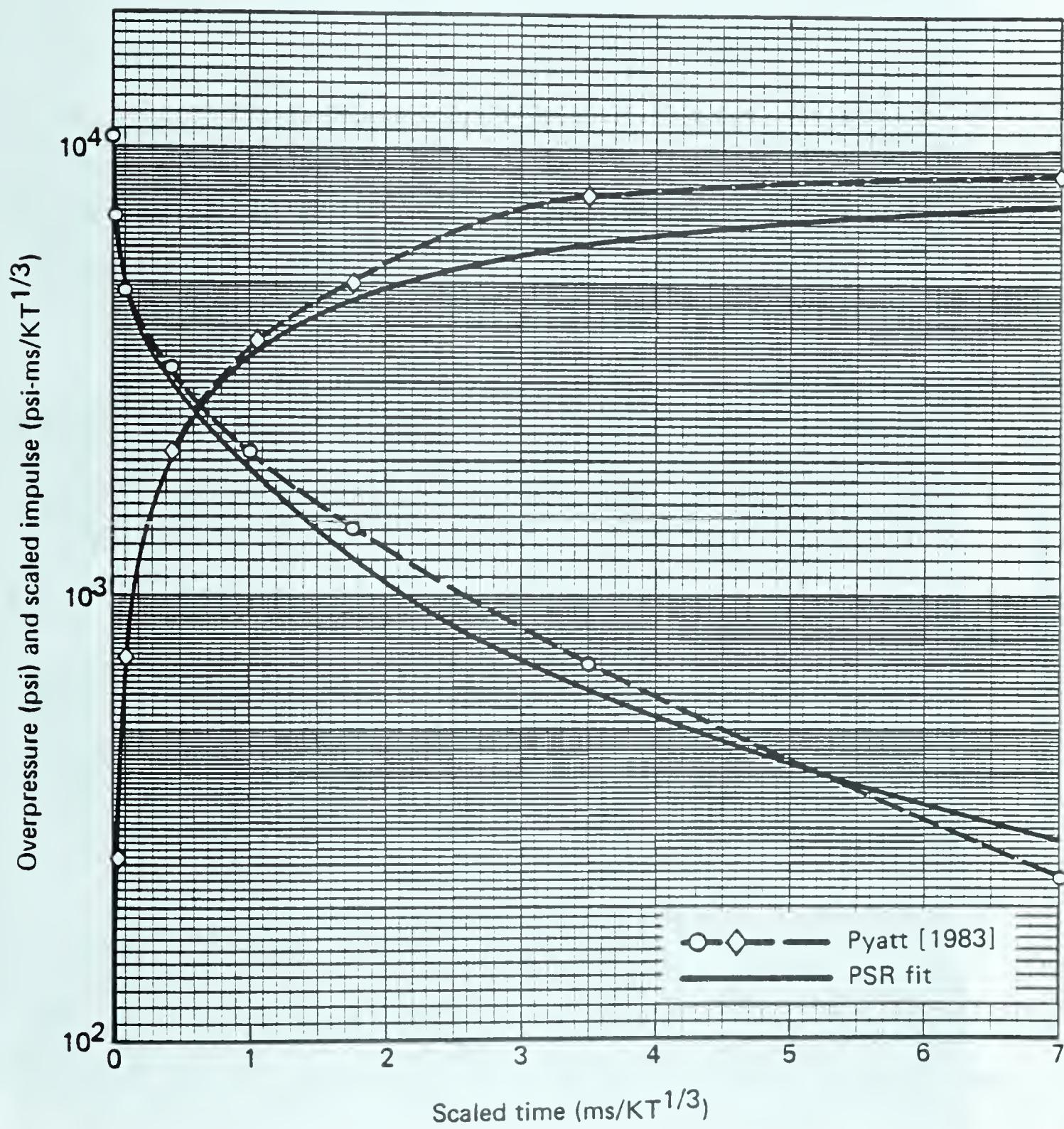


Figure 48. Fit compared to S-Cubed calculation: overpressure and scaled impulse versus scaled time to 7 ms, for $\Delta P_s \approx 10,760$ psi, $y = 0$, $x = 69$ ft/ $\text{KT}^{1/3}$.

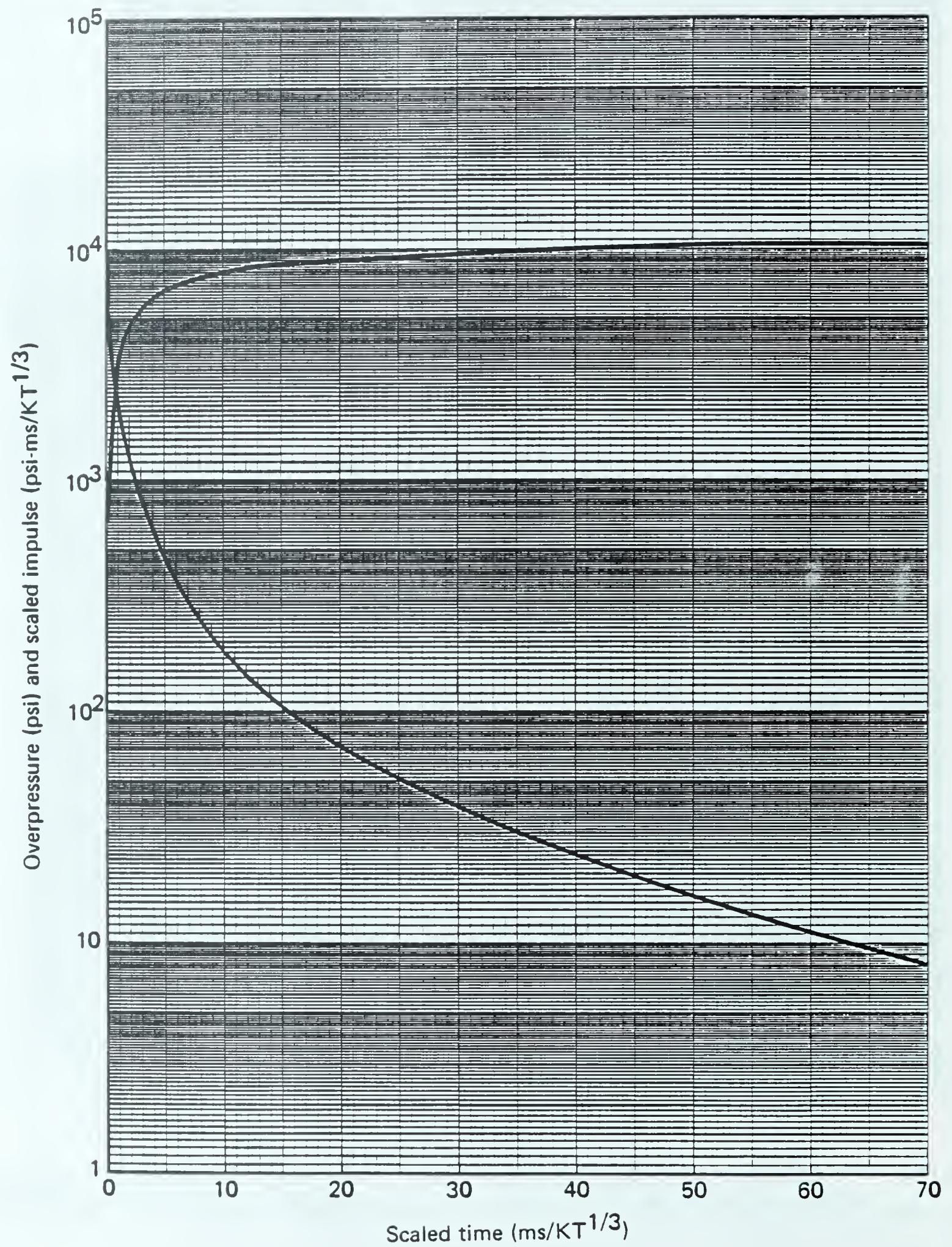


Figure 49. Fit for overpressure and scaled impulse versus scaled time to 70 ms, for $\Delta P_S \approx 10,760$ psi, $y = 0$, $x = 69$ ft/ $KT^{1/3}$.

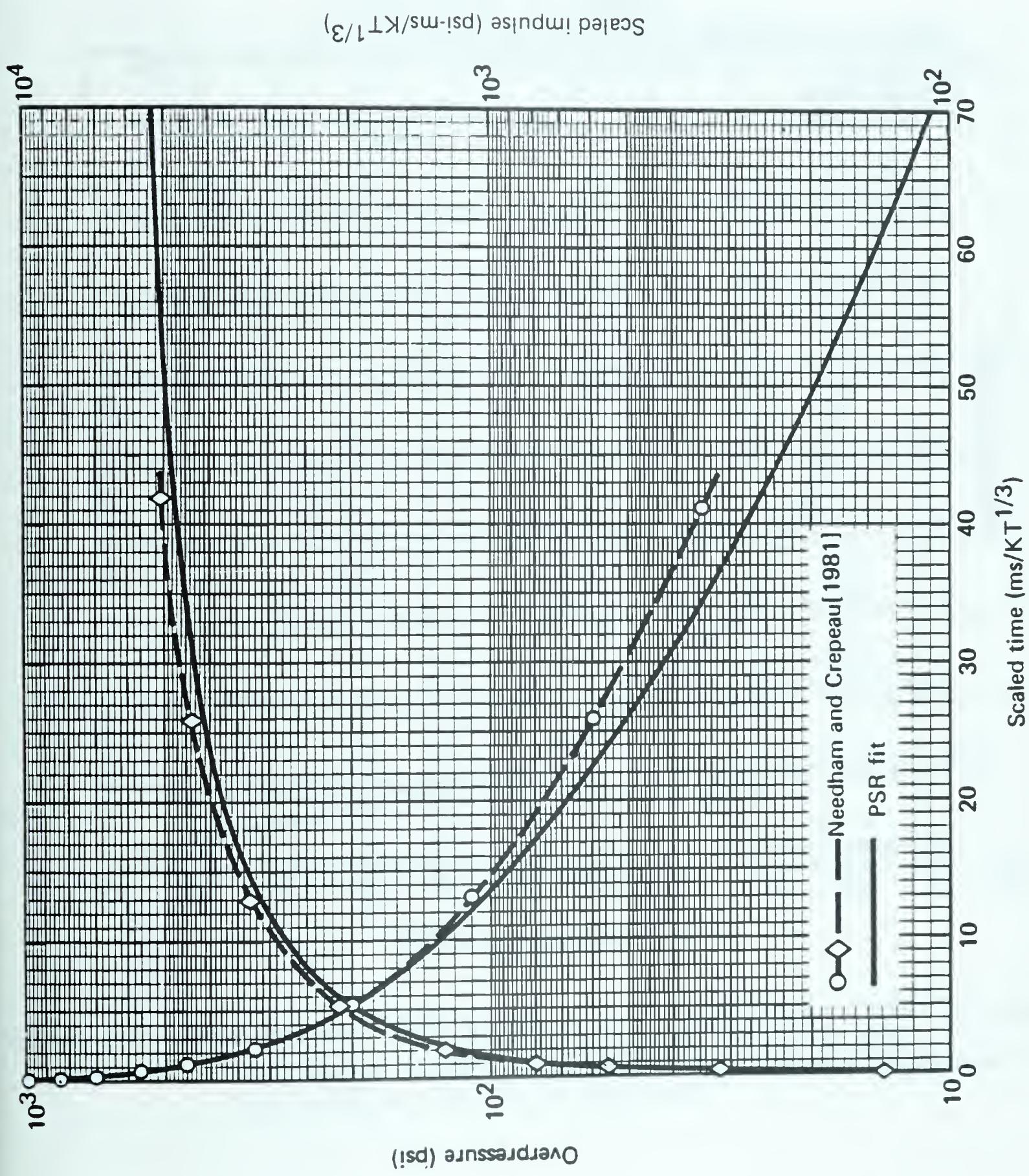


Figure 50. Fit compared to DNA 1-KT standard (2W): overpressure and scaled impulse versus scaled time to 70 ms, for $\Delta P_S \approx 99.1$ psi, $y = 0$, $x = 154.6$ ft/KT $^{1/3}$.

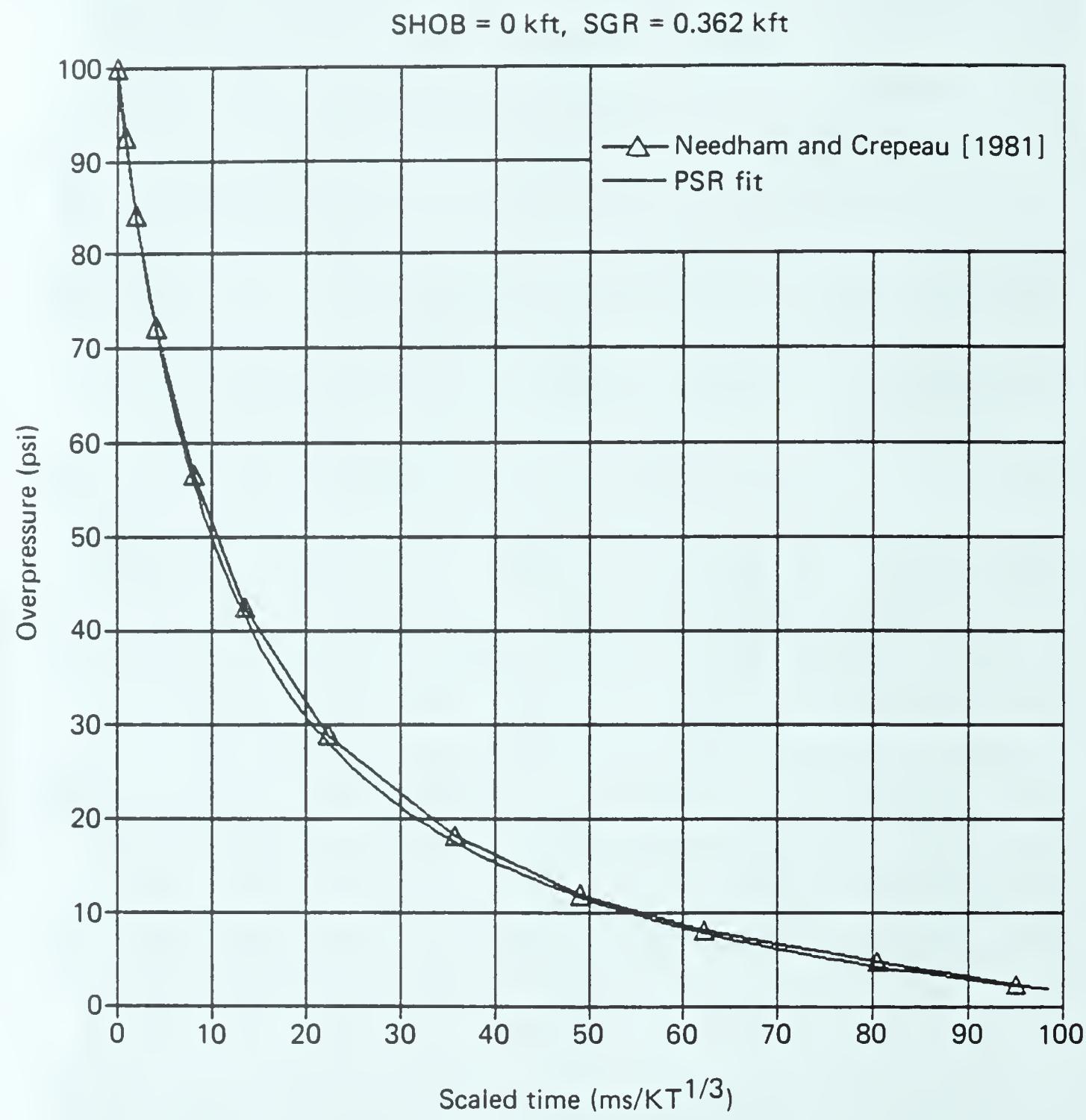


Figure 51. Fit compared to DNA 1-KT standard (2W): overpressure versus scaled time to 100 ms, for $\Delta P_s \approx 98.59$ psi.

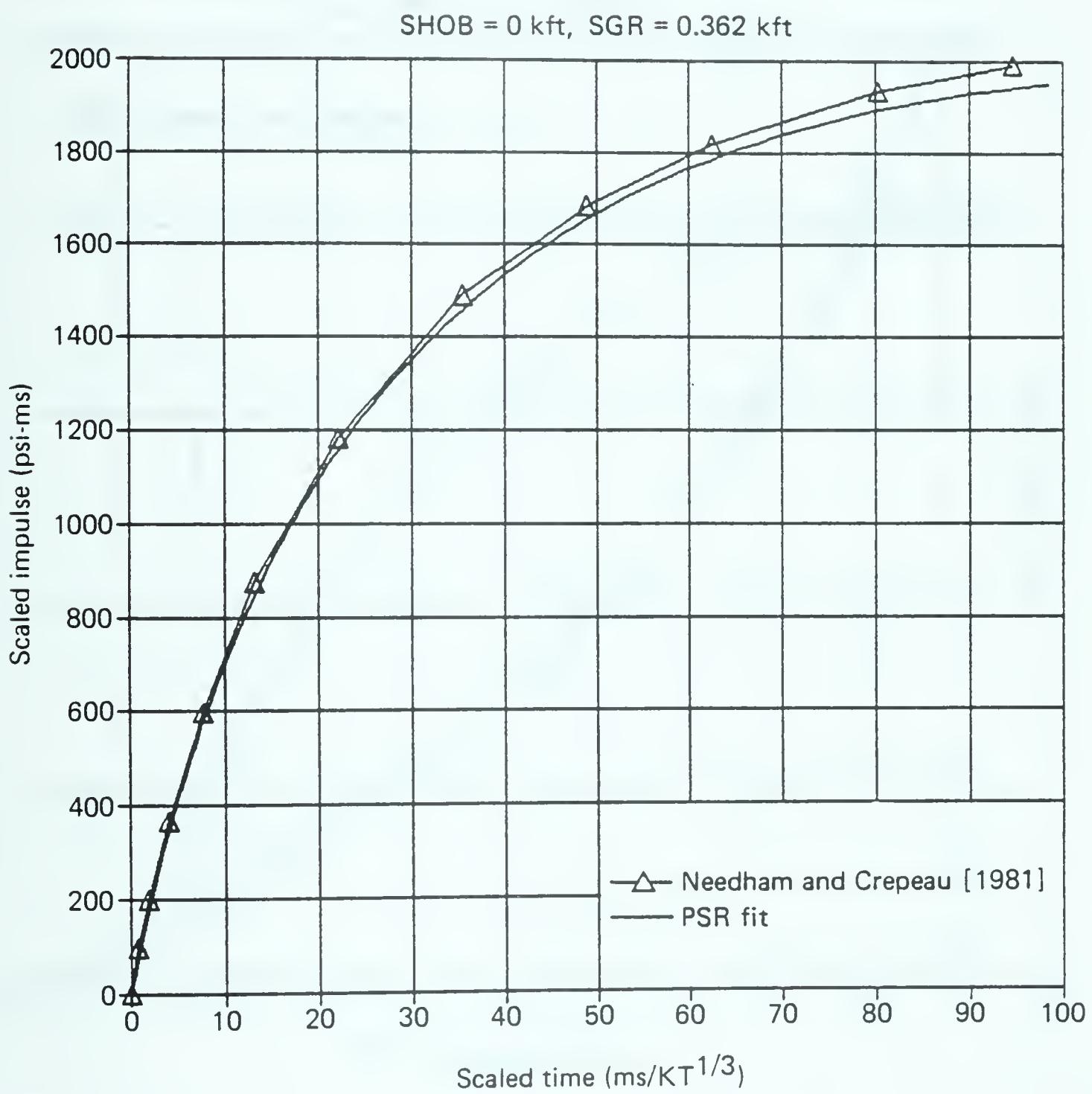


Figure 52. Fit compared to DNA 1-KT standard (2W): scaled impulse versus scaled time to 100 ms, for $\Delta P_s \approx 98.59$ psi.

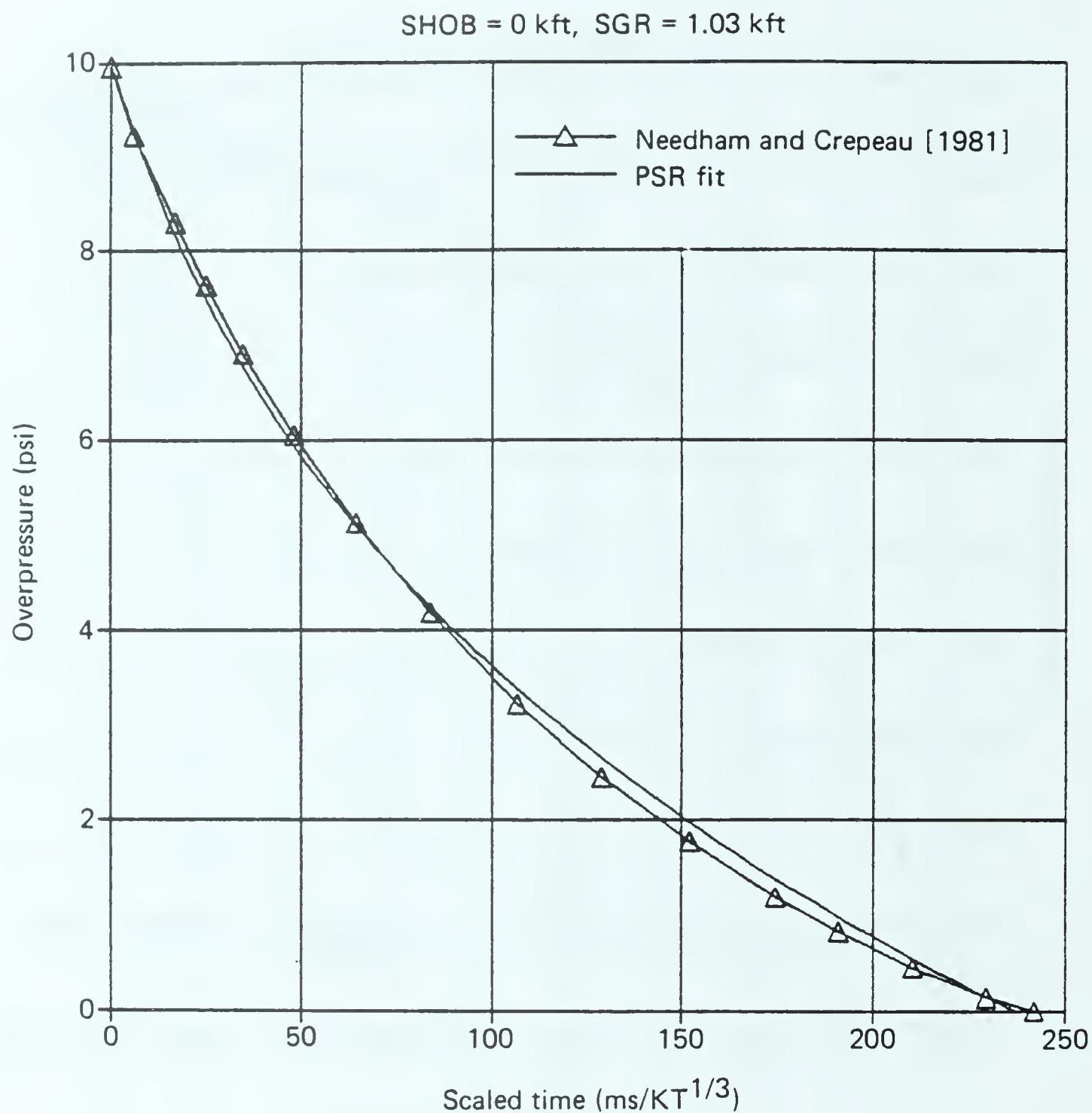


Figure 53. Fit compared to DNA 1-KT standard (2W): overpressure versus scaled time to 250 ms, for $\Delta P_S \approx 10.01$ psi.

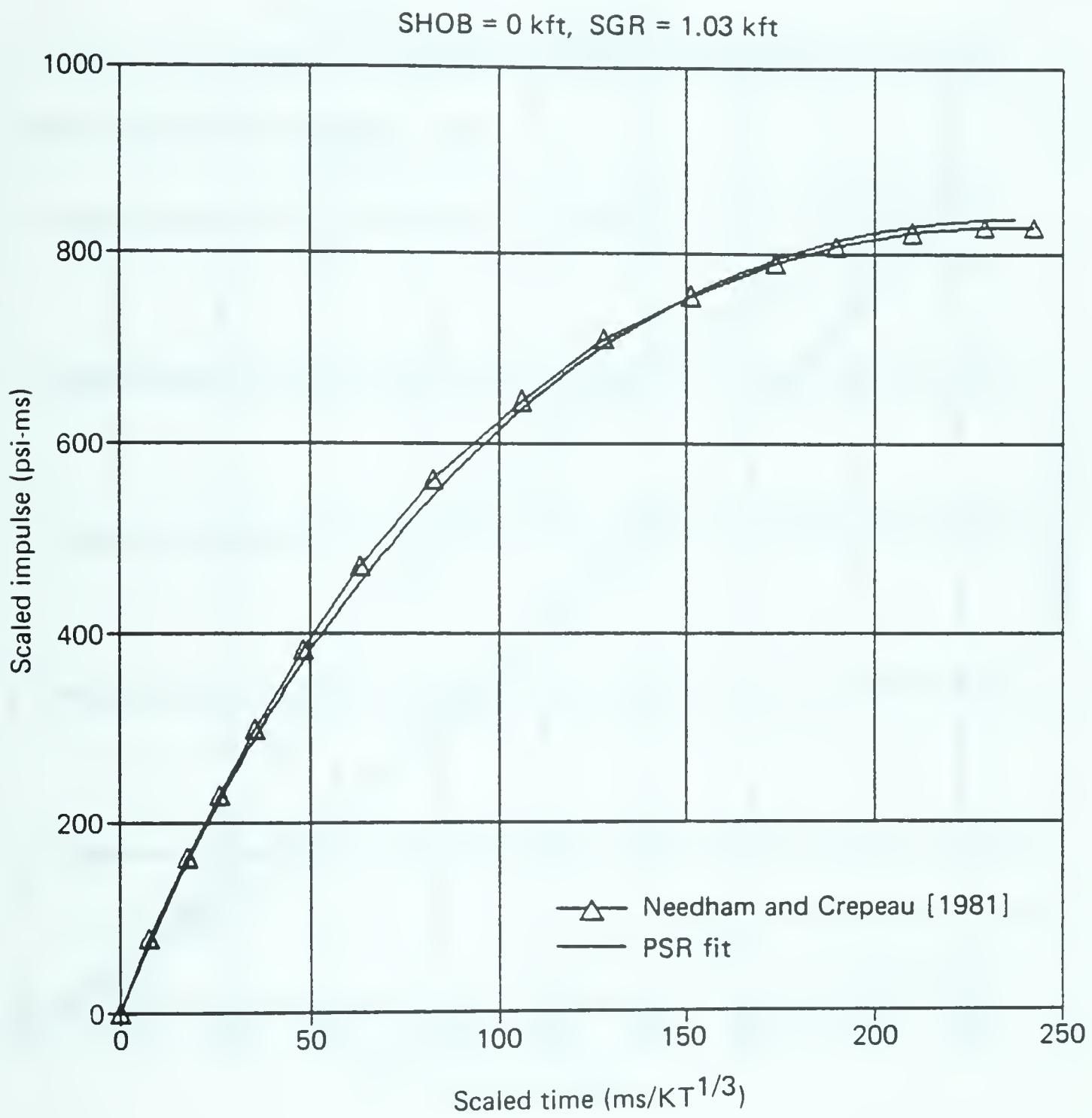


Figure 54. Fit compared to DNA 1-KT standard (2W): scaled impulse versus scaled time to 250 ms, for $\Delta P_S \approx 10.01$ psi.

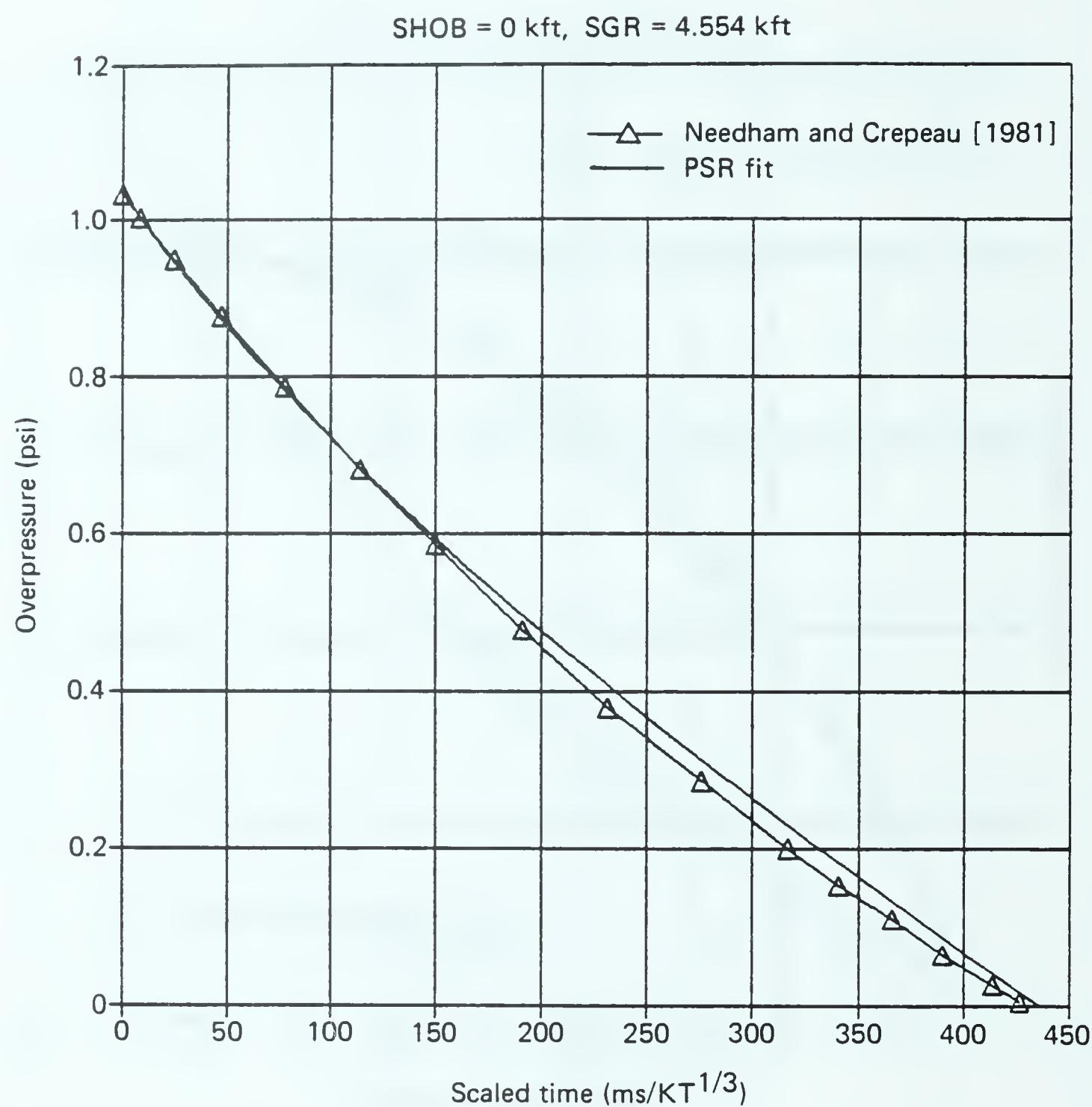


Figure 55. Fit compared to DNA 1-KT standard (2W): overpressure versus scaled time to 450 ms, for $\Delta P_s \approx 1.036$ psi.

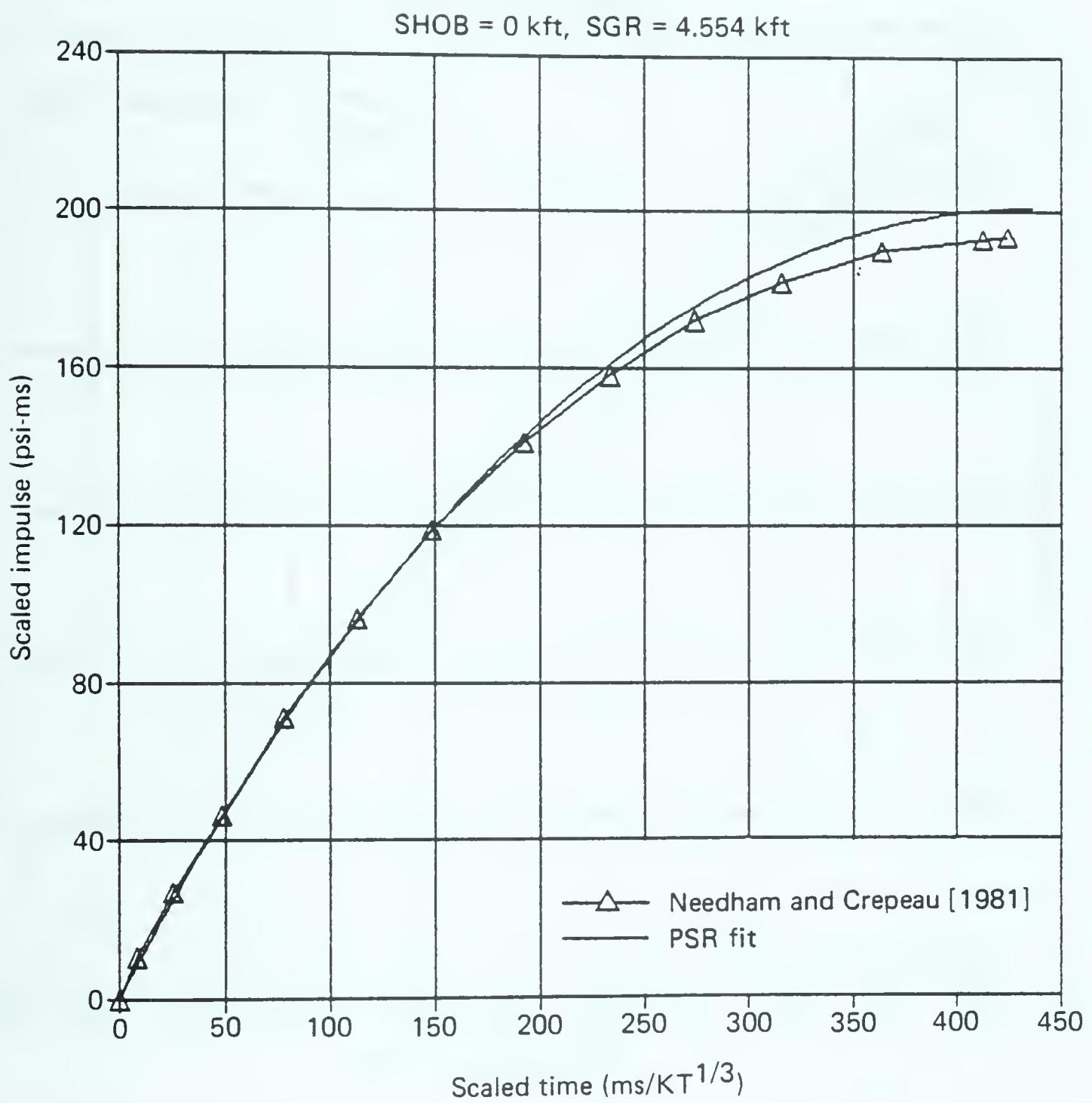


Figure 56. Fit compared to DNA 1-KT standard (2W): scaled impulse versus scaled time to 450 ms, for $\Delta P_s \approx 1.036$ psi.

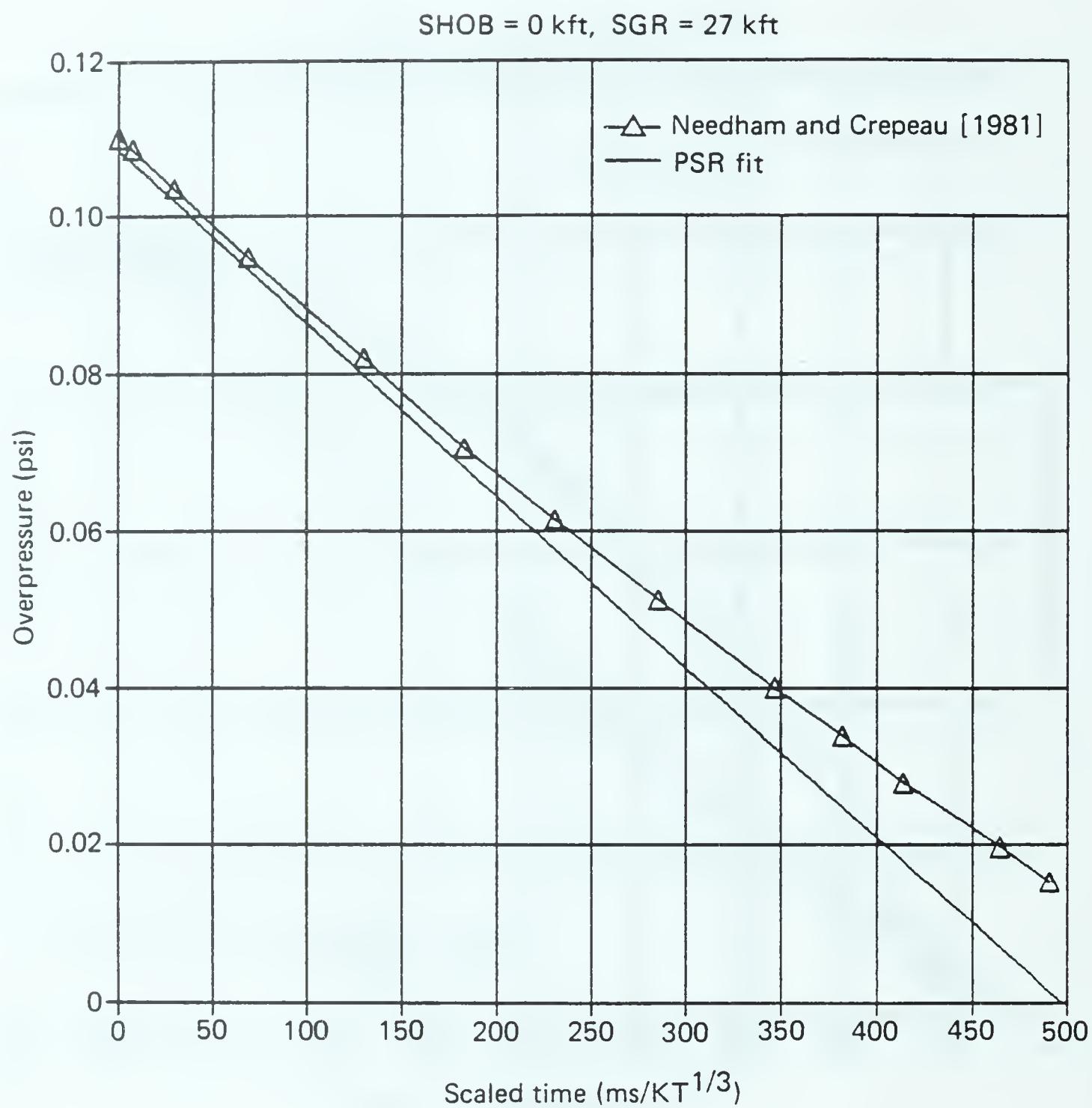


Figure 57. Fit compared to DNA 1-KT standard (2W): overpressure versus scaled time to 500 ms, for $\Delta P_s \approx 0.1086$ psi.

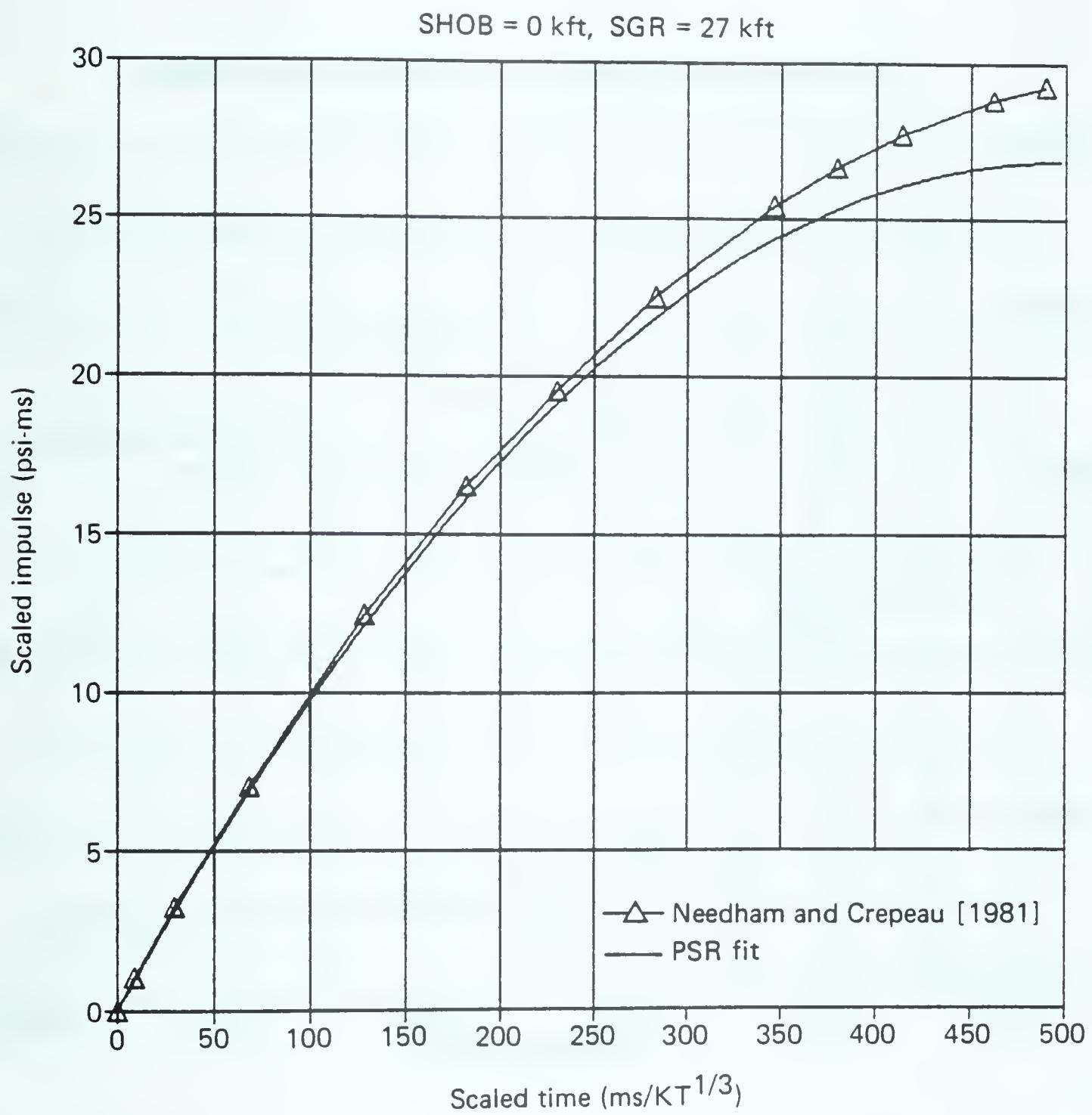


Figure 58. Fit compared to DNA 1-KT standard (2W): scaled impulse versus scaled time to 500 ms, for $\Delta P_S \approx 0.1086$ psi.

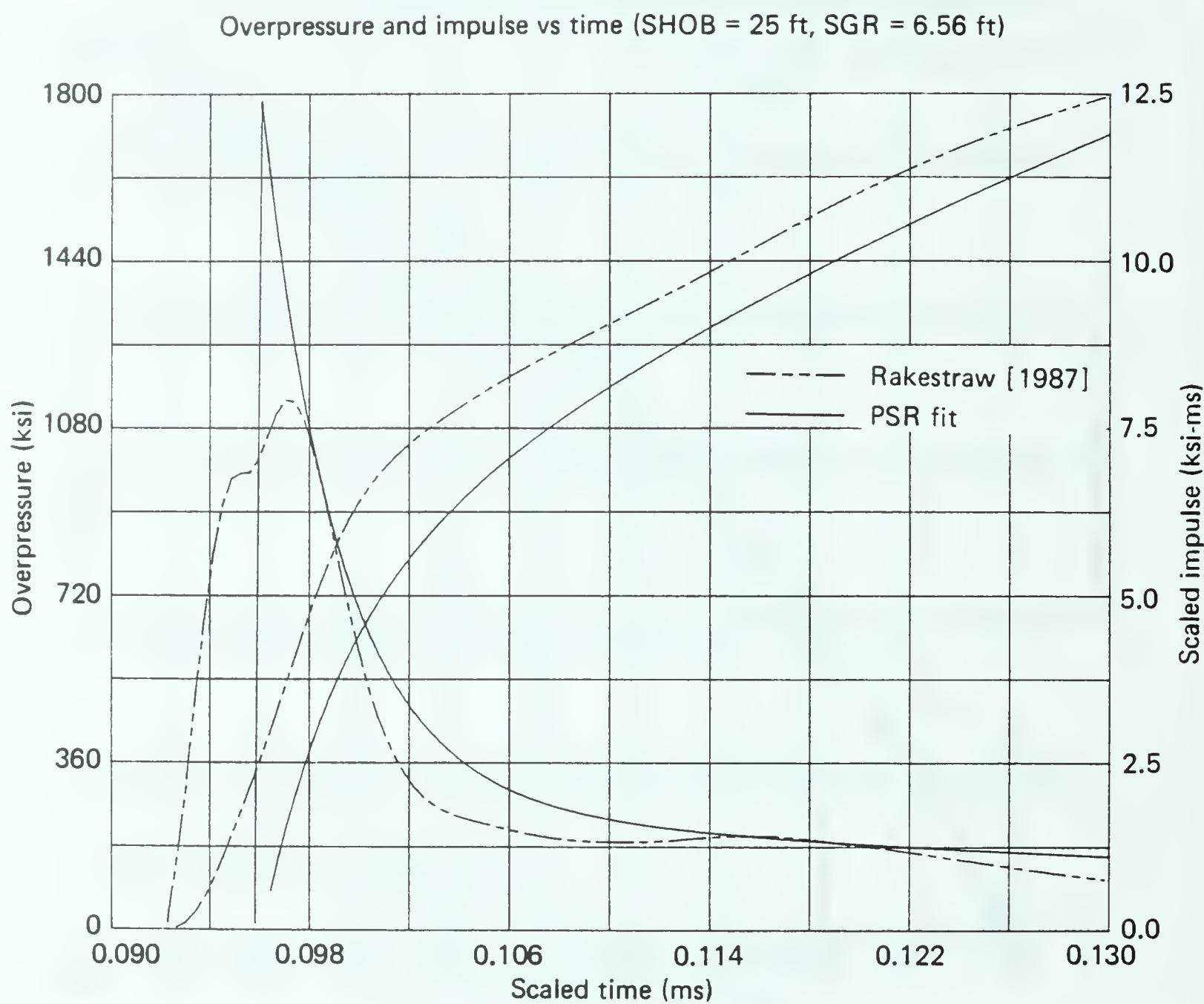


Figure 59. Fit compared to scaled SAI calculation: overpressure and scaled impulse versus scaled time to .13 ms, for 25 ft HOB $\Delta P_s \approx 1,785,000$ psi.

Overpressure and impulse vs time (SHOB = 25 ft, SGR = 6.56 ft)

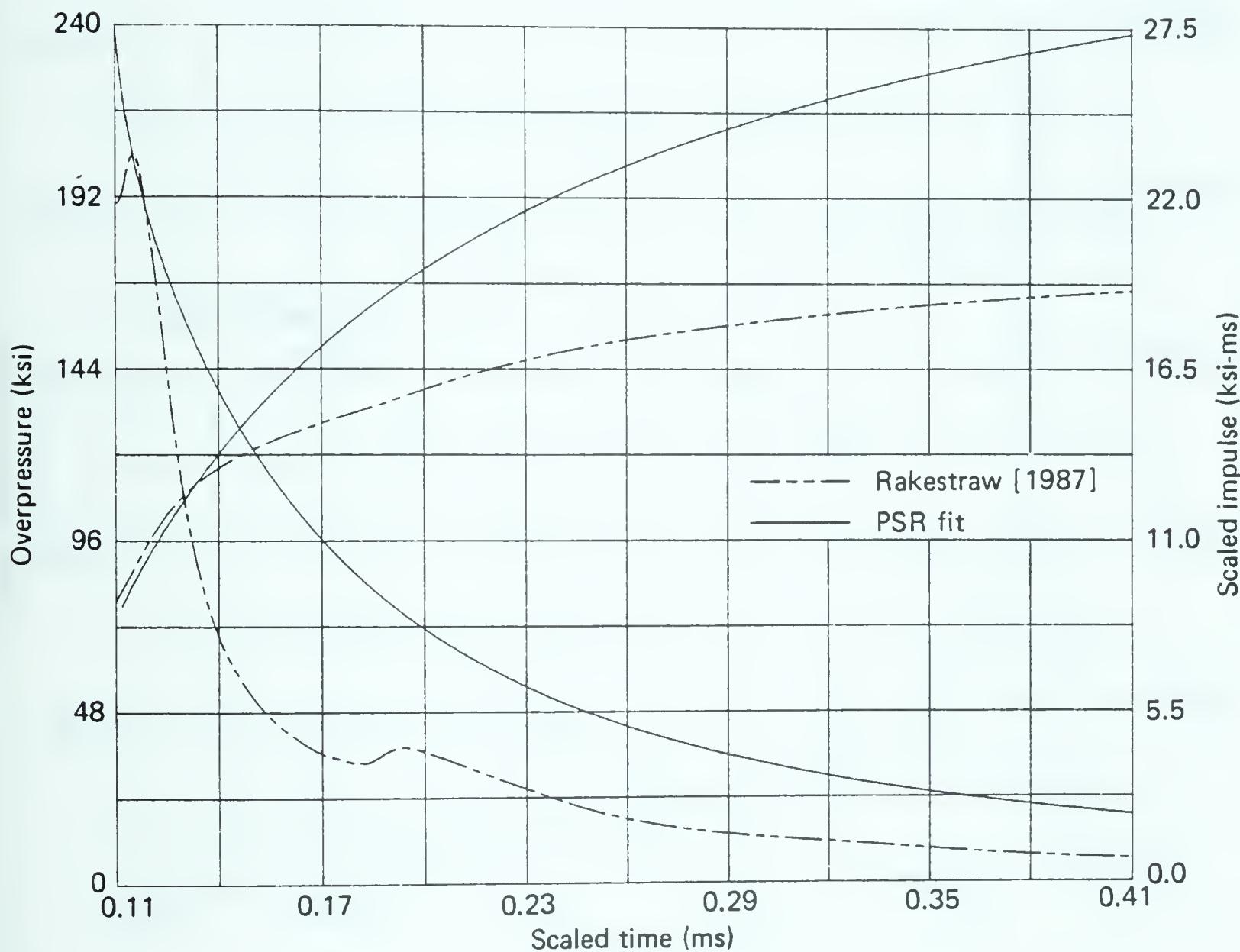


Figure 60. Fit compared to SAI calculation: overpressure and scaled impulse versus scaled time to .41 ms, for 25 ft SHOB, $\Delta P_s \approx 1,785,000$ psi.

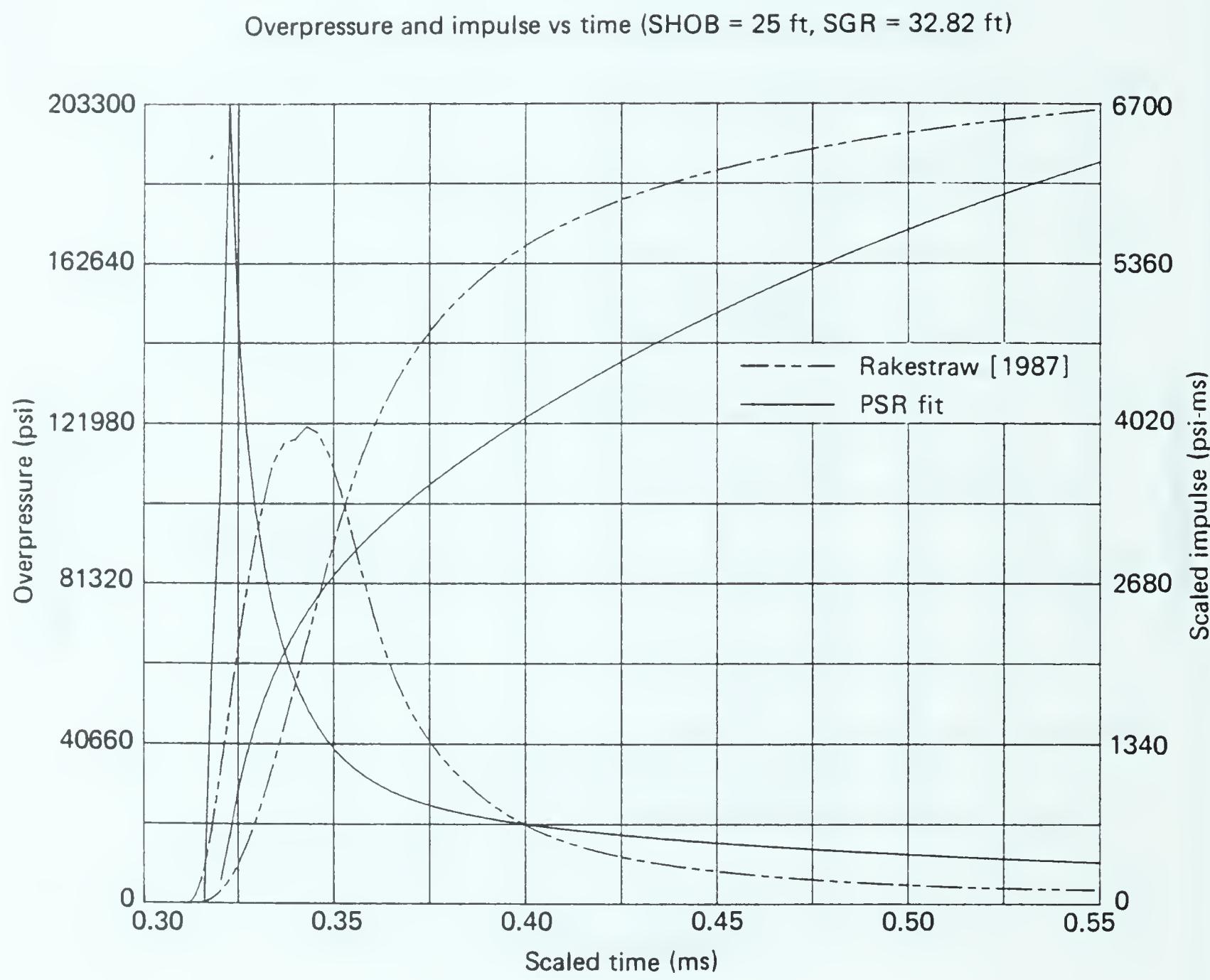


Figure 61. Fit compared to SAI calculation: overpressure and scaled impulse versus scaled time to .55 ms, for 25 ft SHOB, $\Delta P_s \approx 233,300$ psi.

Overpressure and impulse vs time (SHOB = 25 ft, SGR = 32.82 ft)

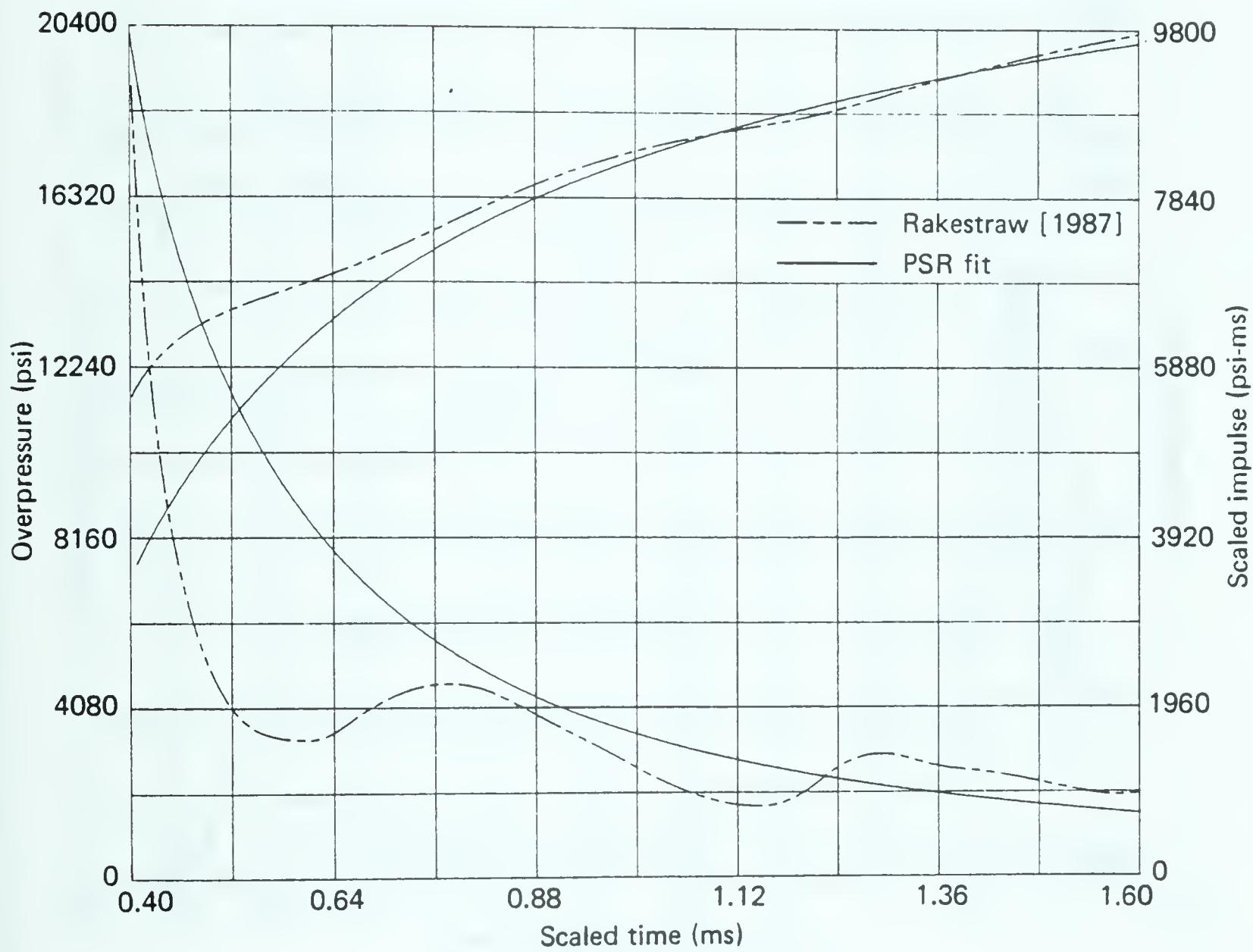


Figure 62. Fit compared to SAI calculation: overpressure and scaled impulse versus scaled time to 1.6 ms, for 25 ft SHOB, $\Delta P_s \approx 233,300$ psi.

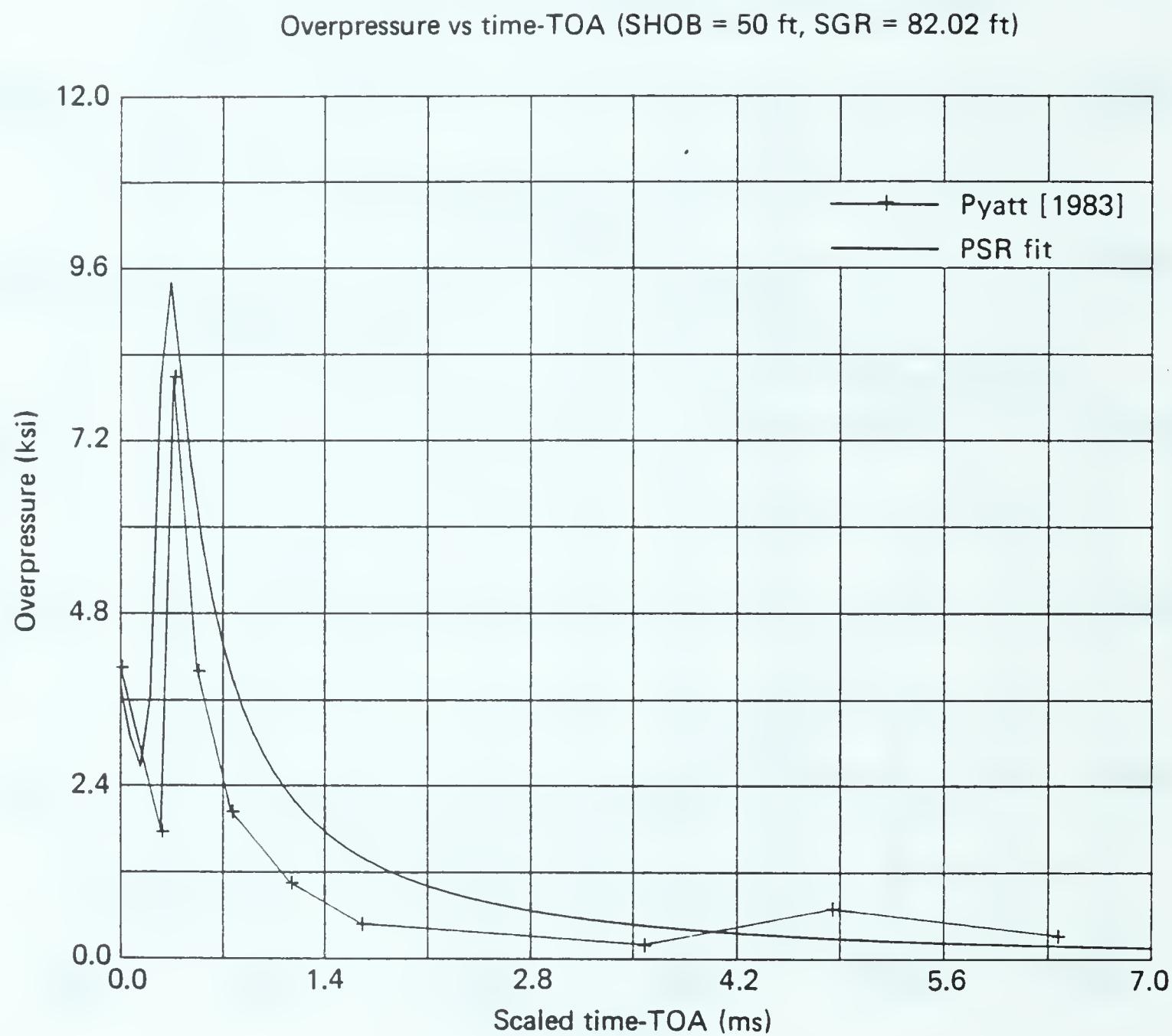


Figure 63. Fit compared to S-CUBED calculation: overpressure versus scaled time minus time-of-arrival to 7 ms, for 50 ft SHOB, $\Delta P_s \approx 9,000$ psi.

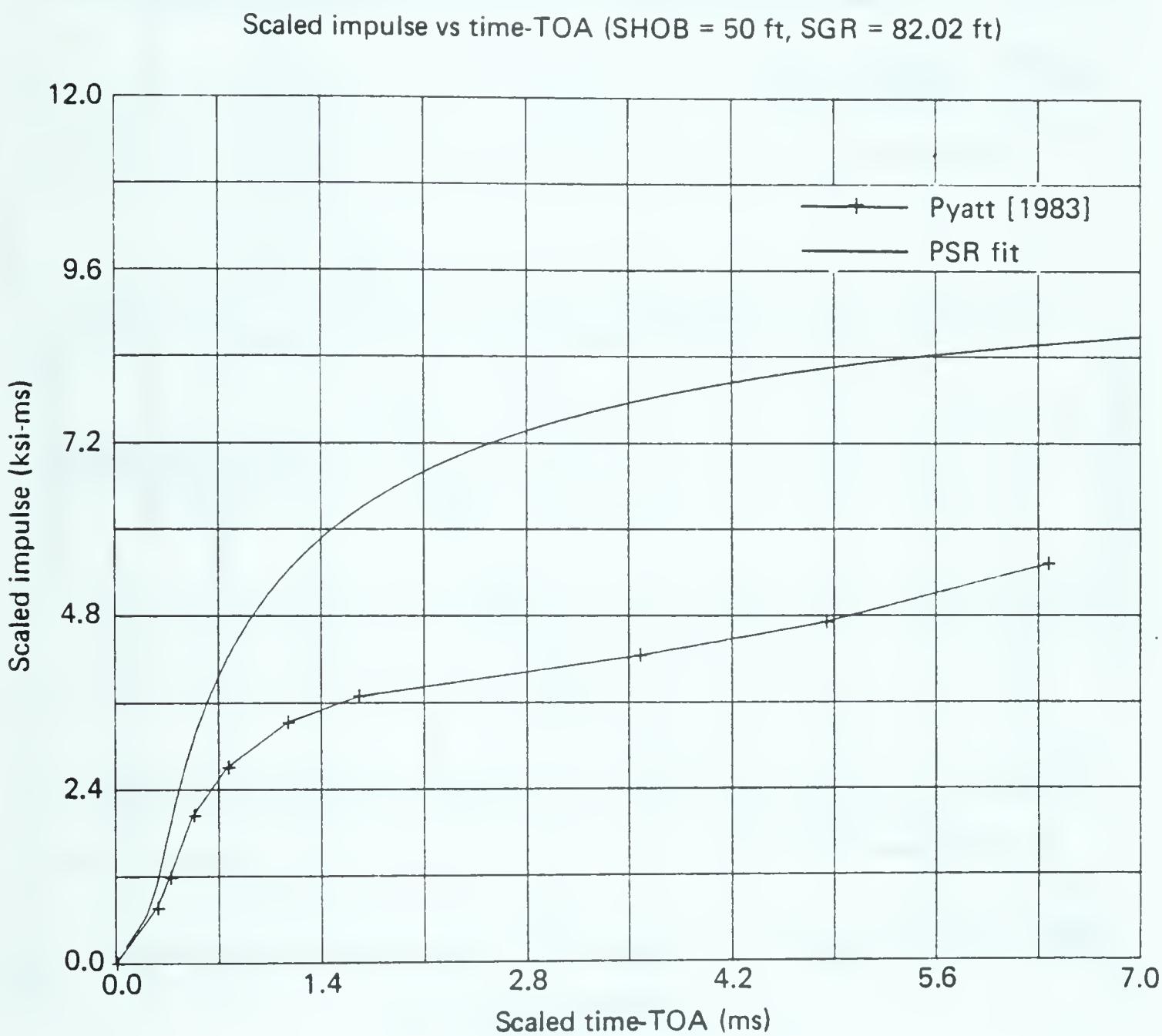


Figure 64. Fit compared to S-CUBED calculation: scaled impulse versus scaled time minus time-of-arrival to 7 ms, for 50 ft SHOB, $\Delta P_s \approx 9,000$ psi.

Scaled impulse vs time-TOA (SHOB = 50 ft, SGR = 82.02 ft)

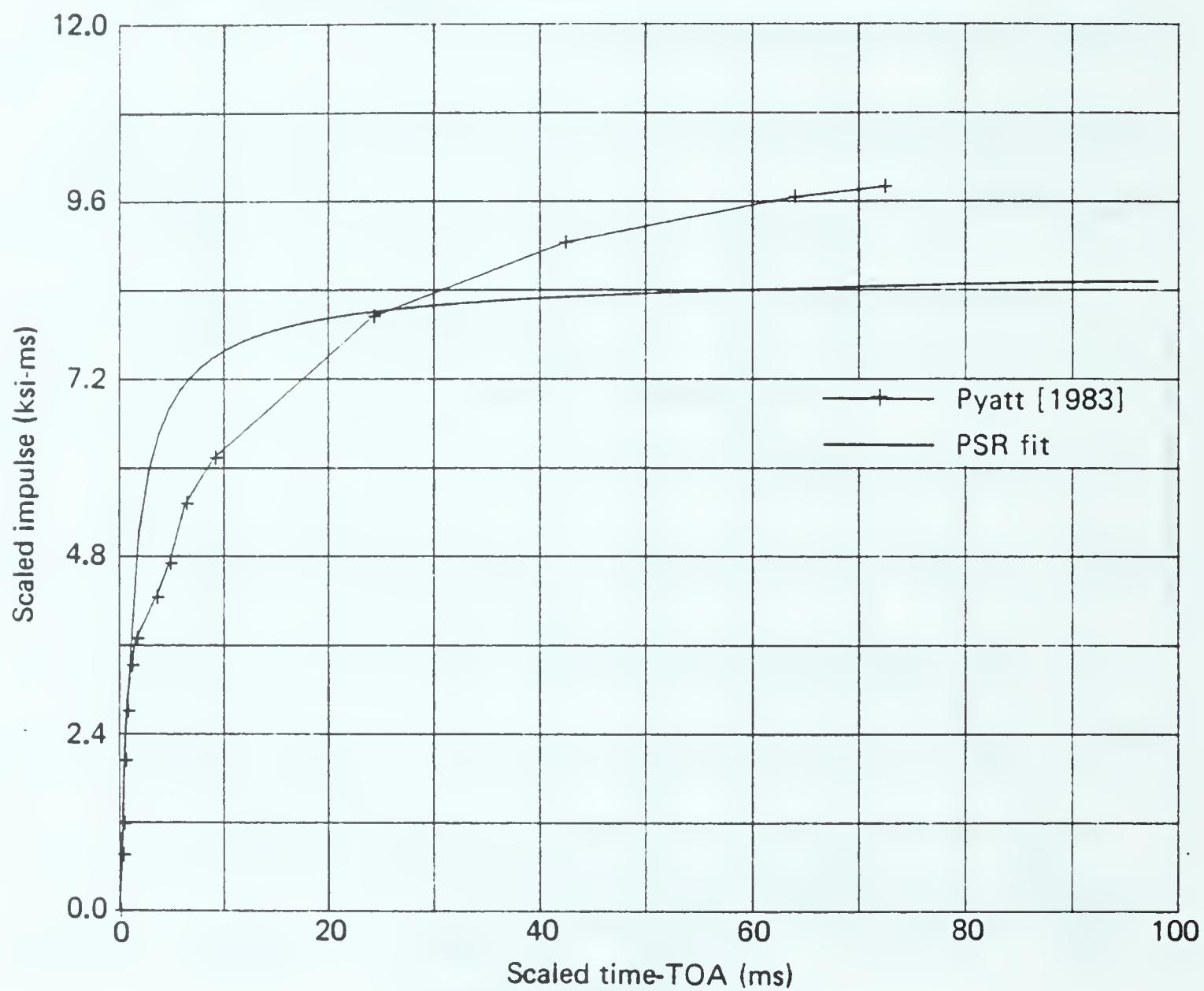


Figure 65. Fit compared to S-CUBED calculation: scaled impulse versus scaled time minus time-of-arrival to 100 ms, for 50 ft SHOB, $\Delta P_s \approx 9,000$ psi.

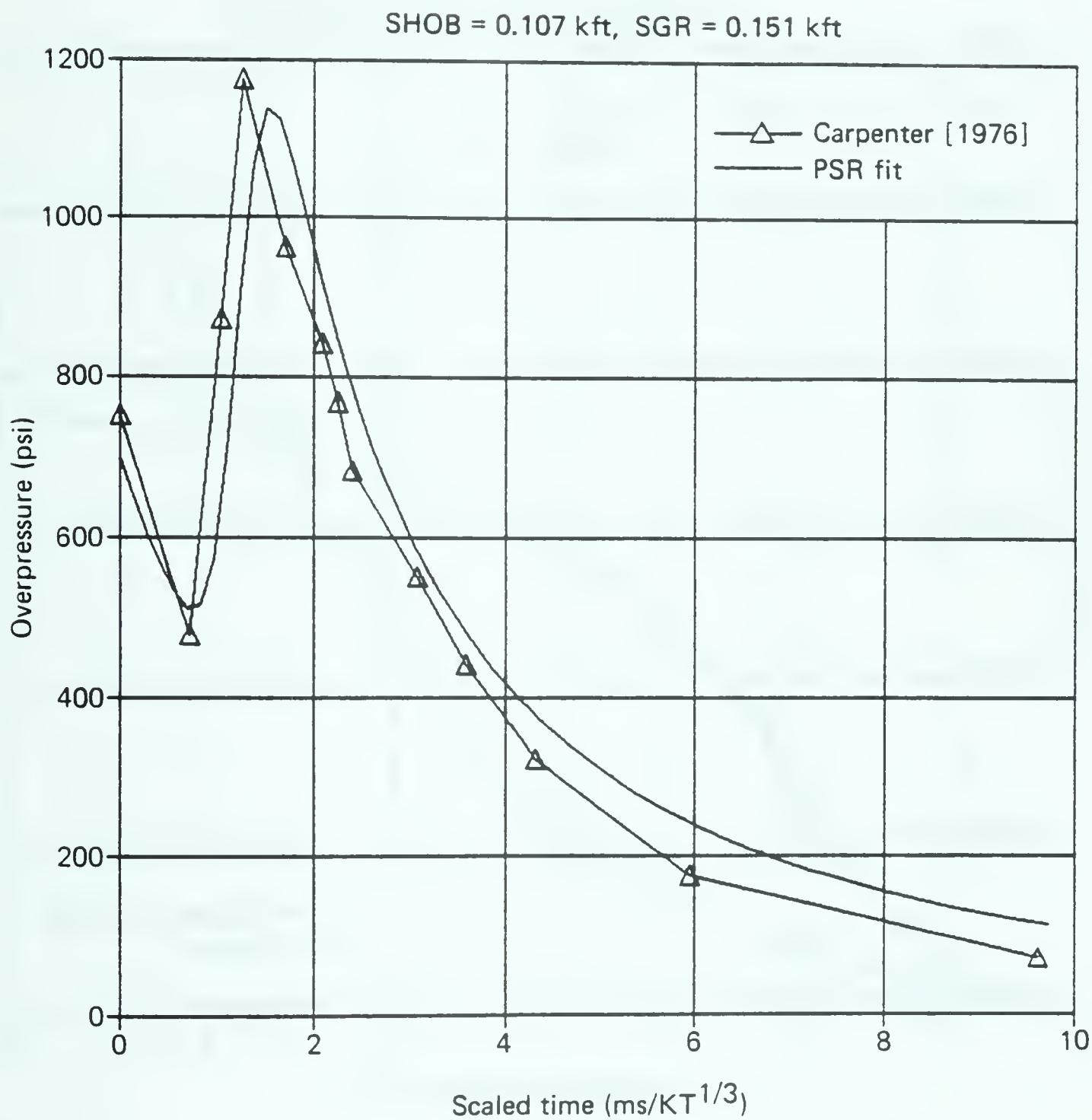


Figure 66. Fit compared to 8-lb charge data: overpressure versus scaled time to 10 ms, for 107-ft SHOB, $\Delta P_s \approx 1199$ psi.

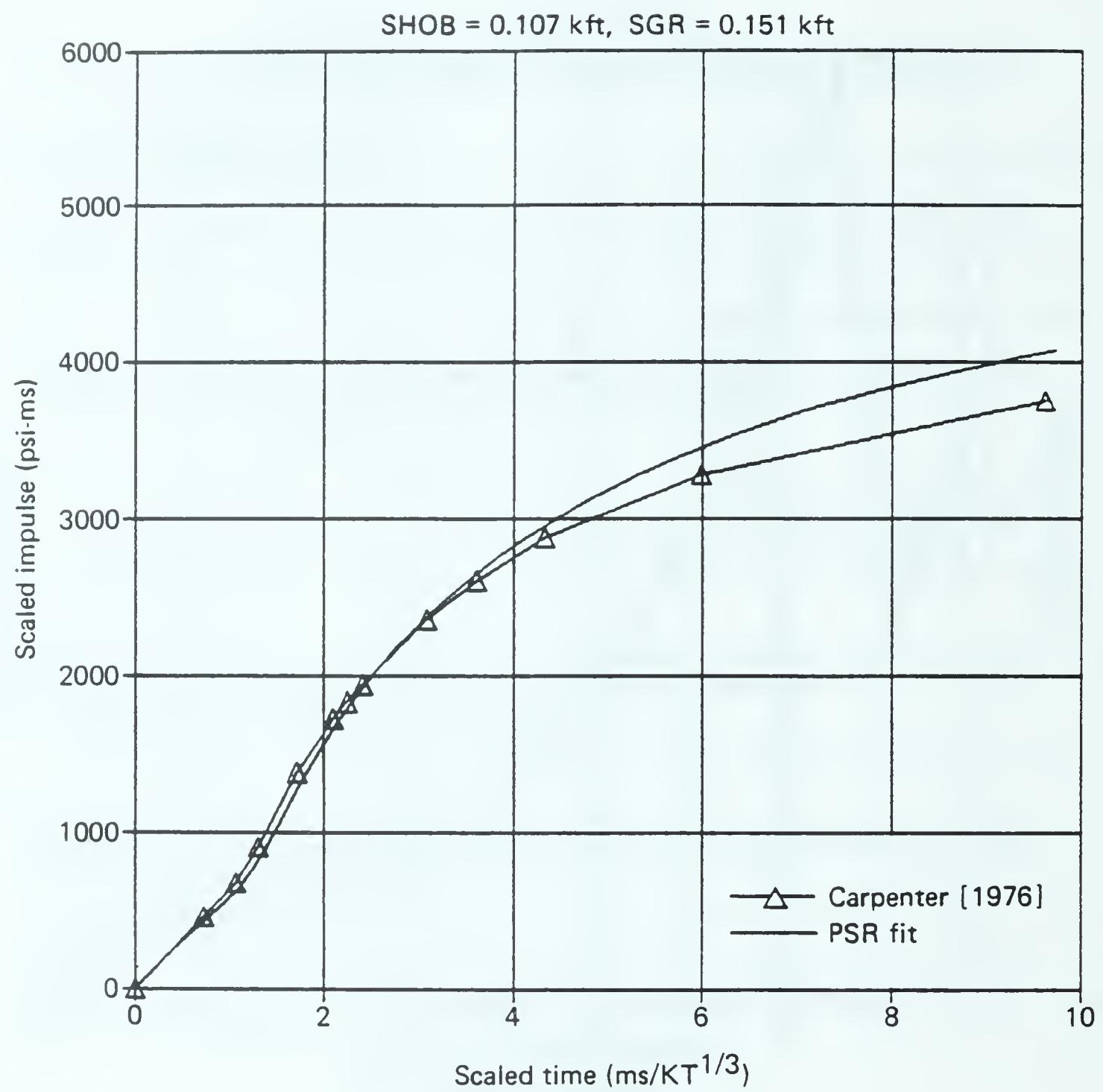


Figure 67. Fit compared to 8-lb charge data: scaled impulse versus scaled time to 10 ms, for 107-ft SHOB, $\Delta P_s \approx 1199$ psi.

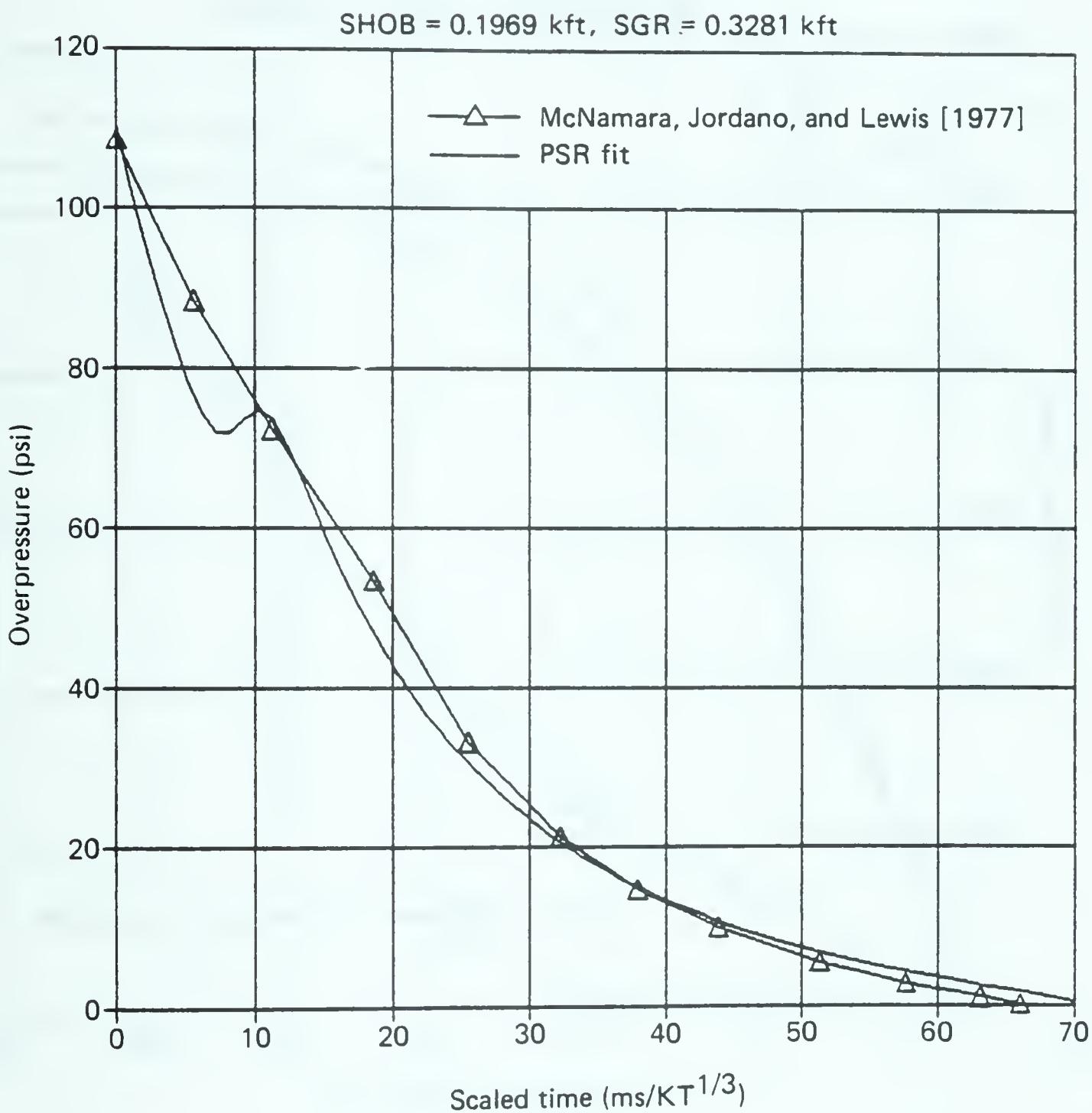


Figure 68. Fit compared to General Electric-TEMPO calculation: overpressure versus scaled time to 70 ms, for 60-m SHOB, $\Delta P_s \approx 110.5$ psi.

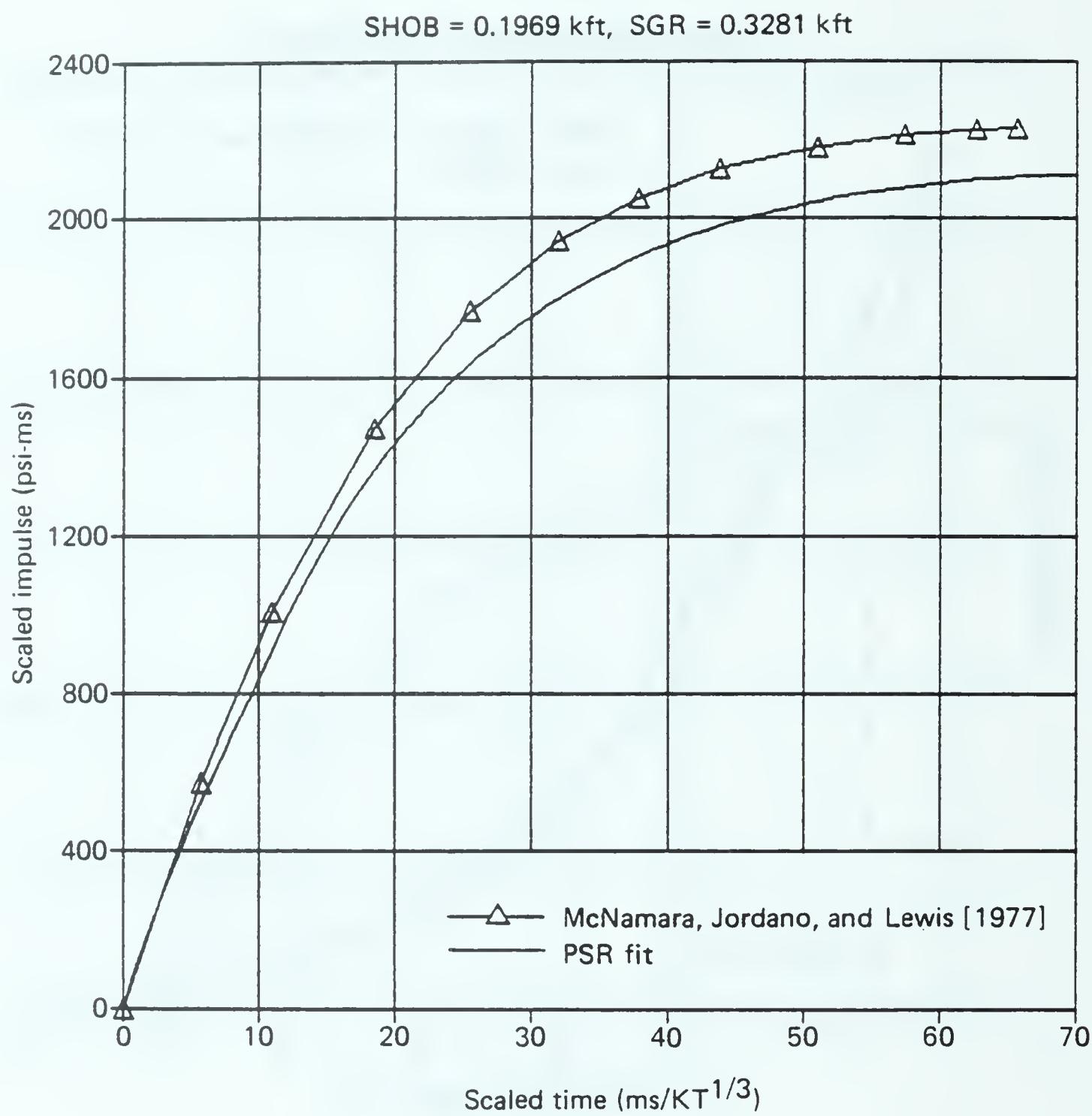


Figure 69. Fit compared to General Electric-TEMPO calculation: scaled impulse versus scaled time to 70 ms, for 60-m SHOB, $\Delta P_s \approx 110.5$ psi.

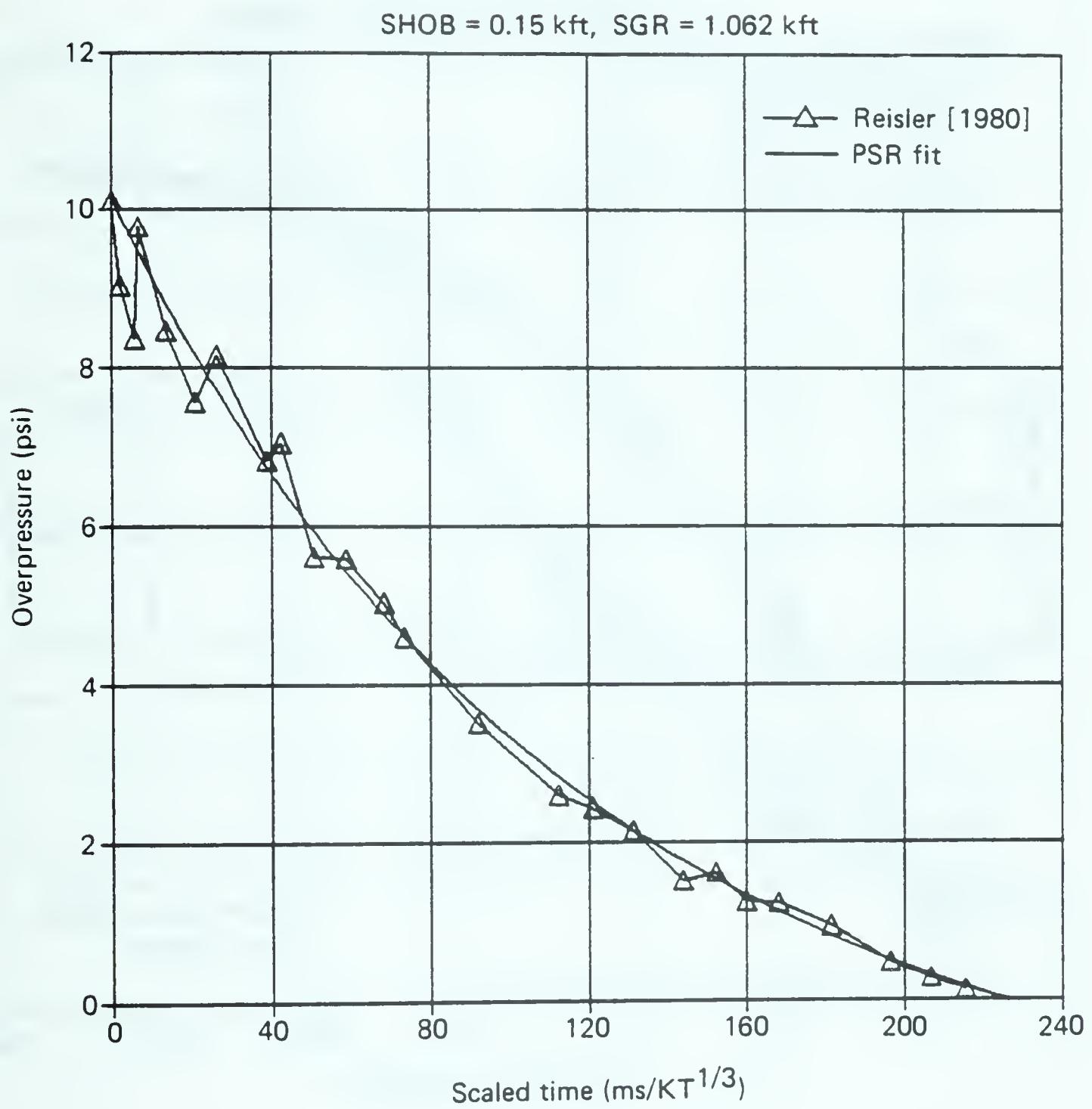


Figure 70. Fit compared to DIPOLE WEST data: overpressure versus scaled time to 220 ms, for 150-ft SHOB, $\Delta P_s \approx 10.15$ psi.



Figure 71. Fit compared to DIPOLE WEST data: scaled impulse versus scaled time to 220 ms, for 150-ft SHOB, $\Delta P_s \approx 10.15$ psi.

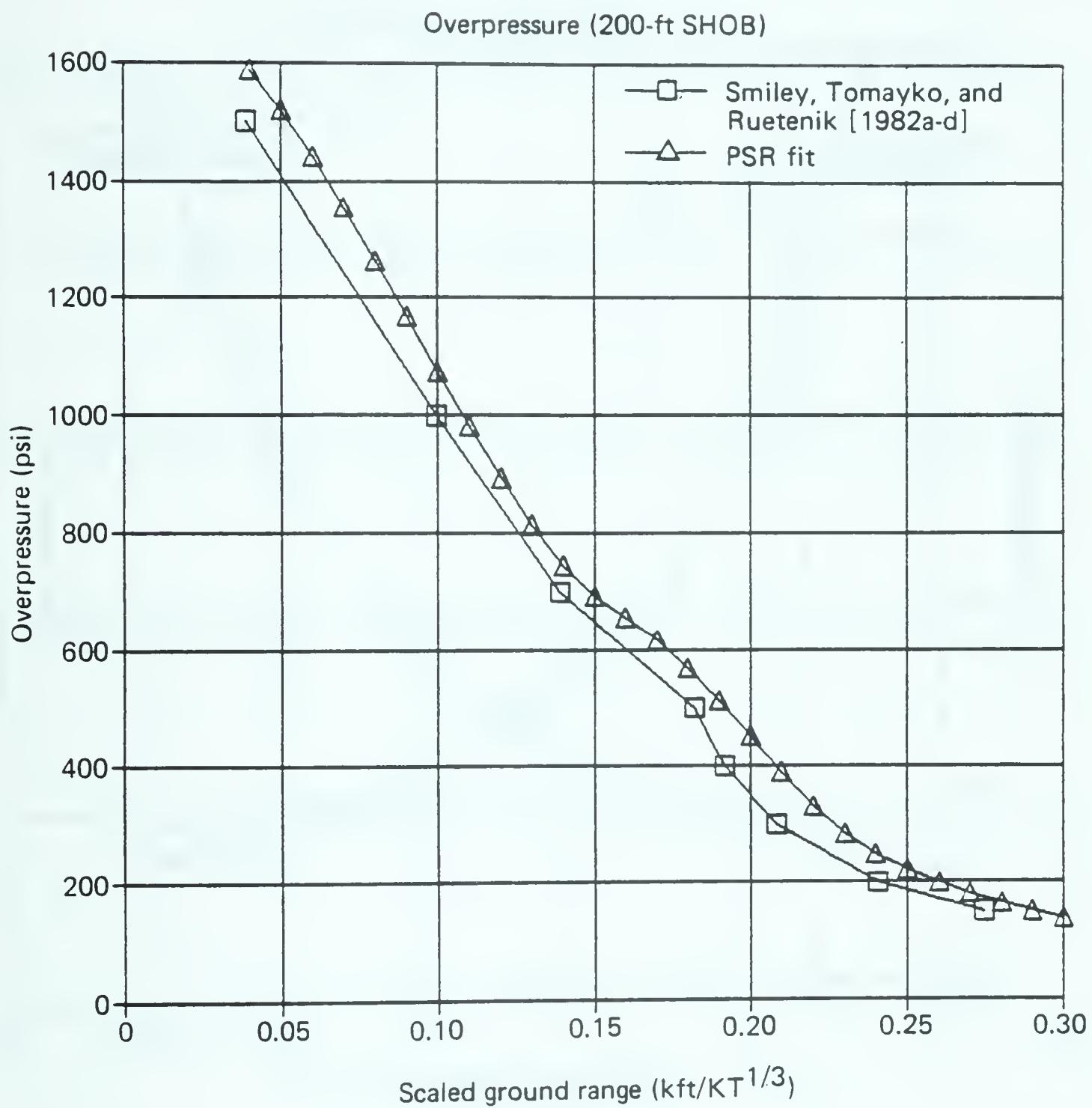


Figure 72. Fit compared to 200-ft SHOB Kaman AviDyne calculation: peak overpressure (from 1600 psi) versus scaled ground range (0 to 0.3 kft).

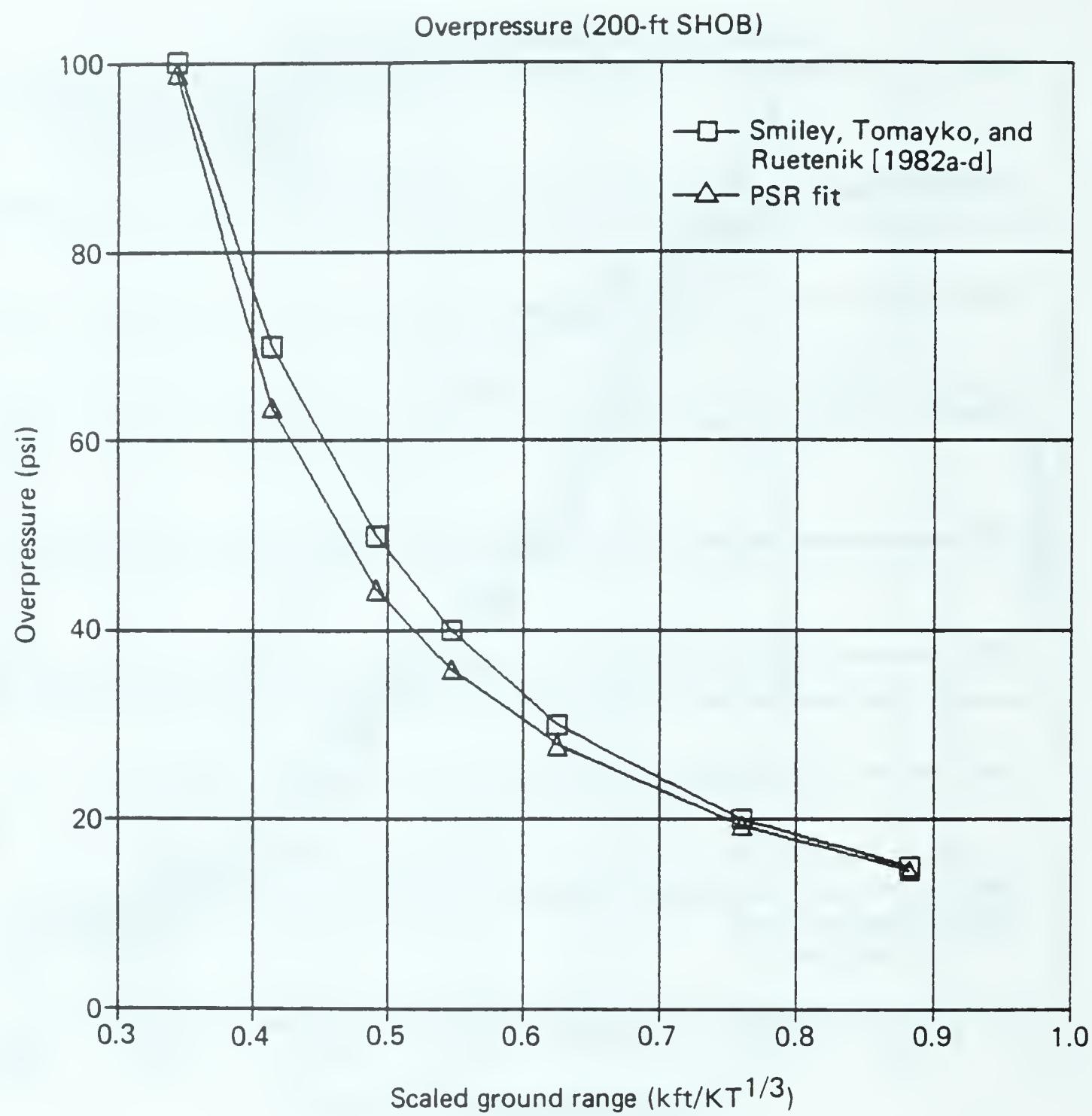


Figure 73. Fit compared to 200-ft SHOB Kaman AviDyne calculation: peak overpressure (100 to 15 psi) versus scaled ground range (0.3 to 0.9 kft).

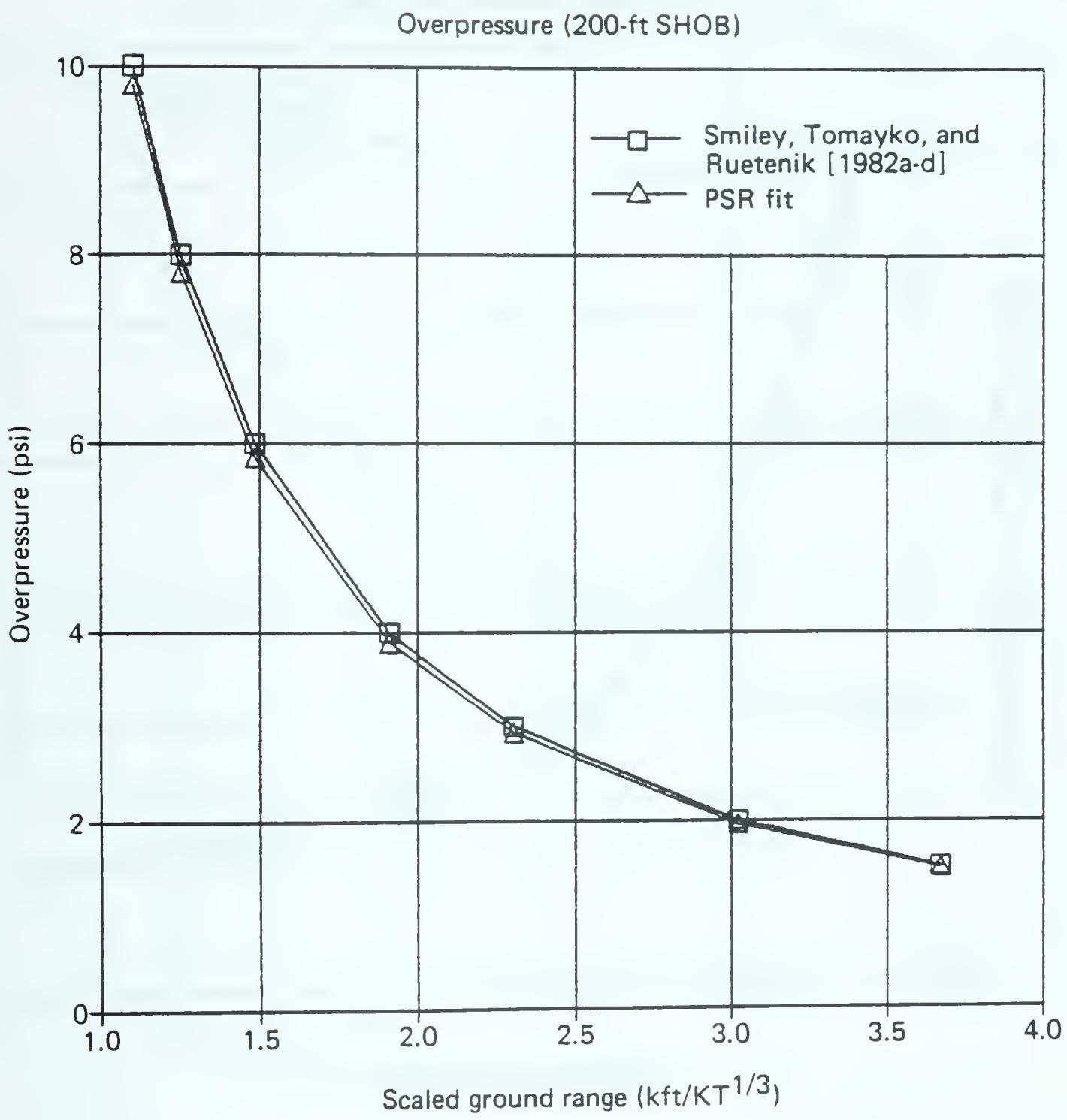


Figure 74. Fit compared to 200-ft SHOB Kaman AviDyne calculation: peak overpressure (10 to 1.5 psi) versus scaled ground range (1 to 3.7 kft).

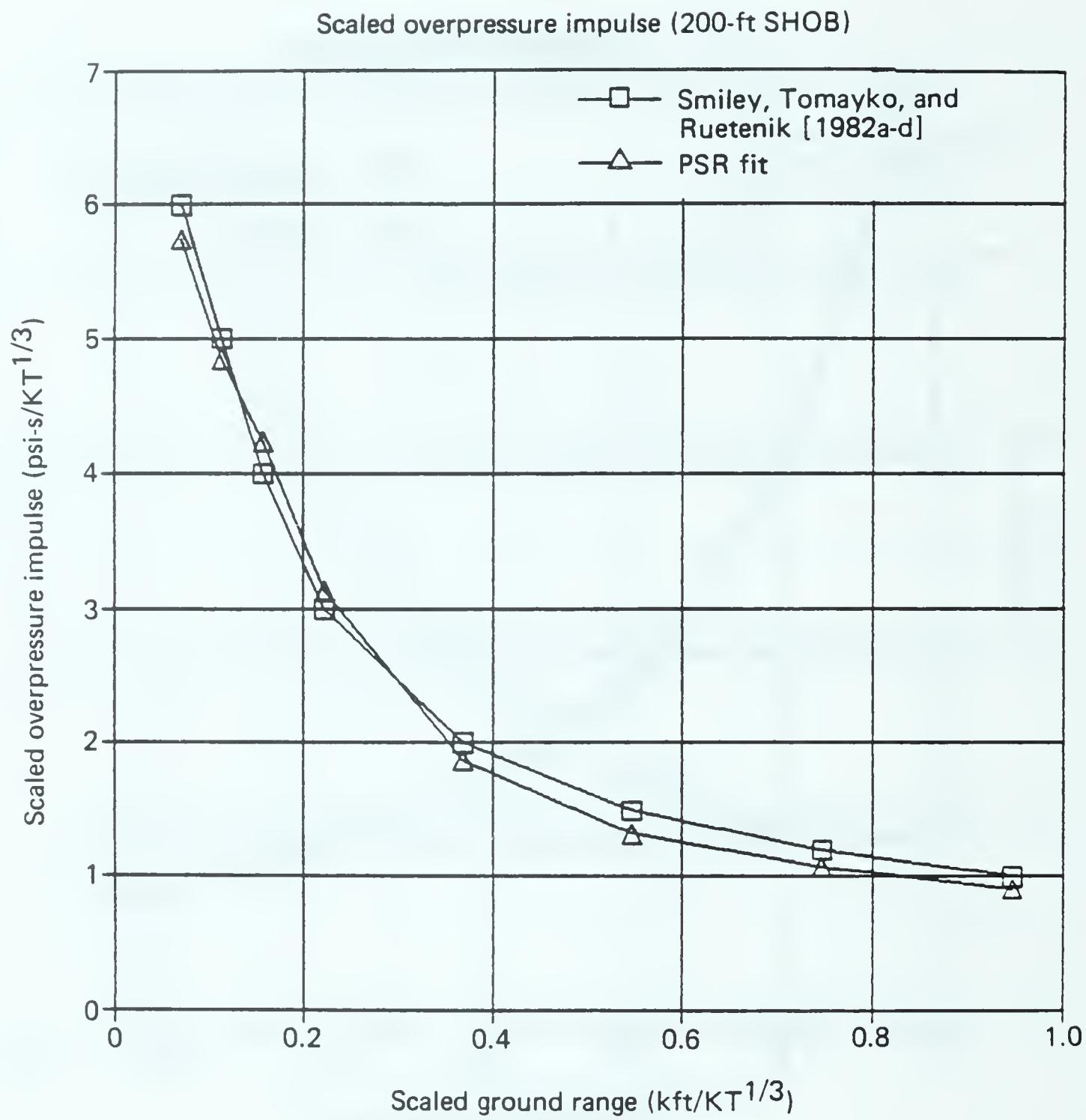


Figure 75. Fit compared to 200-ft SHOB Kaman AviDyne calculation: scaled overpressure impulse versus scaled ground range (to 1 kft).

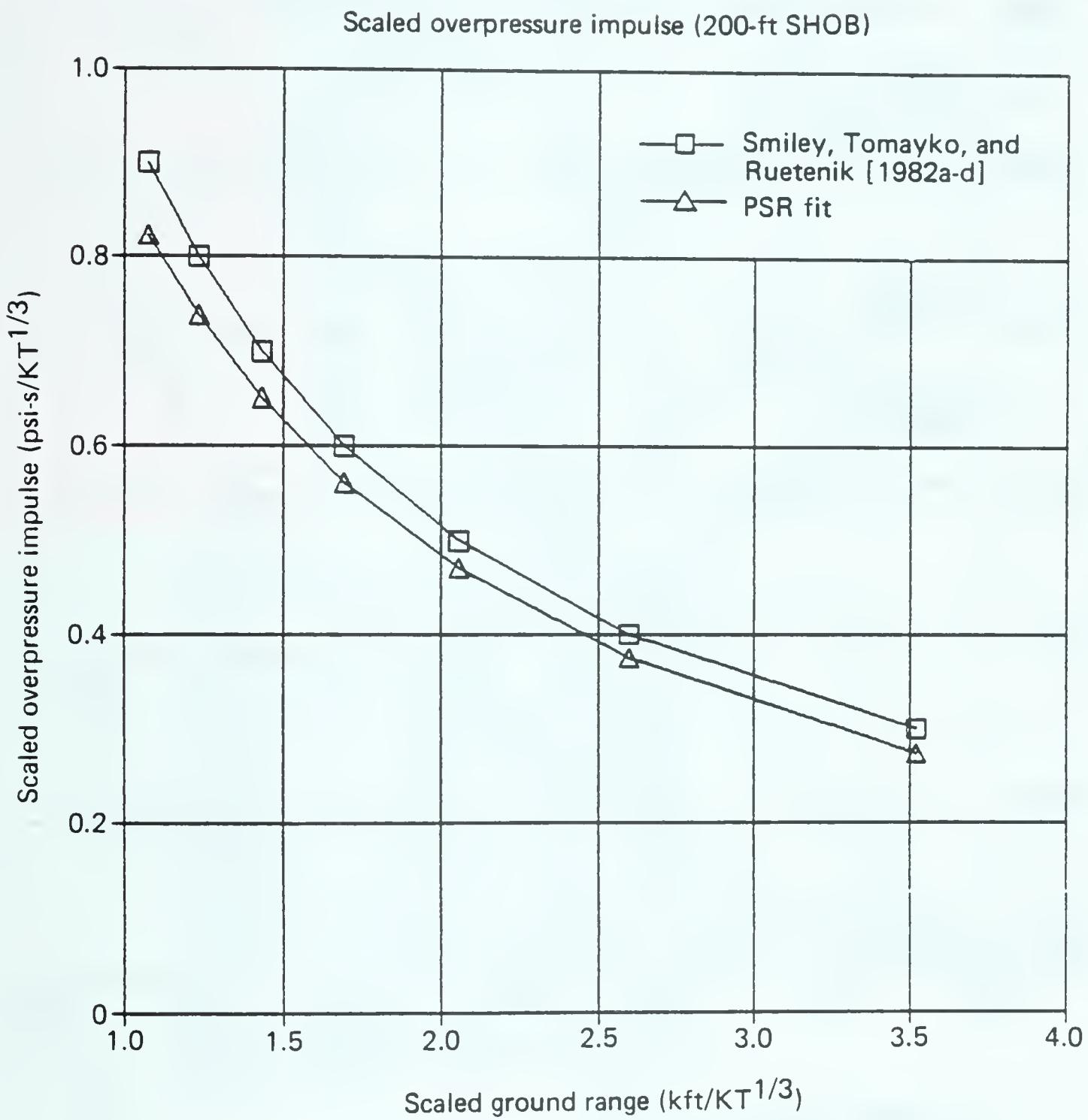


Figure 76. Fit compared to 200-ft SHOB Kaman AviDyne calculation: impulse versus scaled ground range (1 to 3.5 kft).

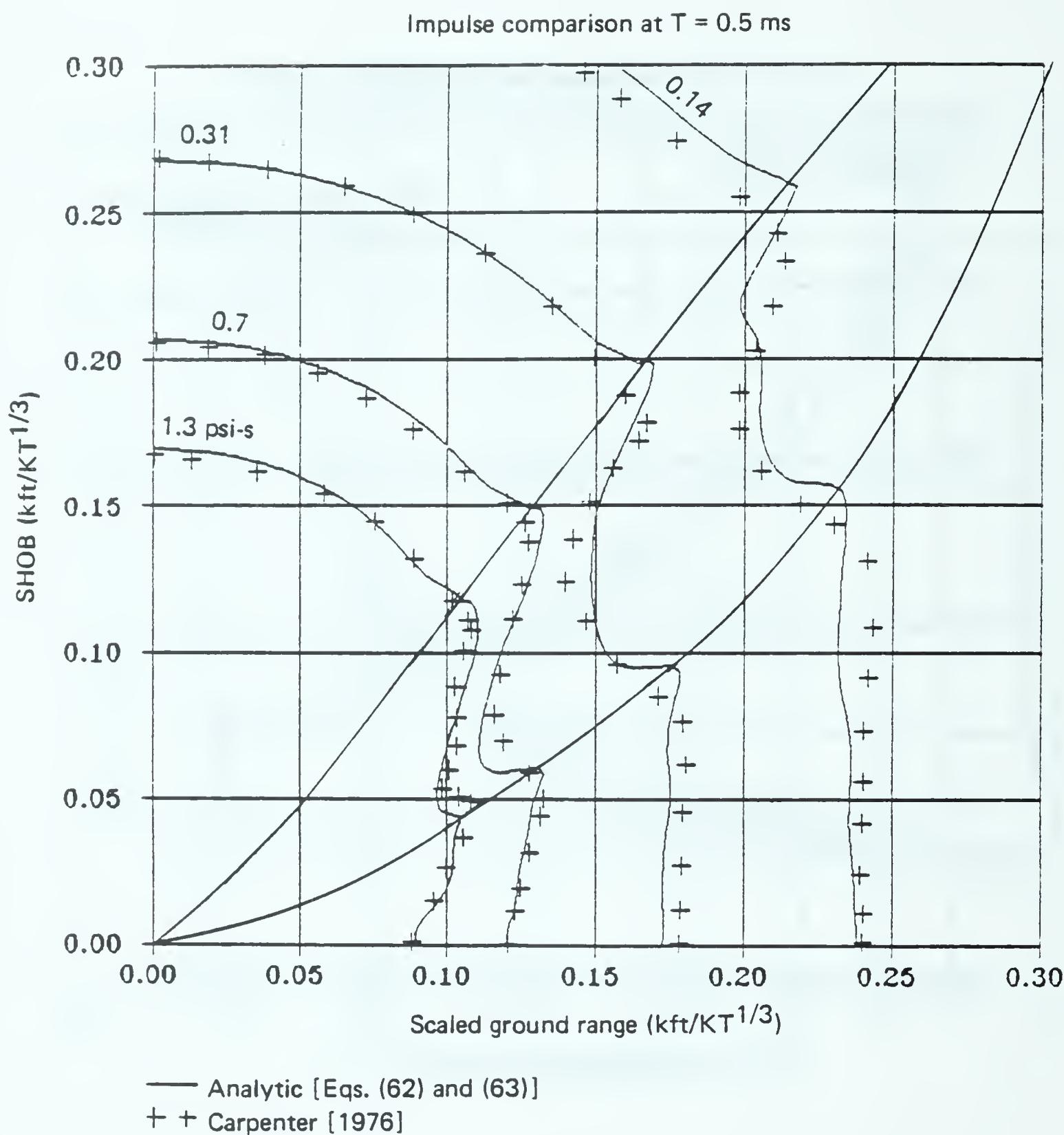


Figure 77. HOB isoimpulse curves: fit compared to 8-1b charge data, showing partial impulse contours for $0.5 \text{ ms}/\text{KT}^{1/3}$.

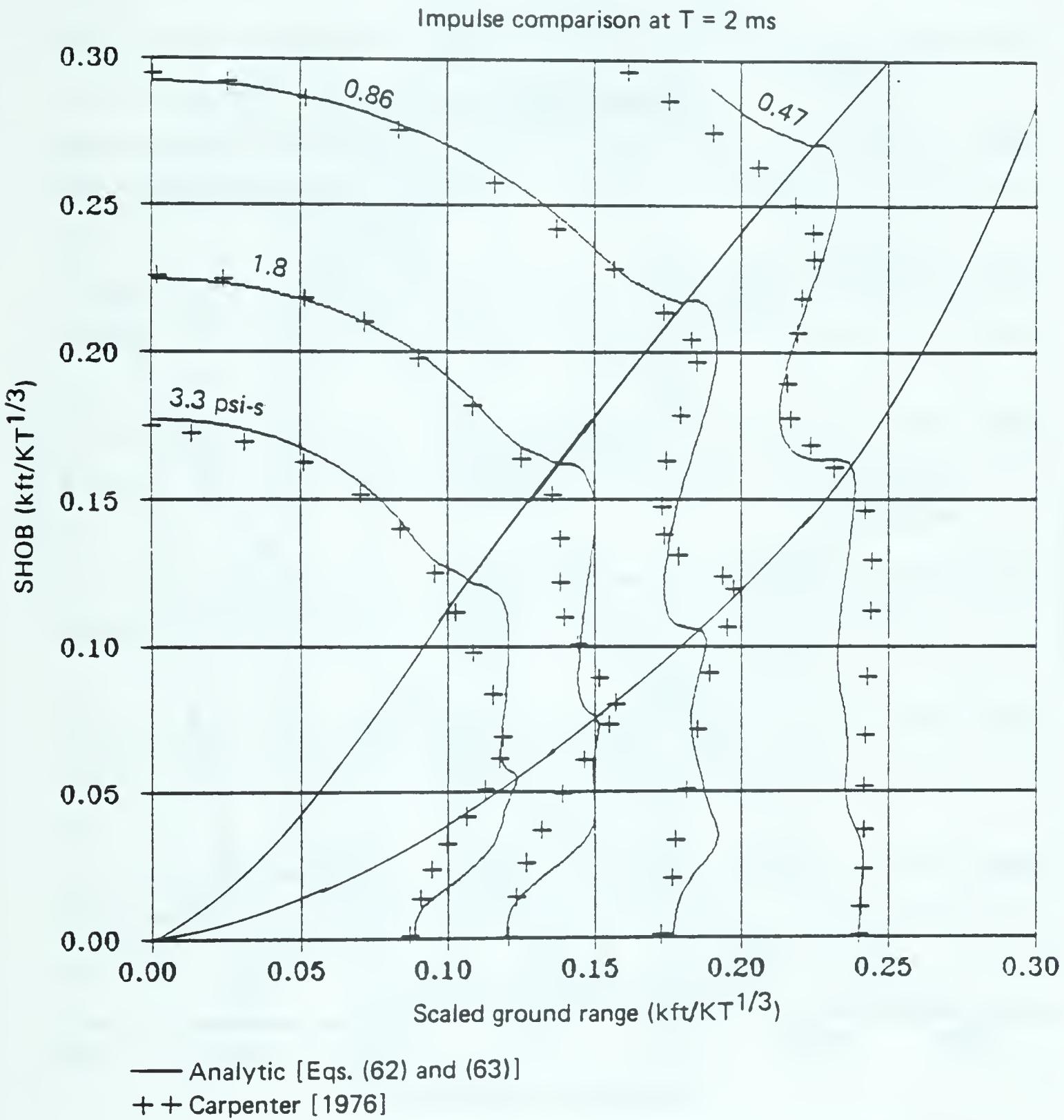


Figure 78. HOB isoimpulse curves: fit compared to 8-lb charge data, showing partial impulse contours for $2 \text{ ms}/\text{KT}^{1/3}$.

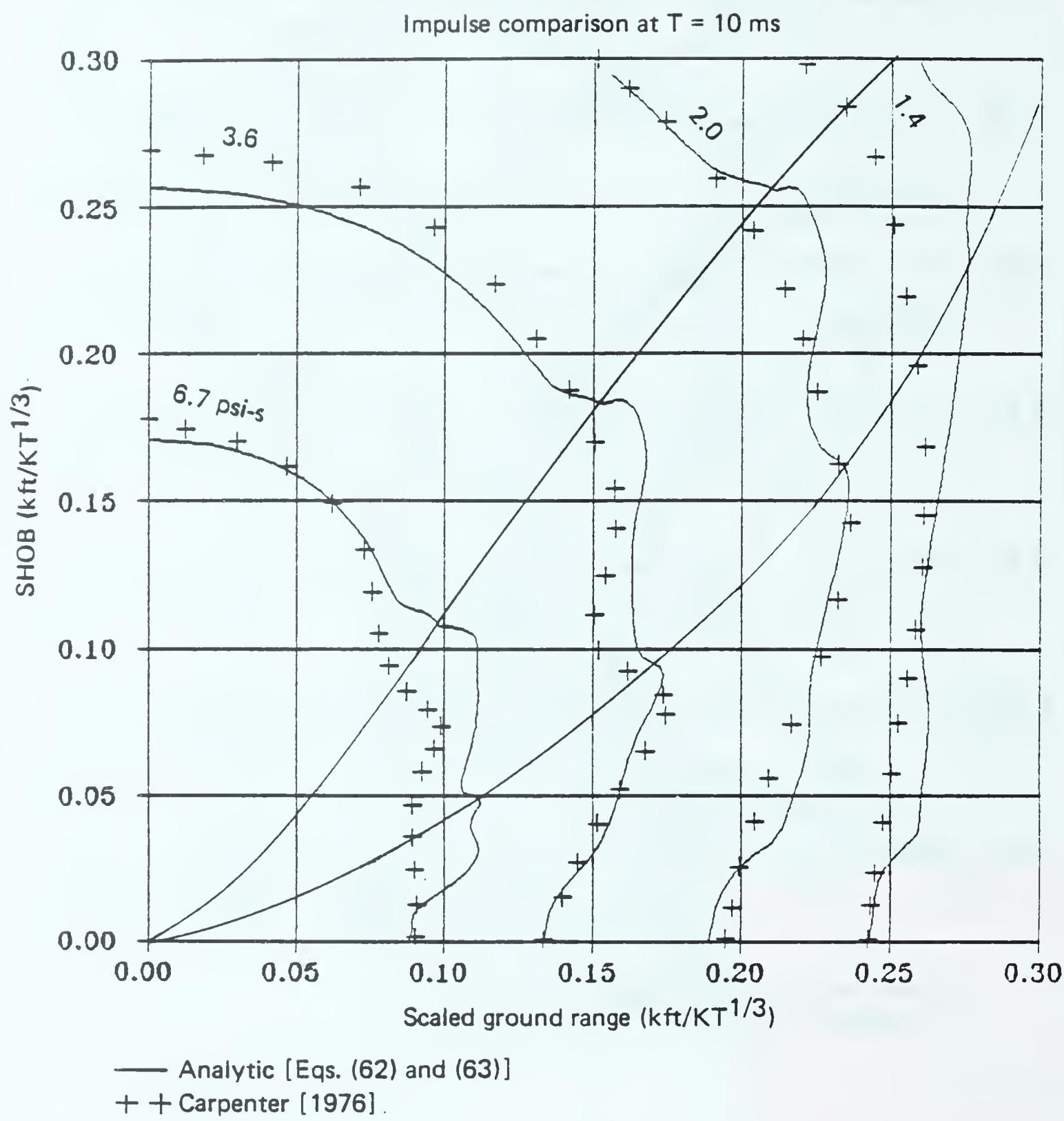


Figure 79. HOB isoimpulse curves: fit compared to 8-1b charge data, showing partial impulse contours for 10 ms/KT^{1/3}.

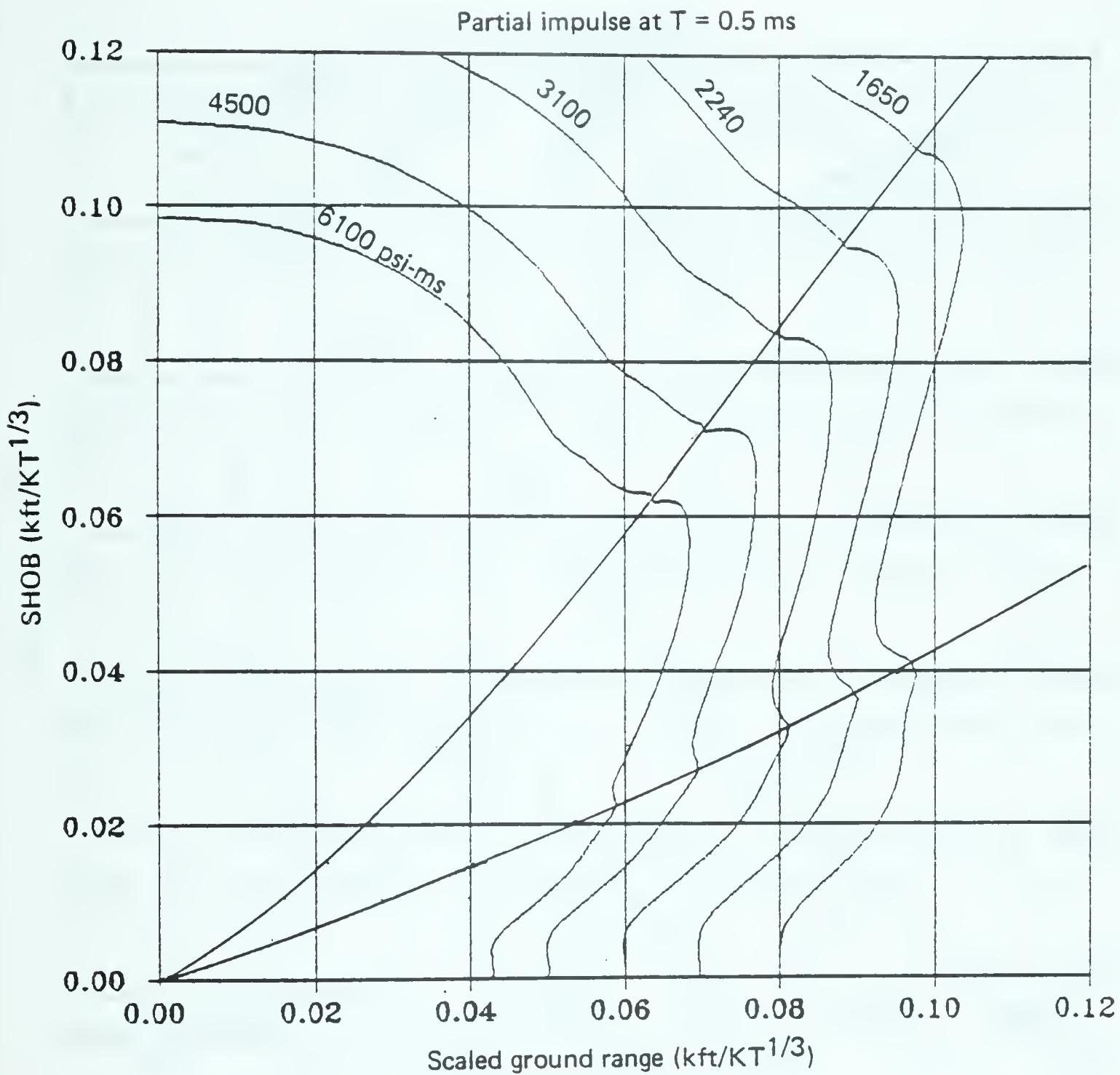


Figure 80. Partial impulse contours at very high overpressure for $0.5 \text{ ms}/\text{KT}^{1/3}$.

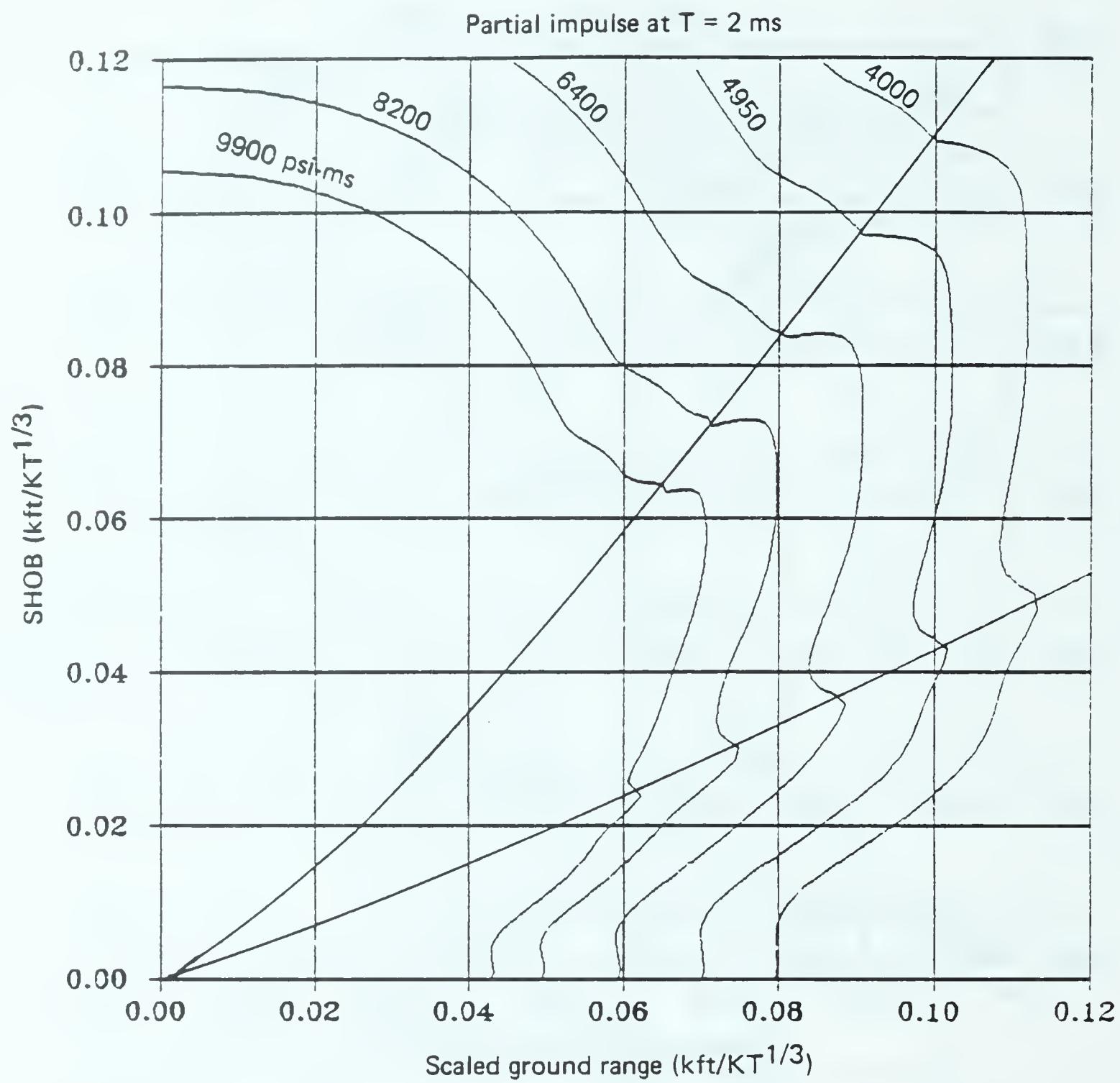


Figure 81. Partial impulse contours at very high overpressure for $2 \text{ ms}/\text{KT}^{1/3}$.

Partial impulse at $T = 10$ ms

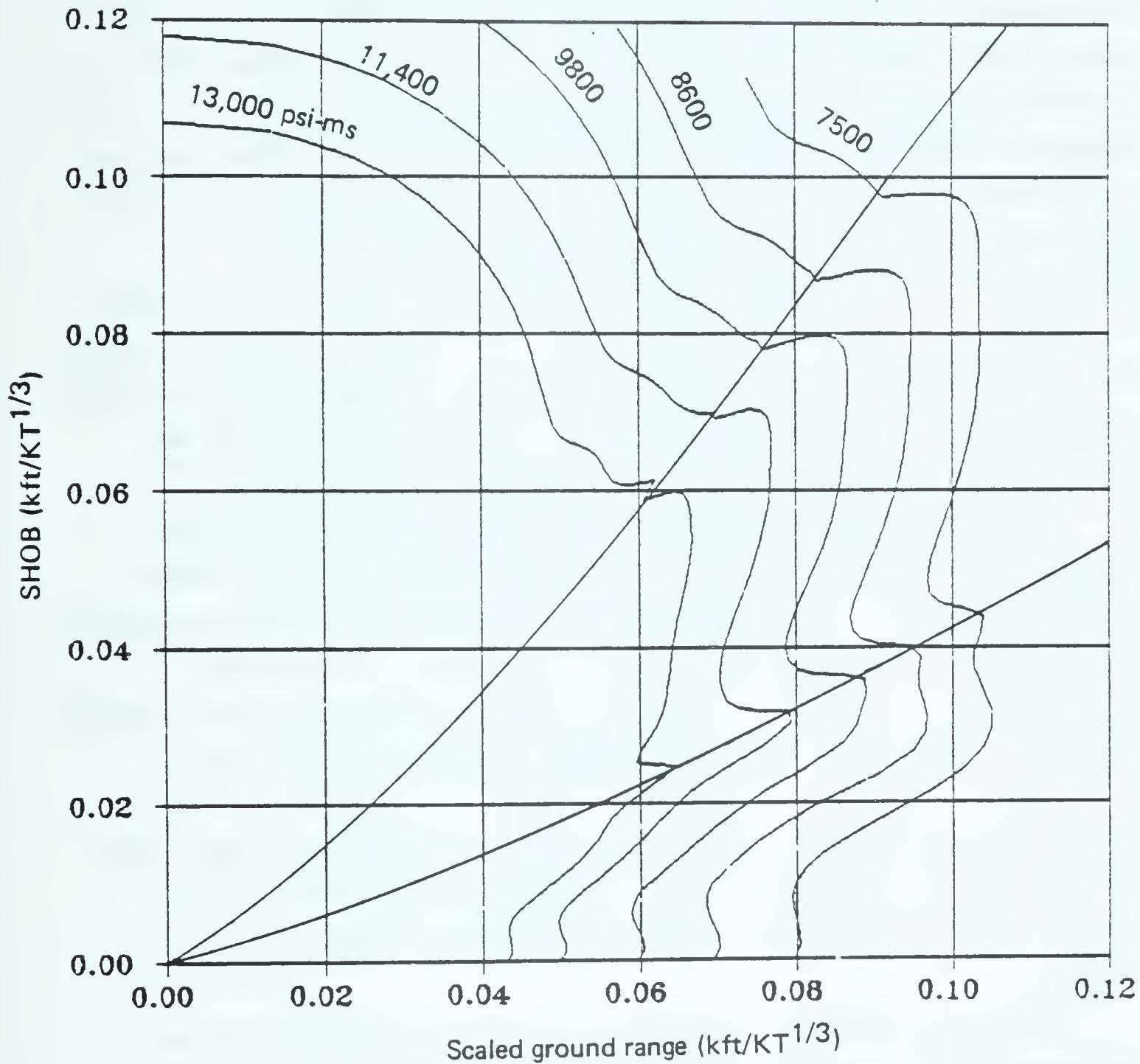


Figure 82. Partial impulse contours at very high overpressure for $10 \text{ ms}/\text{KT}^{1/3}$.

Although the Kaman AviDyne (KA) calculations by Smiley, Tomayko, and Ruetenik [1982a-d] and the NRL calculations of Fry, Kamath, and Book [1985] were not available when this fit was generated, comparisons of the fit to those calculations are quite favorable. Figures 77 through 81 show the peak overpressures and total positive overpressure impulse as functions of scaled ground range for the KA calculations of the fit [Eqs. (62) and (63)] at an SHOB of 200 ft/KT^{1/3}. The largest disparity is shown in Fig. 77 at a range just after the onset of Mach reflection, where the fit (based on the 8-lb charge data) shows considerable pressure increase, while the KA calculations for the same range do not. The KA calculations may suffer most from lack of fine grid zoning in this region.

The overpressure impulse delivered with a time interval comparable to the time to fail for a structure is relevant to dynamic response analyses. For stiff structures designed to survive at high overpressures, the scaled times of interest are the first few milliseconds. Figures 82 through 87 illustrate scaled partial impulse contours (versus SHOB and scaled ground range) for 0.5, 2, and 10 ms/KT^{1/3}. Figures 82 through 84 compare the integral of Eqs. (62) and (63) with the partial impulses scaled from the 8-lb charge tests using PBX-9404 [Carpenter, 1976]. Figures 85 through 87 present partial impulse contours to higher overpressure levels (at closer ranges).

Appendix A contains test values of this fit for the purpose of code checking. A Fortran subroutine for the same fit is given in Appendix B.

PEAK DYNAMIC PRESSURE VERSUS SCALED BURST HEIGHT AND SCALED RANGE.

Speicher [1983] has provided an improved fit to the horizontal peak dynamic pressure from calculations by KA [Smiley, Tomayko, and Ruetenik, 1982; Smiley, Ruetenik, and Tomayko, 1984a,b]; and by [Brode, 1959b]. It follows the general form suggested earlier by Brode [1983]. However, it extends the fit over the entire range inside the regular reflection region, and is valid for dynamic pressures from 1000 psi to 0.05 psi. The form for the peak dynamic pressure Q_s is as follows:

$$Q_s = Q_1 = \frac{Ar^D}{1 + Br^E} + \frac{C}{r^F} \quad \text{for } x \geq x_q ,$$

$$Q_s = Q_m \exp \left[\frac{GL^I}{1 + 649L^I} - \frac{4.01L^J}{1 + HL^J} + 7.67 \times 10^{-6} \right. \\ \left. \times \left(\frac{1}{K + L^{3.22}} - \frac{1}{K} \right) \right] \quad \text{for } x < x_q , \quad (64)$$

where r = scaled slant range in kilofeet per cube-root kiloton,
 $= \sqrt{x^2 + y^2}$,
 x = scaled ground range in kilofeet per cube-root kiloton,
 y = scaled burst height in kilofeet per cube-root kiloton,
 x_q = approximate interface between regular and Mach reflection
in kilofeet per cube-root kiloton,

$$= \frac{63.5y^{7.26}}{1 + 67.11y^{4.746}} + 0.6953y^{0.808} ,$$

$Q_m = Q_1$ evaluated at $x = x_q$ (at $M = 1$),

i.e., for $r = \sqrt{x_q^2 + y^2}$,

$M = x_q/x$,

$L = \log_{10}(M)$,

$$A = -236.1 + \frac{17.72M^{0.593}}{1 + 10.4M^{3.124}} ,$$

$$B = 12.27 - \frac{21.69M^{2.24}}{1 + 6.976M^{0.484}} ,$$

$$C = 20.26 + \frac{14.7M^2}{1 + 0.08747M^{3.05}} ,$$

$$D = -1.137 - \frac{0.5606M^{0.895}}{1 + 3.046M^{7.48}},$$

$$E = 1.731 + \frac{10.84M^{1.12}}{1 + 12.26M^{0.0014}},$$

$$F = 2.84 + \frac{0.855M^{0.9}}{1 + 1.05M^{2.84}},$$

$$G = 50 - \frac{1843y^{2.153}}{1 + 3.95y^{5.08}},$$

$$H = 0.294 + \frac{71.56y^{8.7}}{1 + 115.3y^{6.186}},$$

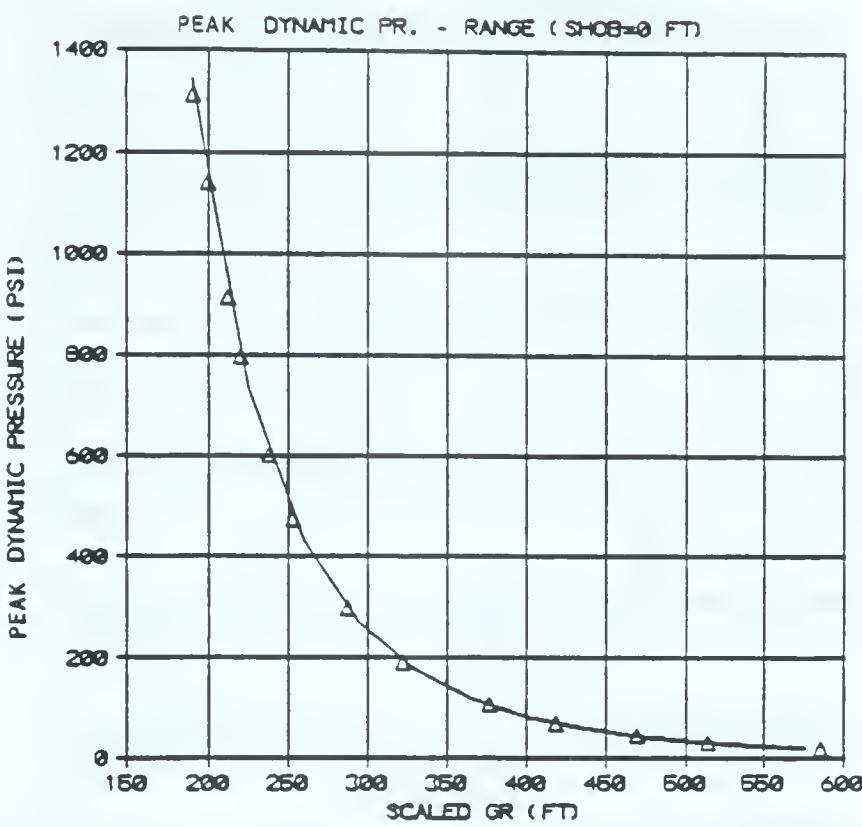
$$I = \left| -3.324 + \frac{987.5y^{4.77}}{1 + 211.8y^{5.166}} \right|,$$

$$J = 1.955 + \frac{169.7y^{9.317}}{1 + 97.36y^{6.513}},$$

$$K = 8.123 \times 10^{-6} + \frac{0.001613y^{6.428}}{1 + 60.26y^{7.358}}.$$

In the above equation, X_q is within 16 percent of X_m [as X_m is defined in Eq. (63)].

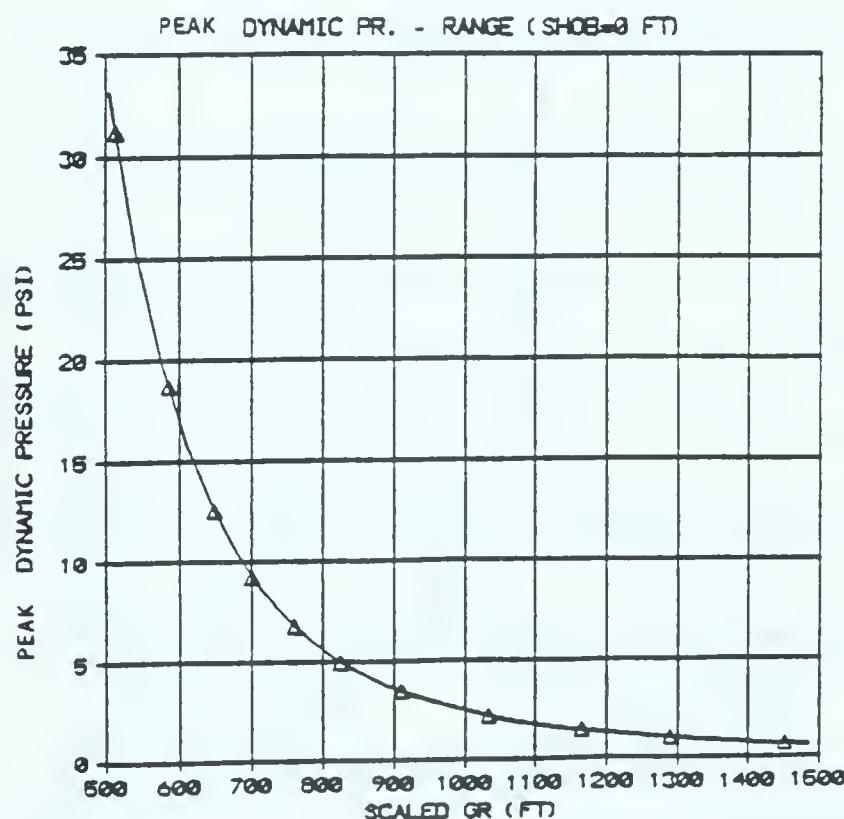
The closeness of this fit is illustrated in Figs. 88 through 106. In those figures, the data points are represented by triangles (Δ). Figures 88 through 90 compare the peak dynamic pressure versus range for a surface burst with the detailed calculation results of KA [Ruetenik, 1984] and the early calculation by Brode [1959b]. The fit is very close at all ranges from 190 to 3000 ft/ $KT^{1/3}$, i.e., from 1400



Note: Δ = calculation result.

Source: Brode [1959b] and Ruetenik [1984].

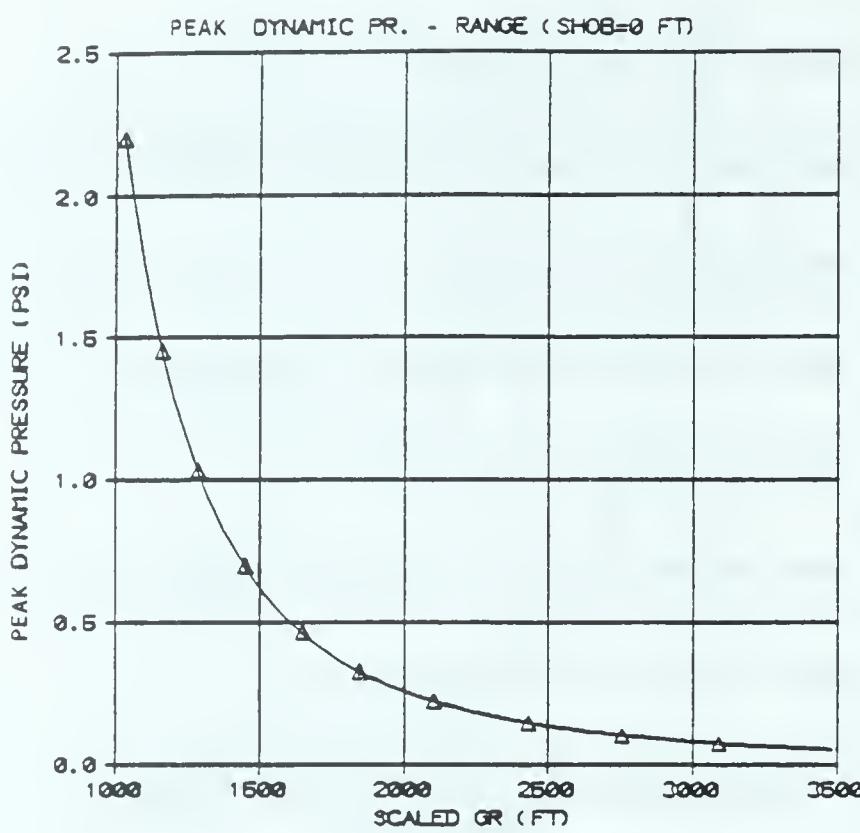
Figure 83. Peak dynamic pressure fit compared to Kaman AviDyne calculation, for surface burst, high-pressure region.



Note: Δ = calculation result.

Source: Brode [1959b] and Ruetenik [1984].

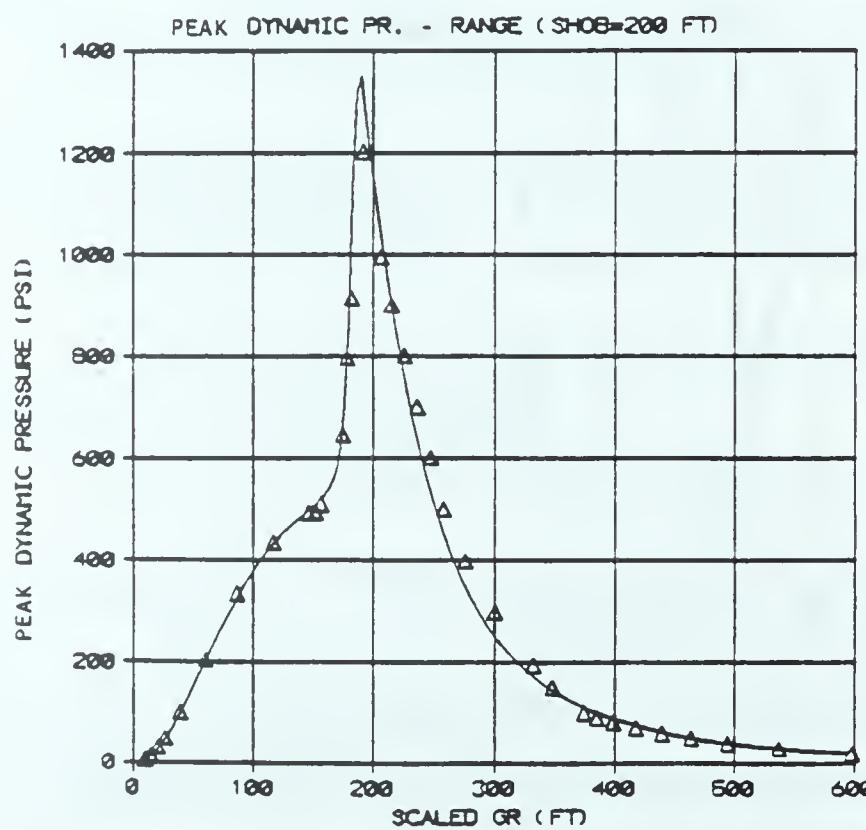
Figure 84. Peak dynamic pressure fit compared to Kaman AviDyne calculation, for surface burst, intermediate region.



Note: Δ = calculation result.

Source: Brode [1959b] and Ruetenik [1984].

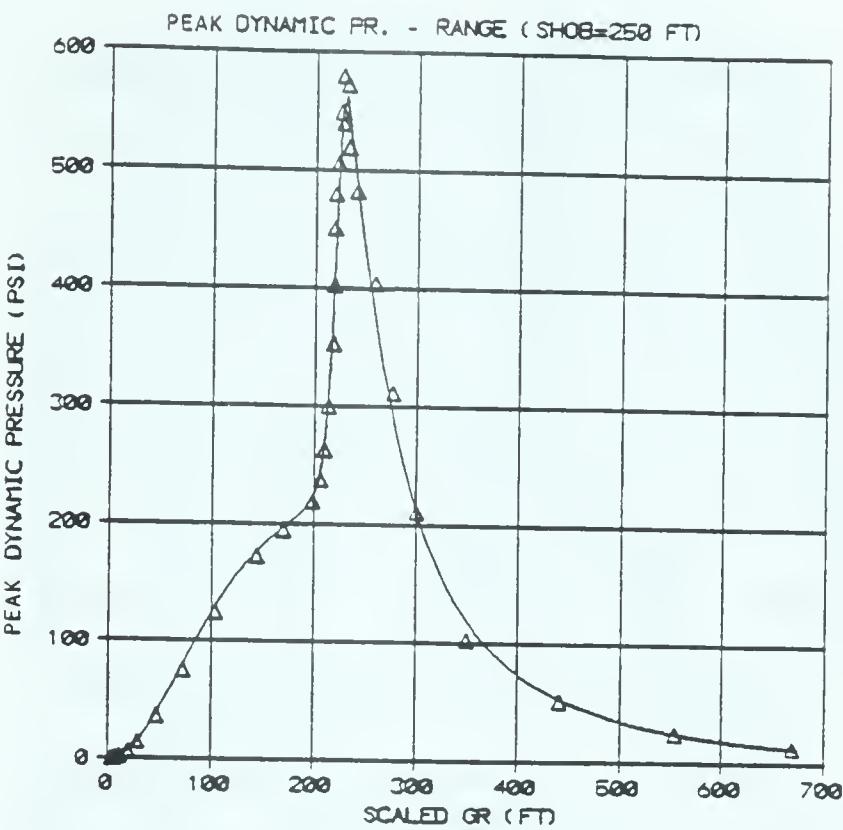
Figure 85: Peak dynamic pressure fit compared to Kaman AviDyne calculation, for surface burst, low-pressure region.



Note: Δ = calculation result.

Source: Smiley, Tomayko, and Ruetenik [1982 a-d].

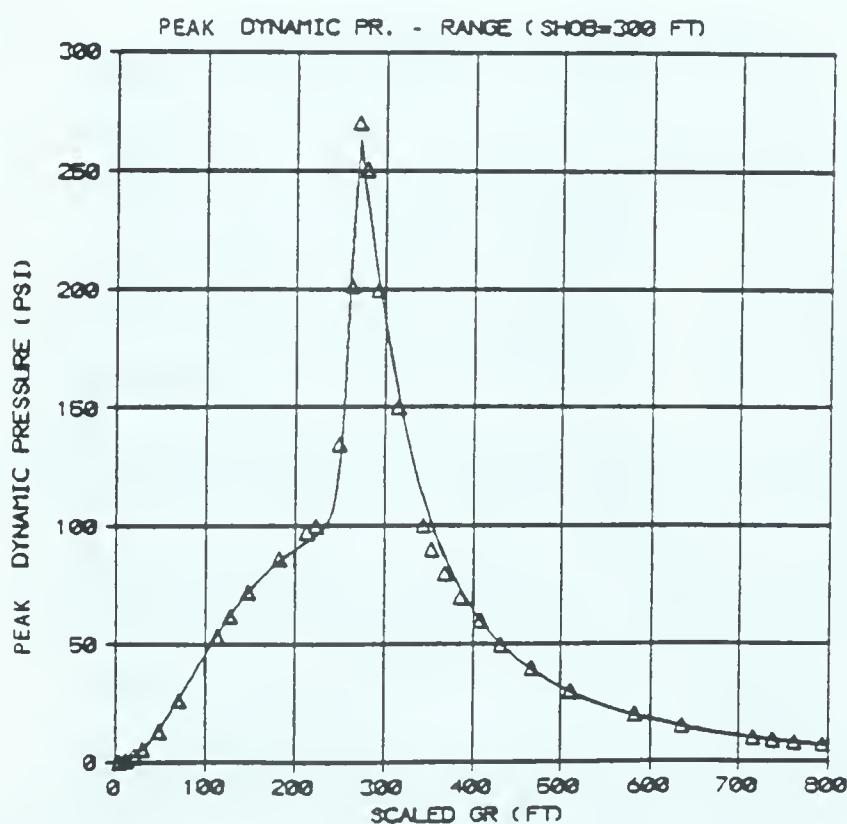
Figure 86. Peak dynamic pressure fit compared to Kaman AviDyne calculation, for scaled burst height of 200 ft/ $KT^{1/3}$.



Note: Δ = calculation result.

Source: Smiley, Tomayko, and Ruetenik [1982 a-d].

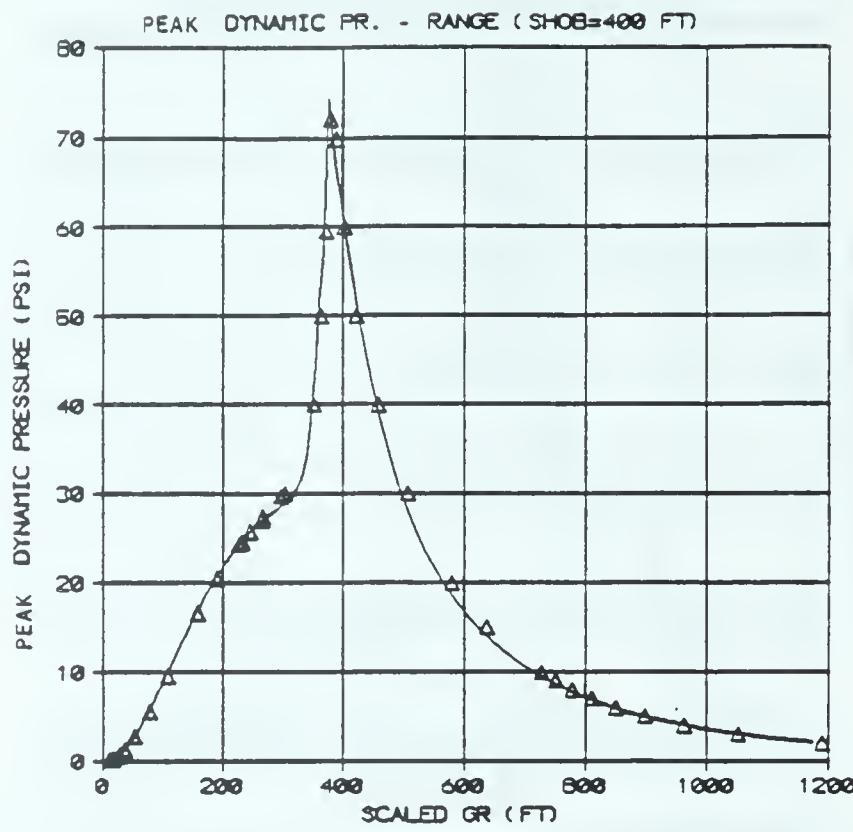
Figure 87. Peak dynamic pressure fit compared to Kaman AviDyne calculation, for scaled burst height of 250 ft/ $KT^{1/3}$.



Note: Δ = calculation result.

Source: Smiley, Tomayko, and Ruetenik [1982 a-d].

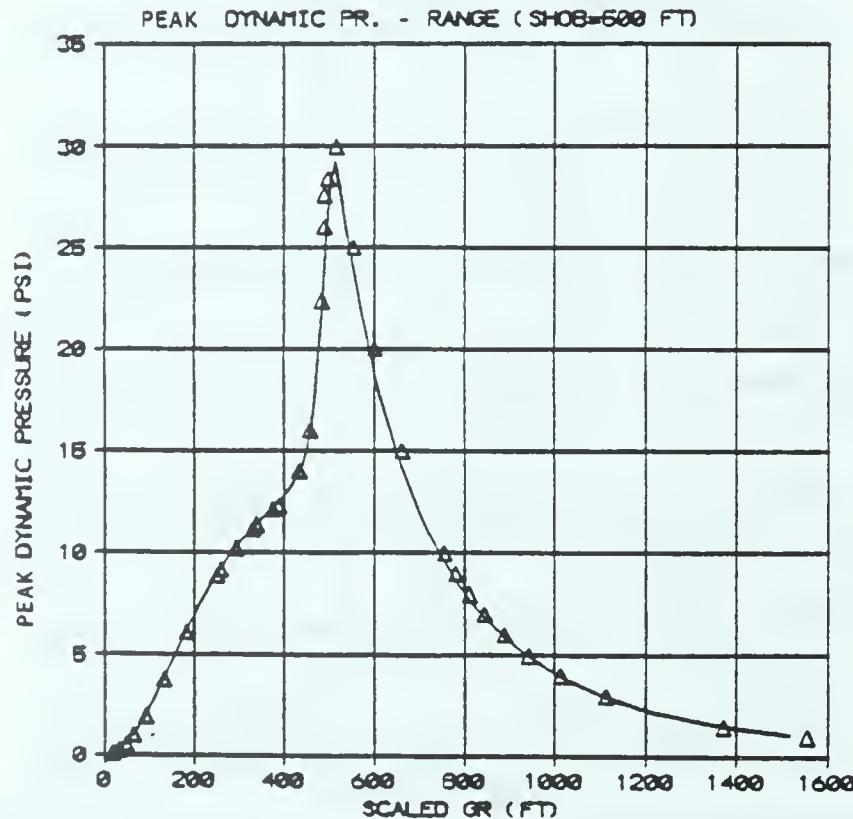
Figure 88. Peak dynamic pressure fit compared to Kaman Avidyne calculation, for scaled burst height of 300 ft/ $KT^{1/3}$.



Note: Δ = calculation result.

Source: Smiley, Tomayko, and Ruetenik [1982a-d].

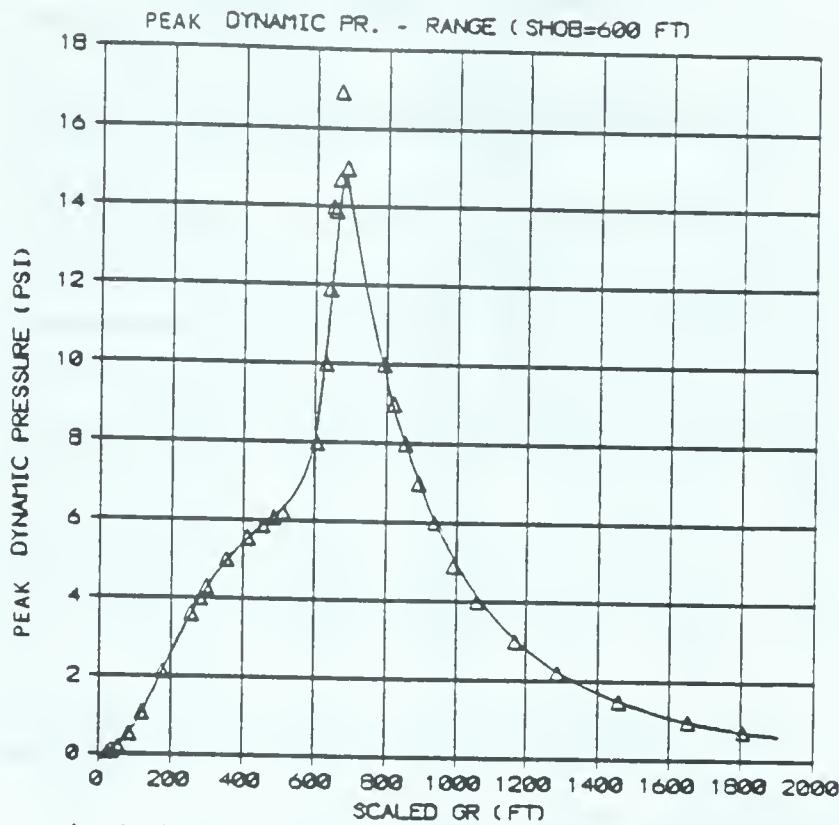
Figure 89. Peak dynamic pressure fit compared to Kaman AviDyne calculation, for scaled burst height of 400 ft/ $KT^{1/3}$.



Note: Δ = calculation result.

Source: Smiley, Ruetenik, and Tomayko [1984b].

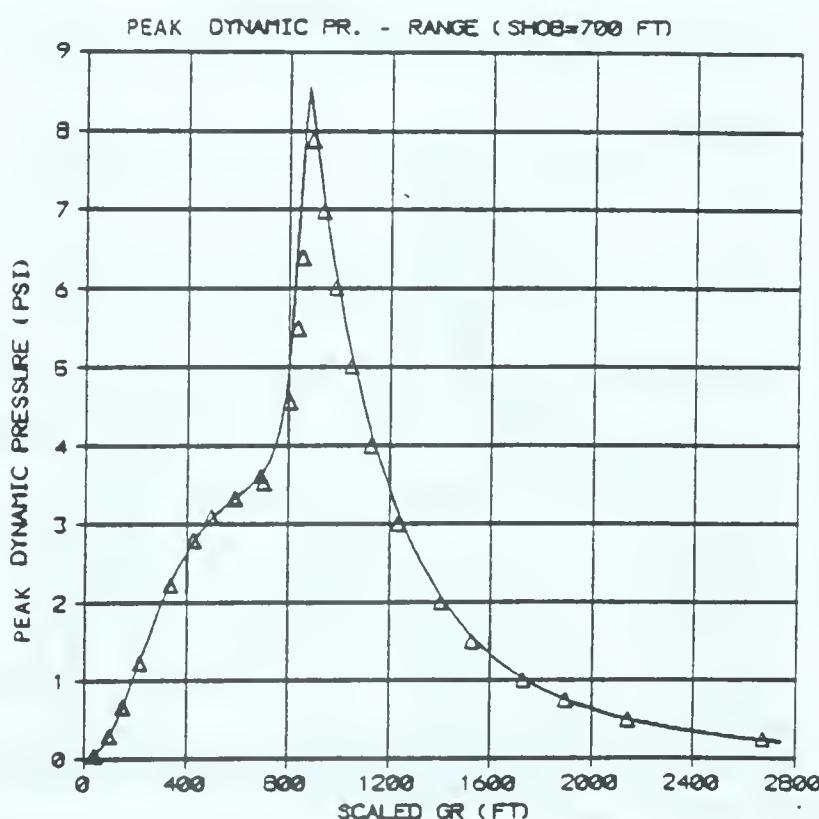
Figure 90. Peak dynamic pressure fit compared to Kaman AviDyne calculation, for scaled burst height of 500 ft/ $KT^{1/3}$.



Note: Δ = calculation result.

Source: Smiley, Ruetenik, and Tomayko [1984b].

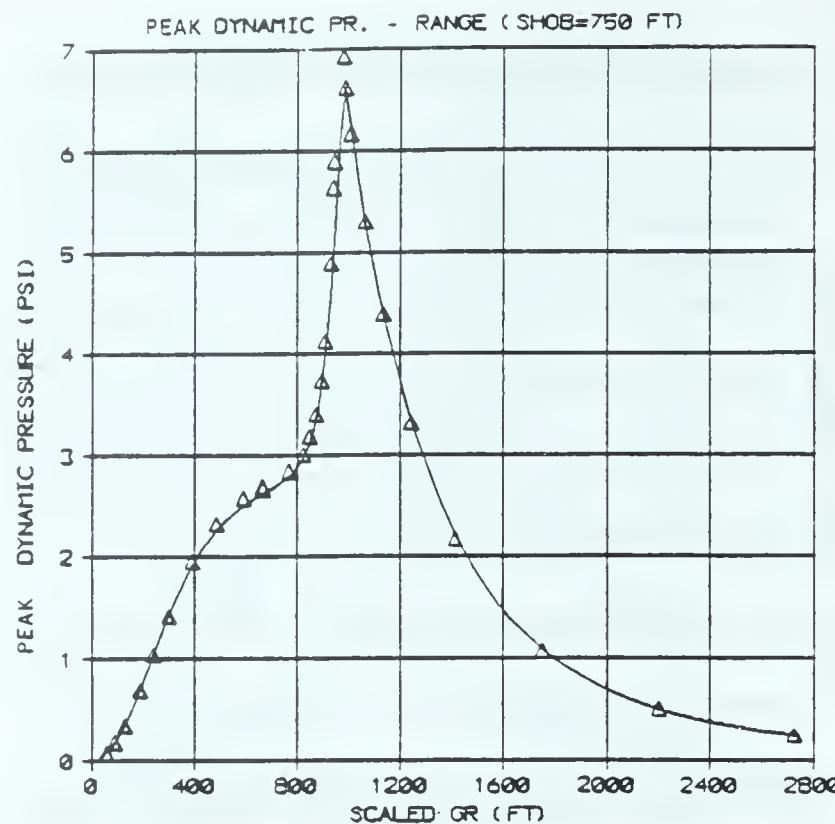
Figure 91. Peak dynamic pressure fit compared to Kaman AviDyne calculation, for scaled burst height of 600 ft/ $KT^{1/3}$.



Note: Δ = calculation result.

Source: Smiley, Tomayko, and Ruetenik [1982a-d].

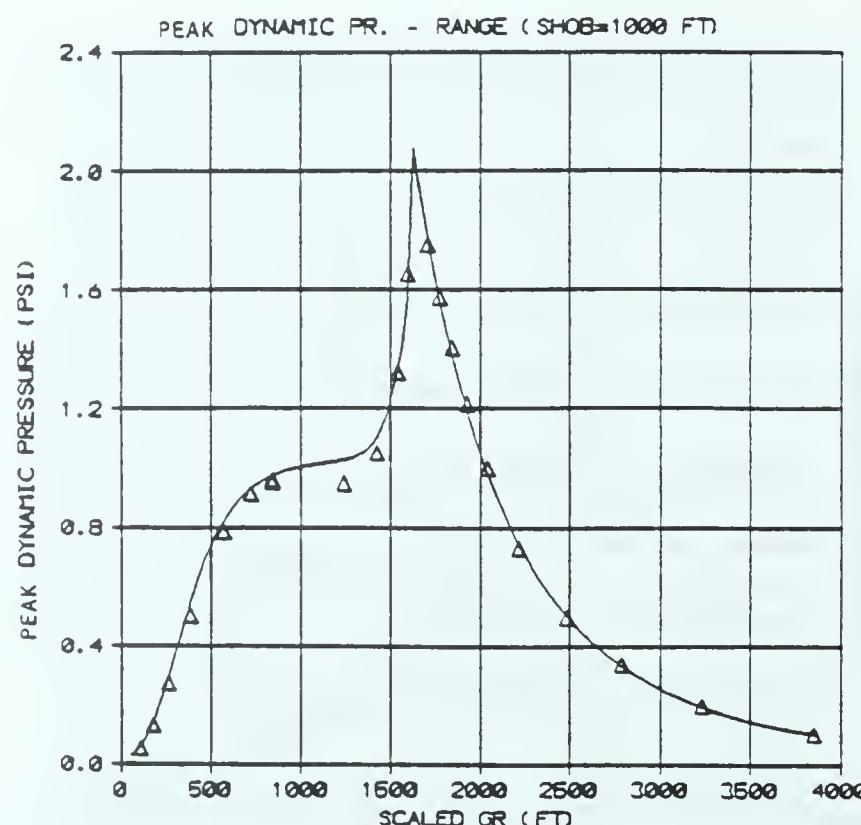
Figure 92. Peak dynamic pressure fit compared to Kaman AviDyne calculation, for scaled burst height of 700 ft/ $KT^{1/3}$.



Note: Δ = calculation result.

Source: Smiley, Ruetenik, and Tomayko [1984a].

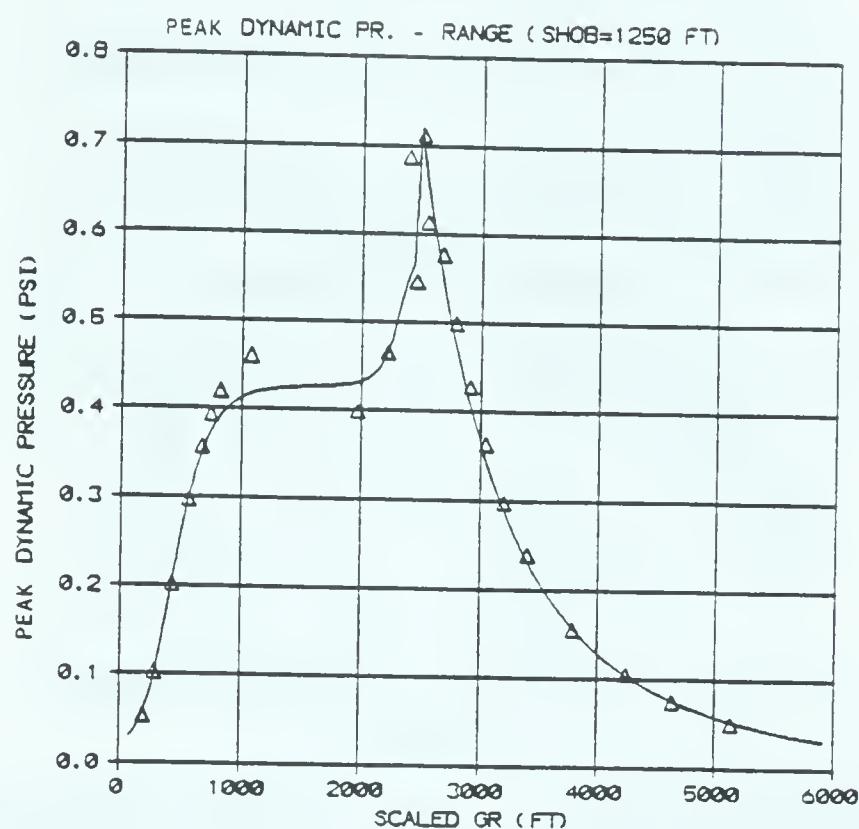
Figure 93. Peak dynamic pressure fit compared to Kaman AviDyne calculation, for scaled burst height of 750 ft/ $KT^{1/3}$.



Note: Δ = calculation result.

Source: Smiley, Ruetenik, and Tomayko [1984a].

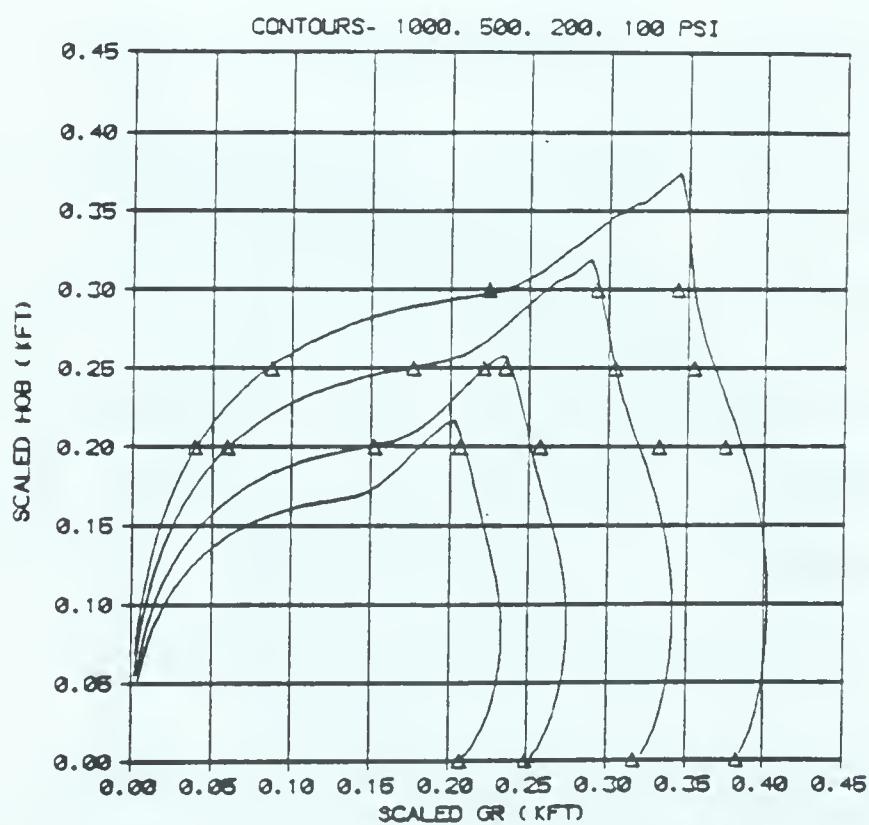
Figure 94. Peak dynamic pressure fit compared to Kaman AviDyne calculation, for scaled burst height of 1000 ft/ $KT^{1/3}$.



Note: Δ = calculation result.

Source: Smiley, Ruetenik, and Tomayko [1984a].

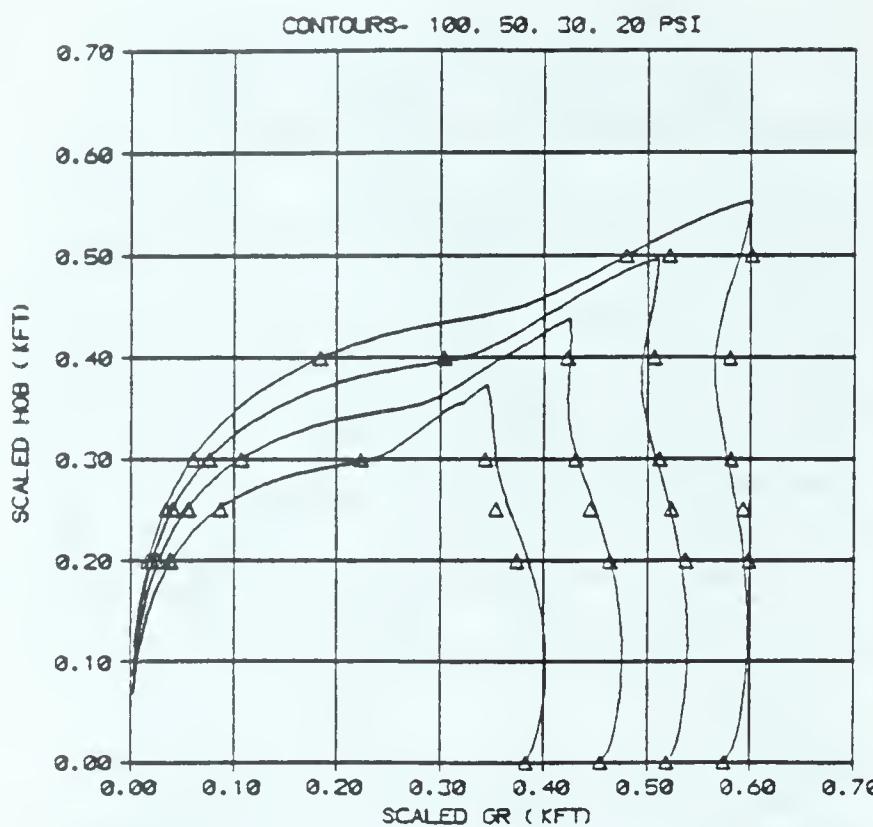
Figure 95. Peak dynamic pressure fit compared to Kaman AviDyne calculation, for scaled burst height of 1250 ft/ $KT^{1/3}$.



Note: Δ = calculation result.

Source: Smiley, Ruetenik, and Tomayko [1984a, b]; Smiley, Tomayko, and Ruetenik [1982 a-d]; Ruetenik [1984]; and Brode [1959b].

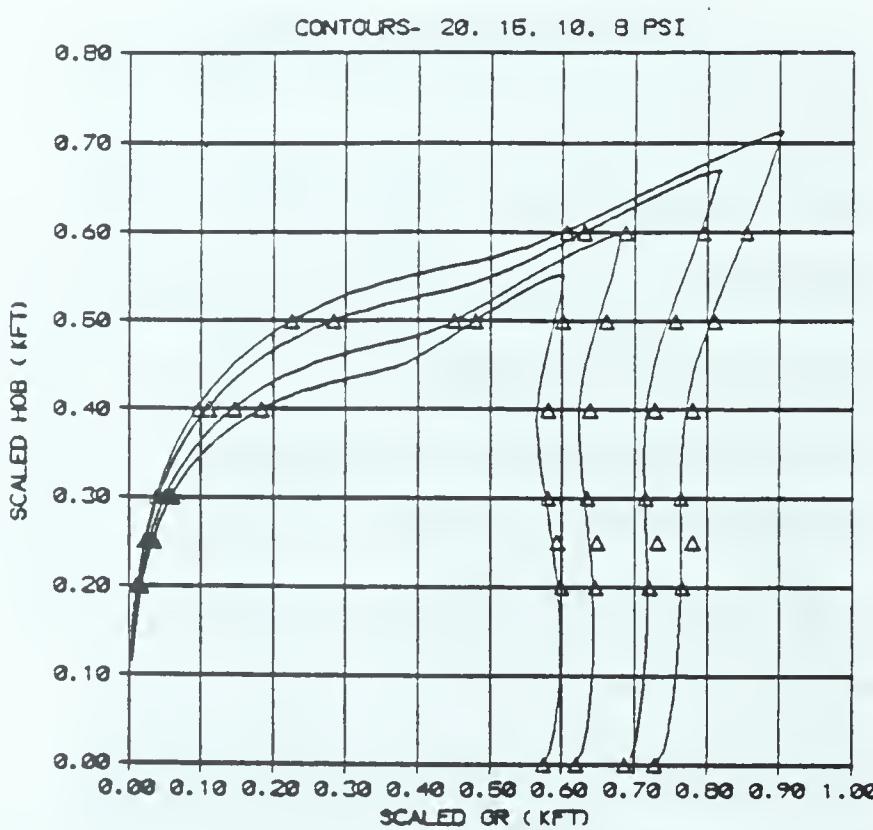
Figure 96. HOB isopicnic contours from Kaman AviDyne calculations compared to fit for peak dynamic pressure (100 to 1000 psi).



Note: Δ = calculation result.

Source: Smiley, Ruetenik, and Tomayko [1984a, b]; Smiley, Tomayko, and Ruetenik [1982 a-d]; Ruetenik [1984]; and Brode [1959b].

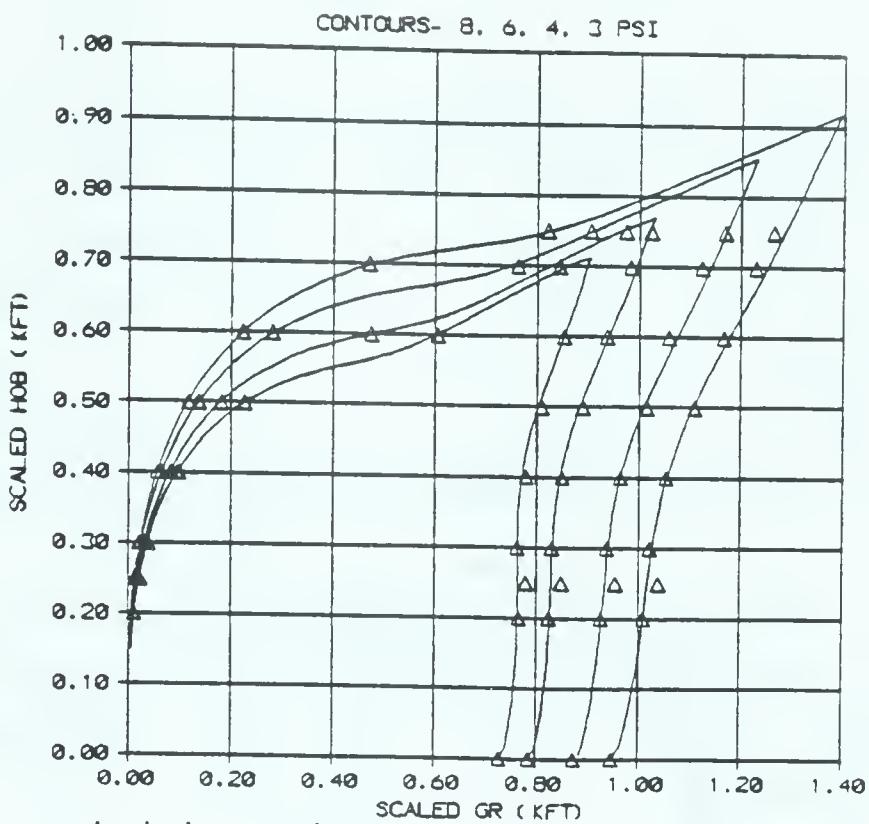
Figure 97. HOB isopicnic contours from Kaman AviDyne calculations compared to fit for peak dynamic pressure (20 to 100 psi).



Note: Δ = calculation result.

Source: Smiley, Ruetenik, and Tomayko [1984a, b]; Smiley, Tomayko, and Ruetenik [1982 a-d]; Ruetenik [1984]; and Brode [1959b].

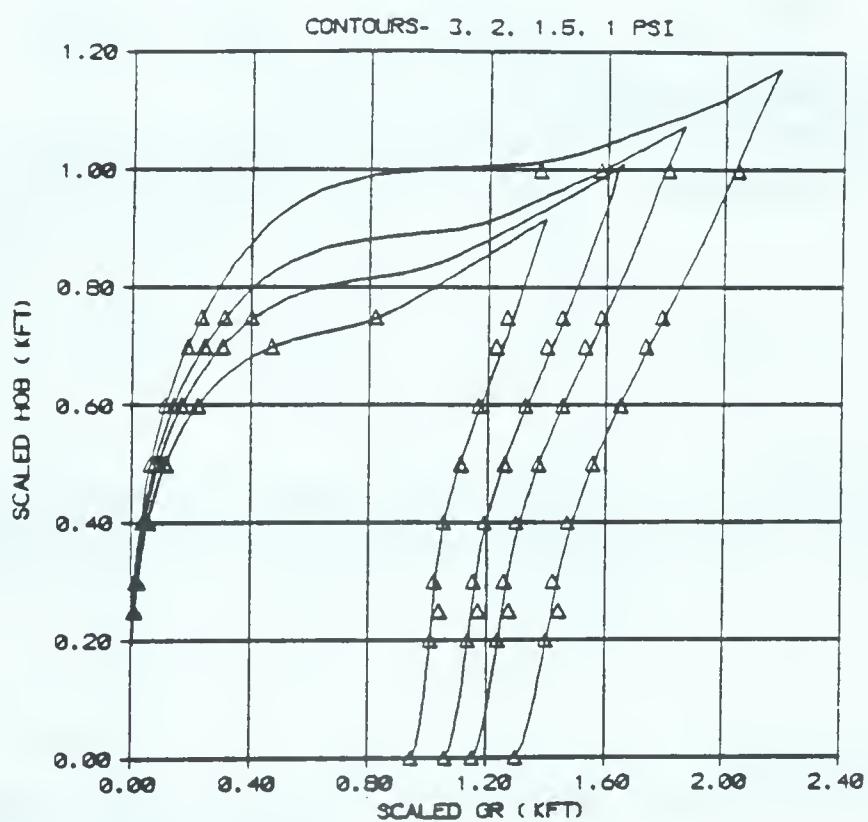
Figure 98. HOB isopicnic contours from Kaman AviDyne calculations compared to fit for peak dynamic pressure (8 to 20 psi).



Note: Δ = calculation result.

Source: Smiley, Ruetenik, and Tomayko [1984a, b] ; Smiley, Tomayko, and Ruetenik [1982 a-d] ; Ruetenik [1984] ; and Brode [1959b].

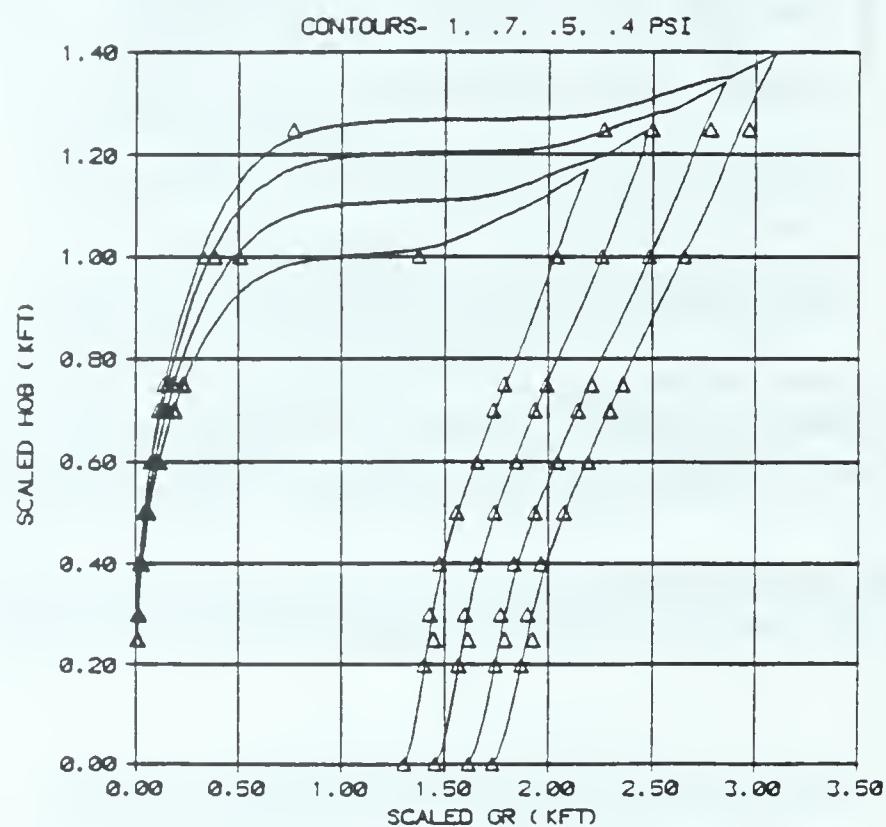
Figure 99. HOB isopicnic contours from Kaman AviDyne calculations compared to fit for peak dynamic pressure (3 to 8 psi).



Note: Δ = calculation result.

Source: Smiley, Ruetenik, and Tomayko [1984a, b] ; Smiley, Tomayko, and Ruetenik [1982 a-d] ; Ruetenik [1984] ; and Brode [1959b].

Figure 100. HOB isopicnic contours from Kaman AviDyne calculations compared to fit for peak dynamic pressure (1 to 3 psi).



Note: Δ = calculation result.

Source: Smiley, Ruetenik, and Tomayko [1984a, b] ; Smiley, Tomayko, and Ruetenik [1982 a-d] ; Ruetenik [1984] ; and Brode [1959b].

Figure 101. HOB isopicnic contours from Kaman AviDyne calculations compared to fit for peak dynamic pressure (0.4 to 1 psi).

down to 0.05 psi. Figures 91 through 100 compare the peak dynamic pressure fit for various scaled burst heights from 200 to 1250 ft/KT^{1/3}, corresponding to KA calculations [Smiley, Tomayko, and Ruetenik, 1982; Smiley, Ruetenik, and Tomayko, 1984a,b]. Again, the fit is very good. It faithfully follows the sharp maximum around the transition from regular reflection to Mach reflection and the change of the character in the regular reflection region as the burst height is increased.

Isopicnic contours of peak dynamic pressure are plotted versus scaled burst height and ground range and compared with data points in Figs. 101 through 109. The dynamic pressure range is 0.05 to 1000 psi.

SCALED DYNAMIC IMPULSE VERSUS SCALED BURST HEIGHT AND GROUND RANGE.

A simple fit exists for the integral of dynamic pressure with time over the positive (outward flow) phase, as defined in Eq. (53). This fit is restricted to the Mach reflection region and has the form

$$I_u^+ = \left(\frac{Ex}{F + x^{3.61}} + \frac{G}{1 + 0.22x^2} \right) \times m \quad \text{psi-ms} , \quad (65)$$

where $E = 183(y^2 + 0.00182)/(y^2 + 0.00222)$,

$F = 0.00058 \exp(9.5y) + 0.0117 \exp(-22y)$,

$G = 2.3 + 29y/(1 + 1760y^5) + 25y^4/(1 + 3.76y^6)$,

but this approximation is valid only for

$$x > x_i = 170\psi/(1 + 337\psi^{1/4}) + 0.914\psi^{2.5} ,$$

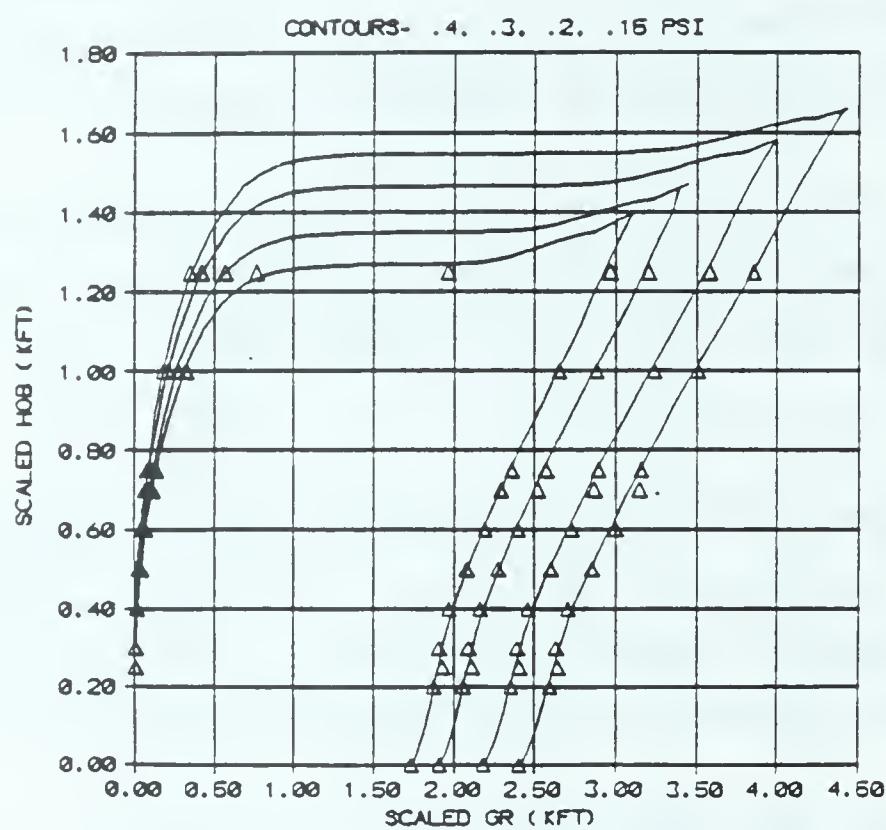
where $\psi = y + 0.09$,

y = scaled burst height H in kilofeet per cube-root kiloton,

$$= H/1000W^{1/3} ,$$

x = scaled ground range GR in kilofeet per cube-root kiloton,

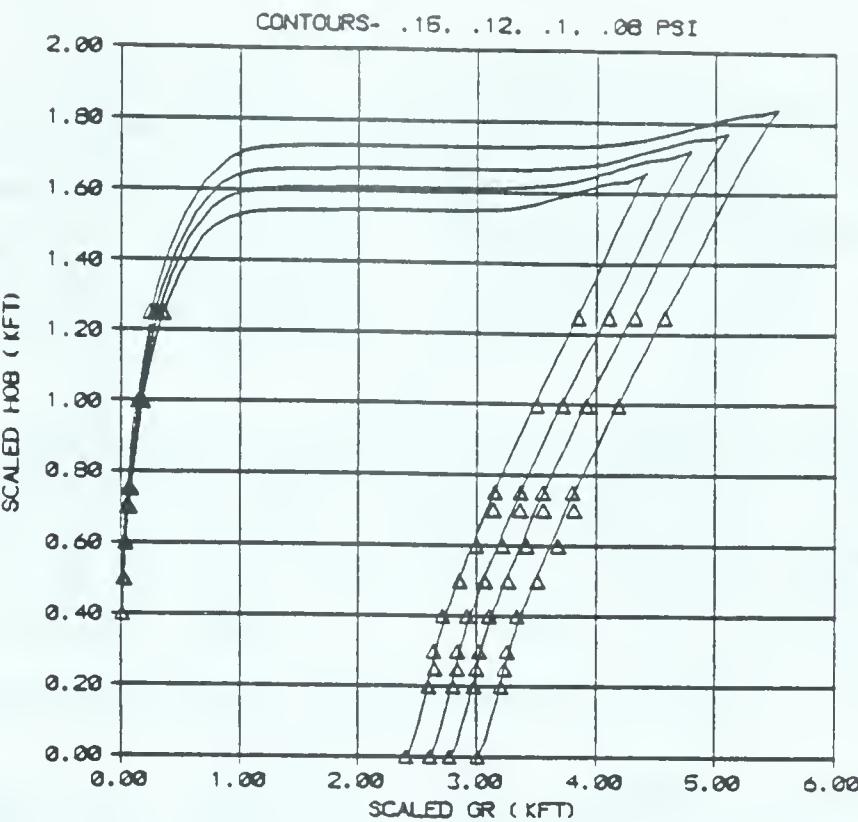
$$= GR/1000W^{1/3} .$$



Note: Δ = calculation result.

Source: Smiley, Ruetenik, and Tomayko [1984a, b]; Smiley, Tomayko, and Ruetenik [1982 a-d]; Ruetenik [1984]; and Brode [1959b].

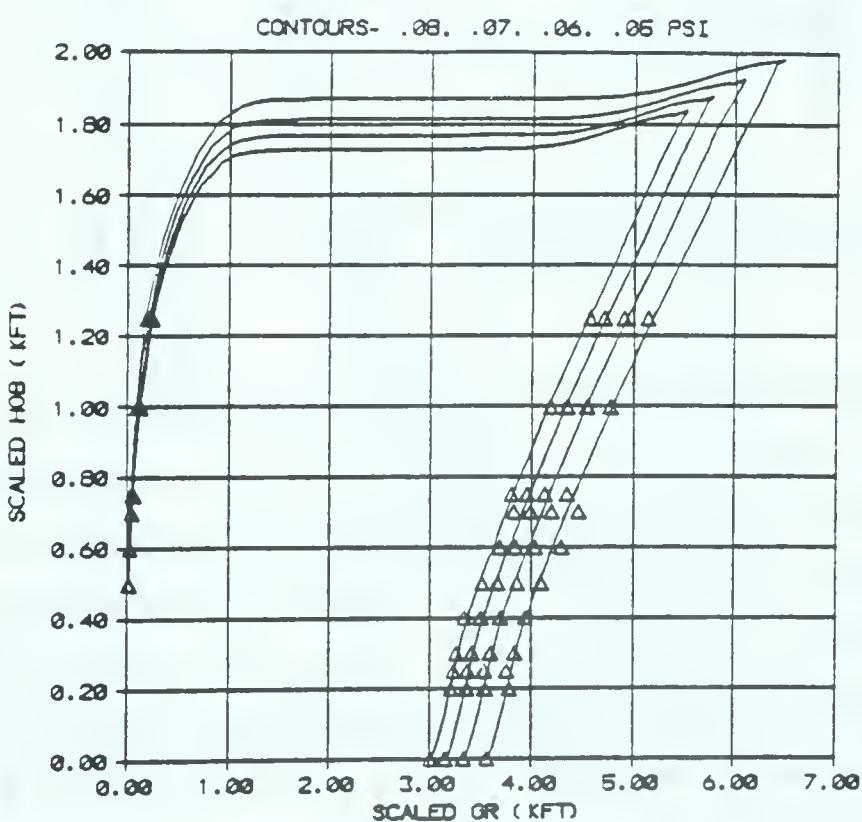
Figure 102. HOB isopicnic contours from Kaman AviDyne calculations compared to fit for peak dynamic pressure (0.15 to 0.4 psi).



Note: \triangle = calculation result.

Source: Smiley, Ruetenik, and Tomayko [1984a, b]; Smiley, Tomayko, and Ruetenik [1982 a-d]; Ruetenik [1984]; and Brode [1959b].

Figure 103. HOB isopicnic contours from Kaman AviDyne calculations compared to fit for peak dynamic pressure (0.08 to 0.15 psi).



Note: \triangle = calculation result.

Source: Smiley, Ruetenik, and Tomayko [1984a, b]; Smiley, Tomayko, and Ruetenik [1982 a-d]; Ruetenik [1984]; and Brode [1959b].

Figure 104. HOB isopicnic contours from Kaman Avidyne calculations compared to fit for peak dynamic pressure (0.05 to 0.08 psi).

This fit differs from the surface burst [1-KT standard (Needham and Crepeau, 1981)] by nearly 7 percent at 700 to 1000 psi-ms ($y = 0$), but is within 5 percent everywhere else. The average difference is less than 2 percent. The fit is compared with the calculations in Fig. 110.

In Fig. 110, the calculation values are indicated by symbols (circles, squares, diamonds, triangles) and the fit by solid curves. The range of applicability is for bursts below $700 \text{ ft/KT}^{1/3}$ and is for $x > X_i$. The scaled ground range is then between 300 and 5500 ft; i.e., the scaled impulses are between 2 and $2000 \text{ psi-ms/KT}^{1/3}$.

DYNAMIC PRESSURE TIME VERSUS SCALED BURST HEIGHT AND RANGE.

The quick fix analytic approximation [Speicher, 1982] has not yet been replaced by a more detailed fit. This fit to the early KA calculations (and the surface burst) is cast in terms of the overpressure fit of Eq. (63).

$$Q \approx \left(\frac{\Delta P}{\Delta P_s} \right)^a \left(\frac{2.5 \Delta P^2}{102.9 + \Delta P} \right) \quad \text{for } X \geq 1.3 X_m , \quad (66)$$

$$Q \approx \left(\frac{\Delta P}{\Delta P_s} \right)^a \left(\frac{2.5 \Delta P^2}{102.9 + \Delta P} \right) \left(\frac{X}{1.3 X_m} \right)^b \quad \text{for } X < 1.3 X_m ,$$

where Q is the dynamic pressure (horizontal component) in pounds per square inch, X_m is the scaled range at which Mach reflection begins for a given burst height (in feet per cube-root kiloton), ΔP_s is the peak overpressure at the scaled burst height and range [Eq. (62)], ΔP is the time-dependent overpressure at that position [Eq. (63)] and X is the scaled ground range in feet per cube-root kiloton, the coefficients a and b are defined as $2 - 2/(1 + 3817y^9)$ and $2 + 1.011/(1 + 33660y^{15})$, respectively, and y is the burst height in kilofeet per kiloton.

One further correction is necessary to alter the effective positive phase duration. That involves replacing the duration of the positive phase D , from Eq. (63), in the overpressure fit by

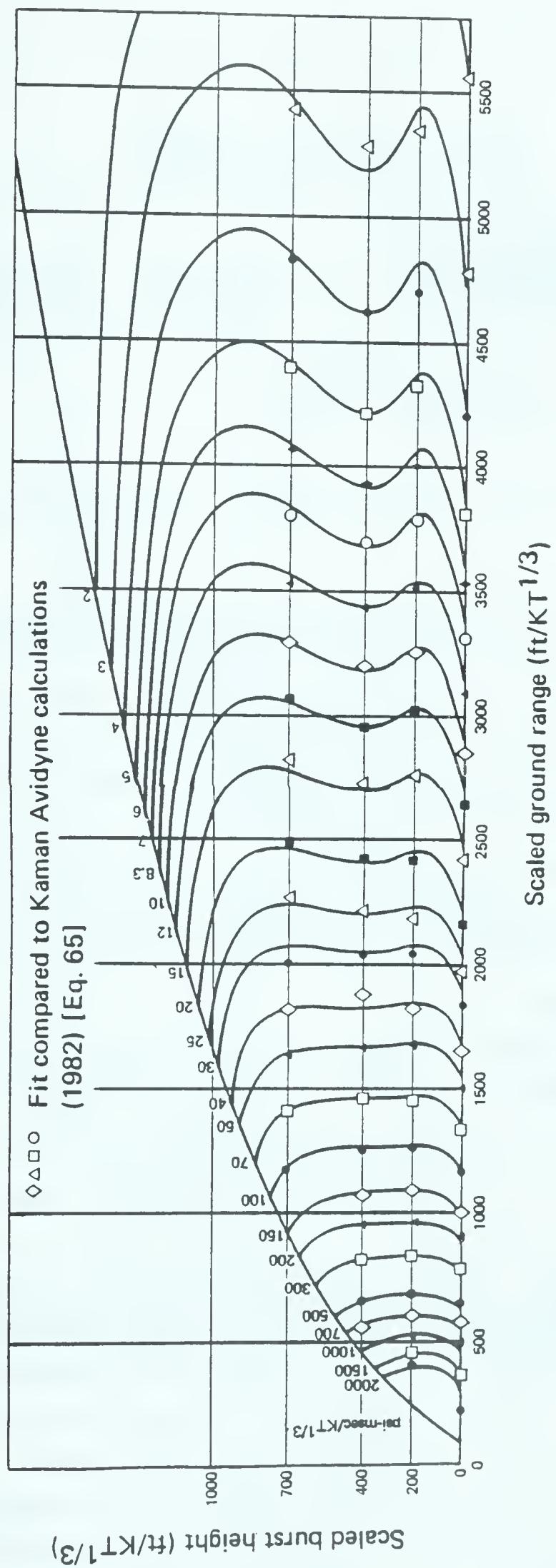


Figure 105. Scaled dynamic impulse fit versus scaled range and scaled burst height.

$$D_u = C \times D \text{ ms} , \quad (67)$$

where

$$C = \frac{89.6y^{5.2}}{(1 + 20.5y^{5.4})} + \frac{4.51}{(1 + 130.7y^{8.6})} + \frac{2.466y^{0.5}}{(1 + 99y^{2.5})} - \frac{12.8(x^2 + y^2)^{1.25}}{1 + 3.63(x^2 + y^2)^{1.25}},$$

and $x = X/1000$ = scaled ground range in kilofeet per cube-root kiloton.

The peak dynamic pressure and the dynamic impulse derived from this quick fix fit are not as accurate as those given by Eqs. (64) and (65). To illustrate the limited usefulness of this approximation [Eqs. (66) and (67)], the peak dynamic pressures are compared with those from the KA calculations in Figs. 111 and 112, all at the scaled burst height of 200 ft/KT^{1/3}. While the peaks from this time-history fit are appreciably low at the innermost range plotted in Fig. 111 (24.5 psi versus 30 psi), the agreement gets better at larger ranges (Fig. 112). The impulses, shown in Figs. 113 and 114, are similarly poor at the closest range shown, but they are in good agreement farther out at intermediate ranges. This fit falls about 30 percent low on peak and impulse at the 100 psi overpressure range. This quick fix time-history fit was provided as an analytic expression useful in dynamic analyses in a limited (low) overpressure range, and should not be used at high overpressures. The expressions for peak dynamic pressure and dynamic impulse [Eqs. (64) and (65)] are more accurate for peaks and total impulse, but they do not provide the time-dependent or transient behavior necessary for calculations of response of structures or vehicles. It is anticipated that this quick fix time-history fit will be improved in the near future.

Figure 115 shows a comparison between the KA calculations and the dynamic pressure iso-impulse contours from the integration of Eq. (66). As expected, this comparison is not as good as that for

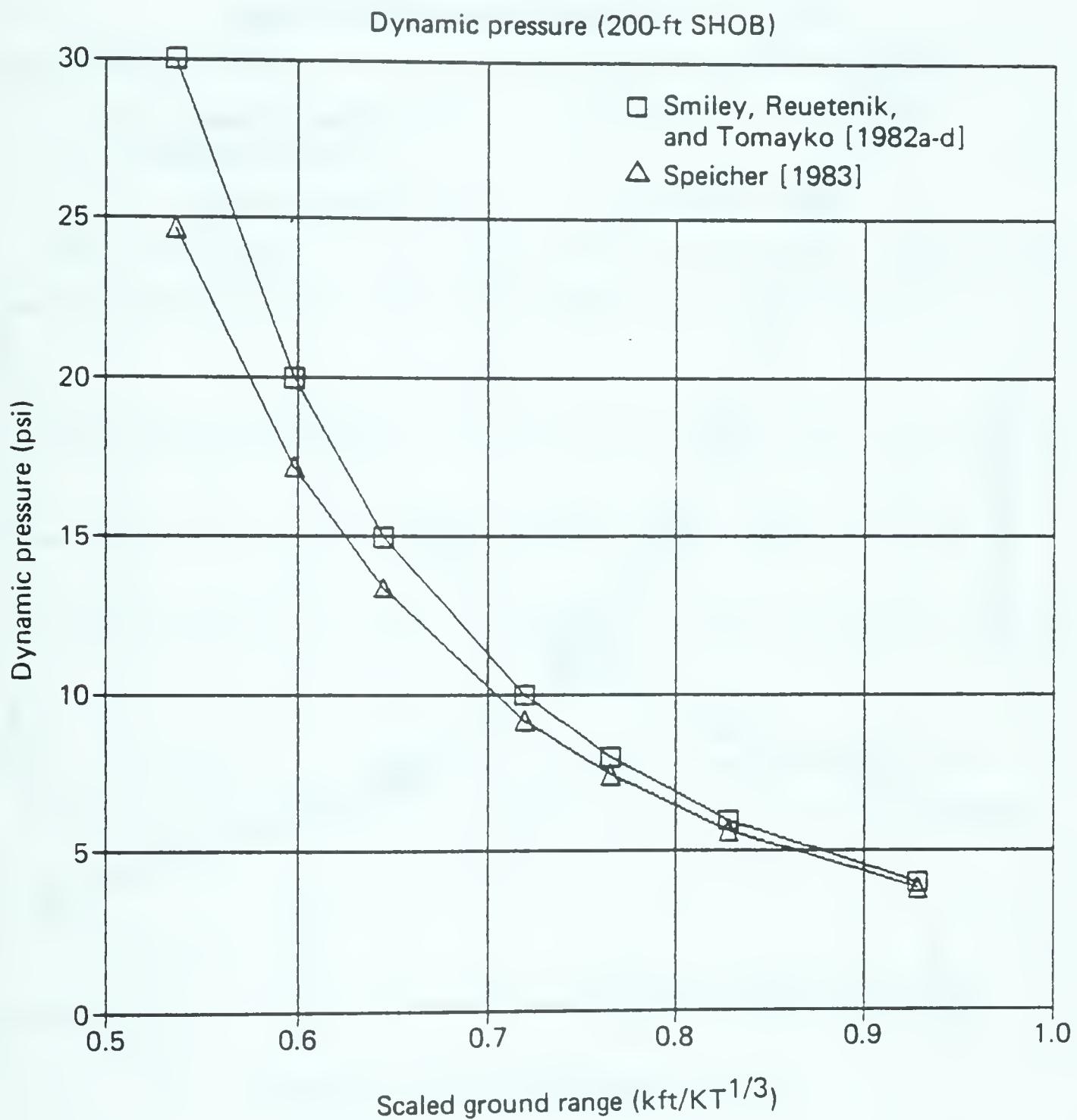


Figure 106. Fit compared to Kaman AviDyne calculation: peak dynamic pressure for 200-ft SHOB versus scaled, close-in ground range.

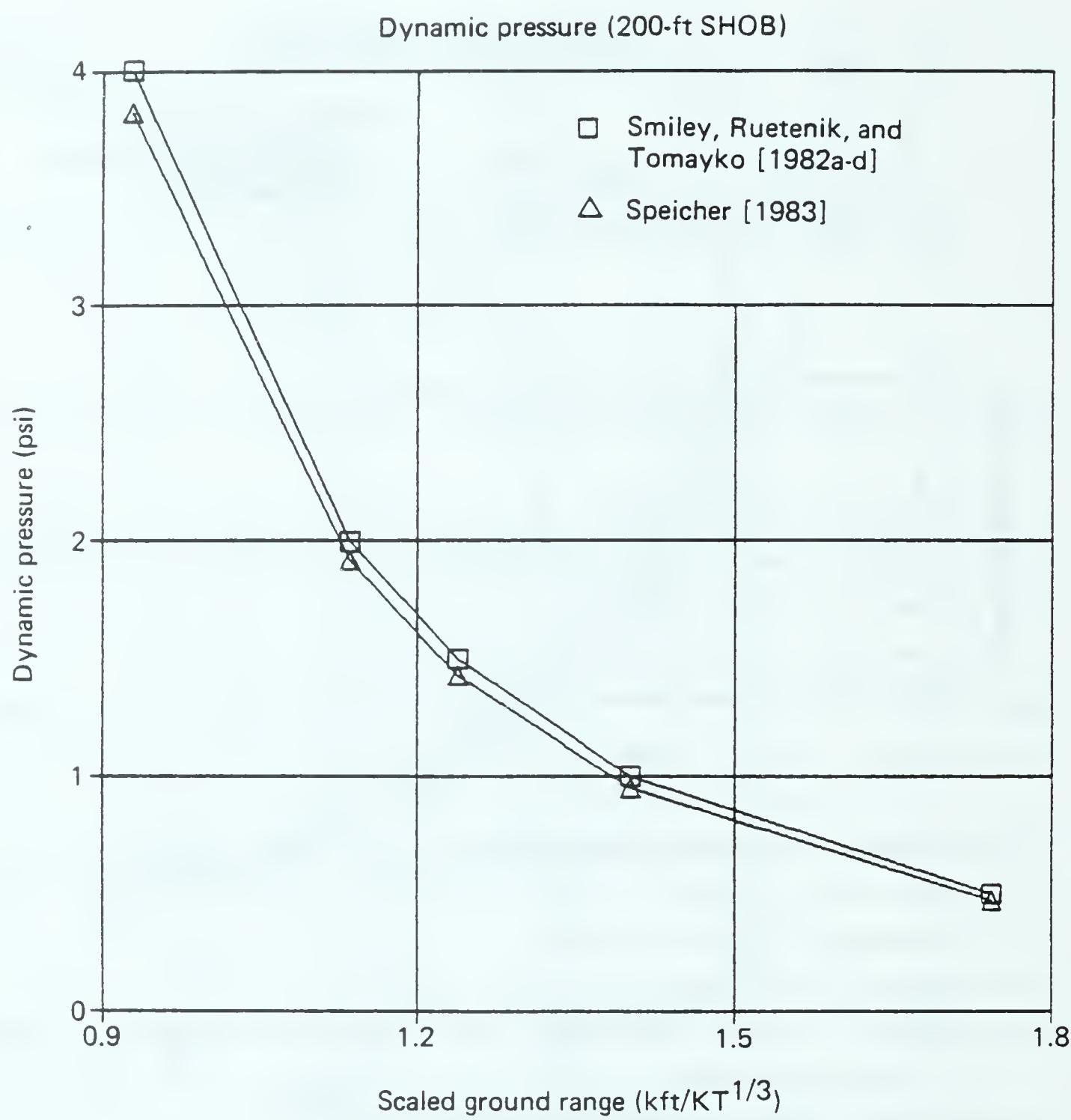


Figure 107. Fit compared to Kaman AviDyne calculation: peak dynamic pressure for 200-ft SHOB versus scaled, intermediate ground range.

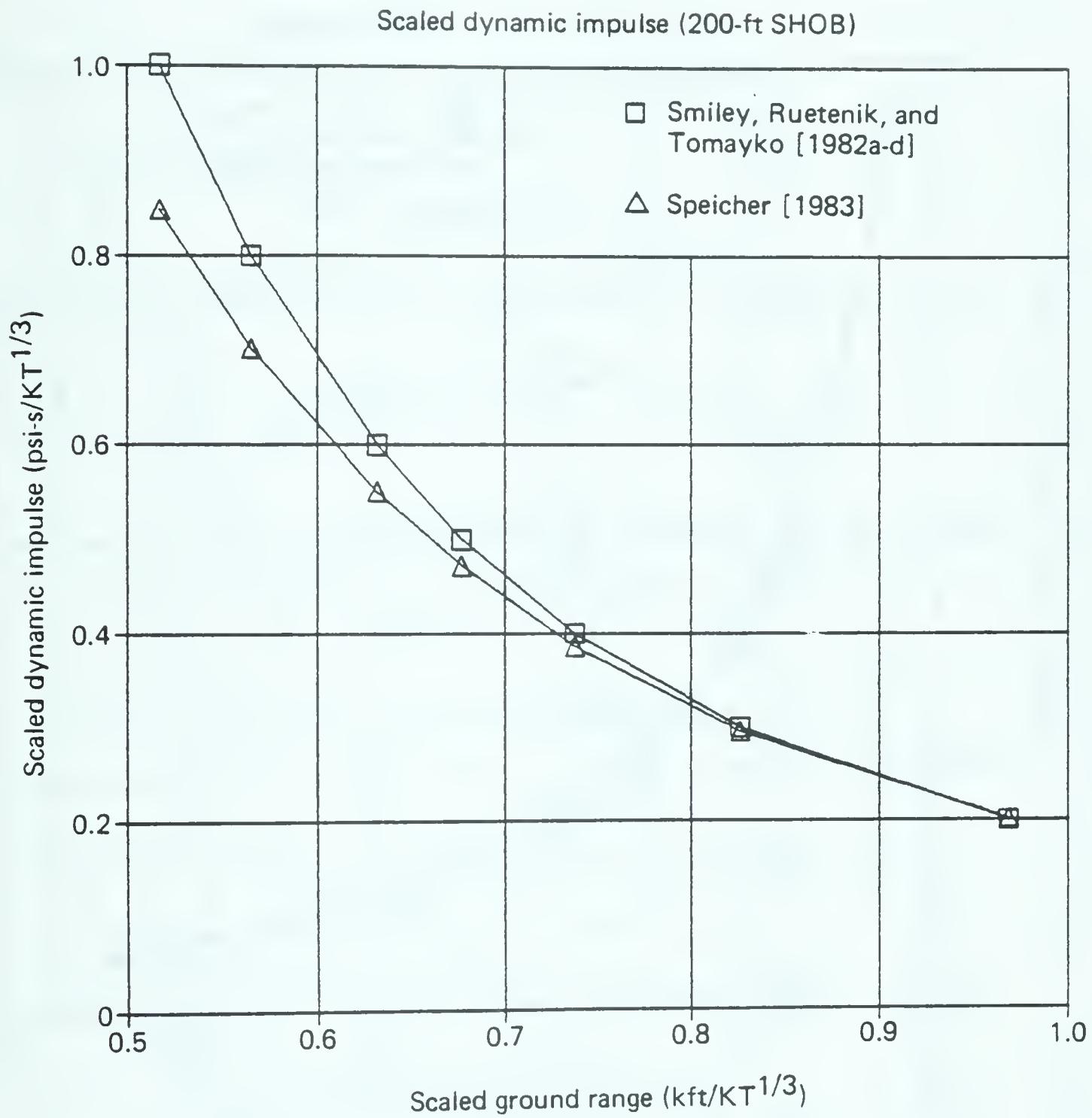


Figure 108. Fit compared to Kaman AviDyne calculation: peak dynamic impulse for 200-ft SHOB versus scaled, close-in ground range.

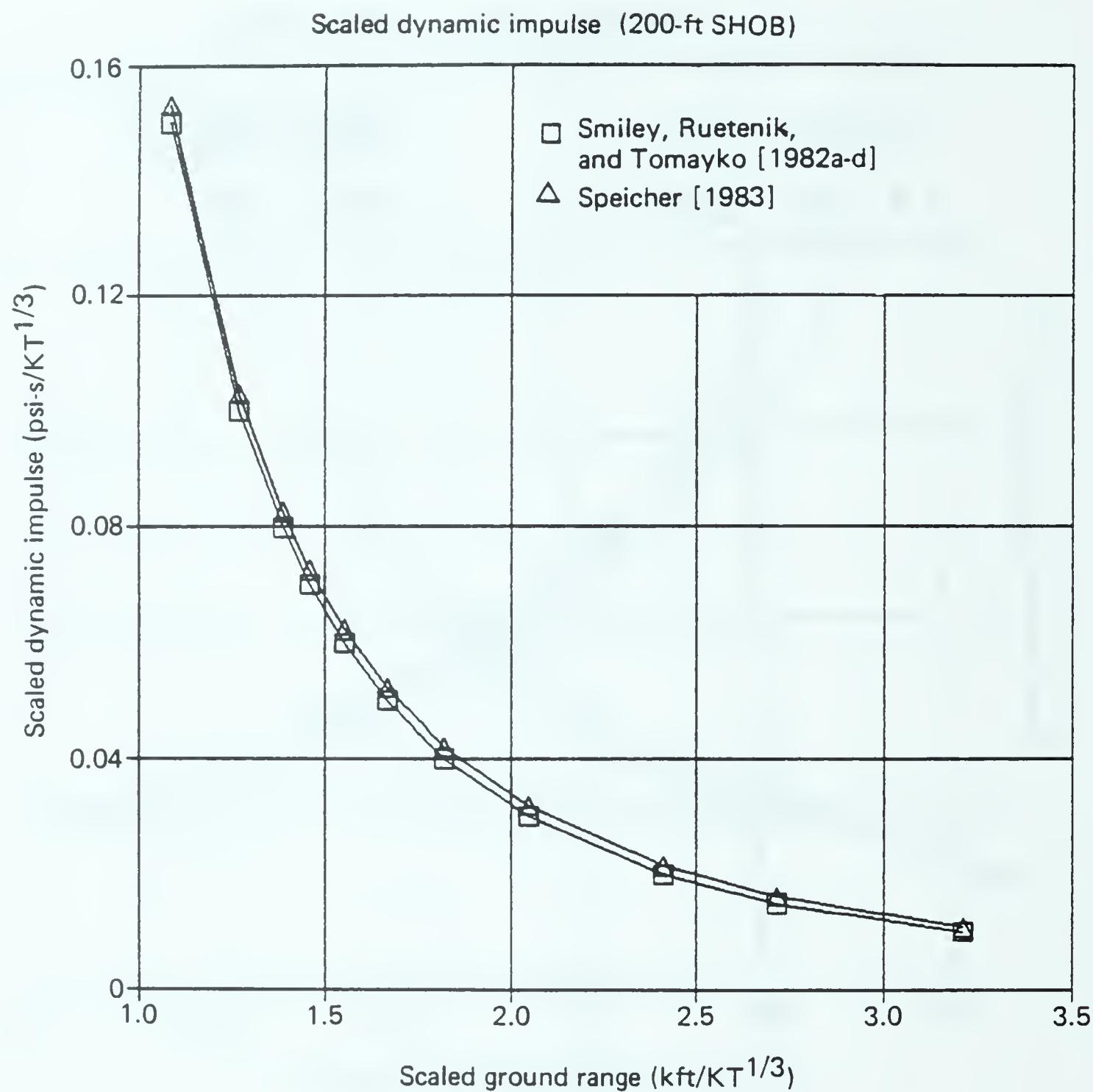


Figure 109. Fit compared to Kaman AviDyne calculation: peak dynamic impulse for 200-ft SHOB versus scaled, intermediate ground range.

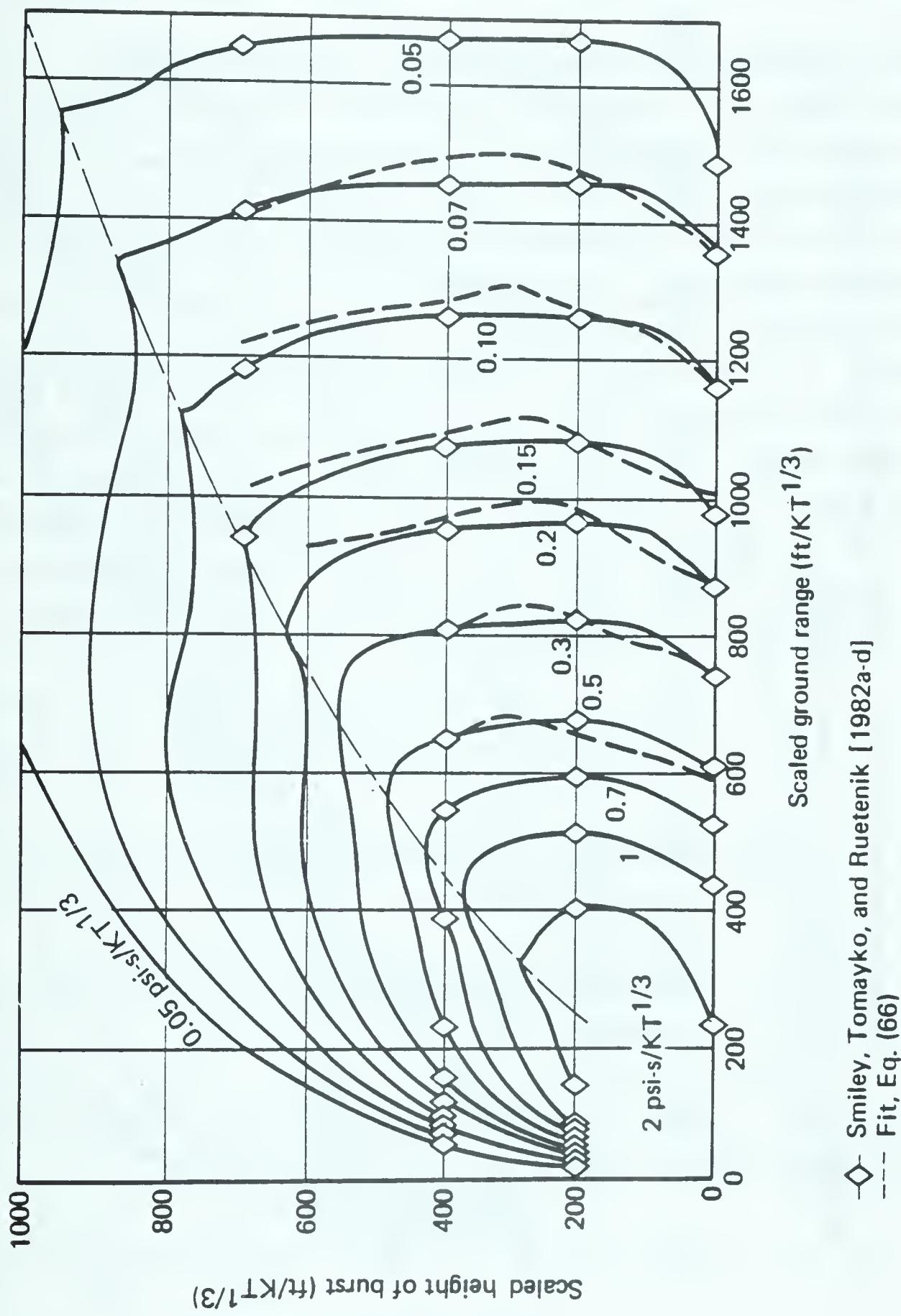


Figure 110. Integration of Eq. (66) over positive phase compared to Kaman AviDyne calculations: dynamic impulse versus SHOB and scaled ground range.

Figure 110 .

Eq. (65), shown in Fig. 110. However, it corresponds reasonably well to the total impulse, while supplying a time-history, which is presumably more useful in dynamic analyses of structural response.

HEIGHT OF TARGET EFFECT ON MAXIMUM DYNAMIC PRESSURE CONTOURS.

As in Figs. 101 through 109, the curves of Fig. 116 show the scaled range to KA calculation peak dynamic pressure values (at scaled burst heights of 0, 200, 250, 400, 500, 700, and 750 ft/KT^{1/3}). Also shown in Fig. 116 are the locus of burst heights and ranges where the peak dynamic pressure at a scaled height above the ground of 1, 2, 3, 5, and 10 ft/KT^{1/3} is less than that at the ground by just 10 percent. At points above the dashed curves in Fig. 116, the peak dynamic pressures are presumably even lower than at the surface for each target height. Below those curves, the peak dynamic pressure at a target height above the surface is within 10 percent of the surface values. In the figure, solid curves are for surface values of peak dynamic pressure. These curves of the 10 percent limit for target heights are closely fit by the expression

$$R_T = a + by + cy^d / (1 + \epsilon y^f) \quad \text{kft/KT}^{1/3}, \quad (68)$$

where y = scaled burst height in kilofeet per cube-root kiloton,

$$a = -1.49 + 0.4073(TH)^{-0.81866},$$

$$b = -13.1 + 16(TH)^{+0.023},$$

$$c = 0.06791 + 0.0363(TH) + 3.019 \times 10^{-8}(TH)^7,$$

$$d = -1.5313 + 0.1302(TH),$$

$$\epsilon = 1.039(TH) + 34.83/(TH)^{1.6754},$$

$$f = 2.733 + 4.158/[1 + 0.00159(TH)^{4.246}],$$

TH = target height in feet per cube-root kiloton.

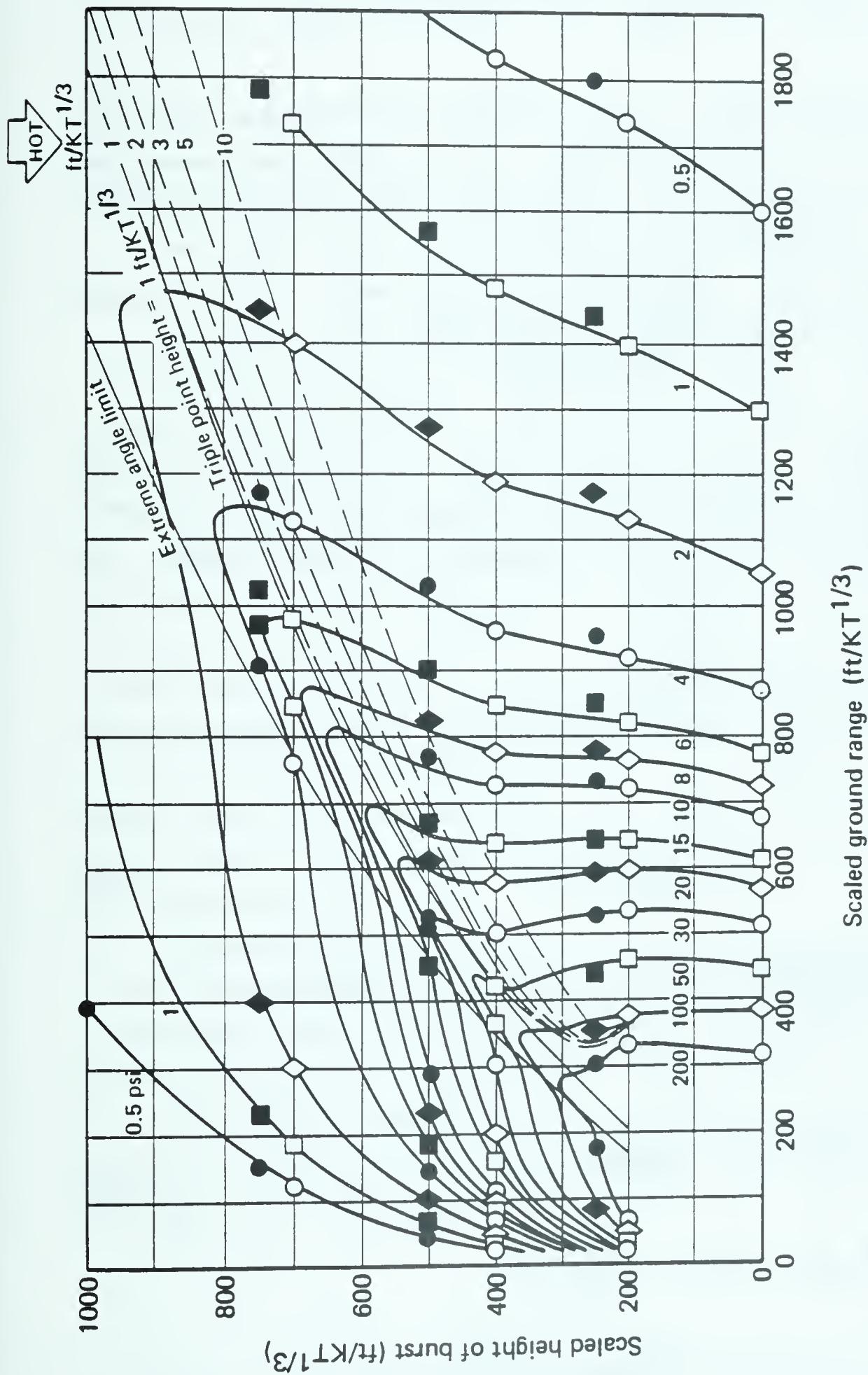


Figure 111. Maximum dynamic pressure HOB/HOT contours for scaled target heights of scaled burst height and ground range where peak dynamic pressure is 90 percent of surface value.

SECTION 5
EQUATION OF STATE FOR AIR

For strong blast waves in the atmosphere, the real gas (nonideal gas) properties of air become important, and the ideal gas assumptions frequently prove inadequate. Air molecules enter a complex energy-density-pressure balance as they dissociate and ionize with rising pressure or temperature. Their behavior is expressed in thermodynamic terms from detailed calculations [Gilmore, 1955, 1959; Hilsenrath, Green, and Beckett, 1957]. The equation of state for air has been closely fit by the author [Brode and Parkin, 1963] and that fit has been used in detailed numerical calculations of the radiation flow and hydrodynamics of nuclear bursts [Brode, 1959a,b, 1966, 1969; Brode et al., 1967], as well as in the KA calculations [Smiley, Tomayko, and Ruetenik, 1982a-d].

CALORIC EQUATION OF STATE FOR AIR.

The usual ideal gas relation for specific internal energy can be written as

$$E = \frac{P}{\rho(\gamma - 1)}, \quad (69)$$

in which E is the energy per unit mass, P is the pressure, ρ is the density, and γ is the ratio of specific heats ($\gamma \equiv C_p/C_v$). Defining $\mu = (\gamma + 1)/(\gamma - 1)$, one can rewrite Eq. (69) as

$$P = \frac{2\rho E}{(\mu - 1)}. \quad (70)$$

Using a dimensionless variable defined as

$$\phi \equiv \left(\frac{P_o}{P} \right) \left(\frac{\rho}{\rho_o} \right)^{1.0553}, \quad (71)$$

in which P_0 is the standard sea level pressure (14.7 psi), P is the air pressure, ρ is the air density, ρ_0 is the standard density (1.293 g/l), and $\xi = \ln(\rho/\rho_0) = \ln n$, then the fit is expressible as

$$\mu = 1 + A + B + C + D + E + F + G + H + I + (27\phi + 3)/(5\phi + 1) , \quad (72)$$

where each literal term A through I has the form

$$J = \frac{(M_0 + M_1\xi + M_2\xi^2)\phi^m(1 - \phi)^n}{(M_3 + M_4\xi)\beta\phi^n + 1} . \quad (73)$$

The coefficients in the literal terms are listed in Table 3 in which powers of ten are abbreviated as follows: 2.236^{+5} means 2.236×10^5 .

This form is valid to better than 5 percent almost everywhere for all pressures up to 10^7 psi and for densities in the range $10^{-6} \leq \rho/\rho_0 < 20$. Radiation energy is not included in the fit; at very high temperatures, the effective specific heat ratio is that of a monoatomic gas ($\gamma = 5/3$). At standard conditions, the ratio is close to that for an ideal diatomic gas ($\gamma = 7/5$). Since the effective specific heat ratio changes slowly with pressure or density, it is usually easy to find the appropriate thermodynamic state by using a few iterative steps.

The data on which this fit is based are represented by the curves of Fig. 117; the corresponding fit is shown in Fig. 118.

THERMAL EQUATION OF STATE FOR AIR.

In defining a temperature, the thermodynamic relation between pressure, density, and temperature becomes more complex than the usual ideal gas form, which is:

$$P = \rho R \theta . \quad (74)$$

The gas constant R becomes a variable. See Sec. 2 [Eq. (24) and Fig. 6] for a fit to that variability.

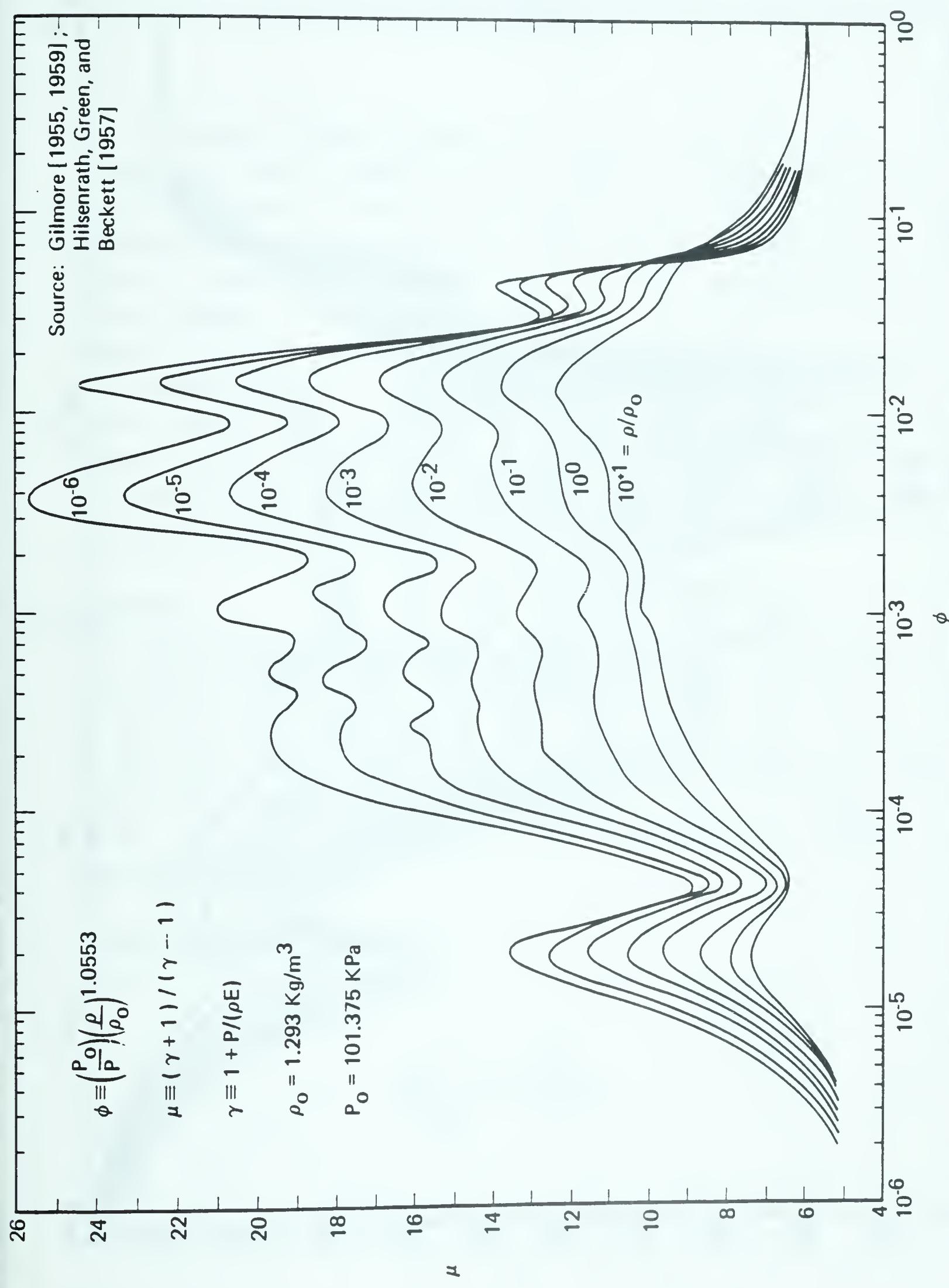
Table 3. Caloric equation of state for air.

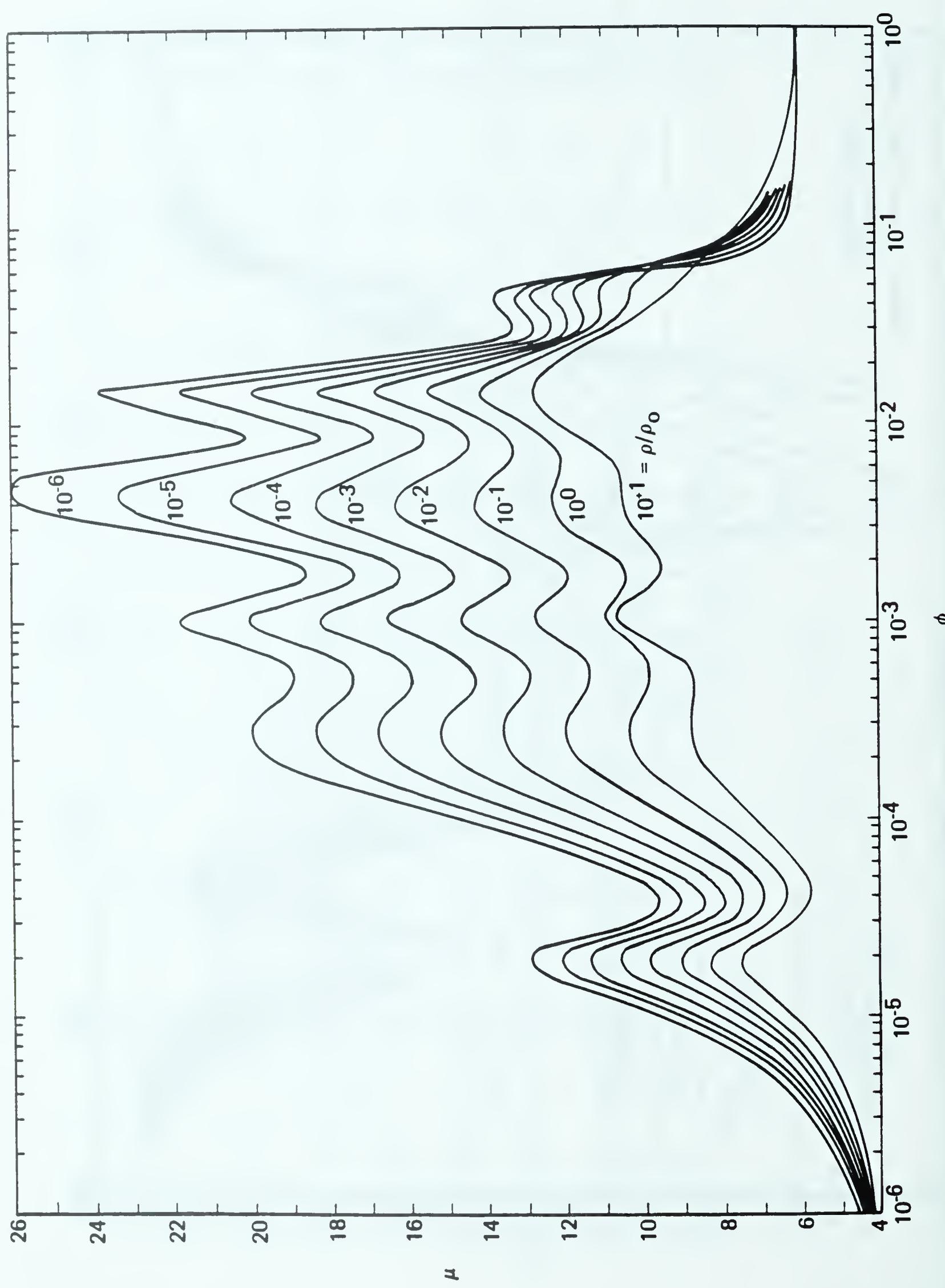
| J | A | B | C | D | E | F * | G | H | I |
|----------------|----------------------|----------------------|----------------------|----------------------|----------------------|----------------------|----------------------|----------------------|----------------------|
| m | 1 | 1 | 2 | 4 | 2 | 3 | 3 | 4 | 10 |
| n | 6 | 2 | 3 | 8 | 3 | 6 | 6 | 6 | 16 |
| M ₀ | 2.236 ⁺⁵ | 4.975 ⁺⁴ | 1.272 ⁺⁶ | 3.892 ⁺⁷ | 8.730 ⁺⁴ | 4.890 ⁺⁹ | 2.774 ⁺⁴ | 1.547 ⁺¹⁰ | 0 |
| M ₁ | -1.509 ⁺⁴ | -5.463 ⁺³ | -1.246 ⁺⁵ | -2.295 ⁺⁷ | 3.190 ⁺³ | 7.125 ⁺⁸ | -7.849 ⁺³ | -1.671 ⁺⁸ | 1.619 ⁺¹¹ |
| M ₂ | 0 | 0 | -3.053 ⁺³ | 0 | 0 | 0 | 0 | -6.617 ⁺⁷ | 0 |
| M ₃ | 5.412 ⁺²⁷ | 1.609 ⁺⁷ | 2.615 ⁺⁷ | 3.330 ⁺¹⁴ | 4.976 ⁺⁵ | 8.368 ⁺¹⁷ | 3.243 ⁺⁷ | 8.490 ⁺⁹ | 7.275 ⁺¹⁸ |
| M ₄ | 0 | 0 | 1.034 ⁺⁶ | 0 | -1.883 ⁺³ | 0 | -5.494 ⁺⁶ | 4.0 ⁺⁸ | 0 |
| α | 1 | 1 | 1 | 1 | 1 | 1 | 1 | α' + 1 | 1 |
| β | 1 | 1 | 100 ϕ + 1 | 1 | 1 | 1 | 1 | 1 | 1 |

Note: Powers of ten are abbreviated. For example, 2.236⁺⁵ means 2.236 × 10⁵.

* $X_i(\xi)$ in the numerator of F is absolute, i.e., $| \xi |$.
[†] Alpha prime (α') = $(1 - \phi)^2(\phi - c)(\phi - d)$,

$$\begin{aligned} \text{where } c &= 7.4^{-2} - 3.764 - 3\xi && \text{if } \xi \leq 0, \\ &= 7.4^{-2} - 3.764 - 3\xi - 5.852 - 3\xi^2 && \text{if } \xi > 0, \\ d &= 2.357^{-2} - 4.255 - 3\xi - 2.52 - 4\xi^2. \end{aligned}$$





SECTION 6
THERMAL RADIATION

A nuclear fireball releases a fair fraction of the explosion energy in a pulse of light and heat or thermal radiation. This burst of radiant energy is complex and variable in time, spectrum, and geometry. It is coupled with the nuclear radiation and the blast wave. It has at least two major peaks, and varies considerably with yield, altitude, and atmospheric conditions. When close to the ground, the earth material ingested into the fireball markedly affects the thermal radiation. When burst at high altitude, the thinner atmosphere leads to more rapid radiation as inner hot regions are exposed earlier, yet the greater transparency leads to low emissivities and low thermal power (radiation) at higher temperatures or earlier in the fireball expansion and cooling.

AIRBURST

For nuclear explosions in the atmosphere, but not on the ground, the thermal radiation may be characterized by a double pulse, the first of which is so short that it contains less than half a percent of the total energy released, yet its peak power is comparable to that in the second pulse which contains more than a third of the total yield. The major or second pulse is well approximated by a simple time dependence:

Thermal Power

$$\frac{P^*}{P_{2ma}^*} \approx \frac{2\tau_r^2}{(1 + \tau_r^4)} , \quad (75)$$

where P^* = power or rate of fireball heat release,

$$\tau_r = t_r/t_{2\max},$$

t_r = time after burst, in seconds,

t_{ma}^* = time to second maximum in power radiated (airburst)

$$\approx 0.0417 \cdot W^{0.44} \text{ s}, \quad \pm 11\%^\dagger \quad (76)$$

P_{ma}^* = power at second maximum from airbursts,

$$= 3.18 W^{0.56} \text{ KT/s}, \quad \pm 34\% \quad (77)$$

W = yield, in kilotons.

Equations (76) and (77) are from Glasstone and Dolan [1977], and represent an empirical approximation to observed and calculated times to maximum and power at maximum.

The pulse approximated by Eq. (75) and the partial integral of that pulse over time are illustrated in Fig. 119. The integral of the power fit to a time $t_{10ma} = 10 t_{ma}$ includes 91 percent of the integral to very late times, i.e., it leaves only 9 percent to be radiated after that time. The curve with which it is compared [Glasstone and Dolan, 1977] leaves 20 percent beyond t_{10ma} . The curve plotted for the fit (Fig. 119) has been renormalized to 80 percent at t_{10ma} .

The expression for thermal power [Eq. (75)], when integrated analytically, leads to:

$$E^*(\tau) = \frac{1}{\sqrt{2}} \arctan(\sqrt{2}\tau/(1 - \tau^2)) - \frac{\sqrt{2}}{4} \ln \left[\frac{\tau^2 + \sqrt{2}\tau + 1}{\tau^2 - \sqrt{2}\tau + 1} \right]. \quad (78)$$

^dThe $\pm 11\%$ indicates that a band around the empirical values of ± 11 span 90% of the atmospheric test data.

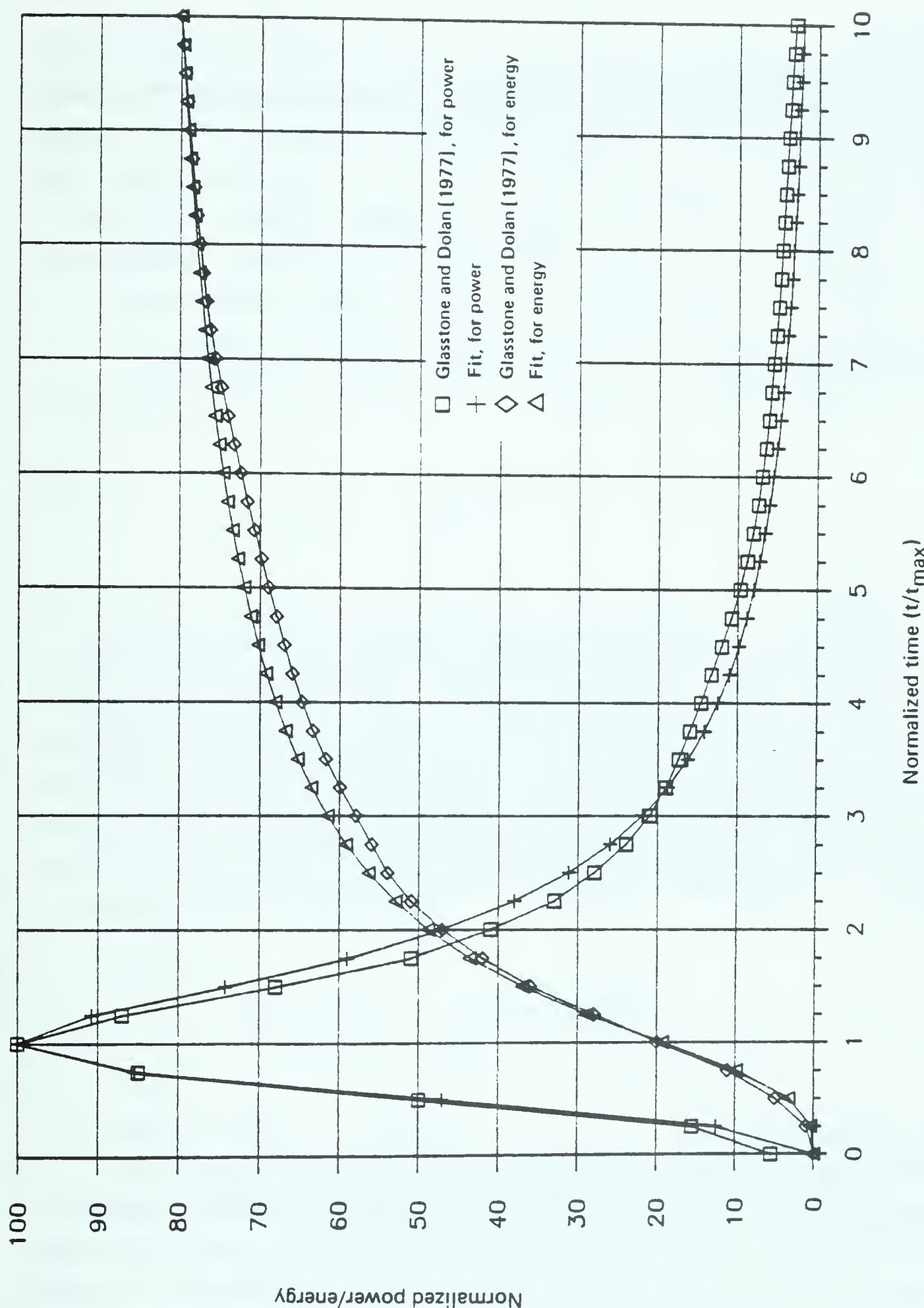


Figure 114. Fit compared to data average: normalized thermal radiation power pulse and thermal energy radiated versus normalized time.

This function (normalized at $t_{10\text{ma}}$ to 80 percent of the total thermal emission) is plotted as the fit in Fig. 119.

First Peak

The main burst of thermal energy is generally preceded by a sharp pulse of light, as the fireball shock breaks through the air surrounding the bomb that has been altered (ionized) by the early nuclear and X-ray radiation and begins to cool as it expands further. That first pulse contains less than 1/2 percent of the total yield, and peaks in a time measured in milliseconds. The time to the first peak is proportional to the cube-root of the yield (compatible with hydrodynamic scaling):

$$t_{f\text{ma}} \simeq W^{1/3} \quad \text{ms.} \quad (79)$$

Thermal Minimum

A minimum in radiated power occurs between the first and main peaks when the expanding and cooling shock front becomes sufficiently transparent that the hotter interior air of the fireball is exposed, allowing an increase in the rate of radiant energy emission. This time to minimum power for air bursts depends on optical properties (mean free paths for light passing through air) as well as fireball dimensions. An approximate empirical scaling from Kieth and Sachs [1985] is as follows:

$$t_{\text{min}} = 3.13 \cdot W^{0.44} \quad \text{ms.} \quad \pm 12 \% \quad (80)$$

Thermal Energy Fraction

For bursts low in the atmosphere, the radiated energy at a time ten times the time to maximum can be approximated by

$$f_{10\text{ma}}^* = E_{10\text{ma}}^* / W = 0.277 \quad \text{KT} \quad \pm 19 \% \quad (81)$$

If radiation at times beyond ten times time to maximum is included in the thermal fraction, the expression becomes [Glasstone and Dolan, 1977]

$$f_\infty^* = E_\infty^* / W = 0.35. \quad (82)$$

An earlier fit to the thermal energy (in visible light) as a function of yield resulted in the expression [Brode, 1968]:

$$f_\infty^* \approx 0.33 + 0.0038 \cdot W^{1/2} / (1 + 0.0316 \cdot W^{1/2}). \quad (83)$$

This latter form (Eq. 83) predicts a rise in the fraction with increasing yield (from 33 to 42 percent between 1 and 10,000 KT), while Glasstone and Dolan [1977] hold the fraction fixed at 35 percent. In contrast, the recent revision of the Thermal Radiation section (Chapter 6) of the Defense Nuclear Agency manual compiled by Kieth and Sachs [1985] predicts a decrease with increasing yield (although they state that $f^* = 0.33$ is equally appropriate. An analytic fit to their curves for a low airburst is:

$$f_\infty^* \approx 34.9 / (1 + 0.00162 \cdot \lambda^{2.447}) \quad (84)$$

in which $\lambda = \ln(W)$ (W in KT).

These three predictions are illustrated in Fig. 120, showing a divergence between the values as yield is increased. Although a good deal of scatter exists in the atmospheric test data, they do not appear to support the reduction of thermal fraction with increasing yield predicted by Kieth and Sachs [1985].

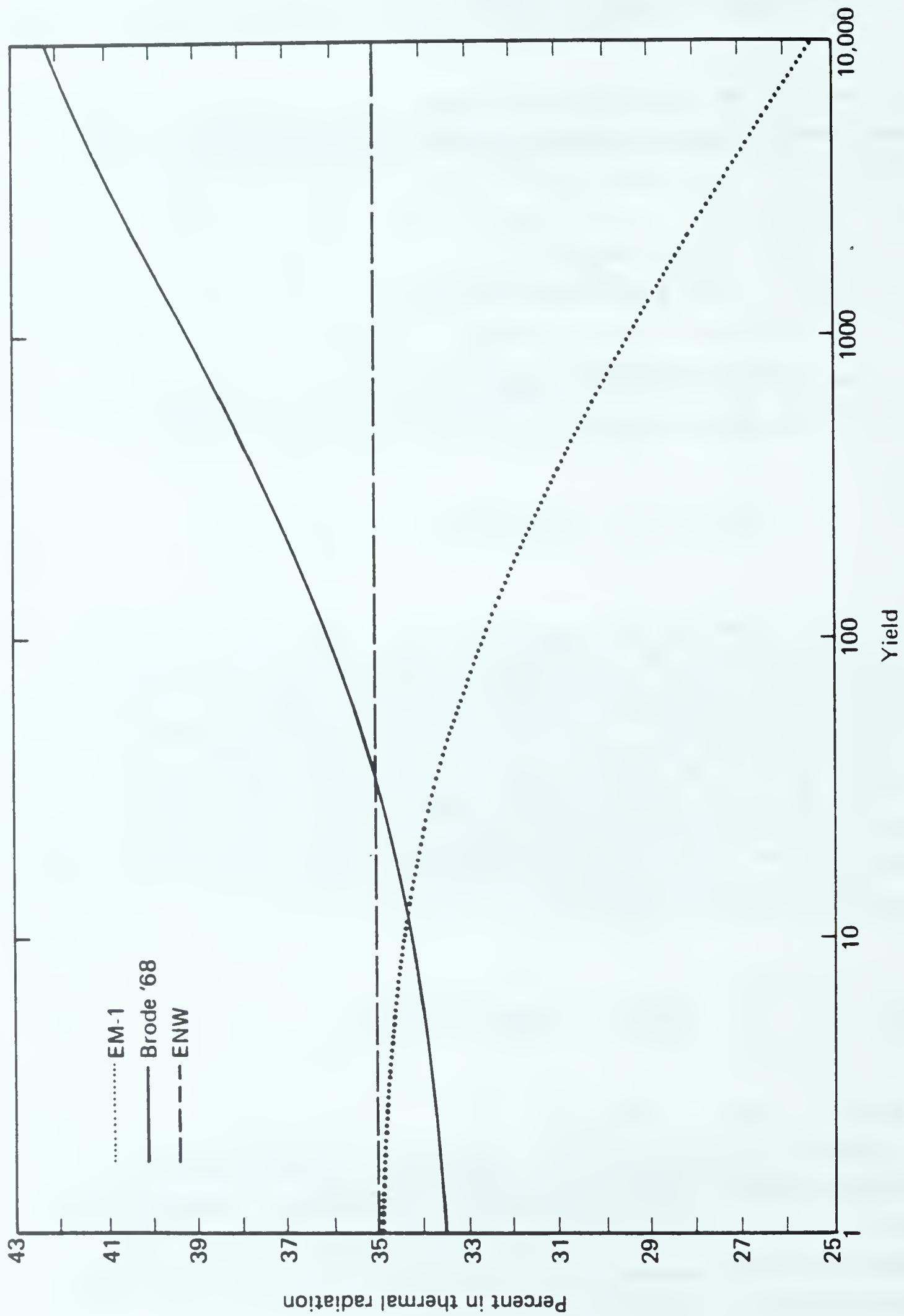


Figure 115. Thermal fraction versus yield, near sea level airburst predictions.

Radiant Exposure

The intensity or fluence of fireball thermal radiation received at a distance from an airburst falls off as the square of the distance, and is also attenuated by absorption and scattering in the intervening air. It may be affected by reflections from ground cover (e.g., snow) or clouds or by absorption in intervening cloud layers, and will depend on burst height and yield. From an airburst weapon, the thermal fluence at a distance can be expressed in the following form:

$$Q^* = A^* \cdot B^* \cdot E^* \cdot T^* / [4\pi \cdot (r^*)^2] \text{ cal/cm}^2 \quad (85)$$

in which A^* = attenuation through clouds

B^* = enhancement due to snow or cloud reflections

E^* = total radiated energy (cal)

T^* = transmissivity of the atmosphere

r^* = distance from burst (cm)

The factor A^* , representing the attenuation through clouds can range from a value of unity (for no clouds) to as much as 1/10 for heavy cloud cover between burst and target. [$1/10 < A^* < 1$]

The enhancement due to snow cover can be as great as 1.9, and nearly as great for reflections from a cloud deck above the burst. [$1 < E^* < 1.9$]

It is conventional to express the energy release in kilotons; there are 10^{12} calories in a kiloton. The fraction of the energy released that appears in thermal radiation for a low altitude airburst [$f^* E_\infty^*/W$] is given variously by Eqs. 82 through 84.

The atmospheric transmission is a complex function of the radiative properties of the air molecules and the suspended contaminants, but can be usefully approximated without reference to its spectral dependence by an absorptive (extinction) property and a forward scattering contribution. The absorption can be characterized by a term [$\exp(-\alpha^* \cdot R^*/V^*)$], and the scattering factor as $(1 + \beta^* \cdot R^*/V^*)$, in

which V^* is a visibility or atmospheric visual distance. Thus,

$$T^* = (1 + \beta^* \cdot R^* / V^*) \cdot \exp(-\alpha^* \cdot R^* / V^*) , \dagger \quad (86)$$

with R^* and V^* in the same length units (e.g., statute miles).

With ground range in statute miles, Eq. (85) becomes

$$Q^* = 3.07 \cdot A^* \cdot B^* \cdot f^* \cdot T^* \cdot W / (R_{mi}^*)^2 \text{ cal/cm}^2 , \quad (87)$$

where $R_{mi}^* = [(H^*)^2 + (GR^*)^2]^{1/2}$ mi,

H_{mi}^* = Burst height mi,

GR^* = Ground Range mi.

With distances in kilometers, the expression becomes

$$Q^* = 7.96 \cdot A^* \cdot B^* \cdot f^* \cdot T^* \cdot W / (R_{km}^*)^2 \text{ cal/cm}^2 . \quad (88)$$

For nautical miles (used in some targeting work):

$$Q^* = 2.32 \cdot A^* \cdot B^* \cdot f^* \cdot T^* \cdot W / (R_{nm}^*)^2 \text{ cal/cm}^2 . \quad (89)$$

Ranges are given in kilofeet elsewhere in this compendium of fits; the thermal fluence versus slant range in kilofeet is written:

$$Q^* = 85.7 \cdot A^* \cdot B^* \cdot f^* \cdot T^* \cdot W / (R_{kft}^*)^2 \text{ cal/cm}^2 \quad (90)$$

[†]The constants α^* and β^* depend on the atmospheric moisture and particulate contents, but best values are $\alpha^* \approx 2.9$, $\beta^* \approx 1.9$. A reasonable range for each might be $1.8 < \alpha < 3.2$ and $1.25 < \beta < 2.1$.

SURFACE BURST

The thermal pulse from a surface burst is less regular and generally less intense than that from an airburst. Soil and other surface material drawn into the fireball, intervening topography and structures, and greater distortion of the fireball radiating surface due to reflections and precursors often degrade the thermal pulse from surface and near-surface bursts. The surface burst power pulse may have the same general shape as the air burst [Eq. (75)], but the time to maximum, the power at maximum, and the total energy emitted are different. [Kieth and Sachs, 1985]:

$$t_{\text{ma}}^* \simeq 0.0419 \cdot W^{0.464} \quad \text{s ,} \quad (91)$$

$$P_{\text{ma}}^* \simeq 1.35 \cdot W^{0.56} \quad \text{KT/s ,} \quad (92)$$

$$f_{10\text{ma}}^* \equiv E_{10\text{ma}}^*/W \simeq 0.118 \cdot W^{0.024} , \quad (93)$$

$$f_{\infty S}^* \equiv E_{\infty S}^*/W \simeq 0.149 \cdot W^{0.024} \quad \text{KT .} \quad (94)$$

Graphical data from Fig. 6II-5 from Kieth and Sachs [1985] is fit by the following expression when extrapolated to zero burst height:

$$f_{\infty S}^* \simeq 0.04475 + 0.002161 \cdot \lambda^3 / (1 + 0.01575 \cdot \lambda^3) , \quad (95)$$

in which, again, $\lambda = \ln(W)$.

In addition, the time to first maximum is less regular, and the time to minimum is greater:

$$t_{\text{min}} \simeq 4.25 \cdot W^{0.44} \quad \text{ms .} \quad (96)$$

Thermal Partition--Transition between Surface and Airburst

Kieth and Sachs [1985] give some guidance as to the transition between surface and airburst thermal partition in their Table 6II-2. When fit with an analytical expression, this transition may be presented as:

$$f_t^* \simeq f_s^* + (f_s^* - f_s^*) \cdot (h/4)^2 / [1 + (h/4)^2]. \quad (97)$$

In this formula, h is the scaled burst height in meters per cube root kiloton, f_s is the surface burst partition [Eq. (95)], and f is the airburst thermal partition [Eq. (83)]. This transition is illustrated as a function of scaled burst height for yields from 1 KT to 10 MT in Fig. 121.

BURIED BURSTS

Burial quickly quenches the thermal radiation from a nuclear burst, but at shallow depths of burst, a fraction of the energy still radiates from the contaminated fireball. Based on the limited experience of a few near surface and shallow buried bursts, the following fit approximates the thermal energy partition for such shallow-buried bursts:

$$\begin{aligned} f_u^* &\simeq .35 \cdot \{1 - 1/[1 + ((h+5.925)/8.144)^4]\}, \\ \text{for } -4.89 \leq h &\leq 100m/(KT)^{1/3}, \\ f_u^* &\simeq 0 \text{ for } h \leq -4.89. \end{aligned} \quad (98)$$

HIGH ALTITUDE BURSTS

For bursts above about 14,00-ft altitude (≈ 4.3 km), the influence of decreased air density on fireball behavior becomes appreciable. The atmospheric density (ρ) is often expressed in terms of the standard

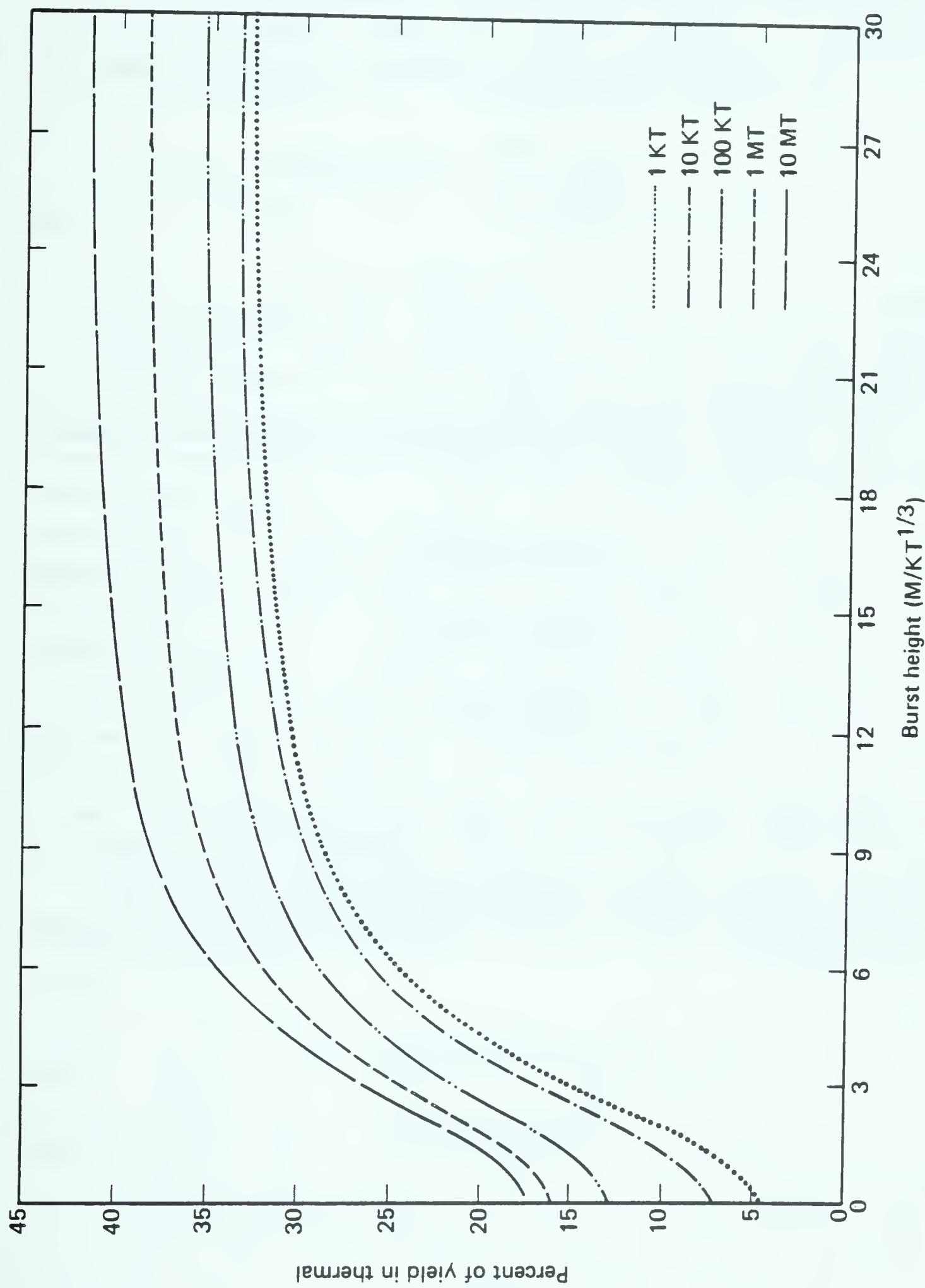


Figure 116. Approximate transition from surface burst to airburst thermal radiation fraction versus burst height for yields from 1 KT to 10 MT Eq. [(97)].

sea-level atmospheric density ($\rho \approx 1.225$ grams per liter), and can be approximated [U.S. Standard, 1962] by the function:

$$\eta = \rho / \rho_0 \simeq [1 + 0.5405 \cdot (h/10)^{0.9852} / (1 + 0.1545 \cdot (h/10)^{3.393}) \\ + 5.591 \cdot (h/100)^{3.909} / (1 + 36.32 \cdot (h/100)^{17.74})] \\ \cdot \exp(-0.14856 \cdot h), \quad (99)$$

in which h is the altitude in kilometers. This expression fits the tabular data to better than 3 percent up to 30 km. It is good to better than 6 percent up to 115 km.

The following expressions approximate the thermal pulse characteristics in the atmosphere ($h < 30$ km):

$$t_{\min}^* \approx 4.3 \cdot W^{0.45} \cdot \eta^{0.23} \text{ ms}, \quad (100)$$

$$t_{\text{ma}}^* \approx 40 \cdot W^{0.45} \cdot \eta^{0.35} \text{ ms}, \quad (101)$$

$$P_{\text{ma}}^* \approx 3.1 \cdot W^{0.55} / \eta^{0.54} \text{ KTs}. \quad (102)$$

The time to first maximum is nearly independent of altitude of burst, so that Eq. (79) can be used for any height. The fraction emitted as thermal radiation can be roughly approximated by [Keith and Sachs, 1985]:

$$f_{10\text{ma}}^* \approx 0.276 / \eta^{0.034}, \quad (103)$$

$$f_\infty^* \approx 0.35 / \eta^{0.34}. \quad (104)$$

This ratio of thermal energy radiated to the total yield of a nuclear explosion at altitude has been approximated earlier [Brode, 1968], based on high altitude tests and a few numerical calculations, for densities as low as $n = 0.001$ and for yields from 1 KT to 10 MT as:

$$f^* \approx 0.27 + 0.06 \cdot n + 0.0038 \cdot W^{1/2} / (1 + 0.0316 \cdot W^{1/2}) \\ + 114 \cdot n / (1 + 82000 \cdot n^2) . \quad (105)$$

The expression in Eq. (105) indicates an increase in thermal radiation fraction with increasing yield, as the emissivity of the fireball remains high longer and to lower fireball temperatures. That allows more radiation to be emitted. The fraction shows a slight initial drop with atmospheric density, because at lower densities, the fireball forms a shock later (thereby becoming a strong radiation source later), and yet it becomes transparent earlier. Eventually, radiative expansion in a rarefied atmosphere creates such a large fireball that it can again radiate effectively in the visible. At extreme altitudes, the lack of atmosphere does not allow for reradiation in the visible, and the thermal fraction once more decreases. Figure 122 shows the fit [Eq. (105)] as a function of yield for burst altitudes up to 30 kilometers.

The thermal fraction versus yield and altitude of burst, as depicted by Glasstone and Dolan [1977] can be approximated by the form:

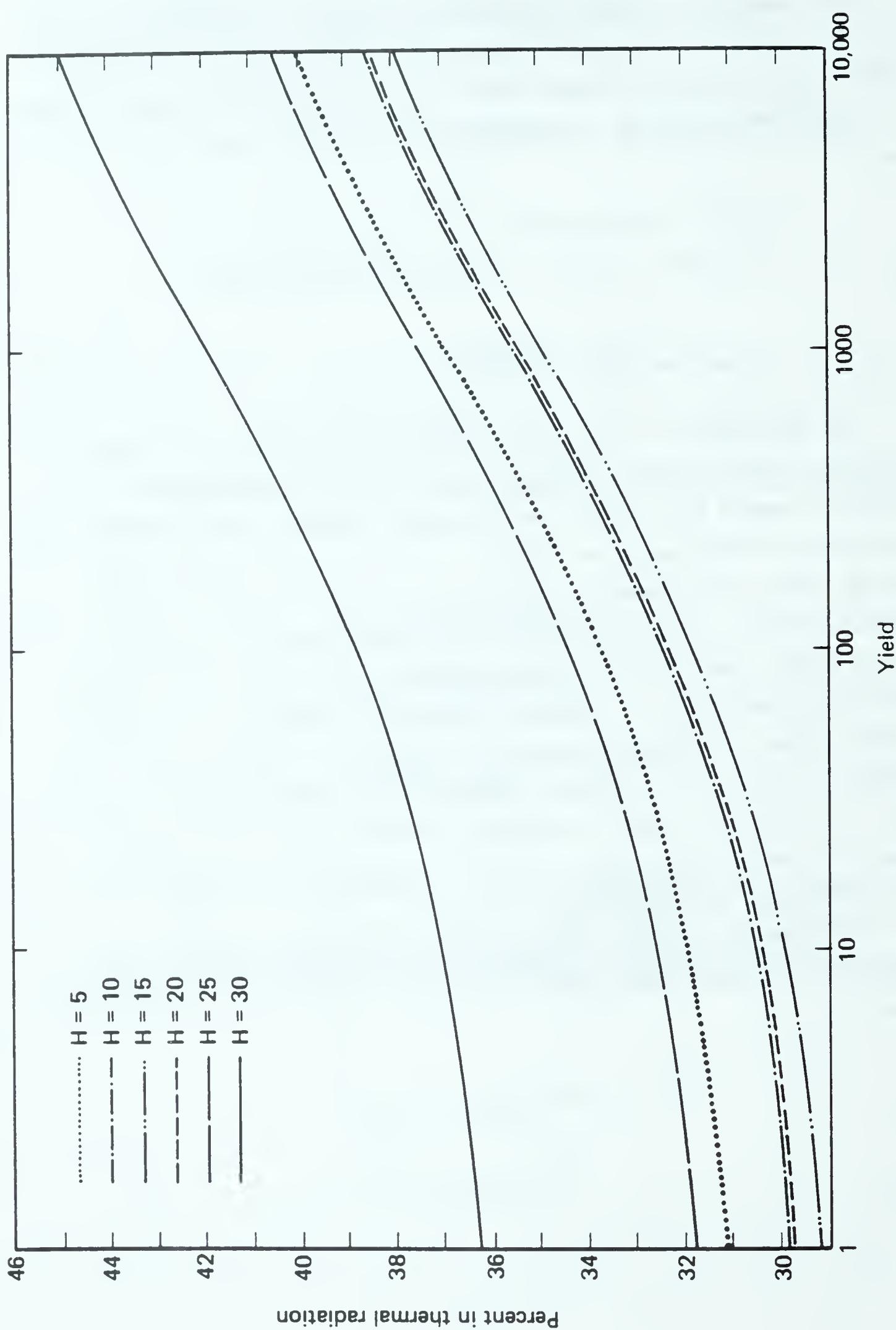


Figure 117. Thermal radiation fraction of total yield versus yield for burst altitudes up to 30 km [Brode, 1968, Eq. (32)].

$$\begin{aligned}
f_{\infty} &\simeq 35 + a \cdot h^{9.5} / (1+b \cdot h^{10}) + c \cdot h^3, \\
a &= 9.621 \cdot 10^{-9} \cdot [\lambda^4 / (1+2.0737 \cdot 10^{-6} \cdot \lambda^9) \\
&\quad + 3.188 \cdot \lambda^2 / (1+0.009269 \cdot \lambda^2)], \\
b &= 4.810 \cdot 10^{-9} [\lambda^4 / (1+0.00001472 \cdot \lambda^9) \\
&\quad + 4.857 \cdot \lambda / (1+0.2895 \cdot \lambda)], \\
c &= 0.0002042 \cdot (1-0.0776 \cdot \lambda + 0.0001181 \cdot \lambda^{3.882}), \quad (106)
\end{aligned}$$

where $\lambda = \ln(W)$, and h = altitude in kilometers.

This approximation [Eq. (106)] is plotted in Fig. 123 versus yield for burst heights up to 30 km.

The thermal fraction versus yield and altitude as depicted by Kieth and Sachs [1985] is at variance with these previous estimates [Eqs. (105) and (106)]. It can be fit by the form:

$$f_{\infty}^* \approx a + b \cdot h + c \cdot h^2 + d \cdot h^3 \quad (107)$$

in which

$$\begin{aligned}
a &= 34.86 / (1+0.001618 \cdot \lambda^{2.447}), \\
b &= 0.1125 / (1+0.08972 \cdot \lambda^{1.545}) - 0.005319, \\
c &= 0.01861 - 0.009506 \cdot \lambda + 0.005402 \cdot \lambda^2 - 0.001008 \cdot \lambda^3 \\
&\quad + 0.0000579 \cdot \lambda^4, \\
d &= -0.0002261 + 0.0003568 \cdot \lambda - 0.0001888 \cdot \lambda^2 \\
&\quad + 0.00003323 \cdot \lambda^3 - 0.000001841 \cdot \lambda^4,
\end{aligned}$$

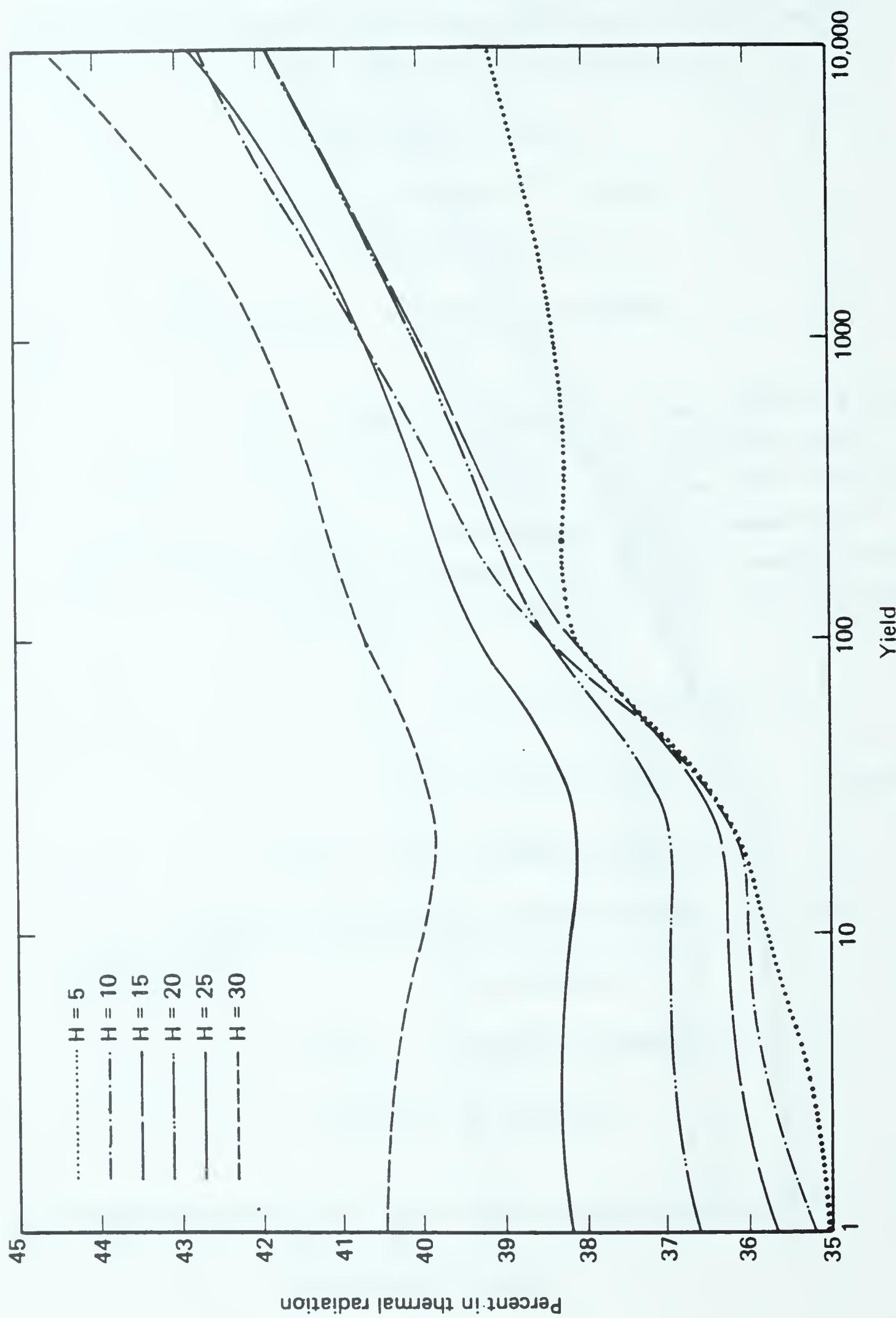


Figure 118. Thermal radiation fraction of total yield versus yield for burst altitudes up to 30 km [ENW, 1977].

again with $\lambda = \ln(W)$ (W in KT) and h = altitude of burst in kilometers. This fit is illustrated in Fig. 124.

The three predictions approximated in Eqs. (105), (106) and (107) are based on many of the same test data and numerical calculations, so the differences are not easily justified. The test data, as well as most of the calculations, contain considerable scatter and variability, and the information at altitude is sparse. However, more and better calculations are possible, and could help to further resolve the uncertainties. The three predictions are plotted versus altitude for 1 KT, 100 KT, and 10 MT in Figs. 125, 126, and 127, respectively. All the forms lead to an increase in the thermal fraction with altitude at high altitudes ($h > 14\text{km}$), but the Kieth and Sachs [1985] values decrease with yield. The test data, although limited, do not seem to support a decreasing thermal fraction with increasing yield at any altitude.

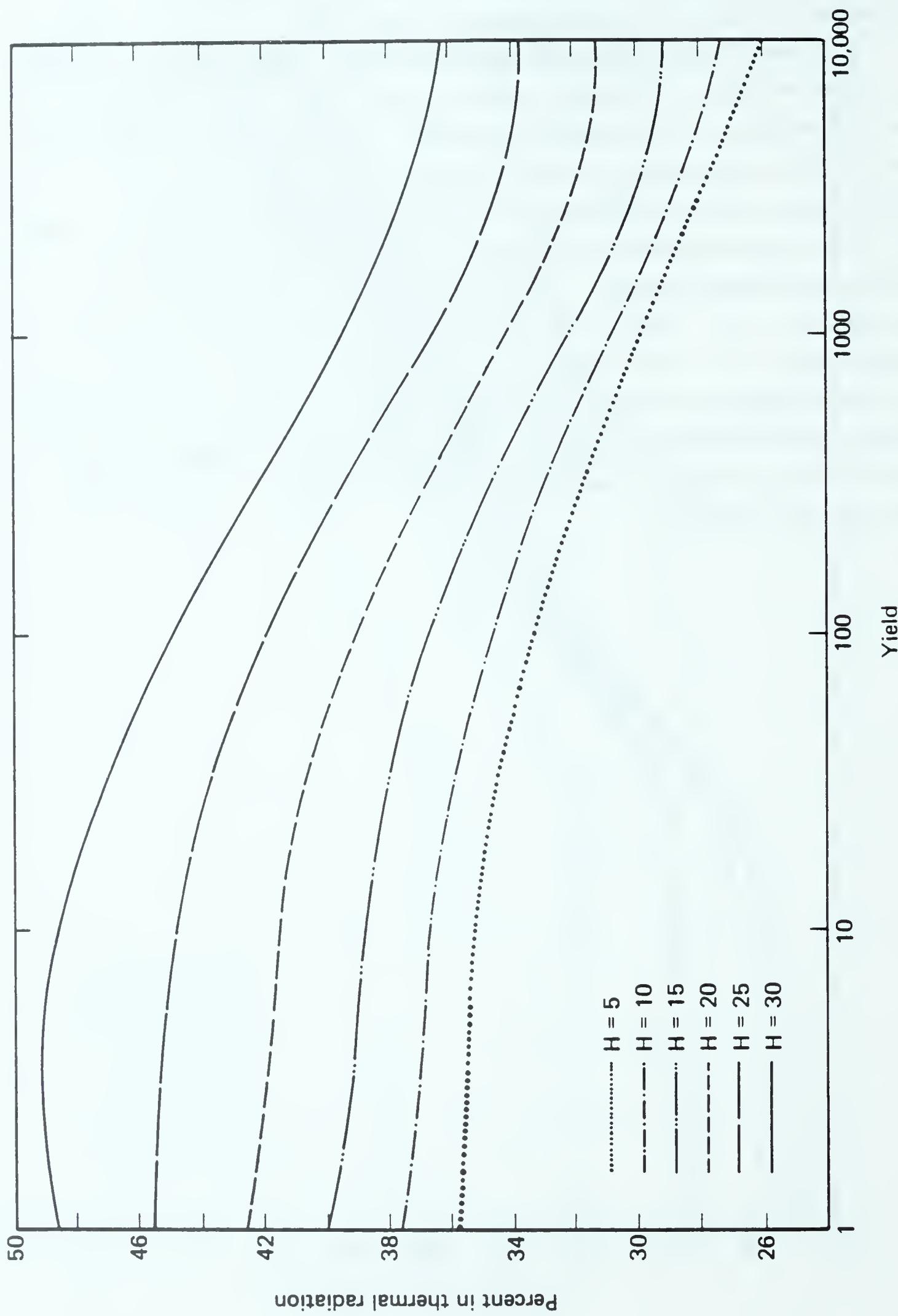


Figure 119. Thermal radiation fraction of total yield versus yield for burst altitudes up to 30 km [FMI, 1985].

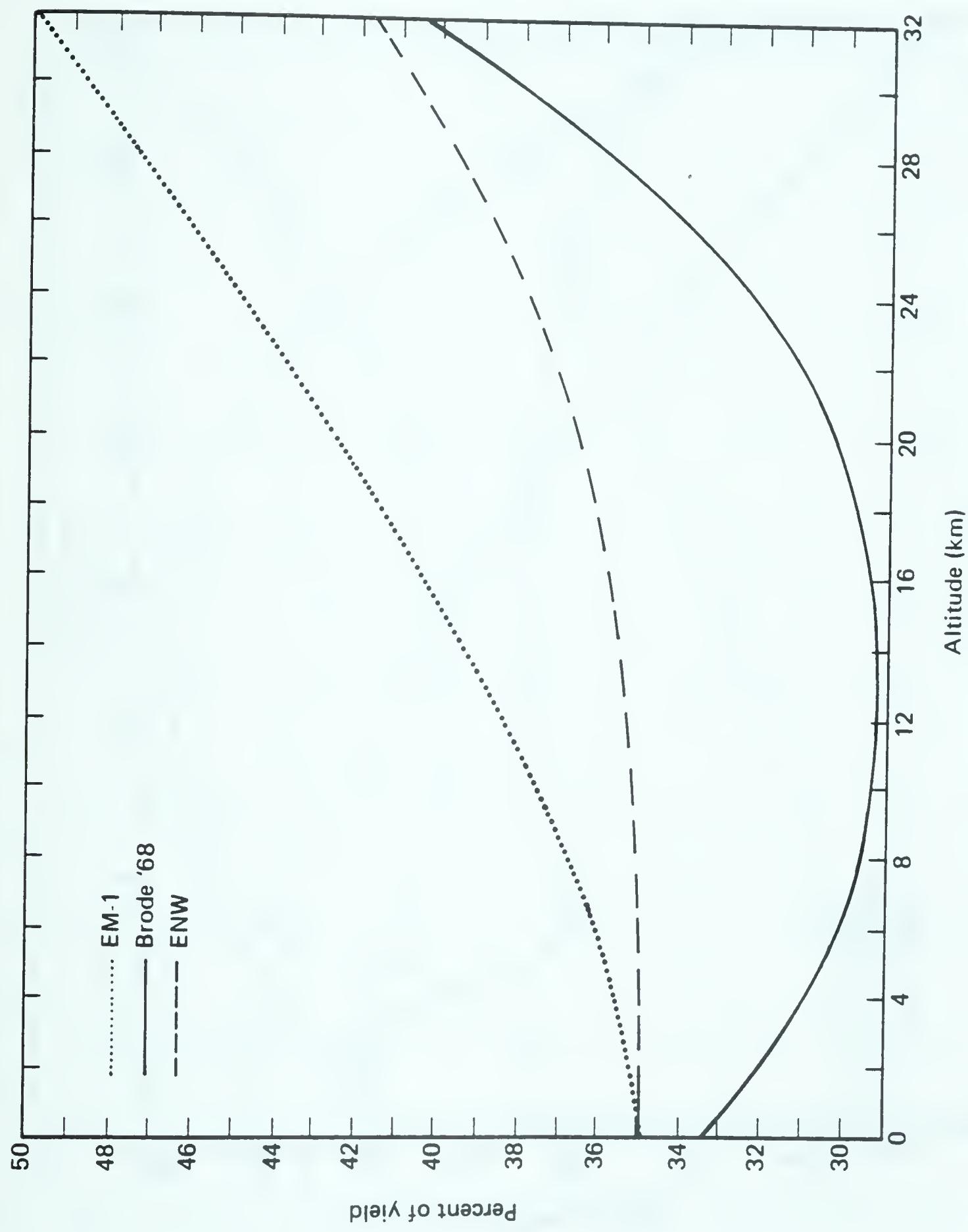
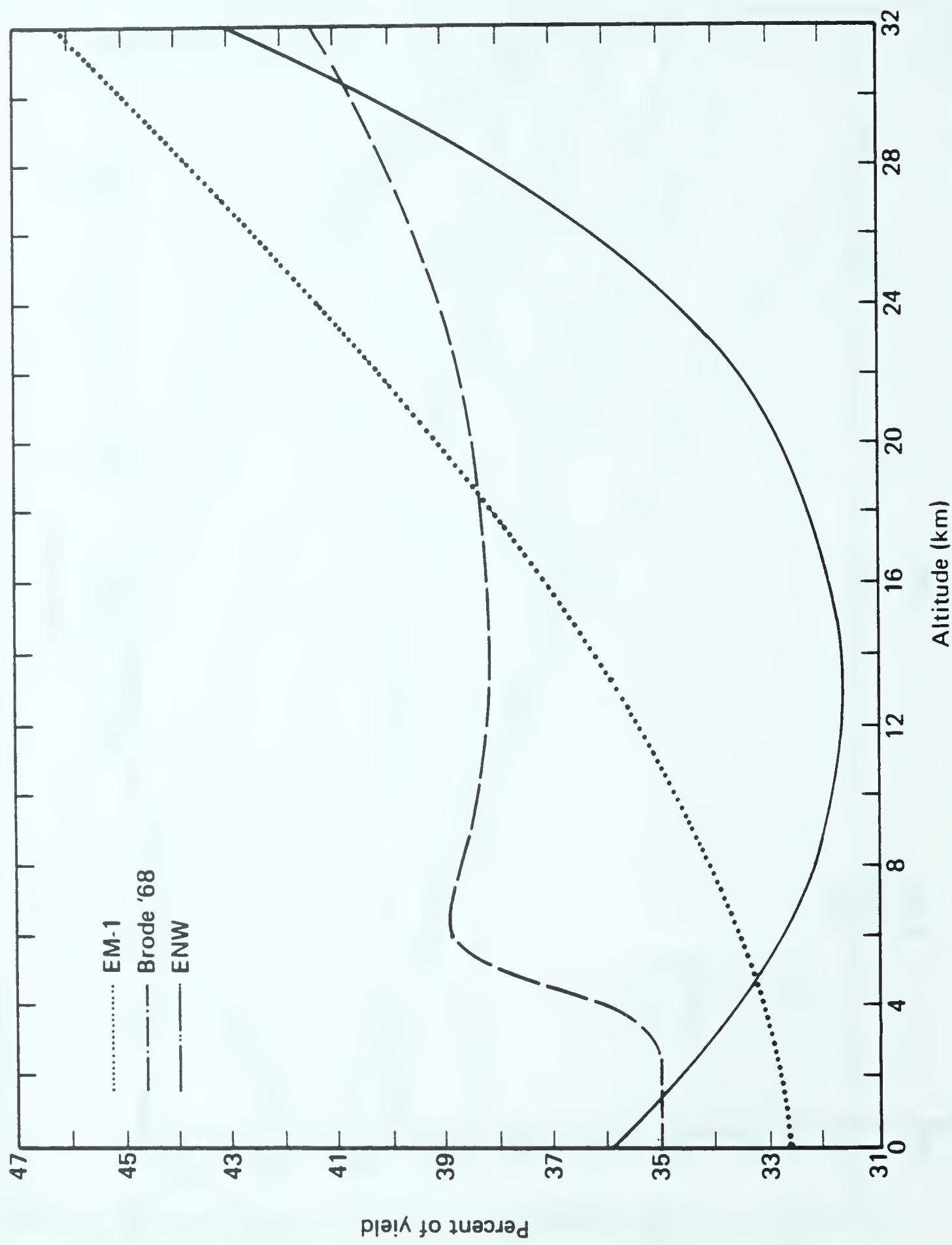


Figure 120. Comparison of thermal fractions as predicted by three formulae (Eqs. (101), (102), (103)) versus burst altitude for 1 KT.

Figure 121. Comparison of thermal fractions as predicted by three formulae (Eqs. (101), (102), (103)) versus burst altitude for 100 kT.



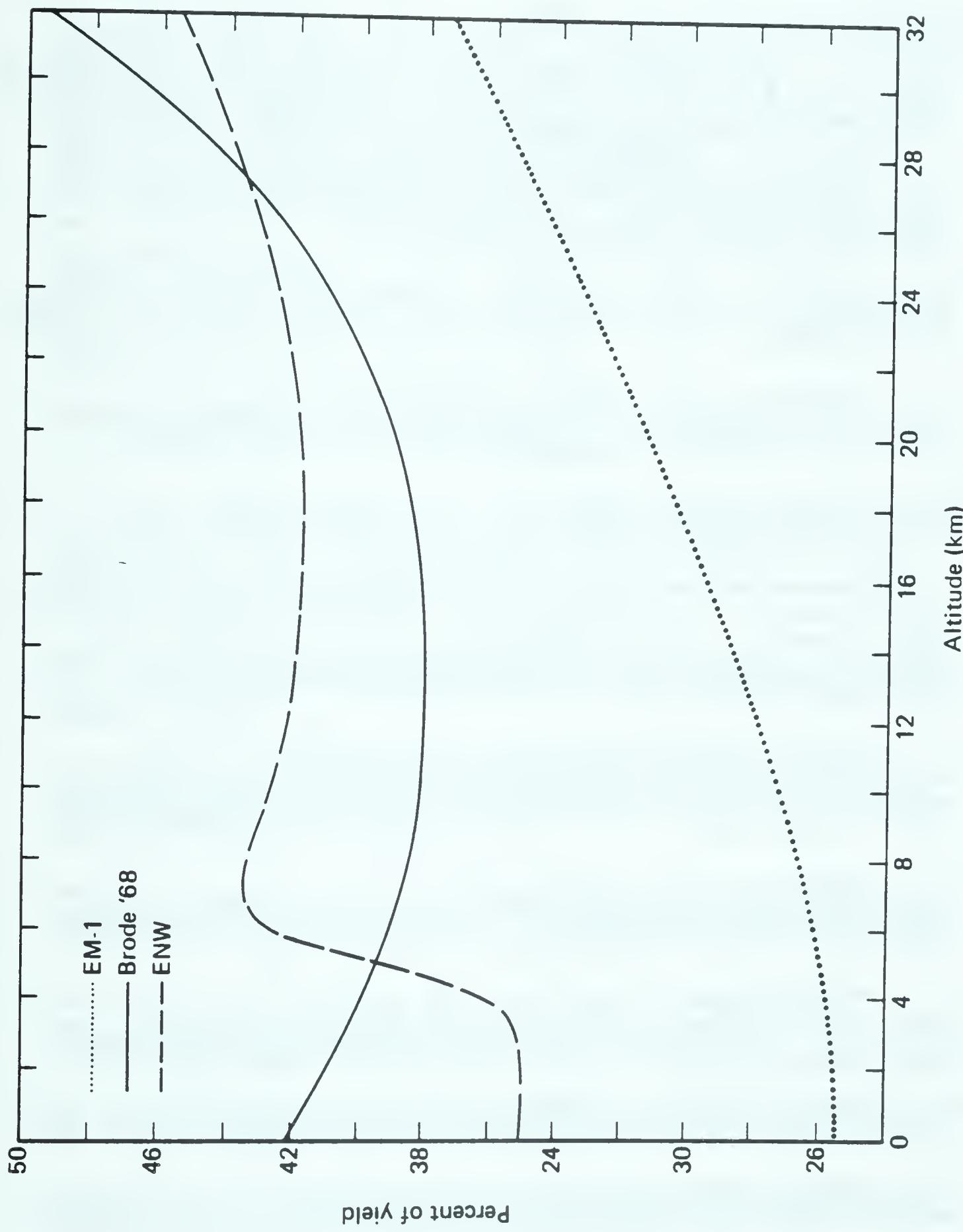


Figure 122. Comparison of thermal fractions as predicted by three formulae (Eqs. (101), (102), (103)) versus burst altitude for 10 MT.

SECTION 7
LIST OF REFERENCES

- Brode, H. L., Calculation of the Blast Wave from a Spherical Charge of TNT, The Rand Corporation, Santa Monica, California, (subsequently published in Physics of Fluids, Vol. 2, March 1959a, pp. 217-229).
- , Theoretical Description of the Blast and Fireball for a Sea-Level Megaton Explosion, The Rand Corporation, Santa Monica, California, RM-2248, September 1959b.
- , A Review of Nuclear Explosion Phenomena Pertinent to Protective Construction, The Rand Corporation, Santa Monica, California, R-425-PR, May 1964.
- , Theoretical Description of the Blast and Fireball for a Sea-Level Kiloton Explosion, The Rand Corporation, Santa Monica, California, RM-2246-PR, January 1966.
- , "Review of Nuclear Weapon Effects," Ann. Rev. Nuc. Sci., Vol. 18, March 1968.
- , "Theoretical Description of the Performance of the UTIAS Hypervelocity Launcher," Astronautica Acta, Vol. 15, Pergamon Press, Oxford, England, 1970, pp. 301-309; presented at the International Colloquium on Gas Dynamics of Explosions, Novosibirsk, USSR, 24-29 August 1969.
- , Height of Burst Effects at High Overpressures, The Rand Corporation, Santa Monica, California, RM-6301-DASA, July 1970 (subsequently published by Defense Atomic Support Agency, Washington, D.C., as DASA 2506).
- , "Improvements and Corrections to DASA 2506, Height of Burst Effects at High Overpressures," R & D Associates, Marina Del Rey, California, private communication, 30 November 1978.
- , "The Real Thing: Blast Waves from Atmospheric Nuclear Explosions," Proceedings of the 12th International Symposium on Shock Tubes and Waves, Jerusalem, Israel, 16-19 July, 1979.
- , Review of Nuclear Test Peak Overpressures Height-of-Burst Data, Pacific-Sierra Research Corporation, Note 353, November 1981.
- , Analytic Fits to Dynamic Pressure and Impulse, Pacific-Sierra Research Corporation, Note 529, February 1983.

Brode, H. L., and B. R. Parkin, "Calculations of the Blast and Close-In Elastic Response of the Cavity Explosions in the COWBOY Program," J. Geophys. Res., Vol. 68, No. 9, 1 May 1963.

Brode, H. L., and S. J. Speicher, Analytic Approximation for Dynamic Pressure Versus Time, Pacific-Sierra Research Corporation, Note 315, May 1980.

----, Airblast Overpressure Analytic Expression for Burst Height, Range, and Time Over an Ideal Surface (Summary), Pacific-Sierra Research Corporation, Note 445, February 1982.

Brode, H. L., et al., A Program for Calculating Radiation Flow and Hydrodynamic Motion, The Rand Corporation, Santa Monica, California, RM-5178, April 1967.

Carpenter, H. J., R & D Associates, Marina Del Rey, California, private communication, 31 August 1976.

Fry, M. A., Science Applications International, McLean, Virginia, private communication, 10 April 1986.

Fry, M. A., P. Kamath, and D. L. Book, Height of Burst Study, Calculations of 1 MT at 250, 500, 750, 1000, 1250, 1500 Feet, Science Applications, Inc., McLean, Virginia, in association with Naval Research Laboratory, Washington, D.C., presented to the Defense Nuclear Agency, Headquarters, Washington, D.C., 18 January 1985.

Gilmore, F. R., Equilibrium Composition and Thermodynamic Properties of Air to 24,000 K, The Rand Corporation, Santa Monica, California, RM-1543, August 1955.

----, Additional Values for the Equilibrium Composition and Thermodynamic Properties of Air, The Rand Corporation, Santa Monica, California, RM-2328, December 1959.

Glasstone, S., and P. J. Dolan, The Effects of Nuclear Weapons, U.S. Department of Defense and Department of Energy, Washington, D.C., 1977.

Hilsenrath, J., M. S. Green, and C. W. Beckett, Thermodynamic Properties of Highly Ionized Air, Air Force Special Weapons Center, AFSWC-TR-56-35, April 1957.

Kuhl, A., Evaluation of Recent HE and Nuclear HOB Calculations, R & D Associates, Marina Del Rey, California, revised ed., March 1983.

McNamara, W., R. J. Jordano, and P. S. Lewis, Air Blast from a 1 KT Nuclear Burst at 60 Meters Over an Ideal Surface, General Electric Corporation-TEMPO, BRL-CR-353, November 1977.

Moulton, J. F., ed., Nuclear Weapons Blast Phenomena, Vol. 1, Defense Atomic Support Agency, Washington, D.C., DASA 1200, March 1960.

Needham, C. E., and J. E. Crepeau, The DNA Nuclear Blast Standard (1 KT), S-Cubed, La Jolla, California, SSS-R-81-4845, January 1981.

Needham, C. E., M. L. Havens, and C. S. Knauth, Nuclear Blast Standard (1 KT), Air Force Weapons Laboratory, Kirtland Air Force Base, New Mexico, AFWL-TR-73-55, April 1975.

Pyatt, K. D., Jr., Surface Airblast Overpressure Impulse at Extremely High Overpressure, S-Cubed, La Jolla, California, SSS-R-83-6069, March 1983a.

-----, S-Cubed, La Jolla, California, private communication, May 1983b.

-----, S-Cubed, La Jolla, California, private communication, December 1985.

Pyatt, K. D., Jr., and D. Wilkins, S-Cubed, La Jolla, California, private communication, August 1983.

Reisler, R., U.S. Army Ballistics Research Laboratory, Aberdeen Proving Ground, Aberdeen, Maryland, private communication, August 1980.

Ruetenik, J. R., Kaman AviDyne, Burlington, Massachusetts, private communication, November 1984.

Sachs, D. C., Ideal Airblast, Kaman Tempo, Santa Barbara, California, C5180-02, September 1985.

Smiley, R. F., J. R. Ruetenik, and M. A. Tomayko, Reflect-4 Code Computations of 1 MT Nuclear Blast Waves Reflected from the Ground, Kaman AviDyne, Burlington, Massachusetts, Vols. 1-3, KA-TR-221, May 1984a.

-----, Reflect-4 Code Computations of 40 KT Nuclear Blast Waves Reflected from the Ground for Four Heights of Burst, Vols. 1 and 2, Kaman AviDyne, Burlington, Massachusetts, KA-TR-222, September 1984b.

Smiley, R. F., M. A. Tomayko, and J. R. Ruetenik, Reflect-4 Code Overpressure, Dynamic Pressure, and Impulse Time-Histories at the Ground for a 40-KT Burst at 684-FT HOB, Kaman AviDyne, Burlington, Massachusetts, KA-TR-136, August 1982a.

-----, Reflect-4 Code Overpressure, Dynamic Pressure, and Impulse Time-Histories at the Ground for a 40-KT Burst at 1368-FT HOB, Kaman AviDyne, Burlington, Massachusetts, KA-TR-137, August 1982b.

-----, Reflect-4 Code Overpressure, Dynamic Pressure, and Impulse Time-Histories at the Ground for a 40-KT Burst at 2394-FT HOB, Kaman AviDyne, Burlington, Massachusetts, KA-TR-138, August 1982c.

-----, Reflect-4 Code Computations of 40 KT Nuclear Blast Waves Reflected from the Ground, Kaman AviDyne, Burlington, Massachusetts, KA-TR-201, November 1982d.

Speicher, S. J., Corrections to Dynamic Pressure "Quick Fix", Pacific-Sierra Research Corporation, private communication, 21 December 1982.

-----, Improvement to Dynamic Pressure "Quick Fix", Pacific-Sierra Research Corporation, private communication, 20 June 1983.

Speicher, S. J., and H. L. Brode, Revised Procedure for the Analytic Approximation of Dynamic Pressure Versus Time, Pacific-Sierra Research Corporation, Note 320, May 1980a.

-----, An Analytic Approximation for Peak Overpressure Versus Burst Height and Ground Range Over an Ideal Surface, Pacific-Sierra Research Corporation, Note 336, September 1980b.

-----, Airblast Overpressure Analytic Expression for Burst Height, Range, and Time--Over an Ideal Surface, Pacific-Sierra Research Corporation, Note 385, November 1981.

-----, An Analytic Expression for Extremely High Peak Overpressure Over an Ideal Surface, Pacific-Sierra Research Corporation, Note 597, May 1984a.

-----, Extremely High Overpressure Analytic Expression for Burst Height, Range, and Time--Over an Ideal Surface, Pacific-Sierra Research Corporation, Note 611, October 1984b.



APPENDIX A
OVERPRESSURE VALUES AS FUNCTION OF
GROUND RANGE, BURST HEIGHT, AND TIME

| X | Y | $\sigma - \tau$ | ΔP |
|--------|--------|-----------------|------------|
| 18.2 | 0.0 | 0.042 | 107926.6 |
| 28.1 | 0.0 | 0.363 | 10113.7 |
| 37.9 | 0.0 | 1.22 | 2069.0 |
| 47.1 | 0.0 | 0.0045 | 27696.0 |
| 66.3 | 0.0 | 6.39 | 306.5 |
| 80.3 | 0.0 | 19.8 | 78.34 |
| 0.0 | 25.0 | 0.137 | 55580.0 |
| 19.7 | 25.0 | 25.3 | 9.284 |
| 32.8 | 25.0 | 0.00417 | 255273.1 |
| 49.2 | 25.0 | 0.046 | 10462.5 |
| 64.7 | 25.0 | 0.189 | 15346.0 |
| 83.0 | 25.0 | 57.8 | 7.799 |
| 97.6 | 25.0 | 124.0 | 1.265 |
| 0.0 | 50.0 | 0.0416 | 110106.0 |
| 6.72 | 50.0 | 0.116 | 43739.3 |
| 24.2 | 50.0 | 3.07 | 270.9 |
| 41.5 | 50.0 | 56.1 | 0.1174 |
| 55.9 | 50.0 | 0.137 | 21674.8 |
| 72.6 | 50.0 | 0.251 | 15168.9 |
| 90.6 | 50.0 | 11.7 | 70.46 |
| 14.9 | 22.5 | 0.0139 | 201704.4 |
| 33.1 | 18.9 | 1.35 | 1397.0 |
| 37.7 | 8.22 | 0.214 | 16365.0 |
| 82.8 | 1410.0 | 6.95 | 8.374 |
| 157.0 | 257.0 | 0.448 | 375.8 |
| 393.0 | 682.0 | 10.9 | 24.23 |
| 1250.0 | 220.0 | 22.1 | 6.593 |
| 1160.0 | 2520.0 | 0.538 | 3.1185 |
| 3140.0 | 4260.0 | 13.4 | 1.233 |

NOTE: X = scaled ground range ($ft/KT^{1/3}$),
 Y = scaled burst height ($ft/KT^{1/3}$),
 $\sigma - \tau$ = scaled time - time of arrival ($ms/KT^{1/3}$),
 ΔP = overpressure (psi).



APPENDIX B
FORTRAN PROGRAM FOR OVERPRESSURE
VERSUS TIME, BURST HEIGHT, AND GROUND RANGE.

```

SUBROUTINE PT(Y,X,SIGMA,DELTAP)
C
C
C
C THIS IS A FORTRAN IMPLEMENTATION OF THE ANALYTIC EXPRESSION FOR
C PRESSURE TIME HISTORY (BRODE AND SPEICHER, MAY 1986)
C
C THE PARAMETERS ARE:
C
C X = SCALED GROUND RANGE (FT/KT**(1/3))
C Y = SCALED HOB (FT/KT**(1/3))
C SIGMA = SCALED TIME (MSEC/KT**(1/3))
C           ** NOTE THAT SIGMA IS THE TIME AFTER BURST IN THE      **
C           ** ANALYTIC EXPRESSION. FOR PURPOSES OF CALCULATION    **
C           ** SIGMA IN THIS ROUTINE IS TIME AFTER TIME OF ARRIVAL,   **
C           ** WHICH IS THEN ADDED TO THE CALCULATED TIME OF ARRIVAL **
C DELTAP = PRESSURE (PSI)
C
C IF PRESSURE IS DESIRED IN KPA THEN MULTIPLY RESULT
C BY 100/14.504
C
C NOTE THAT LIMITS ARE PLACED ON VALUES SUCH AS X,Y,Z, ETC...
C THIS IS DONE TO AVOID OVERFLOWS AND THE VALUES ARE MACHINE
C DEPENDENT.
C
C
C
IF (X.LT.1E-9) X=1.E-9
IF (Y.LT.1E-9) Y=1.E-9
CAPR = (X*X + Y*Y)**.5

R = CAPR/1000
Z = Y/X

IF (Z.GT.100.) Z=100
CALL PPEAK(X,Y,CAPR,Z,DELTPS)
XM = 170*Y / (1. + 60.* (Y**.25)) + 2.89*((Y/100)**2.5)
U = (0.543 - 21.8*R + 386*(R**2) + 2383*(R**3))*(R**8)
# / (2.99E-14 - 1.91E-10*(R**2) + 1.032E-6*(R**4) -
# 4.43E-6*(R**6) + (1.028 + 2.087*R + 2.69*(R**2))* (R**8))
TAU = U
IF (X.LT.XM) GOTO 100
W = (1.086 - 34.605*R + 486.3*(R**2) + 2383*(R**3))
# * (R**8) / (3.0137E-13 - 1.2128E-9*(R**2)
# + 4.128E-6*(R**4) - 1.116E-5*(R**6) + (1.632 +
# 2.629*R + 2.69*(R**2))* (R**8))
TAU = U*XM/X + W*(1 - XM/X)
100 CONTINUE
SIGMA = SIGMA + TAU
S2 = 1 - 15.18*((Y/100)**3.5) / (1 + 15.18*((Y/100)**3.5)) -

```

```

# (0.02441*((Y/1.E6)**2) / (1 + 9000*((Y/100)**7)) * (1.E10 /
# (0.441 + ((X/100)**10)))
CAPD = ((1640700 + 24629*TAU + 416.15*(TAU**2)) / (10880 +
# 619.76*TAU + (TAU**2)) * (0.4 + 0.001204*(TAU**1.5) /
# (1 + 0.001559*(TAU**1.5)) + (0.6126 + 0.5486*(TAU**.25) /
# (1 + 0.00357*(TAU**1.5)) - 3.47*(TAU**0.637) / (1 +
# 5.696*(TAU**0.645))) * S2)
S = 1 - 1100*((Y/100)**7) / (1 + 1100*((Y/100)**7)) -
# (2.441E-14*Y*Y / (1 + 9000*((Y/100)**7))) * (1.E10 / (0.441 +
# ((X/100)**10)))
F2 = (0.445 - 5.44*(R**1.02) / (1 + 100000*(R**5.84)) +
# 7.571*(Z**7.15) / (1 - 5.135*(Z**12.9)) - 8.07*(Z**7.31) /
# (1 + 5.583*(Z**12.23)) * (0.435*((Y/10)**1.26) / (1 +
# 0.03096*((Y/10)**3.12)) * (1 - 0.000019*(TAU**8) / (1 +
# 0.000019*(TAU**8)))
F = (0.01477*(TAU**.75) / (1 + 0.005836*TAU) + 7.402E-5*(TAU**2.5)
# / (1 + 1.429E-8*(TAU**4.75)) - 0.216) * S + 0.7076 -
# 3.077E-5*(TAU**3) / (1 + 4.367E-5*(TAU**3)) + F2 - (0.452 -
# 9.94E-7*(X**4.13) / (1 + 2.1868E-6*(X**4.13))) * (1 -
# 1.5397E-4*(Y**4.3) / (1 + 1.5397E-4*(Y**4.3)))
G = 10 + (77.58 - 64.99*(TAU**.125) / (1 + 0.04348*(TAU**5))) * S
H = 3.003 + 0.05601*TAU / (1 + 1.473E-9*(TAU**5)) + (0.01769*TAU /
# (1 + 3.207E-10*(TAU**4.25)) - 0.03209*(TAU**1.25) / (1 +
# 9.914E-8*(TAU**4)) - 1.6) * S - 0.1966*(TAU**1.22) / (1 +
# 0.767*(TAU**1.22))
B = (F * ((TAU/SIGMA)**G) + (1 - F) * ((TAU/SIGMA)**H)) *
# (1 - (SIGMA - TAU)/CAPD)
IF (X.LT.XM .OR. Y.GT.380.) GOTO 1000
XE = 3.039*Y / (1 + 0.0067*Y)
AK = ABS((X - XM)/(XE - XM))
IF (AK.GT.50.) AK=50
D2 = 2.99 + 31240*((Y/100)**9.86) / (1 + 15530*((Y/100)**9.87))
D = 0.23 + 0.583*Y*Y / (26667 + Y*Y) + 0.27*AK + (0.5 - 0.583*Y*Y /
# (26667 + Y*Y)) * (AK**D2)
A = (D - 1) * (1 - (AK**20) / (1 + (AK**20)))
AJ = 11860 * (SIGMA - TAU) / (Y * ((X - XM)**1.25))
IF (AJ.GT.200) AJ=200
V = 1 + (0.003744*((Y/10)**5.185) /
# (1 + 0.004684*((Y/10)**4.189)) +
# 0.004755*((Y/10)**8.049) / (1 + 0.003444*((Y/10)**7.497)) -
# 0.04852*((Y/10)**3.423) / (1 + 0.03038*((Y/10)**2.538)) * *
# (AJ**3) / (6.13 + (AJ**3)) * (1 / (1 + 9.23*(AK**2))) *
C3 = 1 + (1.094*(AK**.738) / (1 + 3.687*(AK**2.63)) * (1 -
# 83.01*((Y/100)**6.5) / (1 + 172.3*((Y/100)**6.04)) - 0.15)) * *
# (1 / (1 + 0.5089*(AK**13)))
C2 = 23000*((Y/100)**9) / (1 + 23000*((Y/100)**9))
TEMP = (X/100)**4
C = (1.04 - 0.02409*TEMP / (1 +
# 0.02317*TEMP)) * (AJ**7) / (((1 + A) * (1 +
# 0.923*(AJ**8.5))) * (C2 + (1 - C2) * (1 -
# 0.09*(AK**2.5) / (1 + 0.09*(AK**2.5)))) *
# * C3 * (1 - (((SIGMA - TAU)/CAPD)**8)))
DELTAP = DELTPS * (1 + A) * (B*V + C)
RETURN
1000 CONTINUE
DELTAP = DELTPS * B
RETURN
END

```

```

C
C
C SUBROUTINE PPEAK(X,Y,CAPR,Z,DELTPS)
C
C THIS IS A FORTRAN IMPLEMENTATION OF THE ANALYTIC EXPRESSION FOR
C PEAK OVERPRESSURE (BRODE AND SPEICHER, MAY 1986)
C
C THE PARAMETERS ARE:
C
C X = SCALED GR          (FT/KT**(1/3))
C Y = SCALED HOB          (FT/KT**(1/3))
C CAPR = (X*X + Y*Y)**(1/2) (FT/KT**(1/3))
C Z = Y/X
C DELTPS = PEAK PRESSURE (PSI)
C
C
C R = CAPR/1000
C A = 1.22 - (3.908*Z*Z) / (1 + 810.2*Z**5)
C B = 2.321 + (6.195*(Z**18)/(1 + 1.110*(Z**18))) -
# (0.03831*(Z**17)/(1 + 0.02415*(Z**17))) + (0.6692/(1 +
# 4164*(Z**8)))
# BB = .0629*((X/Y)**8.34) / (1 + .00509*((X/Y)**13.05)) *
# .05*Y / (1 + 2.56E-8*(Y**5))
C = 4.153 - (1.149*(Z**18)) / (1 + 1.641*(Z**18)) - (1.1 / (1 +
# 2.771*(Z**2.5)))
D = (-4.166) + 25.76*(Z**1.75) / (1 + 1.382*(Z**18)) + 8.257*Z /
# (1 + 3.219*Z)
E = 1 - 0.004642*(Z**18) / (1 + 0.003886*(Z**18))
F = 0.6096 + 2.879*(Z**9.25) / (1 + 2.359*(Z**14.5)) - 17.15*Z*Z /
# (1 + 71.66*(Z**3))
G = 1.83 + 5.361*Z*Z / (1 + .3139*(Z**6))
H = -(0.2905 + 64.67*(Z**5)) / (1 + 441.5*(Z**5)) - 1.389*Z / (1
# + 49.03*(Z**5)) + 8.808*(Z**1.5) / (1 + 154.5*(Z**3.5)) +
# 1.094*(CAPR**2) / ((0.7813E9 - 1.234E5*CAPR + 1201*(CAPR**1.5) +
# (CAPR**2)) * (1 + 2*Y))
P = 1.8008E-7*(Y**4) / (1 + 0.0002863*(Y**4)) - 2.121*Y*Y /
# (794300 + (Y**4.3))
Q = 5.18 + 8.864*(Y**3.5) / (3.788E6 + (Y**4))
DELTPS = (10.47)/(R**A) + (B - BB)/(R**C) + (D*E)/(1 +
# F*(R**G)) + H + P/(R**Q)

RETURN
END

```



APPENDIX C
LIST OF SYMBOLS

| | |
|---|------------|
| air density, in kilograms per cubic meter; Eqs. (6) through (8) | ρ |
| air temperature, in degrees kelvin; Eq. (24) | θ |
| ambient air density | ρ_0 |
| ambient air sound speed = 1.0872 kft/s | c_0 |
| ambient air specific heat ratio ≈ 1.400 | γ_0 |
| ambient air temperature = 273.2 K; Eqs. (20), (21) | θ_0 |
| ambient pressure, in pounds per square inch ≈ 14.7 psi at sea level | p_0 |
| burst height, in feet | H |
| duration of negative overpressure phase, in milliseconds | D_p^- |
| duration of positive overpressure phase, in milliseconds; Eqs. (43) through (48) | D_p^+ |
| duration of positive dynamic pressure, or outward flow; Eq. (52) | D_u^+ |
| dynamic pressure, in pounds per square inch $(\rho u^2/2)$; Eqs. (15) through (18), (56), (57), (63), (64), (66) | Q |
| fireball temperature maximum, in 10^3°C ; Eq. (59) | θ_m |
| free-air or surface-burst range, in kilofeet; Eqs. (36), (40), (41), (55) | sr |
| ground range, or shock radius, in feet | GR |

NOTE: Subscripts "o" refer to ambient air (preshock) conditions;
subscripts "s" refer to shock conditions; and subscripts "R" refer
to reflected shock values.

| | |
|--|--------------|
| impulse in dynamic pressure positive phase, in pounds per square inch millisecond; Eqs. (53) through (55), (65) | I_u^+ |
| impulse in positive overpressure phase, in pounds per square inch millisecond; Eqs. (47), (48) | I_p^+ |
| interface between regular and Mach reflection, approximate; Eq. (64) | X_q |
| locus of scaled burst heights and scaled ranges for second peak equal to shock overpressure, in kilofeet per cube-root kiloton; Eq. (63) | X_e |
| lower limit to range of validity of dynamic impulse fit; Eq. (65) | X_i |
| Mach number (u/C) | M |
| Mach reflection onset, in kilofeet per cube-root kiloton; Eq. (63) | X_m |
| overpressure, in millions of pounds per square inch | ζ |
| overpressure, in pounds per square inch; Eqs. (49), (50), (63) | ΔP |
| overpressure, in thousands of pounds per square inch = $\Delta P_s / 1000$ | π |
| particle velocity | u |
| peak density | ρ_s |
| peak dynamic pressure at transition between regular and Mach reflection; Eq. (64) | Q_m |
| peak dynamic pressure, in pounds per square inch; Eqs. (16) through (18) | Q_s |
| peak overpressure, in pounds per square inch; Eqs. (33) through (35), (37), (38), (50), (62) | ΔP_s |
| peak particle velocity, in kilofeet per second; Eqs. (12) through (14) | u_s |

NOTE: Subscripts "o" refer to ambient air (preshock) conditions;
subscripts "s" refer to shock conditions; and subscripts "R" refer
to reflected shock values.

| | |
|---|--------------|
| peak pressure, in pounds per square inch; Eqs. (2) through (6) | P_s |
| positive dynamic pressure duration; Eq. (58) | D' |
| positive overpressure duration; Eqs. (50), (51) | D |
| power, or rate, of heat release | p^* |
| pressure = $\Delta P + P_o$, in pounds per square inch | P |
| radiant fluence, in calories per square centimeter | Q^* |
| range for height of target at which dynamic pressure is lower by 10 percent from surface value for corresponding burst height; Eq. (67) | R_T |
| range for thermal radiation, in statute miles | R_r |
| ratio of scaled burst height to scaled ground range (y/x); Eqs. (62), (63) | z |
| reflected peak overpressure (normal reflection), in pounds per square inch; Eq. (30) | ΔP_R |
| reflected pressure, in pounds per square inch; Eqs. (26) through (30) | P_R |
| reflected shock velocity; Eq. (25), (26) | U_R |
| reflection factor = $\Delta P_R / \Delta P_s$; Eqs. (30) through (32) | RF |
| scaled burst height, in feet per cube-root kiloton = H/m | Y |
| scaled burst height, in kilofeet per cube-root kiloton = $Y/1000$ | y |
| scaled ground range, in feet per cube-root kiloton = GR/m | X |
| scaled ground range, in kilofeet per cube-root kiloton = $X/1000$ | x |

NOTE: Subscripts "o" refer to ambient air (preshock) conditions;
subscripts "s" refer to shock conditions; and subscripts "R" refer
to reflected shock values.

| | |
|--|------------------|
| scaled slant range, in feet per cube-root kiloton = $(x^2 + y^2)^{1/2}$ | R |
| scaled slant range, in kilofeet per cube-root kiloton = $(x^2 + y^2)^{1/2}$; Eq. (33) | r |
| scaled time after detonation (t/m), in milli-seconds per cube-root kiloton | σ |
| scaled time of arrival (T/m), in milli-seconds per cube-root kiloton | τ |
| shock density ratio | η_s |
| shocked air specific heat ratio | γ_s |
| shock temperature | θ_s |
| shock temperature increase, in degrees centigrade; Eqs. (20) through (23) | $\Delta\theta_s$ |
| shock velocity, in kilofeet per second; Eqs. (10), (11) | U_s |
| specific heat at constant pressure | C_p |
| specific heat at constant volume | C_v |
| specific heat ratio = C_p/C_v ; Eq. (9) | γ |
| specific internal energy, in ergs per gram; Eqs. (4), (5), (69), (70) | E |
| specific volume, in cubic centimeters per gram = $1/\rho$ | V |
| speed of sound | C |
| standard deviation | Σ |
| thermal gas constant = PV/θ | |
| thermal gas constant for air at shock conditions | s |
| thermal gas constant for air at ambient conditions | o |

NOTE: Subscripts "o" refer to ambient air (preshock) conditions; subscripts "s" refer to shock conditions; and subscripts "R" refer to reflected shock values.

| | |
|--|--------|
| thermal gas constant ratio = $\gamma_0 = PV/(v_0 \theta)$; Eqs. (24), (25) | v |
| thermodynamic variable, equation of state for air, dimensionless; Eq. (71) | ϕ |
| time after detonation, in milliseconds | t |
| time after detonation, in seconds (thermal) | t_r |
| time of arrival, in milliseconds; Eqs. (39) through (41) | T |
| time to maximum fireball temperature; Eq. (60) | t_m |
| time to negative phase | t_n |
| total energy radiated | E^* |
| transmissivity | T^* |
| visibility, in statute miles | V_i |
| yield, in kilotons | W |
| yield scaling factor = cube-root yield in cube-root kilotons | m |

$$\alpha = \theta \eta^{-0.086} \times 10^{-4}; \text{ Eq. (25)}$$

$$\beta = \beta(\alpha, \eta); \text{ Eq. (25)}$$

$$\eta = \rho/\rho_0$$

$$\mu = (\gamma + 1)(\gamma - 1) = 1 + 2E\rho/P; \text{ Eq. (72)}$$

$$\omega = (t - T)/D_u^+ = (\sigma - \tau)/D; \text{ Eq. (56)}$$

$$\psi = h + 0.09 \text{ (a parameter in } Q_s \text{ and } I_u^+ \text{ fits versus HOB);}
Eqs. (64), (65)$$

$$\xi = \ln \eta$$

NOTE: Subscripts "0" refer to ambient air (preshock) conditions; subscripts "s" refer to shock conditions; and subscripts "R" refer to reflected shock values.

QC 168-85 D46 B864 1987
BRODE HAROLD L
AIRBLAST FROM NUCLEAR
BURSTS--ANALYTIC
M1 40104537 SCI



000034043141

B27609⁹